MONASH University

The evolution of a high temperature/low pressure crustal block and its thick ultramylonitic shear zone:
An insight into the Famatinian Orogen, the Sierra de Quilmes, Sierras Pampeanas, NW Argentina.

Melanie A. Finch

A thesis submitted for the degree of Doctor of Philosophy at

Monash University in 2015

School of Earth, Atmosphere and Environment

Monash University, Clayton, Victoria, 3800, Australia

Copyright notice

Abstract

This thesis investigated the evolution of a high temperature, low pressure crustal block of the Late Cambrian to Silurian Famatinian orogeny in the Sierra de Quilmes mountain range of the Sierras Pampeanas, NW Argentina. The crustal block is bound by the El Pichao-Ovejería shear zone, of which the eastern strand, the El Pichao shear zone, is a focus for this thesis. The El Pichao shear zone contains a 1 km-thick ultramylonite at its base and thrusts the granulite facies Tolombón complex, onto the amphibolite facies Agua del Sapo complex. The aims of this project were (1) to characterise the structural and metamorphic evolution of the Tolombón complex and its significance for understanding the western margin of Gondwana during the Famatinian orogeny, and (2) to determine the processes that formed the thick ultramylonitic layer.

Mapping in the Tolombón complex revealed that metamorphic zones increased from greenschist facies in the NE to granulite facies migmatites in the SW (chapter 2). Rocks are sheared with top-to-W or -NW thrust shear sense that intensifies near major thrust shear zones, which repeat metamorphic zones (chapters 2, 4). We determined that thrusting in the Tolombón complex began during peak metamorphism (chapter 2), between 485 and 465 Ma (U-Pb monazite, chapter 4). The kinematics remained the same as rocks were thrust to shallower structural levels and shearing localised to the amphibolite facies El Pichao shear zone (chapters 2 and 4). Major- and trace- element geochemistry revealed that the mylonitic rocks of the El Pichao shear zone define a geochemical field narrower than their protolith, suggesting that they underwent mixing and homogenisation during shearing and did not experience substantial alteration (chapter 2). Peak metamorphism in the footwall of the PSZ occurred between ~435 and 420 Ma (U-Pb monazite, chapter 4) suggesting that the Tolombón complex was thrust onto the Agua del Sapo complex prior to this time, coinciding with the activation of other mylonitic shear zones in the Sierras Pampeanas.

We speculate that the heat flux during peak metamorphism in the Tolombón complex may be a result of contact metamorphism, increased rates of shallow convection in the asthenosphere, or inherited high geothermal gradients from an earlier period of shearing (chapter 4). We suggest that the Sierra de Quilmes may have been part of the Famatinian back-arc at this time, indicated by a shared high geothermal gradient and position inboard of the Famatinian magmatic arc (chapter 4). Pervasive shortening in the Sierra de Quilmes from early in the Famatinian orogeny suggests that the Famatinian back-arc was dominantly convergent and any period of extension was brief, concluding before peak metamorphism.

Ultramylonites 1 km thick are rare and suggest the layer may have widened over time, perhaps a result of weakening of the host rock or hardening of the ultramylonite. These processes may be facilitated by water migration, so we used FTIR to measure the water content of mylonitic rocks (chapter 3). We found that water content decreased as strain increased, the opposite of previous studies. We speculate that water and heat diffusion out of the ultramylonitic

layer caused the ultramylonite to harden and the neighbouring rocks to weaken (chapter 3). This caused shearing to refocus to the neighbouring rocks and widened the shear zone. Repetition of this cycle gradually built up the 1 km-thick layer of ultramylonite (chapter 3).

The work presented in this thesis provides insight into strain localisation in shear zones and the role of water and heat diffusion in generating thick layers of ultramylonite. This work also demonstrates that the Sierra de Quilmes provides a unique insight into the tectono-metamorphic evolution of Famatinian back-arc, suggesting shortening was dominant during its development.

Thesis including published works

General Declaration

I hereby declare that this thesis contains no material which has been accepted for the award of any other degree or diploma at any university or equivalent institution and that, to the best of my knowledge and belief, this thesis contains no material previously published or written by another person, except where due reference is made in the text of the thesis.

This thesis includes one original paper published in a peer reviewed journal. The core theme of the thesis is the evolution of a high temperature/low pressure crustal block and its thick ultramylonitic shear zone. The ideas, development and writing up of all the papers in the thesis were the principal responsibility of myself, the candidate, working within the School of Earth, Atmosphere and Environment under the supervision of Roberto Weinberg.

In the case of chapter 2 my contribution to the work involved the following:

Thesis chapter	Publication title	Publication status*	Nature and extent (%) of students contribution
2	One kilometre-thick ultramylonite, Sierra de Quilmes, Sierras Pampeanas, NW Argentina	Published	87.5% Fieldwork, structural and microstructural analysis, geochemical analysis, preparation of the manuscript

I have not renumbered sections of submitted or published papers in order to generate a consistent presentation within the thesis.

Student signature: Date:

The undersigned hereby certify that the above declaration correctly reflects the nature and extent of the student and co-authors' contributions to this work.

Main Supervisor signature: Date:

Table of contents

List of figures

List of tables

Acknowledgements

I truly believe that I could not have asked for a better supervisor than Roberto. He is an excellent judge of when to provide assistance and when to let things go. He has always provided a high level of support, from reviewing work and talking about ideas, to opportunities for career and skills development. He has taught me much of what I know about structural geology and a lot about writing and being a scientist. I am extremely grateful for the time, energy, ideas, and resources he has spent on me and my research and I hope we will have cause to work together in the future. I really enjoyed doing this project and that is due in no small part to Roberto's supervisory style.

Pavlína Hasalová was also a great supervisor and helped me with the metamorphic work in chapter 4. In the early stages of my PhD and in the field she provided a great insight into metamorphic processes and melting which provided the background that underlies the metamorphic work.

Andy Tomkins was always available to run ideas past and to read parts of my work. Having someone to discuss findings, thin sections, and ideas with was extremely valuable. I really valued his support and willingness to drop whatever he was doing to help me.

I would like to thank Laurent Ailleres and Pete Betts who made me part of their demonstrating team. Our time in the field together, your respect for my opinions, your trust in my point of view and ability to teach, and your open mindedness to new ideas gave me belief in my own

abilities when I doubted them. I learnt a great deal about what it is to be a scientist from both of you and you gave me the confidence to continue to pursue my chosen career path. I cannot thank you enough.

Thank-you to Chris Wilson who assisted in the ideas for chapter 3 and provided feedback on an early draft.

Thanks also to the members of my review panel: Sandy Cruden, Sasha Wilson, Chris Wilson, and Pete Betts. Your suggestions were always useful and thoughtful and contributed to the direction of my work.

Thanks to Finlay Shanks, Martin Racek, Junnel Alegado, Rachelle Pierson, Robert Douglass who assisted with various analyses and sample preparation.

Thanks to the STRUMET group, particularly Lauren Wolfram and Nikk Hunter who both worked in Sierra de Quilmes and assisted me with data and questions. To our field team: Ivan Semenov, Gaby Fuentes, Tato Becchio, Alfonso Sola, and Nestor Suzaño, thanks for the hard work in the field, the local knowledge, and the laughs. Particular thanks to Gaby with whom I have worked most closely and who has always been extremely helpful, friendly, and supportive. No job was too big or small to ask for her help with. Thank-you to the Quilmes people, owners of the land on which this research was conducted, whose permission was granted for this work.

To my family: home of three

Earth Science PhD candidates. I couldn't ask for a more supportive family. Thanks to Mum and Dad for their excellent and prompt proof reading of chapters of the thesis. Thanks also to best friends club who I think actually understand what I do all day – a credit to their own reckoning and patience. Apologies to the Jones-O'Mearas for not holding up my side of the bet.

Thanks to mgfer1, who supported me, brought me back to reality, and lifted me up when none of my analyses worked and I feared I might never figure out "the answers". Thank-you for proof reading, for talking to me about ideas, for asking intelligent questions, for being excited every time I thought I discovered something new, and for having the patience, understanding, and thoughtfulness that made the stressful times better.

And finally, to Emily Finch. I wish everyone could be so fortunate as to have their sister working so close by, willing to do any arduous favours, and always on my side in any situation. Thanks for all your help and being the best cheerleader, sister, and friend I could want.

To my sister Karen and Grandpa Max

"Look again at that dot. That's here. That's home. That's us. On it everyone you love, everyone you know, everyone you ever heard of, every human being who ever was, lived out their lives. The aggregate of our joy and suffering, thousands of confident religions, ideologies, and economic doctrines, every hunter and forager, every hero and coward, every creator and destroyer of civilization, every king and peasant, every young couple in love, every mother and father, hopeful child, inventor and explorer, every teacher of morals, every corrupt politician, every "superstar," every "supreme leader," every saint and sinner in the history of our species lived there-on a mote of dust suspended in a sunbeam...It has been said that astronomy is a humbling and character-building experience. There is perhaps no better demonstration of the folly of human conceits than this distant image of our tiny world. To me, it underscores our responsibility to deal more kindly with one another, and to preserve and cherish the pale blue dot, the only home we've ever known."

— An excerpt from Pale Blue Dot by Carl Sagan

Chapter 1

Introduction

Summary of research aims and methods and literature reviews of the evolution of the Sierras Pampeanas and the development of shear zones

Previous page: One of the donkeys that carried our gear between camps on our trek through Sierra de Quilmes.

1. Background and rationale to the thesis

The movement of tectonic plates on Earth is accommodated by discrete shear zones that accumulate strain and allow rocks to move past each other. Understanding the development and evolution of shear zones is fundamental to our understanding of major processes, from the uplift of mountain belts to the initiation of subduction (Zhong and Gurnis, 1996, Bercovici and Ricard, 2014). Rocks accommodate strain in shear zones in a multitude of ways and deformation may partition into a network of anastomosing shear zones (Carreras, 2013) or it may be accommodated in single shear zones that take up most of the movement (Finch et al., 2015, chapter 2). Shear zones within networks may form relatively thin (mm- to cm- wide) zones of high strain that distribute the movement associated with plate convergence between them. Alternatively, singular shear zones may accommodate most of the plate convergence at a width that is controlled by the balance between shear heating and thermal diffusion (Regenauer-Lieb and Yuen, 2003). Thin zones of high strain are a relatively common occurrence in the upper crust where rocks are strong (Vauchez et al., 2012). At greater depths rocks become weaker and strain distributes over a wider area, forming thick regions of rocks at lower strain (Vauchez et al., 2012). Thick zones of high strain are not predicted in either setting but are occasionally reported, suggesting that the shear zone may have widened or narrowed over time through processes such as heat or water diffusion (Means, 1984).

This thesis focuses on one such thick, high-strain shear zone, the El Pichao shear zone (PSZ), and the evolution of its hanging wall, the Tolombón complex, in the Sierra de Quilmes, part of the Sierras Pampeanas mountain range in NW Argentina (Figs. 1,2). The PSZ is 3.5 km-thick and includes a 1 km-thick ultramylonite at its base, a thickness far greater than that reported for analogous ultramylonites worldwide. The PSZ is part of a longer shear zone, the El Pichao-Ovejería shear zone (Fig. 2), which thrusts the Tolombón complex, a tilted high T/low P, granulite facies crustal block, over the amphibolite facies Agua del Sapo complex. Understanding the development of the complex and its bounding shear zone requires determination of the physical processes active within the shear zone as well as the regional context of the shear zone, placing it within its paleo-tectonic setting. Accordingly, the aims of this project were (1) to characterise the structural and metamorphic evolution of the Tolombón complex and its significance for understanding the western margin of Gondwana during the Famatinian orogeny, and (2) to determine the processes that formed the thick ultramylonitic layer.

In order to achieve these aims a number of geological methods were employed. Research began with two field seasons in Sierra de Quilmes (Fig. 2) creating maps, collecting data and samples, and forming an initial understanding of the structures and metamorphism. Thin sections were made for petrographical analysis and enabled refinement of field-based maps (chapters 2 and 4). Key samples were selected for geochemical analysis of major and trace elements, and data were analysed for trends (chapter 2). Whole-rock analyses were also used as the
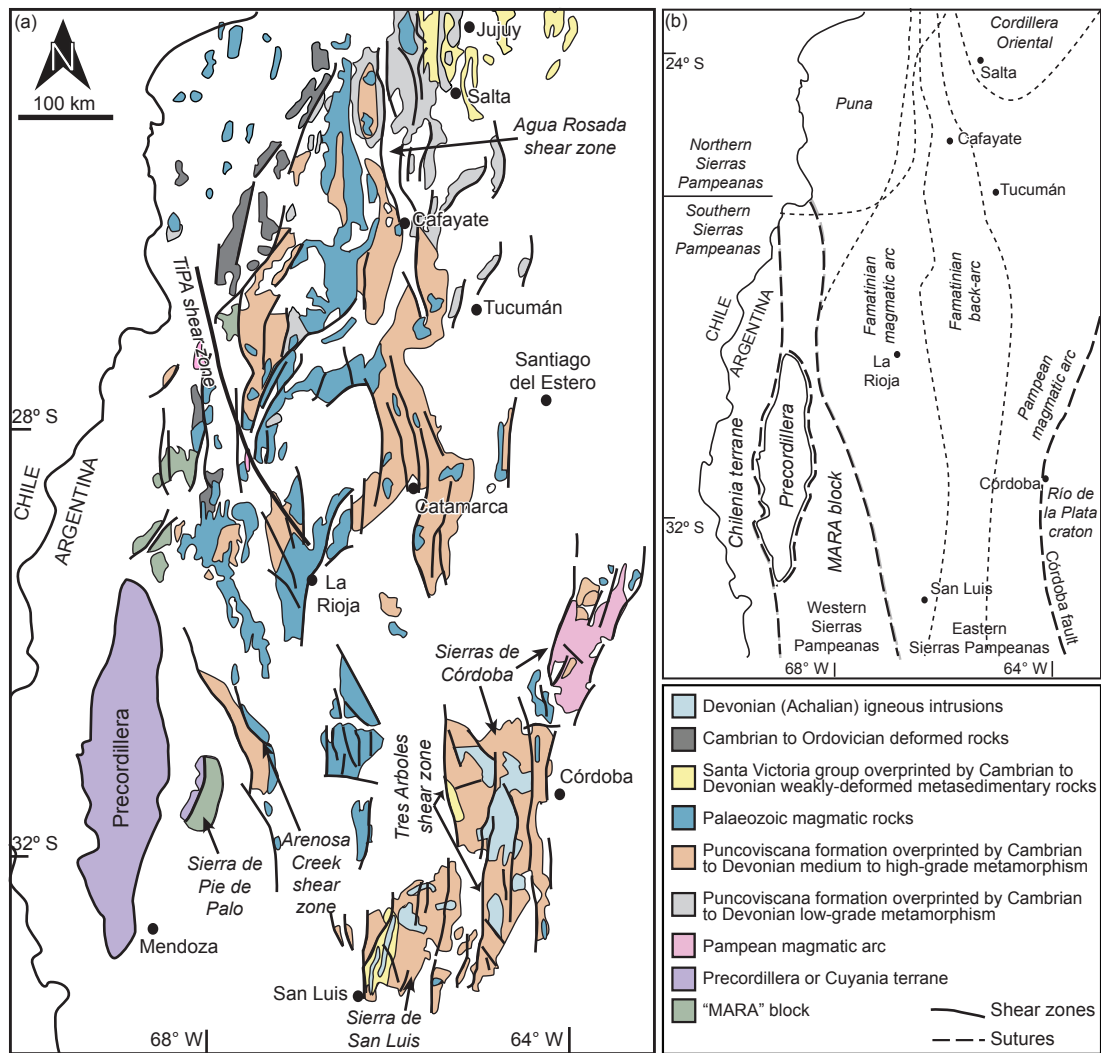
Fig. 1. (a) The mountain blocks of the Sierras Pampeanas with the location of major faults and shear zones indicated (modified from Hongn et al., 2010). (b) Schematic outline of the cratons and terranes of NW Argentina (modified from Rapela et al., 2015).

starting composition for thermodynamic models, intended to provide information about the P-T-t path and the nature of shear zones that separate rocks of different metamorphic grade (chapter 4). To understand the timing of metamorphism and constrain the timing of shearing, U-Pb analysis of monazite was conducted using the SHRIMP (chapter 4). These data were collated with results from previous research to assist in understanding relationships between events in different areas of the range. The role of water in the PSZ was investigated using fourier transform infrared spectroscopy on quartz and feldspar in rocks with different deformation intensity (chapter 3). Together, this diverse suite of methods provided a relatively complete picture of the processes that controlled formation of the PSZ and the Tolombón complex.

The tectono-metamorphic context that is revealed for the Sierra de Quilmes in this thesis is that of a high T/low P terrane, consistent with previous interpretations of an ancient back-arc region. Present day analogues in South America are located west of the Sierras Pampeanas, under kilometres of sediment and sedimentary rocks and marked by a low seismic-velocity

anomaly in the upper mantle indicating high temperatures (van der Lee et al., 2001, Hyndman et al., 2005). Knowledge of currently active back-arcs is limited to what can be known from indirect methods, mainly geophysical. Consequently, ancient terranes uplifted to Earth's surface are the main source of information about processes active in back-arc regions, including the nature of anatexis and how these regions deform during plate convergence. The increased heat flow in back-arc regions is not necessarily tied to extension, rather, it is primarily a result of increased shallow asthenospheric convection due to devolatisation of the underlying downgoing slab (Hyndman et al., 2005). Increased heat flow causes thermal weakening and renders back-arcs weaker than surrounding cratonic and forearc regions (Hyndman et al., 2005). Consequently, back-arcs often accommodate the majority of the plate convergence (Hyndman et al., 2005), making them an important region for understanding the processes that occur during plate subduction.

The Sierra de Quilmes is a key site for understanding the Paleozoic back-arc region of South America because it is a tilted metamorphic complex that preserves rocks from greenschist to granulite facies, metamorphosed during the Late Cambrian to Early Silurian Famatinian orogeny, which caused deformation and sequence repetition by ductile shear zones. Despite this, it has received little attention in the literature and we have made a number of important discoveries within the region that we report for the first time in this work.

2. Thesis structure

This thesis reports our discoveries and their meaning in five parts. The first chapter provides the context for the work with two literature reviews. The first is a review of the regional geology of the Sierras Pampeanas and the orogenic events that took place in the Paleozoic. The protolith to the Sierras Pampeanas and the timing and environment of its deposition are described before the different regions within the mountain range are detailed. The second review describes how shear zones develop and what controls their width.

Chapters 2 to 4 are the three research chapters of the thesis that detail the main findings. Monash University allows theses to be structured as a col-
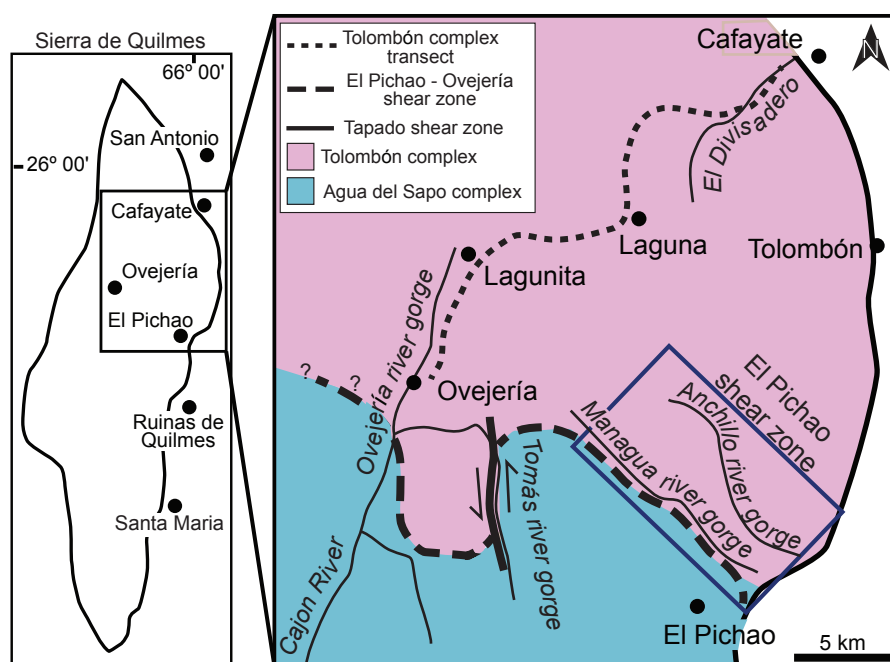
Fig. 2. The location of the field area studied in this thesis.

lection of research papers that are either published or prepared for submission, so these research chapters are structured as journal articles. Chapter 2 was published in the Journal of Structural Geology and although chapters three and four are planned for submission to different journals, they are formatted in the style of the Journal of Structural Geology for consistency.

Chapter 2 is a detailed description of the PSZ that we described for the first time in a paper published in early 2015. The paper describes the lithologies, structures, metamorphism, and geochemistry of the PSZ and speculates on the large-scale physical processes that may allow such a thick shear zone to develop. The journal version is reproduced in this thesis, which therefore differs aesthetically from the other chapters.

Chapter 3 focuses on the water content in rocks of the PSZ, returning to the question of why the ultramylonitic layer of the PSZ became so thick. Here, we examine the role of water in the ultramylonitic layer by measuring the water content in quartz and feldspar using fourier transform infrared spectroscopy. We found that water content decreased with increasing deformation and recrystallisation and conclude that water removal from the shear zone, hardening of the core of the shear zone and the weakening of its shoulders may explain shear zone widening and the thickness of the ultramylonite layer.

Chapter 4 zooms out of the PSZ to examine the nature of its hanging wall, the high-grade Tolombón complex of the Sierra de Quilmes. This chapter describes the gradation in metamorphic conditions from unmelted greenschist-facies rocks in the NE to granulite-facies migmatites. In this chapter another shear zone, the Tolombón thrust, is described and compared to the PSZ. This paper also presents new geochronological and thermodynamic data on the region, which assists in understanding the development of these shear zones and the mountain range more broadly.

The findings of chapters 2 to 4 are brought together in the final summarising chapter 5. In order to avoid repetition the regional geology common to chapters 2–4 is fully reviewed in the next section. Some repetition however is unavoidable because the published chapter 2 had to be made self-contained.

3. Literature review of the Sierras Pampeanas

3.1. Introduction

The Sierras Pampeanas in Argentina are a series of ~12 mountain ranges that were uplifted in the foreland of the Andean orogeny (Jordan and Allmendinger, 1986), comprised of two provinces, east and west, which formed from different protoliths (Fig. 1). The eastern province consists of metamorphic and anatectic equivalents of a thick package of turbidites called the Puncoviscana Formation, deposited on the paleo-Pacific margin in the Ediacaran to early Cambrian (Turner, 1960, Bachman et al., 1987, Acenolaza et al., 1988). These rocks were deformed and metamorphosed during three periods of subduction: the Cambrian Pampean orogeny, the

Late Cambrian - Silurian Famatinian orogeny, and the Devonian Achalian orogeny (Sims et al., 1998). The magmatic arc formed during the Pampean orogeny is preserved in the Sierras de Córdoba, located in the SE of the Sierras Pampeanas (Fig. 1; Simpson et al., 2003). The Famatinian magmatic arc and back-arc basin are preserved in N-S trending zones that span the length of the Sierras Pampeanas, from 22° to 33° S (Fig. 1). The Achalian orogeny caused minor overprinting of the earlier events with localised shearing, folding, and granitic intrusions (Sims et al., 1998). The three Palaeozoic orogenies culminated in the accretion of exotic terranes characterised by high-pressure, mafic assemblages with Laurentian affinities that form the western Sierras Pampeanas (Fig. 1; Caminos, 1979).

The Sierras Pampeanas generally increase in structural depth and metamorphic grade from the north, where rocks are weakly metamorphosed (~25° S), to the south, where high-grade metamorphic rocks and migmatites are exposed near Córdoba (33° S; Piñán-Llamas and Simpson, 2006) due to flat slab subduction during the Andean orogeny between 27° and 33° 30′ S (Ramos et al., 2002). The exception to this overall increase in metamorphic grade is the Famatinian back-arc that intermittently records high T/low P conditions over a region 1000 km long (22°–33° S) and 250 km wide (65°–68° W; Larrovere et al., 2011). This implies high heat flux, which would have caused thermal weakening of this zone, suggesting it may have been a key site for strain localisation during plate convergence.

Tectono-metamorphic models for the Sierras Pampeanas describe evidence for continental collision and terrane accretion in the southern Sierras Pampeanas (Ramos et al., 1986, Ramos, 1988) but no such evidence is found in the north (Lucassen et al., 2000). This may be because terranes did not extend into the northern Sierras Pampeanas, or alternatively because the evidence is not preserved or does not outcrop in the shallow structural levels preserved in the north.

This review details the main features of the Sierras Pampeanas and its tectonic evolution in order to provide the background for chapters 2–5 that focus on the northern Sierras Pampeanas. There are several different terrane accretion models for western Argentina and Chile and they each propose different terranes, time of collision, and terrane origin. A review of these models is beyond the scope of this work, particularly since many have been abandoned in light of new evidence. The models presented here are those that have the greatest acceptance. We begin with the early evolution of the Sierras Pampeanas including the source and deposition of its protolith, before describing the features of the eastern and western Sierras Pampeanas and the orogenies that affected them.

3.2. Evolution of the Puncoviscana Formation, the Mesón group, and Ordovician sedimentary sequences

The protolith to the eastern Sierras Pampeanas, the Puncoviscana Formation (Turner, 1960), outcrops over an area of 1200 x 300 km in NW Argentina (Jezek et al., 1985) and consists

of a >2000 m-thick package dominated by sedimentary rocks. The base consists of conglomer-ate, diamictite, and sandstone intruded by ultra-potassic dykes and mafic volcanics, and this is overlain by marine sequences including flysch turbidites, thick layers of sandstone, siltstone, ar-gillite, and laterally-discontinuous lenses of conglomerate, pyroclastic, volcanic, and volcaniclas-tic rocks (Omarini, 1983, Acenolaza et al., 1988, Omarini et al., 1999). The sandstones comprise grain sizes from silt to medium sand and are lithologically classified as greywackes and lithic greywackes (Jezek et al., 1985, Omarini et al., 1999) with volcanogenic, arc-related geochemical affinities (Zimmermann, 2005). Various primary structures are evident, particularly in the low-er-grade regions, including flaser, graded, and cross bedding, Bouma sequences, parallel lami-nation, flame structures, and submarine-fan facies (Omarini, 1983, Jezek et al., 1985, Omarini et al., 1999, Piñán-Llamas, 2007) with sediment transport directions toward the west or northwest (Jezek et al., 1985). Compaction soon after deposition led to the development of a pronounced bedding-parallel cleavage due to pressure solution and dissolution of quartz (Piñán-Llamas and Simpson, 2009).

Deposition of sediments into the Puncoviscana basin began by the late Neoproterozoic (K-Ar authigenic mica 670±25 Ma; Do Campo et al., 1999) and ended in the early Cambrian (youngest trace fossils: 534–530 Ma; Durand, 1996, youngest zircons: 535–515 Ma; Adams et al., 2011). The early stages of deposition were coeval with the rifting of Laurentia from Rodinia, which began the Terra Australis orogen on the 18000 km-long rifted margin of Gondwana (Fig. 3; Cawood, 2005). The break-away of Laurentia from the core of Rodinia opened the Iapetus (paleo-Pacific) Ocean on the eastern side of Laurentia and the Pacific Ocean on the west, form-ing West and East Gondwana respectively (Cawood, 2005). West Gondwana consisted of cratons from South America and Africa, and East Gondwana included sections of Australia, Antarctica, and India (Cawood, 2005). The Puncoviscana basin was located on the newly-formed Iape-tus-West Gondwana margin and deposition during rifting is evidenced in basal sections of the Puncoviscana Formation by interbedded mafic volcanic flows and intrusion of ultra-potassic dykes that show mantle geochemical affinities (Omarini et al., 1999). The age of these rocks is poorly constrained due to resetting by later orogenesis (Omarini et al., 1999, Cawood, 2005). After rifting, the West Gondwana-Iapetus margin was passive and the Puncoviscana Formation was dominated by marine shelf and slope sequences (Jezek et al., 1985, Schwartz et al., 2008). Subduction commenced on the margins of East and West Gondwana at around 540 Ma, indicat-ed in the Puncoviscana Formation by the presence of thin, intercalated layers of 540–535 Ma pyroclastic rocks attributed to the proximal calc-alkaline Pampean magmatic arc (Escayola et al., 2011). At this time, the Puncoviscana Formation depocentre was located between the Pampean magmatic arc to the east and the trench to the west, a fore-arc position (Keppie and Bahlburg, 1999, Zimmermann, 2005, Ramos, 2008, Escayola et al., 2011). Gondwana was established in the late Neoproterozoic (by ~530 Ma) when East and West Gondwana collided (Fig. 3; Cawood, 2005). In some regions, the Puncoviscana formation is divided into facies or complexes based on

local differences in lithology (e.g., unique carbonatic or clastic horizons; e.g. Aparicio González et al., 2014) and/or structural style (e.g. Mon and Hongn, 1991). These facies and complexes are discontinuous and vary between localities.

The multi-stage evolution recorded in the Puncoviscana Formation is also seen in other sedimentary basins on the Iapetus-Pacific margin of Gondwana during the late Neoproterozoic to Cambrian (Fig. 3). For example, sedimentary rocks of the Transantarctic mountains record a passive margin, shallow-shelf setting from 670–580 Ma, with contributions from Archean to Mesoproterozoic cratons, overlain by arc-derived sedimentary rocks aged 580–515 Ma, syn-orogenic sedimentary rocks aged 515–490 Ma and late-orogenic rocks aged 490–480 Ma that are intruded by dykes as a result of trenchward migration of magmatism (Goodge et al., 2004).

Rocks of the Eastern Australian Kanmantoo group and Lachlan fold belt record a similar evolution with an early passive margin setting and later contributions from the actively deforming Pacific margin (Ireland et al., 1998). The striking similarities in timing and sedimentation type between rocks on the Iapetus-Pacific margin of Gondwana in the Neoproterozoic to Cambrian reflects the extensive subduction system of the Terra Australis Orogen active at this time on the margin of Gondwana (Fig. 3).

The sediment source for the Puncoviscana Formation has been widely debated since the first description of the sequence more than 50 years ago (Turner, 1960). The Río de la Plata craton was originally thought to be the main sediment source since it underlies most of NE Argentina between approximately 25°–38° S and 54°–64° W (Rapela et al., 2007) and is now located directly east of the Sierras Pampeanas. It consists of continental crust that underwent deformation and anatexis during the Palaeoproterozoic Trans-Amazonian cycle (Pankhurst et al., 2003, Massonne et al., 2012). Early models contended that prior to the commencement of subduction,
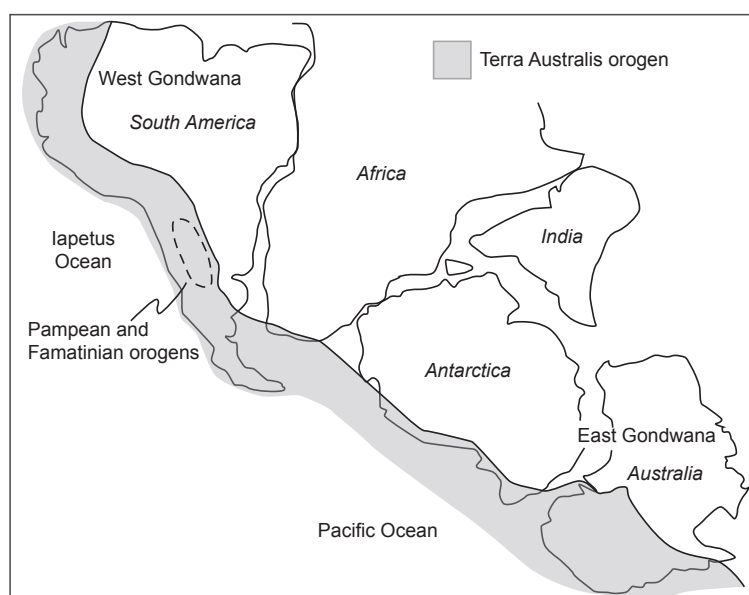
Fig. 3. Distribution of the Terra Australis Orogen (grey) on the cratons that formed the paleo-Pacific margin of Gondwana during the late Neoproterozoic to Cambrian (Cawood, 2005).

the Río de la Plata craton was located on the West Gondwana-Iapetus margin and eroded into the submarine Puncoviscana basin, which extended from Bolivia to central Argentina (Jezek et al., 1985). However, more recent reviews of Puncoviscana Formation detrital zircon data indicate that there are two dominant age ranges: 670–545 Ma and 1200–900 Ma (Miller et al., 2011), suggesting that the Río de la Plata craton (with its dominant ~2100 Ma zircons) is unlikely to be the source (Rapela et al., 2007,

Miller et al., 2011). These zircon populations are consistent with orogens within an extensive mountain range in south-east and south-central Brazil: the Neoproterozoic Brasiliano Orogen and the Mesoproterozoic Sunsás Orogen (e.g. Adams et al., 2011, Miller et al., 2011). It is contended that a major river system developed in the rising Brasiliano Orogen, which drained sediment from the mountain ranges across the craton, to the Puncoviscana basin (Adams et al., 2011).

The overlying Mesón group is in angular unconformity contact with the Puncoviscana Formation (Turner, 1960). It consists dominantly of sandstone and conglomerate with layers of siltstone, mudstone, and alkaline volcanic rocks (Kumpa and Sanchez, 1988, Augustsson et al, 2011). The minimum deposition age is not known because index fossils are not preserved. The Mesón group contains the same zircon populations as the Puncoviscana Formation in addition to a population of zircons aged between 1900 and 2200 Ma and another population at ~500 Ma (Miller et al., 2011). The late Cambrian ages are taken as the maximum deposition age of the Mesón group (Adams et al., 2011, Miller et al., 2011). The Paleoproterozoic zircons are the same age as those in the Río de la Plata craton, which suggests that the craton became available for erosion at this time, either because of denudation of overlying sequences of rocks (Miller et al., 2011), or because it reached juxtaposition with the Mesón group in the Cambrian (Rapela et al., 2007). Models for the latter suggest that prior to this time, the Río de la Plata craton was located south of the Brazilian shield and its northwards movement in the Cambrian was accommodated by a dextral strike-slip shear zone, the Transbrasiliano Mega-Shear Zone, now located between Sierras de Córdoba and the Río de la Plata craton (Rapela et al., 2007).

The volcanic rocks intercalated with Mesón group sedimentary rocks have an alkaline geochemical signature consistent with a rift-related, intraplate extensional setting (Coira et al., 1999, Hongn et al., 2010). Consequently, the Mesón group is generally regarded to have infilled an extensional basin, thought to have formed in the early stages of the Famatinian orogeny in a back-arc setting (Hongn et al., 2010) and arc rocks eroded into this basin.

Overlying the Mesón group there are km-thick marine sedimentary sequences, deposited from the Early to Middle Ordovician (graptolites; Bahlburg, 1990, 1991), preserved in Puna and the Cordillera Oriental (Fig. 1b; Turner, 1960). The eastern part of the Cordillera Oriental, furthest from the arc, consists of the Ordovician Santa Victoria group, consisting of shallow-water pelites interbedded with arenites (Turner, 1960, Moya, 1988). Faunal and lithological data indicate the sediments were deposited on a shallow-marine shelf that underwent several periods of marine transgression and regression (Moya, 1988). Rocks are not deformed or metamorphosed and there was no volcanigenic input (Moya, 1988). Further west, Ordovician sedimentary rocks in Puna and the western part of the Cordillera Oriental contain several formations largely sourced from the Puncoviscana Formation and Mesón group with input from the Famatinian magmatic arc, situated in west Puna (Zimmermann and Bahlburg, 2003). The two oldest Ordovician sedimentary sequences, the Tolar Chico and the Tolillar Formations, consist of non-fossiliferous turbidite packages that contain flute marks, ripples, and cross and parallel laminations, indicative

of a shallow marine depositional environment (Zimmermann and Bahlburg, 2003). These packages contain volcaniclastic sandstones and debris that increases in volume toward the overlying sequence, the Diablo Formation, which consists of turbidite sequences intercalated with rhyolitic and andesitic lavas including pillowed andesites, and rare peperites and volcaniclastic flows (Zimmermann and Bahlburg, 2003). Volcanism within the sequence was submarine and attributed to the Famatinian magmatic arc (Fig. 1; Zimmermann and Bahlburg, 2003). Evidence for volcanism is absent in rocks above the Diablo Formation, suggesting that the Famatinian magmatic arc was not active in southern Puna by this time (Bahlburg, 1990, Zimmermann and Bahlburg, 2003). Coincident with the cessation of magmatism in the arc, there was a rapid increase in sedimentation rate in the back-arc basin in Puna, while further east, deposition of the Santa Victoria group ceased (Bahlburg, 1991; Bahlburg and Furlong, 1996; Bahlburg and Herve, 1997). This is thought to be due to eastward thrusting of the magmatic arc, which increased loading on the basin and caused development of a peripheral bulge in the Cordillera Oriental, uplifting the Santa Victoria group (Bahlburg and Herve, 1997). After this, the 3500m-thick Puna turbidite sequences were deposited into the basin (Bahlburg and Herve, 1997), in the late Arengian to early Llanvirnian (~475–460 Ma, graptolites; Bahlburg, 1990). The basal Coquena Formation consists of turbidites that fine upwards into the black shales of the Falda Ciénaga Formation, deposited in a deep-marine setting, indicated by the absence of shallow water sedimentary structures and lack of debris flows (Bahlburg, 1990, Zimmerman et al., 2002). This upwards fining indicates that sediments were deposited into a tectonically subsiding basin. Overlying this, the Lina Formation consists of shales and sandstones deposited in submarine channels (Aceñolaza et al., 2013) suggesting marine regression. In the Late Ordovician a period of shortening caused inversion of the basin, the development of west-vergent folds, and shearing on vertical planes (Mon and Hongn, 1987). Lower Silurian strata were deposited on Ordovician sequences forming an angular unconformity (Isaacson et al., 1976). The relationship between the deposition of sedimentary formations and the orogenic events of the Sierras Pampeanas is discussed further in section 3.3.2.

3.3. Eastern and western Sierras Pampeanas

The Sierras Pampeanas is separated into eastern and western provinces that formed from different protoliths. The eastern Sierras Pampeanas consists of deformed and metamorphosed equivalents of the Puncoviscana Formation (Fig. 1). It is dominated by high T/low P metamorphic assemblages (Caminos, 1979) and contains longitudinally continuous zones of intrusive and extrusive igneous rocks that record magmatism and deformation during Palaeozoic subduction (Fig. 1). The western Sierras Pampeanas (Fig. 1) is compositionally and geochronologically distinct from the eastern region, and consists of a number of basement uplifts of exotic terranes (Fig. 1; Rapela et al., 2015). We first describe the western Sierras Pampeanas and its tectonic history before outlining the orogenic events that overprinted the Puncoviscana Formation in the

eastern Sierras Pampeanas.

3.3.1. Western Sierras Pampeanas

The western Sierras Pampeanas consists of two allochthonous terranes that accreted at the end of the Pampean and Famatinian orogenies respectively. The easternmost terrane consists of Paleoproterozoic basement overprinted by Mesoproterozoic magmatism and metamorphism and outcrops in the Arequipa massif in Peru, the Sierras of Toro Negro, Umango, Maz, Espinal, and Pie de Palo in Argentina, and Río Apa in Brazil, all of which are grouped together as the "MARA block" in Rapela et al. (2015; Fig. 1). These outcrops are characterised by high-grade metasedimentary rocks including quartzites, metasandstones, metapelites, and calcsilicate rocks with associated igneous-intrusive rocks and anorthosite-mangerite-charnockite-granite complexes (Casquet et al., 2008) that have been dated to 1330–1070 (U-Pb zircon; Rapela et al., 2010). The MARA block rifted from Laurentia in the Ediacaran - Early Cambrian (Thomas et al., 2012, Rapela et al., 2015) and began accreting to the Iapetus-Gondwana margin at 530–525 Ma, toward the end of the Pampean orogeny (Rapela et al., 2015). To the west of the MARA block is the Mesoproterozoic Precordillera or Cuyania terrane (Davis et al., 2000, Vujovich et al., 2004, van Staal et al., 2011). It is dominated by high pressure metamorphic rocks including ultramafic, mafic, and carbonate sequences with ages of 1330–1030 Ma (Rapela et al., 2007) intruded by igneous rocks that crystallised from the Late Proterozoic through to the Ordovician with geochemical affinities consistent with an extensional setting (Davis et al., 2000). These intrusions, combined with stratigraphic, faunal, and geochemical data, have led to the interpretation of the Precordillera terrane as Laurentian in origin, rifting in the Cambrian to Early Ordovician (Davis et al., 2000, Vujovich et al., 2004, van Staal and Hatcher, 2010). The Precordillera terrane accreted in the early Silurian to Devonian (Thomas and Astini, 2003) at the end of the Famatinian orogeny (described in section 3.3.2.2). To the west of the Precordillera terrane is the Chilenia terrane that docked at the end of the Achalian orogeny (~350 Ma) and lies west of (outside) the Sierras Pampeanas (Fig. 1b).

3.3.2. Orogenesis in the Eastern Sierras Pampeanas

The Eastern Sierras Pampeanas underwent deformation, anatexis, and metamorphism during the Pampean, Famatinian, and Achalian orogenies. These orogenies and their effect on the Eastern Sierras Pampeanas are described below.

3.3.2.1. Pampean orogeny (540–?520 Ma)

The initiation of subduction on the western margin of Gondwana (present day coordinates; Rapela et al., 1998a) began the Pampean orogeny in the Early Cambrian (U-Pb zircon rims; Sims et al., 1998). Sedimentary rocks in the Puncoviscana basin, located in the arc-trench gap were progressively assembled into an accretionary prism (Escayola et al., 2011). The Pam-

pean arc formed on the easternmost part of the accretionary prism and the western margin of the Río de la Plata craton (Rapela et al., 1998b). It is exposed in northern Sierras de Córdoba (Fig. 1) and consists of I-type plutonic rocks (Simpson et al., 2003) and less-voluminous peraluminous intrusions, dated at 523±2 Ma (U-Pb zircon; Rapela et al., 1998b). Metamorphism was generally upper-amphibolite to lower-granulite facies (Rapela et al., 1998b, Drobe et al., 2011) with peak metamorphism between 540 and 520 Ma (U-Pb zircon rims; Sims et al., 1998). Deformation during the Pampean orogeny involved penetrative, metre-scale, NE-trending chevron folds (Simpson et al., 2003, Piñán-Llamas, 2007), tight folds, late minor shear zones, and fabric reorientation (Simpson et al., 2003). The end of the Pampean orogeny is recorded in the Sierras de Córdoba with ophiolite obduction and crustal shortening and thickening, followed by isothermal decompression with associated magmatism and the development of mylonitic shear zones (Rapela et al., 1998b). Dating of a granite that formed during decompression suggests that the Pampean orogeny ceased by 525–519 Ma (U-Pb zircon and Rb-Sr whole rock; Rapela et al., 1998b). The Pampean orogeny ended with accretion of the MARA block in the western Sierras Pampeanas (Rapela et al., 1998b).

3.3.2.2. Famatinian orogeny (?490–430 Ma)

There is some debate over whether subduction of the Iapetus underneath the margin of Gondwana ceased at the end of the Pampean orogeny or continued into the Famatinian orogeny (e.g. Becchio and Lucassen, 2002). Arguments for the cessation of subduction suggest that there was a period of magmatic quiescence indicated by a gap in the geochronological record (Rapela et al., 1998b). While this gap is seen in many data sets, it is not ubiquitous through the Sierras Pampeanas (e.g. Becchio and Lucassen, 2002) and where present does not necessarily indicate subduction ceased, only that magmatism ceased.

Another argument for cessation in subduction is the deposition of the Mesón group, the sedimentary sequence that unconformably overlies the Puncoviscana Formation. Prior to deposition of the Mesón group, the Puncoviscana Formation experienced uplift and erosion, consistent with decompression at the end of the Pampean orogeny described by Rapela et al. (1998b). After this, the basin became extensional, as indicated by intercalated alkaline igneous rocks of the Mesón group with rift-related geochemical affinities (Coira et al., 1999, Hongn et al., 2010). However, this is not necessarily indicative of a cessation in subduction since it may represent the beginning of extension in a back-arc basin setting related to the westward shift from the Pampean to the Famatinian arc (detailed in section 3.3.2.2.2). Therefore, we find no compelling reason to suggest that there was a break in subduction between the Pampean and Famatinian orogenies.

3.3.2.2.1. Famatinian magmatic arc

Subduction on the Iapetus-Pacific margin of Gondwana caused the development of the Famatinian magmatic arc, now preserved in a zone up to 600 km wide at ~67° W that trends N-S for ~1000 km through the entire Sierras Pampeanas, from Puna to San Luis (Fig. 1; Rapela et al., 1998a, Saavedra et al., 1998). As mentioned previously, flat subduction of the NAZCA plate south of 27° S caused the exposure of progressively deeper rocks toward the south. Accordingly, shallow levels of the arc are exposed in a relatively narrow band between 22° and 27° S in Sierra de Famatina and the Puna region (Coira et al., 1999), whereas deeper plutonic levels are exposed over a wider section between 27° and 33° S (Tibaldi et al., 2013, Ducea et al., 2015).

Arc magmatism was pre- and syn-tectonic and consisted of three main types: I-type, S-type, and tonalite-trondhjemite-granodiorite (Toselli et al., 1978, Rapela et al., 1990, DeBari, 1994, Pankhurst et al., 2000). I-type granitoids grade into S-type granitoids toward the east and away from the arc, indicative of crustal melting (Steenken et al., 2011). While fractionation of a calc-alkaline parent magma has been used to explain compositional diversity of the Famatinian arc rocks (Bellos et al., 2015), field-based studies, zircon inheritance patterns, and geochemical modelling suggest that the entire compositional diversity of the Famatinian magmatic arc is better explained by hybridisation processes between mantle-derived gabbro and diorite magmas and melt derived from the supracrustal Puncoviscana Formation wall rock (Ducea et al., 2015). There is no evidence of basement contributions to arc rocks, which suggests that the lithosphere was thinned prior to deposition of the Puncoviscana Formation (Ducea et al., 2015), perhaps a result of the rifting of Rodinia, which formed the passive margin, described in section 3.2. Ages of zircons in magmatic rocks indicate the arc was active between 490 and 440 Ma with the most voluminous activity around 470 Ma (Pankhurst et al., 1998, Bellos et al., 2015). Successive intrusions built up batholiths over time, and the prevalence of magmatic contacts between different intrusion pulses that vary in age by >5 Ma suggest that rocks remained liquid for extended periods (Bellos et al., 2015). Bellos et al. (2015) demonstrated that magmas were recycled while still liquid with ages that span >20 Ma in zircons within a single sample, and examples of back-veining and magma intrusion into a liquid host rock in plutonic rocks separated by 15 Ma. This argues for a prolonged high-temperature regime during the Famatinian orogeny (Lucassen and Becchio, 2003).

I-type intrusions are occasionally associated with km-scale thermal aureoles, such as the Cerro Toro thermal aureole exposed in western Sierra de Famatina adjacent to a sheeted-tonalite complex (Alasino et al., 2014). The aureole was described by Alasino et al. (2014) and consists of two concentric metamorphic regions, the external and intermediate zones, that surround a 25 km pluton of tonalite, which forms the internal zone. The external zone is the outermost region of the aureole and consists of fibrolite-bearing stromatic metatexites and tabular amphibolites that are intercalated with foliation-parallel, <1 km-wide sheets of tonalite and granodiorite that contain mafic enclaves of gabbro. The intermediate zone is 3 km wide and adjacent to the tonalite pluton. It consists of hybrid mixes of tonalitic magma and migmatitic metasedimenta-

ry rocks that lose coherence toward the pluton, grading into leucogranites and leucotonalites. Enclaves and xenoliths of mafic rocks are common. Migmatites increase in metamorphic grade toward the pluton with Bt+Sil±Crd diatexites that grade into Bt+Sil±Grt±Crd diatexites and into Bt±Amp±Cpx±Kfs hybrid rocks. At the contact with the internal zone, leucogranitoids from the intermediate zone intrude the tonalitic pluton. In summary, the Cerro Toro thermal aureole consists of a tonalitic pluton at its core surrounded by high T/low P rocks that decrease metamorphic grade and proportion of in situ melting away from the pluton.

3.3.2.2.2. Famatinian back-arc basin

East of the preserved Famatinian arc, between 65° and 66° W, there is a longitudinally continuous zone that contains intermittent outcrops of high T/low P rocks, which typically contain cordierite at lower T, garnet at moderate T, and orthopyroxene-bearing metatexites and diatexites in the highest-grade rocks (e.g., Grissom et al., 1998, Büttner et al., 2005, Larrovere et al., 2011). High T/low P metamorphism has been recognised from the northern Sierras Pampeanas in Sierra de Quilmes (Büttner et al., 2005), Sierra de Cachi (Hongn et al., 2014), and Sierras de Ancasti, Ambato, and Aconquija (Larrovere et al., 2011), through to the southern Sierras Pampeanas in Sierras Valle Fértil-La Huerta (Otamendi et al., 2008) and Sierra de San Luis (Hauzenberger et al., 2001). High T/low P metamorphism over this ~ 1000 km-long zone (Fig. 1b) implies a regional process for large-scale, uniform heat input into the crust (de los Hoyos et al., 2011, Larrovere et al., 2011). The catalyst for such a process may be lithospheric thinning in a back-arc basin. This is supported by the deposition of km-thick packages of Ordovician sediments into a tectonically-subsiding submarine basin in Puna and the Cordillera Oriental (section 3.2) and Famatinian bimodal volcanism including mafic rocks with a back-arc basin geochemical signature, dated to 480–475 Ma (Coira et al 2009) and purported to be a result of subduction rollback during the Famatinian orogeny (Hongn et al., 2014). Lithospheric thinning in the back-arc basin, combined with dehydration of the underlying subducting slab, may have caused shallow asthenosphere convection (Hyndman et al., 2005), high T/low P metamorphism in the overlying lithosphere, and large-scale heat flux that thermally weakened the middle crust (Larrovere et al., 2011). Thermally weakened back-arcs are often the locus of deformation in continental settings because they are an order of magnitude weaker than the craton interior (Hyndman et al., 2005). This is evidenced in the Famatinian back-arc by ubiquitous ductile shear zones, thought to be a result of basin inversion at the end of the Famatinian orogeny during the Oclóyic tectonic phase (see below; Hongn et al., 2014).

High T/low P metamorphism may alternatively be a result of regional contact metamorphism with intrusive rocks of the Famatinian magmatic arc (Alasino et al., 2014). While there is no clear evidence for contact metamorphism (e.g., plutons at the centre of metamorphic aureoles) or even the presence of intrusive arc rocks within the metamorphic sequence, the narrowing of the outcrop exposure of the Famatinian arc toward the northern Sierras Pampeanas suggests the possibility that the arc width is constant but in the north it may be buried below the Famatinian

high T/low P Puncoviscana Formation.

3.3.2.2.3. Oclóyic tectonic phase (470–430 Ma)

Toward the end of the Famatinian orogeny, the back-arc basin region underwent shortening on a number of mylonitic shear zones, defining the Oclóyic tectonic phase (Rapela et al., 1998a). This phase is thought to be coincident with either collision of the Precordillera terrane with the continent margin (e.g. Pankhurst et al., 1998) or accelerated approach of the terrane, prior to collision (Rapela et al., 1998a). Mylonitic shear zones from this period are pervasive in the Sierras Pampeanas, including, the Tres Arboles shear zone (32° S; Simpson et al., 2003), Arenosa Creek shear zone (31° S; Castro de Machuca et al., 2012), shear zones in the Sierra de Pie de Palo (31° S; Ramos et al., 1998), the El Pichao shear zone (26° S; Finch et al., 2015), and the Agua Rosada shear zone (25–26° S; Wegmann et al., 2008; Fig. 1).

The age of ductile shearing is difficult to determine because it relies on the preservation of features (minerals, dykes, etc.) that formed before, during, and after shearing. This rarely occurs, typically only the start, middle, or end of shearing can be determined. Some shear zones in the Famatinian back-arc have been dated using minerals that grew during shearing. For example, the age of shearing on the greenschist facies Agua Rosada shear zone was dated to 441–424 using Rb-Sr on syn-tectonic white mica (Wegmann et al., 2008). However, minerals that can be shown to have grown during deformation are rare and more often the time of shearing is bracketed by dating deformed minerals using a system that closed after shearing. For example, shearing on the Arenosa Creek shear zone was dated to ~445–435 Ma using ^{40}Ar/^{39}Ar in hornblende from mylonitic rocks (Castro de Machuca et al., 2012). Shearing took place at temperatures up to 700 °C and hornblende has a closure temperature of 450–550 °C so this is a minimum age for shearing (Castro de Machuca et al., 2012). Alternatively, features that cross-cut the shear zone can be dated to determine the end of ductile shearing. For example, the end of mylonitisation in Sierras de Córdoba was dated using pseudotachylites that cross-cut ductile shear zones, which gave ages of 428±12 and 365±10 Ma (Northrup et al., 1998). Field relationships also assist in the determination of the relative time of shearing. For example, using the relationship between outcrop structures and in situ melting, Büttner et al. (2005) demonstrated that shearing in Sierra de Quilmes began during anatexis and continued through retrogression to amphibolite facies and solid-state deformation. They dated migmatites using U/Pb in monazite and titanite to determine that peak metamorphism occurred at ~470 Ma, suggesting that shearing had begun by this time. Dating by Rb/Sr (muscovite and plagioclase) of undeformed pegmatite dykes that cross-cut the shear zones indicated that ductile shearing had ceased by ~440 Ma (Büttner et al., 2005). While this approach suggests that shearing occurred in the Mid-Late Ordovician it is susceptible to errors due to possible migration of strain.

Despite the difficulties in determining the age of shearing, this data taken together indicates that top-to-W thrusting occurred between ~470 and 430 Ma, coinciding with the accretion

of the Precordillera terrane (Davis et al., 2000, Vujovich et al., 2004, van Staal et al., 2011) south of 29 °S, which ended the Famatinian orogeny (Thomas and Astini, 2003 and references therein, Varela et al., 2011).

3.3.3. Achalian orogeny (400–350 Ma)

Renewed subduction on the margin of the eastern Sierras Pampeanas caused the Achalian orogeny (Ramos et al., 1986, Sims et al., 1998). This orogeny spanned the Devonian and caused minor top-to-W thrust shear zones, NNW-trending sinistral shear zones, folding, and localised voluminous granitic intrusions (Sims et al., 1998). Magmatism included major juvenile magmas that mixed with granitic compositions (Steenken et al., 2011). Large, syn-tectonic batholiths were emplaced in Sierra de Córdoba and Sierra de San Luis (Siegesmund et al., 2004, Pinotti et al., 2006). There is no evidence to suggest that a magmatic arc developed during the Achalian orogeny. Rather, the generation of large volumes of magma is speculated to be a result of mafic underplating (López de Luchi, 1996) or slab break-off toward the end of subduction (Steenken et al., 2011). The orogeny ceased when the allochthonous, Laurentia-derived Chilenia terrane accreted onto the western margin of Gondwana at the end of the Devonian (Ramos et al., 1986, Ramos, 1988).

3.4. Eastern Sierras Pampeanas: north and south

The eastern Sierras Pampeanas is divided into northern and southern regions largely because there is no evidence for terrane accretion in the north, including the lack of ophiolites (Mon and Hongn, 1991, Bahlburg and Herve, 1997, Bock et al., 2000), suture zones (Franz and Lucassen, 2001), and absence of high P/low T metamorphism (Lucassen et al., 2000). Between 18° and 26° S there is a gradual decrease in the age of the crust from east of Puna to the Pacific margin on the west, and geochronological and petrological breaks or anomalies are absent (Lucassen et al., 2000, Lucassen et al., 2011). Instead, it is suggested that the northern Sierras Pampeanas experienced subduction without collision and formed a mobile belt that accommodated consecutive Pampean and Famatinian orogenies (Lucassen et al., 2000, Becchio and Lucassen, 2002). Presumably, the terranes that collided with the southern Sierras Pampeanas did not extend to the north, in fact, many of the accretion models only extend the three proposed exotic terranes as far north as 27° S (e.g. Lucassen et al., 2000, Varela et al., 2011, Iannizzotto et al., 2013). Apart from the lack of collision-related features, the north and south Sierras Pampeanas are similar, with the Famatinian arc and back-arc basin continuous from 22°–33° S (Rapela et al., 1998a).

3.5. Summary

The Sierras Pampeanas record the development of NW Argentina on the Iapetus

(paleo-Pacific) margin of Gondwana during the Terra Australis orogeny. The Puncoviscana Formation, protolith to the eastern Sierras Pampeanas, consists of sediments eroded from Proterozoic orogens on the Brazilian craton that were transported to the Iapetus margin in a major river system. The Puncoviscana basin originated during rifting of Rodinia and passive margin development but with the initiation of subduction and the development of the Pampean arc and orogen, it became situated between the arc and trench, and sedimentary rocks from the basin accumulated into an accretionary complex. The Pampean orogeny is best preserved in the Sierras de Córdoba where rocks of the Puncoviscana Formation were deformed, melted, and metamorphosed. The Pampean orogeny is associated with a magmatic arc, I-type plutonic rocks, granulite-facies metamorphism, structures that indicate shortening and top-to-W ductile shearing, and ophiolites that obducted at the end of the orogeny when the MARA block accreted to the Iapetus margin of West Gondwana. Subduction from the Late Cambrian to Silurian caused the Famatinian orogeny and magmatic arc, preserved in a longitudinally continuous zone from the north to the south of the Sierras Pampeanas. The Famatinian back-arc is also preserved in a continuous zone and shows high T/low P metamorphism due to lithospheric thinning and shallow convection of the asthenosphere. The development of thick, mylonitic shear zones in the back-arc during the Oclóyic tectonic phase may be a result of the thermally-weakened middle crust accommodating most of the plate velocity when the Precordillera terrane accreted onto the western margin of the MARA block in the southern Sierras Pampeanas. These exotic terranes rifted from Laurentia and are now uplifted in the western Sierras Pampeanas. Minor Devonian overprint in the Sierras Pampeanas is attributed to the Achalian orogeny, which ended with the collision of the Chilenia terrane. It has been suggested that only the southern Sierras Pampeanas underwent terrane accretion since there is no evidence for it in the north. Apart from the lack of collision-related features, the north and south Sierras Pampeanas are similar, with the Famatinian arc and back-arc basin continuous from 22°–33° S (Rapela et al., 1998a).

4. Literature review of shear zone development and width

Localisation of strain during ductile deformation creates strongly deformed layers known as shear zones (Ramsay and Graham, 1970). Shear zones nucleate at sites of (i) pre-existing heterogeneities, either compositional (e.g., layering) or mechanical (faults, cracks, joints; inherited localization model; e.g., Pennacchioni and Mancktelow, 2007), (ii) weak, anastomosing micro-shear instabilities (widening model; e.g., Ingles et al., 1999), (iii) strain softening caused by grain size reduction and change of active deformation mechanisms and/or fluid ingress (dynamic localization model; Montési and Zuber, 2002, Jessell et al., 2005, Oliot et al., 2010), and (iv) shear heating (Regenauer-Lieb and Yuen, 1998, Regenauer-Lieb et al., 2006).

Shear zones are usually narrow relative to the width of the deforming region due to strain localization. Shear zone width may be optimised to minimise work (strain rate times stress; Vauchez et al., 2012), or may be a result of the combination of yield stress (a function of tem-

perature and depth), plate velocity, and strain rate which increases as the shear zone weakens at constant stress (Platt and Behr, 2011). Shear zone width also depends on the balance between shear heating (a function of strain rate) and heat diffusion away from the fault, modulated by the sensitivity of rock viscosity to temperatures (Regenauer-Lieb and Yuen, 1998). Regenauer-Lieb et al. (2012) demonstrated that the temperature of the lithosphere controlled the spatial distribution and width of shear zones, as well as how effectively deformation localized into them. Shear zone networks in hot, weak lithospheres are wider and less efficient at weakening the lithosphere when compared to networks in colder lithospheres. Consequently, shear zones are narrow in the upper crust where rocks are strong, and widen with depth as temperature increases and rocks become weaker. Shear zones in the middle to lower crust can be tens of kilometres wide but are usually of low strain intensity (Vauchez and Tommasi, 2003, Vauchez et al., 2007).

Strain localisation within shear zones evolves over time, as shear zones develop they may harden and thicken (type 1 of Means, 1995) or weaken further (type 2) due to further strain softening (e.g., White et al., 1980, Fliervoet et al., 1997, Kilian et al., 2011). Weakening in shear zones is a result of grain size decrease (Poirier, 1980), re-orientation of minerals to foliation parallel planes (White et al., 1980, Ji et al., 2004), reaction softening (e.g., Hippertt and Hongn, 1998, Jefferies et al., 2006, Oliot et al., 2010, Goncalves et al., 2012), and shear heating (Regenauer-Lieb et al., 2006). Weakening processes are related to fluid ingress into the shear zone which facilitates the retrogression of minerals and enhances recrystallization mechanisms (e.g. White et al., 1980, Stunitz and Gerald, 1993, Hippertt, 1998, O'Hara, 2007), particularly dissolution-precipitation (e.g., Sinha et al., 1986, Jefferies et al., 2006, O'Hara, 2007) and diffusive mass transfer (Hippertt, 1998, Hippertt and Hongn, 1998, Jefferies et al., 2006). Shear zone weakening allows the maintenance of a steady-state width, or causes narrowing as the strain rate increases (Platt and Behr, 2011). Alternatively, the strength of shear zones may increase due to strain hardening, which can be caused by the accumulation of dislocations, the growth of new, harder minerals (reaction hardening), dehydration of the shear zone, or changes in the deformation style of the rock (Hull, 1988, Passchier and Trouw, 2005, Groome et al., 2006, Johnson et al., 2011, Oliot et al., 2014). Strain hardening can cause the shear-zone interior to become stronger than the host rock, causing shearing to shift to the margin of the shear zone (Means, 1995). This process causes widening of the shear zone and, if repeated, can form apparently thick zones of high strain as the locus of deformation progressively moves outwards (e.g. Oliot et al., 2014, Finch et al., 2015).

Shear zones commonly show a strain gradient from low strain protomylonites at the edge, to high strain ultramylonites in the centre of the shear zone (e.g., Kilian et al., 2011). The degree of mylonitization is indicated by a progressive increase in the proportion of recrystallized matrix relative to porphyroclasts (Sibson, 1977). Ultramylonites, defined as rocks where more than 90% of the crystals are recrystallized (Sibson, 1977), are the ultimate product of mylonitisation. Ultramylonitic shear zones are commonly fluid conduits and show mass loss or gain in comparison to adjacent protomylonites and mylonites (e.g., Hippertt, 1998, Hippertt and Hongn, 1998, Jefferies et al., 2006). However, some ultramylonitic shear zones expel water, the fate

of water in shear zones is controlled by the pressure difference between the shear zone and the matrix, which depends on the angle between the shear zone and the shear direction (Mancktelow, 2002). Ultramylonites are usually synonymous with high strain. However, because they are defined by recrystallization of grains generally accompanied by the loss of porphyroclasts, they can form at lower strains when the protolith is fine grained with few porphyroclasts (Trouw et al., 2010) or when deformation is at high temperatures and feldspar porphyroclasts become as ductile as quartz (e.g., Hanmer et al., 1995, Tullis and Yund 1985).

Thick ultramylonitic shear zones are rare in the Earth's crust because in the upper crust strain typically localises to thin bands whereas in the lower crust strain is distributed over a wide area of lower strain (Vauchez et al., 2012). Despite these expectations, thick sequences of ultramylonites are occasionally reported. Ultramylonites 300–400 m thick are found in the shear zones related to the Pan-African orogeny and amalgamation of West Gondwana in NW Africa (Ferkous and Leblanc, 1995, Arthaud et al., 2008). Similarly, the Mulgandinnah shear zone in Western Australia contains a 500 m thick zone of ultramylonite which formed in response to accretion and formation of the Pilbara terrane (Zegers et al., 1998). The Corredoiras detachment in NW Spain also contains a 500 m wide section of ultramylonite and gneiss which accommodated at least 10 km of thrusting during Variscan plate convergence (Díaz García et al., 1999). The evolution of thick ultramylonitic shear zones and the role of shear zone widening in generating these thick layers has not previously been investigated. In chapters 2 and 3, this thesis examines strain localisation in a 1 km-thick ultramylonite and explores the role of water and heat diffusion in the progressive widening of shear zones.

References

Aceñolaza, F. G., Miller, H. and Toselli, A. J., 1988. The Puncoviscana Formation (Late Precambrian - Early Cambrian) - Sedimentology, tectonometamorphic history and age of the oldest rocks of NW Argentina. In: Lecture Notes in Earth Sciences, The Southern Central Andes (edited by Bahlburg, H., Breitkreuz, C. & Giese, P.) 17. Springer-Verlag, Berlin.

Aceñolaza, G., Bayetgoll, A., Nieva, S. and Aráoz, L., 2013. Environmental constraints of a Middle Ordovician trace fossil association from the Lina Formation (Puna of Jujuy province, NW Argentina). In: Second Latin American Symposium on Ichnology (edited by Bedatou, E., Sostillo, R. & Varela, J. A.), Universidad Nacional de La Pampa, 23.

Augustsson, C., Rüsing, T., Adams, C. J., Chmiel, H., Kocabayoğlu, M., Büld, M., Zimmermann, U., Berndt, J. and Kooijman, E., 2011. Detrital quartz and zircon combined: The production of mature sand with short transportation paths along the Cambrian west Gondwana margin northwestern Argentina. Journal of Sedimentary Research 81(4), 284-298.

Adams, C. J., Miller, H., Aceñolaza, F. G., Toselli, A. J. and Griffin, W. L., 2011. The Pacific Gondwana margin in the late Neoproterozoic–early Paleozoic: Detrital zircon U–Pb ages from metasediments in northwest Argentina reveal their maximum age, provenance and tectonic setting. Gondwana Research 19(1), 71-83.

Alasino, P. H., Casquet, C., Larrovere, M. A., Pankhurst, R., Galindo, C., Dahlquist, J., Baldo, E. and Rapela, C. W., 2014. The evolution of a mid-crustal thermal aureole at Cerro Toro, Sierra de Famatina, NW Argentina. Lithos 190-191, 154-172.

Aparicio González, P. A., Pimentel, M. M., Hauser, N. and Moya, M. C., 2014. U–Pb LA-ICP-MS geochronology of detrital zircon grains from low-grade metasedimentary rocks (Neoproterozoic – Cambrian) of the Mojotoro Range, northwest Argentina. Journal of South American Earth Sciences 49, 39-50.

Arthaud, M. H., Caby, R., Fuck, R. A., Dantas, E. L. and Parente, C. V., 2008. Geology of the northern Borborema Province, NE Brazil and its correlation with Nigeria, NW Africa. In: West Gondwana: Pre-Cenozoic correlations across the South Atlantic region (edited by Pankhurst, R., Trouw, R. A. J., Brito Neves, B. B. & de Wit, M. J.) 294. Geological Society of London, 49-67.

Bachman, G., Grauert, B., Kramm, U., Lork, A. and Miller, H., 1987. El magmatismo del Cambrico medio/Cambrico superior en el basamento del noroeste Argentino: investigaciones isotopicas y geocronologicas sobre los granitoides de los complejos intrusivos de Santa Rosa de Tastil y Canani. In: 10 Congreso Geologico Argentino, Actas, vol. 4, Tucuman, 125-127.

Bahlburg, H., 1990. The Ordovician basin in the Puna of NW Argentina and N Chile: Geodynamic evolution from back-arc to foreland basin. Geotektonische Forschungen 75, 1-107.

Bahlburg, H., 1991. The Ordovician back-arc to foreland successor basin in the Argentinian-Chilean Puna: tectono-sedimentary trends and sea-level changes. Special Publication, International Association of Sedimentologists 12, 465-484.

Bahlburg, H. and Furlong, K. P., 1996. Lithospheric modeling of the Ordovician foreland basin in the Puna of northwestern Argentina: on the influence of arc loading on foreland basin formation. Tectonophysics 259, 245-258.

Bahlburg, H. and Herve, F., 1997. Geodynamic evolution and tectonostratigraphic terranes of northwestern Argentina and nothern Chile. Geological Society of America Bulletin 109(7), 869-884.

Becchio, R. and Lucassen, F., 2002. Concordant titanite U-Pb ages of Cambrian to Silurian high

T metamorphism at the western edge of Gondwana (Southern Puna and western Sierras Pampeanas, Argentina, 26-29°). In: 5th International Symposium on Andean Geodynamics, Toulouse.

Bellos, L. I., Castro, A., Díaz-Alvarado, J. and Toselli, A., 2015. Multi-pulse cotectic evolution and in-situ fractionation of calc-alkaline tonalite-granodiorite rocks, Sierra de Velasco batholith, Famatinian belt, Argentina. Gondwana Research 27(1), 258-280.

Bercovici, D. and Ricard, Y., 2014. Plate tectonics, damage and inheritance. Nature 508(7497), 513-516.

Bock, B., Bahlburg, H., Worner, G. and Zimmermann, U., 2000. Tracing crustal evolution in the Southern Central Andes from Late Precambrian to Permian with Geochemical and Nd and Pb isotope data. The Journal of Geology 108, 515-535.

Büttner, S. H., Glodny, J., Lucassen, F., Wemmer, K., Erdmann, S., Handler, R. and Franz, G., 2005. Ordovician metamorphism and plutonism in the Sierra de Quilmes metamorphic complex: Implications for the tectonic setting of the northern Sierras Pampeanas (NW Argentina). Lithos 83(1-2), 143-181.

Caminos, R., 1979. Sierras Pampeanas Noroccidentales, Salta, Tucuman, Catamarca, La Rioja, San Juan. Academia Nacional de Ciencias de Cordoba, II Simposio de Geologia Regional Argentina 1, 225-291.

Carreras, J., 2013. Anastomosing network of shear zones across schists in Cap de Creus. Journal of Structural Geology 50, 5-6.

Casquet, C., Pankhurst, R. J., Rapela, C. W., Galindo, C., Fanning, C. M., Chiaradia, M., Baldo, E., González-Casado, J. M. and Dahlquist, J. A., 2008. The Mesoproterozoic Maz terrane in the Western Sierras Pampeanas, Argentina, equivalent to the Arequipa–Antofalla block of southern Peru? Implications for West Gondwana margin evolution. Gondwana Research 13(2), 163-175.

Castro de Machuca, B., Delpino, S., Previley, L., Mogessie, A. and Bjerg, E., 2012. Tectono-metamorphic evolution of a high- to medium-grade ductile deformed metagabbro/metadiorite from the Arenosa Creek Shear Zone, Western Sierras Pampeanas, Argentina. Journal of Structural Geology 42, 261-278.

Cawood, P. A., 2005. Terra Australis Orogen: Rodinia breakup and development of the Pacific and Iapetus margins of Gondwana during the Neoproterozoic and Paleozoic. Earth-Science Reviews 69(3-4), 249-279.

Coira, B., Kirschbaum, A., Hongn, F., Pérez, B. and Menegatti, N., 2009. Basic magmatism in northeastern Puna, Argentina: Chemical composition and tectonic setting in the Ordovician back-arc. Journal of South American Earth Sciences 28(4), 374-382.

Coira, B., Peréz, B., Flores, P., Kay, S. M., Woll, B. and Hanning, M., 1999. Magmatic sources and tectonic setting of Gondwana margin Ordovician magmas, northern Puna of Argentina and Chile. Geological Society of America Special Papers 336, 145-170.

Davis, J. S., Roeske, S. M., McClelland, W. C. and Kay, S. M., 2000. Mafic and ultramafic crustal fragments of the southwestern Precordillera terrane and their bearing on tectonic models of the early Paleozoic in western Argentina. Geology 28(2), 171-174.

de los Hoyos, C. R., Willner, A. P., Larrovere, M. A., Rossi, J. N., Toselli, A. J. and Basei, M. A. S., 2011. Tectonothermal evolution and exhumation history of the Paleozoic Proto-Andean Gondwana margin crust: The Famatinian Belt in NW Argentina. Gondwana Research 20(2–3), 309-324.

DeBari, S. M., 1994. Petrogenesis of the Fiambala gabbroic intrusion, Northwestern Argentina, a deep crustal syntectonic pluton in a continental magmatic arc. Journal of Petrology 35(3), 679-713.

Díaz García, F., Martínez Catalán, J. R., Arenas, R. and González Cuadra, P., 1999. Structural and kinematic analysis of the Carredoiras detachment: evidence for early Variscan syn-

convergent extension in the Ordenes Complex, NW Spain. International Journal of Earth Sciences 88, 337-351.

Do Campo, M., Nieto, F., Omarini, R. and Ostera, H., 1999. Neoproterozoic K-Ar ages for the metamorphism of the Puncoviscana formation, Northwestern Argentina. In: 2 Simposio Sudamericano de Geologia Isotopica Actas 1, V. Carlos Paz, Argentina, 48-53.

Drobe, M., de Luchi, M., Steenken, A., Wemmer, K., Naumann, R., Frei, R. and Siegesmund, S., 2011. Geodynamic evolution of the Eastern Sierras Pampeanas (Central Argentina) based on geochemical, Sm–Nd, Pb–Pb and SHRIMP data. International Journal of Earth Sciences 100(2), 631-657.

Ducea, M. N., Otamendi, J. E., Bergantz, G. W., Jianu, D. and Petrescu, L., 2015. The origin and petrologic evolution of the Ordovician Famatinian-Puna arc. In: Geodynamics of a Cordilleran Orogenic System: The Central Andes of Argentina and Northern Chile: Geological Society of America Memoir (edited by DeCelles, P. G., Ducea, M. N., Carrapa, B. & Kapp, P.) 212, 125-138.

Durand, F. R., 1996. La transicion Precambrico-Cambrico en el sur de Sudamerica. In: Early Paleozoic evolution in NW Gondwana (edited by Baldis, B. & Aceñolaza, F. G.) Universidad Nacional de Tucumán, Argentina 12, 195-205.

Escayola, M. P., van Staal, C. R. and Davis, W. J., 2011. The age and tectonic setting of the Puncoviscana Formation in northwestern Argentina: An accretionary complex related to Early Cambrian closure of the Puncoviscana Ocean and accretion of the Arequipa-Antofalla block. Journal of South American Earth Sciences 32, 438-459.

Ferkous, K. and Leblanc, M., 1995. Gold mineralisation in the West Hoggar shear zone, Algeria. Mineralium Deposita 30, 211-224.

Finch, M. A., Weinberg, R. F., Fuentes, M. G., Hasalova, P. and Becchio, R., 2015. One kilometre-thick ultramylonite, Sierra de Quilmes, Sierras Pampeanas, NW Argentina. Journal of Structural Geology 72, 33-54.

Fliervoet, T. F., White, S. H. and Drury, M. R., 1997. Evidence for dominant grain-boundary sliding deformation in greenschist - and amphibolite-grade polymineralic ultramylonites from the Redbank Deformed Zone, Central Australia. Journal of Structural Geology 19(12), 1495-1520.

Franz, G. and Lucassen, F., 2001. Comment on the paper "Puncoviscana folded belt in northwestern Argentina: testimony of Late Proterozoic Rodinia fragmentation and pre-Gondwana collisional episodes" by Omarini et al. International Journal of Earth Sciences 90, 890-893.

Goncalves, P., Oliot, E., Marquer, D. and Connolly, J. A. D., 2012. Role of chemical processes on shear zone formation: An example from the Grimsel metagranodiorite (Aar massif, Central Alps). Journal of Metamorphic Geology 30(7), 703-722.

Goodge, J. W., Williams, I. S. and Myrow, P., 2004. Provenance of Neoproterozoic and lower Paleozoic siliciclastic rocks of the central Ross orogen, Antarctica: Detrital record of rift-, passive-, and active-margin sedimentation. Geological Society of America Bulletin 116(9/10), 1253-1279.

Grissom, G. C., Debari, S. M. and Snee, L. W., 1998. Geology of the Sierra de Fiambala, northwestern Argentina: implications for Early Palaeozoic Andean tectonics. Geological Society, London, Special Publications 142(1), 297-323.

Groome, W. G., Johnson, S. E. and Koons, P. O., 2006. The effects of porphyroblast growth on the effective viscosity of metapelitic rocks: implications for the strength of the middle crust. Journal of Metamorphic Geology 24(5), 389-407.

Hauzenberger, C. A., Mogessie, A., Hoinkes, G., Felfernig, A., Bjerg, E. A., Kostadinoff, J., Delpino, S. and Dimieri, L., 2001. Metamorphic evolution of the Sierras de San Luis, Argentina: granulite facies metamorphism related to mafic intrusions. Mineralogy and Petrol-

ogy 71(1-2), 95-126.

Hippertt, J. F., 1998. Breakdown of feldspar, volume gain and lateral mass transfer during mylo-nitization of granitoid in a low metamorphic grade shear zone. Journal of Structural Geology 20(2-3), 175-193.

Hippertt, J. F. and Hongn, F. D., 1998. Deformation mechanisms in the mylonite/ultramylonite transition. Journal of Structural Geology 20(11), 1435-1448.

Hongn, F. D., Tubia, J. M., Aranguren, A., Vegas, N., Mon, R. and Dunning, G. R., 2010. Magmatism coeval with lower Paleozoic shelf basins in NW-Argentina (Tastil batholith): Constraints on current stratigraphic and tectonic interpretations. Journal of South American Earth Sciences 29(2), 289-305.

Hongn, F. D., Tubia, J. M., Esteban, J. J., Aranguren, A., Vegas, N., Sergeev, S., Larionov, A. and Basei, M., 2014. The Sierra de Cachi (Salta, NW Argentina): geological evidence about a Famatinian retro-arc at mid crustal levels. Journal of Iberian Geology 40(2), 225-240.

Hull, J., 1988. Thickness-displacement relationships for deformation zones. Journal of Structural Geology 10(4), 431-435.

Hyndman, R. D., Currie, C. A. and Mazzotti, S. P., 2005. Subduction zone backarcs, mobile belts, and orogenic heat. GSA today 15(2), 4-10.

Iannizzotto, N. F., Rapela, C. W., Baldo, E. G. A., Galindo, C., Fanning, C. M. and Pankhurst, R. J., 2013. The Sierra Norte-Ambargasta batholith: Late Ediacaran–Early Cambrian magmatism associated with Pampean transpressional tectonics. Journal of South American Earth Sciences 42, 127-143.

Ingles, J., Lamouroux, C., Soula, J.-C., Guerrero, N. and Debat, P., 1999. Nucleation of ductile shear zones in a granodiorite under greenschist facies conditions, Neouvielle massif, Pyrenees, France. Journal of Structural Geology 21(5), 555-576.

Ireland, T. R., Flottmann, T., Fanning, C. M., Gibson, G. M. and Preiss, W. V., 1998. Development of the early Paleozoic Pacific margin of Gondwana from detrital-zircon ages across the Delamerian orogen. Geology 26(3), 243-246.

Isaacson, P. E., Antelo, B. and Boucot, A. J., 1976. Implication of a Llandovery (Early Silurian) brachiopod fauna from Salta province, Argentina. Journal of Palaeontology 50, 1103-1112.

Jefferies, S. P., Holdsworth, R. E., Wibberley, C. A. J., Shimamoto, T., Spiers, C. J., Niemeijer, A. R. and Lloyd, G. E., 2006. The nature and importance of phyllonite development in crustal-scale fault cores: an example from the Median Tectonic Line, Japan. Journal of Structural Geology 28(2), 220-235.

Jessell, M. W., Siebert, E., Bons, P. D., Evans, L. and Piazolo, S., 2005. A new type of numerical experiment on the spatial and temporal patterns of localization of deformation in a material with a coupling of grain size and rheology. Earth and Planetary Science Letters 239, 309-326.

Jezek, P., Willner, A. P., Acenolaza, F. G. and Miller, H., 1985. The Puncoviscana trough - a large basin of Late Precambrian to Early Cambrian age on the Pacific edge of the Brazilian shield. Geologische Rundschau 74(3), 573-584.

Ji, S., Jiang, Z., Rybacki, E., Wirth, R., Prior, D. and Xia, B., 2004. Strain softening and microstructural evolution of anorthite aggregates and quartz-anorthite layered composites deformed in torsion. Earth and Planetary Science Letters 222(2), 377-390.

Johnson, S. E., Jin, Z.-H., Naus-Thijssen, F. M. J. and Koons, P. O., 2011. Coupled deformation and metamorphism in the roof of a tabular midcrustal igneous complex. GSA Bulletin 123(5-6), 1016-1032.

Jordan, T. E. and Allmendinger, R. W., 1986. The Sierras Pampeanas of Argentina; a modern analogue of Rocky Mountain foreland deformation. American Journal of Science 286(10),

737-764.

Keppie, J. D. and Bahlburg, H., 1999. Puncoviscana Formation of northwestern and central Argentina: Passive margin or foreland basin deposit? Geological Society of America Special Papers 336, 139-143.

Kilian, R., Heilbronner, R. and Stunitz, H., 2011. Quartz grain size reduction in a granitoid rock and the transition from dislocation to diffusion creep. Journal of Structural Geology 33(8), 1265-1284.

Kumpa, M. and Sanchez, M. C., 1988. Geology and sedimentology of the Cambrian Grupo Mesón (NW Argentina). In: The Southern Central Andes (edited by Bahlburg, H., Breitkreuz, C. & Giese, P.). Lecture Notes in Earth Sciences 17. Springer Berlin Heidelberg, 39-53.

Larrovere, M. A., de los Hoyos, C. R., Toselli, A. J., Rossi, J. N., Basei, M. A. S. and Belmar, M. E., 2011. High T/P evolution and metamorphic ages of the migmatitic basement of northern Sierras Pampeanas, Argentina: Characterization of a mid-crustal segment of the Famatinian belt. Journal of South American Earth Sciences 31(2-3), 279-297.

López de Luchi, M. G., 1996. Enclaves en un batolito postectónico: petrología de los enclaves microgranulares del batolito de Renca. Revista de la Asociación Geológica Argentina 51(2), 131-146.

Lucassen, F., Becchio, R. and Franz, G., 2011. The Early Palaeozoic high-grade metamorphism at the active continental margin of West Gondwana in the Andes (NW Argentina/N Chile). International Journal of Earth Sciences 100(2), 445-463.

Lucassen, F., Becchio, R., Wilke, H. G., Franz, G., Thirlwall, M. F., Viramonte, J. and Wemmer, K., 2000. Proterozoic-Paleozoic development of the basement of the Central Andes (18-26°S)-a mobile belt of the South American craton. Journal of South American Earth Sciences 13, 697-715.

Mancktelow, N. S., 2002. Finite-element modelling of shear zone development in viscoelastic materials and its implications for localisation of partial melting. Journal of Structural Geology 24(6–7), 1045-1053.

Massonne, H.-J., Dristas, J. A. and Martínez, J. C., 2012. Metamorphic evolution of the Río de la Plata Craton in the Cinco Cerros area, Buenos Aires Province, Argentina. Journal of South American Earth Sciences 38, 57-70.

Means, W. D., 1984. Shear zones of types I and II and their significance for reconstruction of rock history. Geological Society of America Abstracts with Programs 16, 50.

Means, W. D., 1995. Shear zones and rock history. Tectonophysics 247(1–4), 157-160.

Miller, H., Adams, C., Aceñolaza, F. and Toselli, A., 2011. Evolution of exhumation and erosion in western West Gondwanaland as recorded by detrital zircons of late Neoproterozoic and Cambrian sedimentary rocks of NW and Central Argentina. International Journal of Earth Sciences 100(2-3), 619-629.

Mon, R. and Hongn, F. D., 1987. Estructura del Ordovicico de la Puna. Revista de la Asociacion Geologica Argentina 42, 31-38.

Mon, R. and Hongn, F., 1991. The structure of the Precambrian and Lower Paleozoic basement of the Central Andes between 22° and 32°S. Lat. Geologische Rundschau 80(3), 745-758.

Montési, L. G. J. and Zuber, M. T., 2002. A unified description of localization for application to large-scale tectonics. Journal of Geophysical Research 107(B3), 1-21.

Moya, M. C., 1988. Lower Ordovician in the southern part of the Argentine Eastern Cordillera. In: The Southern Central Andes (edited by Bahlburg, H., Breitkreuz, C. & Giese, P.). Lecture Notes in Earth Sciences 17. Springer, Berlin Heidelberg, 55-69.

Northrup, C. J., Simpson, C. and Hodges, K. V., 1998. Pseudotachylite in fault zones of the

Sierras de Córdoba, Argentina; petrogenesis and ^{40}Ar/^{39}Ar geochronology. In: Geological Society of America, Abstracts with Programs 30(7): 325, San Francisco.

O'Hara, K., 2007. Reaction weakening and emplacement of crystalline thrusts: Diffusion control on reaction rate and strain rate. Journal of Structural Geology 29(8), 1301-1314.

Oliot, E., Goncalves, P. and Marquer, D., 2010. Role of plagioclase and reaction softening in a metagranite shear zone at mid-crustal conditions (Gotthard Massif, Swiss Central Alps). Journal of Metamorphic Geology 28(8), 849-871.

Oliot, E., Goncalves, P., Schulmann, K., Marquer, D. and Lexa, O., 2014. Mid-crustal shear zone formation in granitic rocks: Constraints from quantitative textural and crystallographic preferred orientations analyses. Tectonophysics 612-613, 63-80.

Omarini, R. H., 1983. Caracterización litológica diferenciación y génesis de la Formación Puncoviscana entre el Valle de Lerma y la Faja Eruptiva de la Puna. University of Salta, 1-202.

Omarini, R. H., Sureda, R. J., Gotze, H.-J., Seilacher, A. and Pfluger, F., 1999. Puncoviscana folded belt in northwestern Argentina: testimony of Late Proterozoic Rodinia fragmentation and pre-Gondwana collisional episodes. International Journal of Earth Science 88, 76-97.

Otamendi, J. E., Tibaldi, A. M., Vujovich, G. I. and Viñao, G. A., 2008. Metamorphic evolution of migmatites from the deep Famatinian arc crust exposed in Sierras Valle Fértil–La Huerta, San Juan, Argentina. Journal of South American Earth Sciences 25(3), 313-335.

Pankhurst, R. J., Ramos, A. and Linares, E., 2003. Antiquity of the Río de la Plata craton in Tandilia, southern Buenos Aires province, Argentina. Journal of South American Earth Sciences 16(1), 5-13.

Pankhurst, R. J., Rapela, C. W. and Fanning, C. M., 2000. Age and origin of coeval TTG, I- and S-type granites in the Famatinian belt of NW Argentina. Earth and Environmental Science Transactions of the Royal Society of Edinburgh 91(1-2), 151-168.

Pankhurst, R. J., Rapela, C. W., Saavedra, J., Baldo, E., Dahlquist, J., Pascua, I. and Fanning, C. M., 1998. The Famatinian magmatic arc in the central Sierras Pampeanas: an Early to Mid-Ordovician continental arc on the Gondwana margin. Geological Society, London, Special Publications 142(1), 343-367.

Passchier, C. W. and Trouw, R. A. J., 2005. Microtectonics. Springer-Verlag Berlin, Heidelberg.

Pennacchioni, G. and Mancktelow, N. S., 2007. Nucleation and initial growth of a shear zone network within compositionally and structurally heterogeneous granitoids under amphibolite facies conditions. Journal of Structural Geology 29(11), 1757-1780.

Piñán-Llamas, A., 2007. The early Paleozoic evolution of the paleo-Pacific Gondwana margin: A structural, petrographic, and geochemical study in the Puncoviscana Formation., Boston University.

Piñán-Llamas, A. and Simpson, C., 2006. Deformation of Gondwana margin turbidites during the Pampean orogeny, north-central Argentina. Geological Society of America Bulletin 118(9-10), 1270-1279.

Piñán-Llamas, A. and Simpson, C., 2009. Primary structure influence on compositional banding in psammites: Examples from the Puncoviscana Formation, north-central Argentina. Journal of Structural Geology 31(1), 55-71.

Pinotti, L., Tubía, J. M., D'Eramo, F., Vegas, N., Sato, A. M., Coniglio, J. and Aranguren, A., 2006. Structural interplay between plutons during the construction of a batholith (Cerro Aspero batholith, Sierras de Córdoba, Argentina). Journal of Structural Geology 28(5), 834-849.

Platt, J. P. and Behr, W. M., 2011. Lithospheric shear zones as constant stress experiments. Geology 39(2), 127-130.

Poirier, J. P., 1980. Shear localization and shear instability in materials in the ductile field. Journal of Structural Geology 2(1–2), 135-142.

Ramos, V. A., 1988. Late-Proterozoic-Early Paleozoic of South America: A collisional history. Episodes 11, 168-175.

Ramos, V. A., 2008. The basement of the Central Andes: the Arequipa and related terranes. Annual Review of Earth and Planetary Sciences 36, 289-324.

Ramos, V. A., Cristallini, E. O. and Pérez, D. J., 2002. The Pampean flat-slab of the Central Andes. Journal of South American Earth Sciences 15(1), 59-78.

Ramos, V. A., Dallmeyer, R. D. and Vujovich, G., 1998. Time constraints on the Early Palaeozoic docking of the Precordillera, central Argentina. Geological Society, London, Special Publications 142(1), 143-158.

Ramos, V. A., Jordan, T. E., Allmendinger, R. W., Mpodozis, C., Kay, S. M., Cortes, J. M. and Palma, M., 1986. Paleozoic terranes of the Central Argentina-Chilean Andes. Tectonics 5(6), 855-880.

Ramsay, J. G. and Graham, R. H., 1970. Strain variation in shear belts. Canadian Journal of Earth Science 7, 786 - 813.

Rapela, C., Toselli, A., Heaman, L. and Saavedra, J., 1990. Granite plutonism of the Sierras Pampeanas: An inner cordilleran Paleozoic arc in the Southern Andes. Geological Society of America Bulletin Special Papers 241, 77-91.

Rapela, C. W., Pankhurst, R. J., Casquet, C., Baldo, E., Galindo, C., Fanning, C. M. and Dahlquist, J. M., 2010. The Western Sierras Pampeanas: Protracted Grenville-age history (1330–1030 Ma) of intra-oceanic arcs, subduction–accretion at continental-edge and AMCG intraplate magmatism. Journal of South American Earth Sciences 29(1), 105-127.

Rapela, C. W., Pankhurst, R. J., Casquet, C., Baldo, E., Saavedra, J. and Galindo, C., 1998a. Early evolution of the Proto-Andean margin of South America. Geology 26(8), 707-710.

Rapela, C. W., Pankhurst, R. J., Casquet, C., Baldo, E., Saavedra, J., Galindo, C. and Fanning, C. M., 1998b. The Pampean Orogeny of the southern proto-Andes: Cambrian continental collision in the Sierras de Cordoba. Geological Society, London, Special Publications 142(1), 181-217.

Rapela, C. W., Pankhurst, R. J., Casquet, C., Fanning, C. M., Baldo, E. G., González-Casado, J. M., Galindo, C. and Dahlquist, J., 2007. The Río de la Plata craton and the assembly of SW Gondwana. Earth-Science Reviews 83(1–2), 49-82.

Rapela, C. W., Verdecchia, S. O., Casquet, C., Pankhurst, R. J., Baldo, E. G., Galindo, C., Murra, J. A., Dahlquist, J. A. and Fanning, C. M., 2015. Identifying Laurentian and SW Gondwana sources in the Neoproterozoic to Early Paleozoic metasedimentary rocks of the Sierras Pampeanas: Paleogeographic and tectonic implications. Gondwana Research in press.

Regenauer-Lieb, K., Weinberg, R. F. and Rosenbaum, G., 2006. The effect of energy feedbacks on continental strength. Nature 442(7098), 67-70.

Regenauer-Lieb, K., Weinberg, R. F. and Rosenbaum, G., 2012. The role of elastic stored energy in controlling the long term rheological behaviour of the lithosphere. Journal of Geodynamics 55, 66-75.

Regenauer-Lieb, K. and Yuen, D. A., 1998. Rapid conversion of elastic energy into plastic shear heating during incipient necking of the lithosphere. Geophysical Research Letters 25(14), 2737-2740.

Regenauer-Lieb, K. and Yuen, D. A., 2003. Modeling shear zones in geological and planetary sciences: solid- and fluid-thermal–mechanical approaches. Earth-Science Reviews 63(3–4), 295-349.

Saavedra, J., Toselli, A., Rossi, J., Pellitero, E. and Durand, F., 1998. The Early Palaeozoic magmatic record of the Famatina System: a review. Geological Society, London, Special Publications 142(1), 283-295.

Schwartz, J. J., Gromet, L. P. and Miró, R., 2008. Timing and duration of the calc-alkaline arc of the Pampean Orogeny: Implications for the Late Neoproterozoic to Cambrian evolution of Western Gondwana. The Journal of Geology 116(1), 39-61.

Sibson, R. H., 1977. Fault rocks and fault mechanisms. Journal of the Geological Society of London 133, 191-213.

Siegesmund, S., Steenken, A., López de Luchi, M. G., Wemmer, K., Hoffmann, A. and Mosch, S., 2004. The Las Chacras-Potrerillos batholith (Pampean Ranges, Argentina): structural evidence, emplacement and timing of the intrusion. International Journal of Earth Sciences 93(1), 23-43.

Sinha, A. K., Hewitt, D. A. and Rimstidt, J. D., 1986. Fluid interaction and element mobility in the development of ultramylonites. Geology 14, 883-886.

Simpson, C., Law, R. D., Gromet, L. P., Miro, R. and Northrup, C. J., 2003. Paleozoic deformation in the Sierras de Cordoba and Sierra de Las Minas, eastern Sierras Pampeanas, Argentina. Journal of South American Earth Sciences 15(7), 749-764.

Sims, J. P., Ireland, T. R., Camacho, A., Lyons, P., Pieters, P. E., Skirrow, R. G., Stuart-Smith, P. G. and Miro, R., 1998. U-Pb, Th-Pb and Ar-Ar geochronology from the southern Sierras Pampeanas, Argentina: implications for the Palaeozoic tectonic evolution of the western Gondwana margin. Geological Society, London, Special Publications 142(1), 259-281.

Steenken, A., López de Luchi, M., Martínez Dopico, C., Drobe, M., Wemmer, K. and Siegesmund, S., 2011. The Neoproterozoic-early Paleozoic metamorphic and magmatic evolution of the Eastern Sierras Pampeanas: an overview. International Journal of Earth Sciences 100(2), 465-488.

Stunitz, H. and Gerald, J. D. F., 1993. Deformation of granitoids at low metamorphic grade. II: Granular flow in albite-rich mylonites. Tectonophysics 221(3-4), 299-324.

Thomas, W. A. and Astini, R. A., 2003. Ordovician accretion of the Argentine Precordillera terrane to Gondwana: a review. Journal of South American Earth Sciences 16(1), 67-79.

Thomas, W. A., Tucker, R. D., Astini, R. A. and Denison, R. E., 2012. Ages of pre-rift basement and synrift rocks along the conjugate rift and transform margins of the Argentine Precordillera and Laurentia. Geosphere 8(6), 1366-1383.

Tibaldi, A. M., Otamendi, J. E., Cristofolini, E. A., Baliani, I., Walker Jr, B. A. and Bergantz, G. W., 2013. Reconstruction of the Early Ordovician Famatinian arc through thermobarometry in lower and middle crustal exposures, Sierra de Valle Fértil, Argentina. Tectonophysics 589, 151-166.

Toselli, A., Rossi De Toselli, J. N. and Rapela, C. W., 1978. El basamento metamorfico de la Sierra de Quilmes, Republica Argentina. Revista de la Asociación Geológica Argentina 33(2), 105-121.

Turner, J. C., 1960. Estratigrafia de la Sierra de Santa Victoria y adyacencias. Boletin de la Academia Nacional de Ciencias, Cordoba 41(2), 163-206.

van der Lee, S., James, D. and Silver, P., 2001. Upper mantle S velocity structure of central and western South America. Journal of Geophysical Research: Solid Earth 106(B12), 30821-30834.

van Staal, C. R. and Hatcher, J. R. D., 2010. Global setting of Ordovician orogenesis. Geological Society of America Special Papers 466, 1-11.

van Staal, C. R., Vujovich, G. I., Currie, K. L. and Naipauer, M., 2011. An Alpine-style Ordovician collision complex in the Sierra de Pie de Palo, Argentina: Record of subduction of Cuyania beneath the Famatina arc. Journal of Structural Geology 33(3), 343-361.

Varela, R., Basei, M. S., González, P., Sato, A., Naipauer, M., Campos Neto, M., Cingolani, C. and Meira, V., 2011. Accretion of Grenvillian terranes to the southwestern border of the Río de la Plata craton, western Argentina. International Journal of Earth Sciences 100(2-3), 243-272.

Vauchez, A., Egydio-Silva, M., Babinski, M., Tommasi, A., Uhlein, A. and Liu, D., 2007. Deformation of a pervasively molten middle crust: insights from the Neoproterozoic Ribeira-Araçuaí orogen (SE Brazil). Terra Nova 19(4), 278-286.

Vauchez, A. and Tommasi, A., 2003. Wrench faults down to the asthenosphere: geological and geophysical evidence and thermomechanical effects. Geological Society, London, Special Publications 210(1), 15-34.

Vauchez, A., Tommasi, A. and Mainprice, D., 2012. Faults (shear zones) in the Earth's mantle. Tectonophysics 558-559, 1-27.

Vujovich, G. I., van Staal, C. R. and Davis, W., 2004. Age constraints on the tectonic evolution and provenance of the Pie de Palo Complex, Cuyania Composite Terrane, and the Famatinian Orogeny in the Sierra de Pie de Palo, San Juan, Argentina. Gondwana Research 7(4), 1041-1056.

Wegmann, M. I., Riller, U., Hongn, F. D., Glodny, J. and Oncken, O., 2008. Age and kinematics of ductile deformation in the Cerro Durazno area, NW Argentina: Significance for orogenic processes operating at the western margin of Gondwana during Ordovician-Silurian times. Journal of South American Earth Sciences 26(1), 78-90.

White, S. H., Burrows, S. E., Carreras, J., Shaw, N. D. and Humphreys, F. J., 1980. On mylonites in ductile shear zones. Journal of Structural Geology 2(1-2), 175-187.

Zegers, T. E., de Keijzer, M., Passchier, C. W. and White, S. H., 1998. The Mulgandinnah shear zone; an Archean crustal scale strike-slip zone, eastern Pilbara, Western Australia. Precambrian Research 88, 233-247.

Zhong, S. and Gurnis, M., 1996. Interaction of weak faults and non-newtonian rheology produces plate tectonics in a 3D model of mantle flow. Nature 383(6597), 245-247.

Zimmerman, U., Luna Tula, G., Marchioli, A., Narvaez, G., Olima, H. and Ramirez, A., 2002. Analisis de procedencia de la Formacion Falda Cienaga (Ordovicico Medio, Puna Argentina) por petrografia sedimentaria, elementos trazas e isotopia de Nd. Revista de la Asociación Argentina de Sedimentologia 9(2), 165-188.

Zimmermann, U., 2005. Provenance studies of very low- to low-grade metasedimentary rocks of the Puncoviscana complex, northwest Argentina. Geological Society, London, Special Publications 246(1), 381-416.

Zimmermann, U. and Bahlburg, H., 2003. Provenance analysis and tectonic setting of the Ordovician clastic deposits in the southern Puna Basin, NW Argentina. Sedimentology 50, 1079-1104.

Chapter 2

One kilometre-thick ultramylonite, Sierra de Quilmes, Sierras Pampeanas, NW Argentina

M.A. Finch[1], R.F. Weinberg[1], M. G. Fuentes[2], P. Hasalová[1,3], R. Becchio[2]

[1]School of Earth, Atmosphere and Enivronment, Monash University, Clayton, Victoria, 3800, Australia

[2]Instituto Geonorte, National University of Salta, INENCO-CONICET, Av. Bolivia, 5150, 4400 Salta, Argentina

[3]Centre for Lithospheric Research, Czech Geological Survey, Klárov 3, 118 21 Prague 1, Czech Republic

Previous page: Delta clast in an ultramylonitic granitic diatexite from the El Pichao shear zone, Sierra de Quilmes

Monash University

Declaration for Thesis Chapter 2

Declaration by candidate

In the case of Chapter 2, the nature and extent of my contribution to the work was the following:

Nature of contribution	Extent of contribution (%)
Fieldwork, structural and microstructural analysis, geochemical analysis, preparation of the manuscript	87.5 %

The following co-authors contributed to the work. If co-authors are students at Monash University, the extent of their contribution in percentage terms must be stated:

Name	Nature of contribution
R. F. Weinberg	Supervisory role
M. G. Fuentes	Assistance with field work
P. Hasalová	Supervisory role
R. Becchio	Assistance with field work

The undersigned hereby certify that the above declaration correctly reflects the nature and extent of the candidate's and co-authors' contributions to this work*.

Candidate's Signature   **Date**

Main Supervisor's Signature   **Date**

One kilometre-thick ultramylonite, Sierra de Quilmes, Sierras Pampeanas, NW Argentina

M.A. Finch [a, *], R.F. Weinberg [a], M.G. Fuentes [b], P. Hasalová [a, c], R. Becchio [b]

[a] School of Earth, Atmosphere and Environment, Monash University, Clayton, VIC 3800, Australia
[b] Instituto Geonorte, National University of Salta, INENCO-CONICET, Av. Bolivia 5150, 4400 Salta, Argentina
[c] Centre for Lithospheric Research, Czech Geological Survey, Klárov 3, 118 21 Prague 1, Czech Republic

ARTICLE INFO

ABSTRACT

We describe a 1 km-thick ultramylonite forming the high strain base of the >3.5 km-thick El Pichao shear zone in the Sierra de Quilmes. This shear zone thrusted granulite facies migmatites onto amphibolite facies rocks during the 470 Ma Famatinian orogeny. Strain grades upwards from ultramylonites to weakly sheared migmatites across the 3.5 km-zone and the mylonitic rocks define a geochemical field narrower than the protolith, suggesting they underwent mixing and homogenization through shearing. Ultramylonites this thick are uncommon. The width of a shear zone, in the absence of significant compositional rheological contrasts controlling strain localization, is controlled by the balance between shear heat generation and diffusion. Under typical crustal conditions a strain rate of 10^{-12} s^{-1} is required to form a 1 km-thick ultramylonite, and this is achieved when large movement velocities are imposed across the shear zone. We postulate that the El Pichao shear zone and its thick ultramylonite accommodated a significant fraction of convergence velocities driving the orogeny, and that the wide mylonitic shear zones characteristic of the Cambrian—Ordovician deformation of the Sierras Pampeanas result from the convergent movement being taken up by only a few active major shear zones.

1. Introduction

Mylonitic shear zones are localized zones of high strain developed during ductile deformation. Shear zones nucleate at sites of (i) pre-existing heterogeneities, either compositional (e.g. layering) or mechanical (faults, cracks, joints; inherited localization model; e.g. Pennacchioni and Mancktelow, 2007), (ii) weak, anastomosing micro-shear instabilities (widening model; e.g. Ingles et al., 1999), (iii) strain softening caused by grain size reduction and change of active deformation mechanisms and/or fluid ingress (dynamic localization model; Montési and Zuber, 2002; Jessell et al., 2005; Oliot et al., 2010), and (iv) higher shear heating (Regenauer-Lieb and Yuen, 1998; Regenauer-Lieb et al., 2006). After nucleation, mylonitic shear zones may thicken if the shear zone hardens and it becomes easier to deform its margins (type 1 of Means, 1995). Shear zones may also weaken further (type 2) due to strain softening (e.g. White et al., 1980; Fliervoet et al., 1997; Kilian et al., 2011) which is a result of the development of crystallographic preferred orientation (White et al., 1980; Ji et al., 2004), reaction softening (e.g. Hippertt and Hongn, 1998; Jefferies et al., 2006; Oliot et al., 2010; Goncalves et al., 2012), and shear heating (Regenauer-Lieb et al., 2006). Weakening processes are related to fluid ingress into the shear zone which facilitates the retrogression of minerals and enhances recrystallization mechanisms (e.g. White et al., 1980; Stunitz and Gerald, 1993; Hippertt, 1998; O'Hara, 2007), particularly dissolution—precipitation (e.g. Sinha et al., 1986; Jefferies et al., 2006; O'Hara, 2007) and diffusive mass transfer (Hippertt, 1998; Hippertt and Hongn, 1998; Jefferies et al., 2006).

Shear zones are usually narrow relative to the width of the deforming region due to strain localization. It has been argued that shear zone width relates to the combination of yield stress (a function of temperature and depth), plate velocity, and strain rate, which increases as the shear zone weakens at constant stress (Platt and Behr, 2011). However, Vauchez et al. (2012) determined that these variables are not independent because strain rate determines the yield stress of rock and strain rate itself depends on the width of the shear zone. Instead, they proposed that the thickness of the shear zone is optimised to minimise work (strain rate times stress). Shear zones are narrow in the upper crust where rocks are strong, and widen with depth as temperature increases and rocks become

weaker. Indeed, it has been shown that in the middle to lower crust shear zones can be tens of kilometres wide with a concomitant decrease in strain intensity (Vauchez and Tommasi, 2003; Vauchez et al., 2007).

In a homogeneous rock mass, shear zone width depends on the balance between shear heating (a function of strain rate) and heat diffusion away from the fault, modulated by the sensitivity of rock viscosity to temperature (Regenauer-Lieb and Yuen, 1998). Both the strain rate and the stress distribution in shear zones can be variable through time and space due to the contemporaneous evolution of a set of shear zones that together accommodate lithospheric straining, as well as to the role of storage and release of elastic energy (Regenauer-Lieb et al., 2006, 2012). Regenauer-Lieb et al. (2012), investigating the strength of the lithosphere showed how it weakens considerably as a network of shear zones develops to accommodate deformation. They showed that the spatial distribution and width of shear zones, as well as how effectively deformation is localized into them, depend on whether the lithosphere was initially hot or cold. Shear zone networks in hot, weak lithospheres are wider and less efficient at weakening the lithosphere when compared to networks in colder lithospheres. The net effect is that the strength of hot and cold lithospheres tends to converge as the shear zone network matures.

In hot but sub-solidus conditions, mylonites develop readily because of the lack of rheological bimodality between feldspar and quartz (e.g. Tullis and Yund, 1985; Hanmer et al., 1995) so that both minerals recrystallize without development of feldspar porphyroclasts (Hanmer et al., 1995). Cases such as these may be identified by the absence of strain gradient at the margins of the mylonitic zone (Hanmer et al., 1995). In contrast, lower temperature ultramylonites formed at greenschist or amphibolite facies are a result of strong strain localization and most commonly occur as cm-sized bands within mylonitic and protomylonitic shear zones (Whitmeyer and Simpson, 2003).

Shear zones commonly show a strain gradient from low strain protomylonites at the edge, to high strain ultramylonites in the centre of the shear zone (e.g. Kilian et al., 2011). The degree of mylonitization is indicated by a progressive increase in the proportion of recrystallized matrix relative to porphyroclasts (Sibson, 1977). Ultramylonites, defined as rocks where more than 90% of the crystals are recrystallized (Sibson, 1977), are the ultimate product of mylonitization. Ultramylonites can be relatively coarse-grained at high temperatures, and grain size decreases to very fine at greenschist facies (Trouw et al., 2010). Ultramylonitic shear zones are commonly fluid conduits and show mass loss or gain in comparison to adjacent protomylonites and mylonites (e.g. Hippertt, 1998; Hippertt and Hongn, 1998; Jefferies et al., 2006). They are commonly enriched in phyllosilicates (mica and chlorite at low temperatures) due to mineral hydration (Hippertt and Hongn, 1998; O'Hara, 2007) and any porphyroclasts that remain are rounded from shear-induced erosion and recrystallization during rotation (e.g. Hippertt and Hongn, 1998; Griera et al., 2011). In contrast to protomylonites and mylonites, many ultramylonites contain few quartz ribbons and lack compositional layering due to homogenization of the matrix and mixing of the different phases (e.g. Fliervoet et al., 1997; Kanagawa et al., 2008; Kilian et al., 2011). This is a result of grain boundary sliding accommodated by diffusion creep (e.g. Tullis et al., 1982, Garlick and Gromet, 2004) accompanied in some cases by dissolution–precipitation (Kilian et al., 2011). Although rarer, layered ultramylonites can develop if there is high ductility contrast between layers which causes strain to partition into the weakest layer (Ishii et al., 2007). Ultramylonites at amphibolite to greenschist facies commonly have a fine-grained, dark-grey to green or black matrix and consist dominantly of quartz, feldspar, and biotite with fewer than 10% feldspar

porphyroclasts (e.g. Sinha et al., 1986; Jefferies et al., 2006; Ishii et al., 2007). Ultramylonites are usually synonymous with high strain. However, because they are defined by recrystallization of grains generally accompanied by the loss of porphyroclasts, they can form at lower strains when the protolith is fine-grained with few porphyroclasts (Trouw et al., 2010) or when deformation is at high temperatures and feldspar porphyroclasts become as ductile as quartz (e.g. Tullis and Yund, 1985; Hammer et al., 1995).

Thick ultramylonitic shear zones are rare in the Earth's crust because in the upper crust strain typically localises to thin bands, whereas in the lower crust, strain is distributed over a wide area of lower strain. Despite these expectations, thick sequences of ultramylonites are occasionally reported. Ultramylonites 300–400 m thick are found in the shear zones related to the Pan-African orogeny and amalgamation of West Gondwana in NW Africa (Ferkous and Leblanc, 1995; Arthaud et al., 2008). Similarly, the Mulgandinnah shear zone in Western Australia contains a 500 m-thick zone of ultramylonite which formed in response to accretion and formation of the Pilbara terrane (Zegers et al., 1998). The Corredoiras detachment in NW Spain also contains a 500 m-wide section of ultramylonite and mylonite which accommodated at least 10 km of thrusting during Variscan plate convergence (Díaz García et al., 1999). Where they occur, thick ultramylonites are related to major tectonic boundaries. This paper describes the nature of a very thick ultramylonite of the El Pichao shear zone in the Sierra de Quilmes, part of the Sierras Pampeanas mountain range in NW Argentina.

In this paper we follow Sibson's (1977) classification, with protomylonites consisting <50% recrystallized matrix, mylonites consisting of between 50 and 90% recrystallized matrix, and ultramylonites consisting of >90% recrystallized matrix. We use 'mylonitic rocks' as a collective term referring to rocks ranging from ultramylonites to protomylonites and the term 'mylonite' according to Sibson's definition.

2. Geological setting of the Sierra de Quilmes

The Sierras Pampeanas were exhumed in the foreland of the Andean orogen (Fig. 1; Jordan and Allmendinger, 1986; Rapela et al., 1998a) and dominantly consist of metamorphosed rocks of the Puncoviscana formation (Turner, 1960). This formation is a turbidite sequence that consists of sediments eroded from the southwest Gondwana craton (Acenolaza et al., 1988; Schwartz and Gromet, 2004) and deposited on the palaeo-Pacific margin of Gondwana (e.g. Jezek et al., 1985). It was deposited between 600 and 530 Ma (Rapela et al., 1998b; Sims et al., 1998; Schwartz and Gromet, 2004), although the maximum age is unknown because the base of the formation is nowhere seen (Jezek et al., 1985). It outcrops over an area of 1200 km × 300 km from south Bolivia to central Argentina (Fig. 1a; Jezek et al., 1985).

During the Palaeozoic the Puncoviscana formation was metamorphosed and deformed during at least two overlapping tectono-thermal episodes on the paleo-Pacific margin of Gondwana (Acenolaza et al., 1988). The first event was in the Early to Middle Cambrian (535–515 Ma) and caused the Pampean orogeny which resulted in the formation of a magmatic arc and granulite facies metamorphism and anatexis (Rapela et al., 1998a,b). The second event was in the Ordovician (490–450 Ma) and caused the Famatinian orogeny which resulted in continental arc magmatism (Rapela et al., 1998a; Sims et al., 1998) and the development of a back-arc basin (Rapela et al., 1998a). The Ocloyic tectonic phase (450–430 Ma; Bahlburg and Herve, 1997; Rapela et al., 1998a) caused shortening and closure of the Famatinian back-arc basin (Dalla Salda et al., 1992; Rapela et al., 1998a; Astini and Davila, 2004; Castro de Machuca et al., 2012). In the northern Sierras
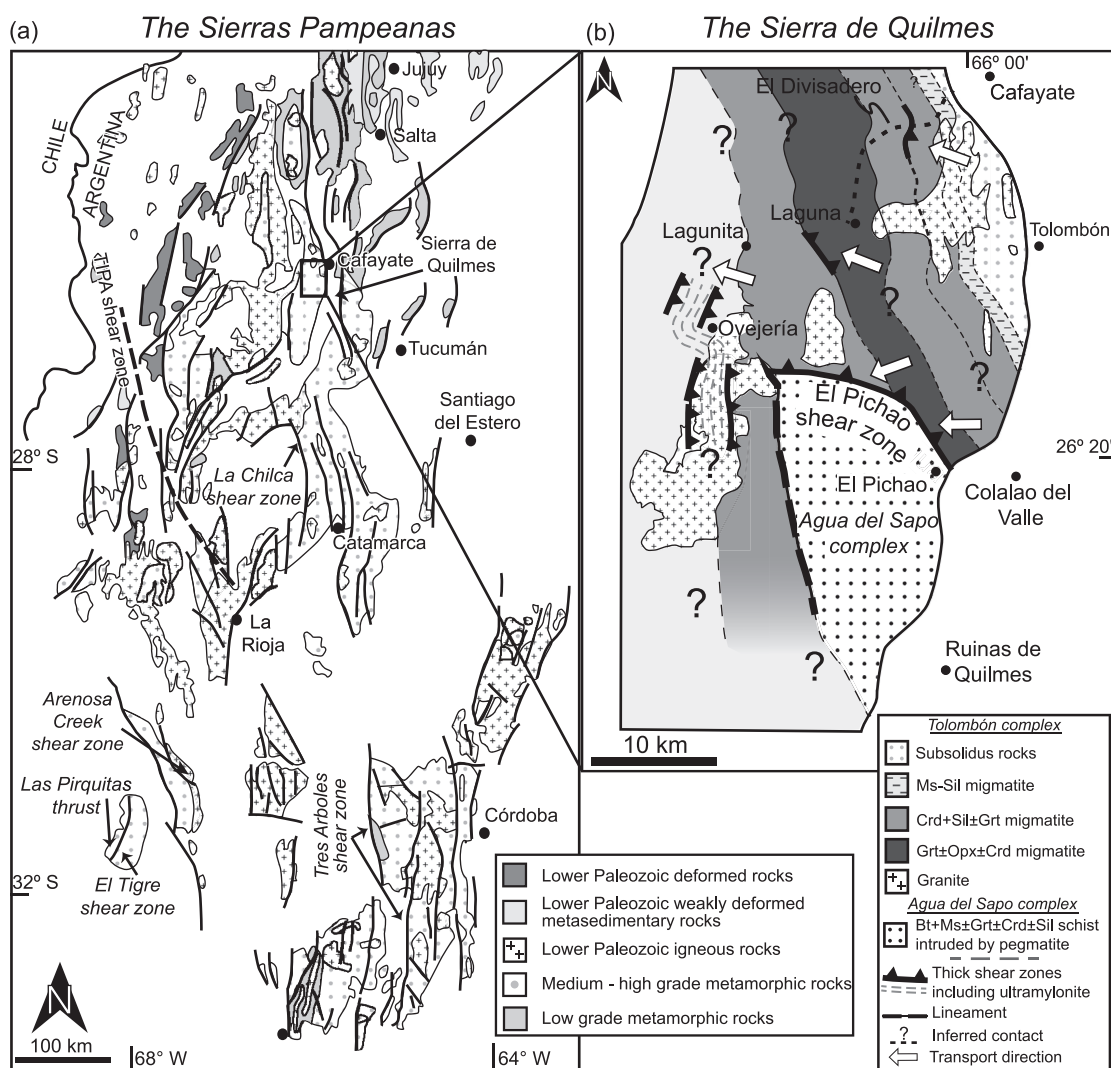
Fig. 1. The Sierras Pampeanas and Sierra de Quilmes of NW Argentina. (a) The Sierras Pampeanas with the location of major faults and shear zones indicated (modified from Hongn et al., 2010). The area shown in (b) is boxed. (b) The studied area in Sierra de Quilmes with El Pichao shear zone indicated in east of range. Granitic bodies are ultramylonitic close to thrusts.

Pampeanas, the absence of exotic terranes, mafic magmatism, and high pressure metamorphism (e.g. Lucassen et al., 2000, 2011) indicate a high-temperature, low-pressure regime between 535 and 430 Ma during consecutive Pampean and Famatinian orogenies (Lucassen et al., 2000, 2011). There is no evidence to support models which propose continental collision and crustal thickening processes (Ramos, 1988 and references therein, Omarini et al., 1999, Loewy et al., 2004) in the northern Sierras Pampeanas.

Shear zones resulting from these orogenies are common in the Sierras Pampeanas and occur discontinuously over 1000 km from 33° S to at least 24° S, and spread over a width of >250 km (Fig. 1a; Höckenreiner et al., 2003). These shear zones are commonly thick zones of mylonite and ultramylonite with thrust-to-west shear sense (Fig. 1; e.g. Le Corre and Rossello, 1994; Whitmeyer and Simpson, 2003; Lopez et al., 2007; Larrovere et al., 2008; Castro de Machuca et al., 2010; Castro de Machuca et al., 2012). One of the most significant shear zones in the northern Sierras Pampeanas is the Tinogasta—Pituil—Antinaco (TIPA) shear zone (Lopez and Toselli, 1993) part of the Las Termas belt in NW Argentina (Fig. 1a). The TIPA shear zone is ~2 km thick, 300 km long and contains mylonites that are increasingly deformed toward the centre of the zone (Höckenreiner et al., 2003). The TIPA shear zone was active at ~400 Ma and thrusts Precambrian—Cambrian rocks west onto

granitoids of the Famatinian magmatic arc (Höckenreiner et al., 2003). It is the largest of several shear zones that trend NNW—SSE in the region between La Rioja and Sierra de Quilmes (Fig. 1a). Clusters of shear zones are also seen in the southern Sierras Pampeanas in Sierras de Córdoba where Martino (2003) recognised 16 shear zones that accommodated thrusting and of these the Tres Arboles shear zone is the most significant at a length of 150 km and width of up to 16 km (Fig. 1a; Whitmeyer and Simpson, 2003). Like the shear zones in the north, the Tres Arboles shear zone trends NNW and thrusts Cambrian schists onto Ordovician rocks (Whitmeyer and Simpson, 2003). Northwest of Sierras de Córdoba, the Sierra de Velasco contains six shear zones which trend NNW. One of the largest is La Horqueta shear zone, which is up to 2 km thick and contains protomylonites and mylonites with a sinstral-thrust shear sense (Lopez et al., 2007). Ductile shear zones have also been recognized in southern Puna and the Eastern Cordillera and overprint igneous and metamorphic rocks (Hongn et al., 1996; Lucassen and Becchio, 2003) including the Brealito shear zone (Hongn and Becchio, 1999), the Agua Rosada shear zone (Hongn and Riller, 2007), and shear zones in Sierra de Molinos (Sola et al., 2010). Combined, these and other shear zones cropping out in the Sierras Pampeanas accommodated major periods of convergence on the paleo-Pacific margin of Gondwana.

The Sierra de Quilmes is a 140 km long N–S trending mountain in the northern Sierras Pampeanas west of the town of Cafayate (Fig. 1; Rossi De Toselli et al., 1976). It consists of two metamorphic complexes: the granulite facies Tolombón complex to the north and west of the range, and the amphibolite facies Agua del Sapo complex in the east and south of the range (Fig. 1b; Toselli et al., 1978). On the east side of the Sierra de Quilmes, the Tolombón complex is thrust onto the Agua del Sapo complex along a NW–SE trending shear zone: the El Pichao shear zone described in this paper. In the centre of Sierra de Quilmes, the western margin of the Agua del Sapo complex is also in fault contact with the Tolombón complex forming an NNW–SSE-trending sub-vertical greenschist facies ultramylonitic shear zone that defines a long lineament (Fig. 1b). Both complexes consist of metamorphosed sedimentary rocks of the Puncoviscana formation that were located in the upper to middle crust during metamorphism and underlie the lower grade rocks exposed in other mountains of the Sierras Pampeanas to the north (Toselli et al., 1978; Becchio et al., 1999; Büttner et al., 2005). The Agua del Sapo complex consists of gneisses and metasedimentary rocks containing Qtz+Pl+Bt+Ms+Ksp±Grt±Tur±Hbl±Crd±Ep (mineral abbreviations after Whitney and Evans, 2010) intruded by Grt-pegmatite dykes (Toselli et al., 1978). Grt-schists are common in the north of the complex, and occasionally contain cordierite. Nodules up to 2 m in length and discontinuous layers of calc-silicate are common.
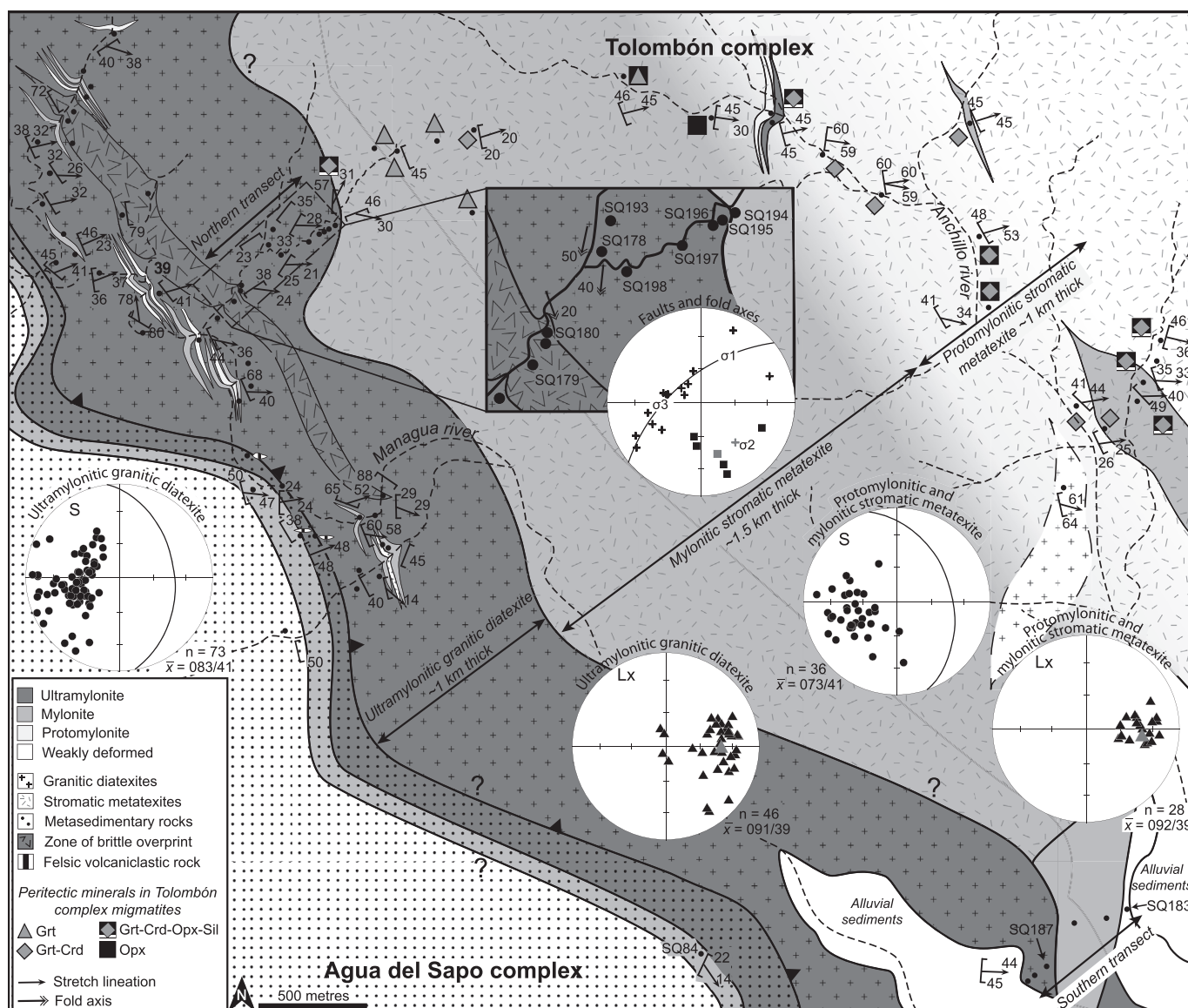
Fig. 2. Geological map of El Pichao shear zone showing thrusting of granulite facies migmatites of the Tolombón complex onto amphibolite facies meta-psammites and -pelites of the Agua del Sapo complex. Mapping mostly followed river gorges due to limited access to mountain ridges, waypoints are marked by black circles. The main shear plane dips NE with a down-dip stretching lineation (stereonets). All stereographic projections are lower hemisphere equal-area, the mean plane ($\bar{x}$) indicated with a great circle and mean lineation with a grey triangle. The stereographic projection for the ultramylonitic diatexite layer shows a spread of foliation measurements from NE to SE dipping. The intersection of these planes is parallel to the stretching lineation and defines the axis of open folds or undulations of thrust planes. Map inset: zoom-in of the northern transect with stereographic projection of poles to fault planes (black crosses) defining great circle, fold axes (black squares), and mean fold axis (grey square). σ_2 is the intersection of all fault planes (pole to great circle, grey cross). σ_1 and σ_3 are on the great circle but remain ill-defined because of lack of striations on the fault planes. σ_1 is inferred to plunge east because of thrusting sense documented in a few of these NE through to SE dipping fault planes.

The Tolombón complex consists of interbedded psammites and pelites, including calc-silicate pods and layers, that grade from greenschist facies in the northeast of the Sierra de Quilmes, to granulite facies migmatites in the southwest, indicating a tilted metamorphic sequence (Fig. 2). Anatexis is linked to the presence of diatexite—granite bodies including the composite Cafayate pluton near El Divisadero (Fig. 2). Büttner et al. (2005) divided the Tolombón complex in the region of El Divisadero, west of Cafayate town, into four metamorphic zones: from northeast to southwest these are the low grade chlorite zone that grades into the biotite—muscovite zone, followed by the garnet—cordierite—sillimanite zone, and finally the highest grade orthopyroxene zone. Ms-dehydration melting begins in the biotite—muscovite zone and continues into the garnet—cordierite—sillimanite zone where it is accompanied by Bt-dehydration melting (Büttner et al., 2005). The orthopyroxene zone contains migmatites produced through Bt-dehydration melting with leucosomes that contain Opx+Grt±Crd±Ksp (Büttner et al., 2005). Metamorphism was high-temperature and low-to medium-pressure (500—800 °C, 3.5—6 kbar, Rapela, 1976; Toselli et al., 1978; Büttner et al., 2005) and peak metamorphism occurred at ~470 Ma (U—Pb monazite and titanite, ICP—MS; Büttner et al., 2005) as part of the Famatinian orogeny. Anatexis and peak metamorphism were coeval with ductile thrusting verging to the west, which ended by ~440 Ma (Büttner et al., 2005). Büttner (2009) suggested that shear zones were originally horizontal and extensional, and later rotated by Andean uplift to show apparent thrust shear sense. This interpretation is not consistent with our findings and will be discussed later.

3. The El Pichao shear zone (PSZ)

The shear zone was named after El Pichao village in its proximity. It thrusts the Grt—Crd—Opx migmatites of the Tolombón complex onto the Grt-bearing metasedimentary rocks of the Agua del Sapo complex (Toselli et al., 1978; Figs. 1 and 2). Above and NE of the shear zone, the Tolombón complex consists of weakly deformed stromatic metatexites and diatexites (described in Section 3.1). These rocks grade to the SW into a 1 km-thick layer of protomylonitic stromatic metatexite (Section 3.2), followed by a 1.5 km-thick layer of mylonitic stromatic metatexite (Section 3.3), and at the base of the shear zone, a 1 km-thick layer of ultramylonitic granitic diatexite (Section 3.4). For simplicity these layers are referred to as protomylonitic metatexite, mylonitic metatexite, and ultramylonitic diatexite respectively. Below the ultramylonitic diatexite there is a sharp contact with the ultramylonitic top of the Agua del Sapo complex that grades downwards into interbedded meta-psammite and -pelite (Section 3.5). The El Pichao shear zone is ~3.5 km thick and comprises the protomylonitic and mylonitic metatexite, the ultramylonitic diatexite and the mylonitic top of the

Agua del Sapo complex. The rocks in each section and transitions between them are described below.

3.1. Tolombón complex: weakly deformed migmatites of the hanging wall

Northeast of and structurally above the PSZ, the Tolombón complex consists of weakly deformed migmatites characterized by leucosomes and melanosomes and evidence for magma flow and extraction (migmatite terminology after Mehnert, 1968). Leucosomes are thick, continuous leucocratic bands which contain peritectic minerals (Grt, Opx, Crd; Fig. 4a), coarse flakes of biotite rimming peritectic minerals (Fig. 4b) interpreted to result from reaction with melt during crystallization, symplectitic garnet—quartz intergrowths (Fig. 4c), and leucosomes which intrude across melanosome layers (Fig. 4a) or are aligned with S—C planes or axial planes of folds (Fig. 4d,e). These features are interpreted to be primary and a result of anatexis with little subsequent modification.

Migmatites are typically stromatic metatexites (Fig. 4a) that grade into regions of diatexite (where the rock loses coherency and behaves as a magma, neosome > paleosome) and granitic diatexite (neosome > 90%). Stromatic migmatites contain >20% leucosome (Fig. 4a) and peritectic minerals appear in both leucosome and melanosome. They also show compositional banding with layers of sand-sized grains of quartz, feldspar, biotite, and garnet that alternate with layers of finer grain size that contain mica, feldspar, quartz, and garnet. This is interpreted as bedding from the protolith which forms well-foliated, leucosome-rich pelitic layers (~80% of total outcrop) and weakly-foliated, leucosome-poor psammitic layers (~20%; Fig. 4a). Leucosomes contain peritectic garnet, cordierite, and orthopyroxene in different combinations and modal proportions: garnet is common to both the psammitic and pelitic rocks but orthopyroxene is more common in psammite, and cordierite in pelite (Fig. 4a,c). Garnet is also found in melanosomes and it is almost always present in metatexites with the exception of a small number of Opx-bearing psammitic layers. Cordierite also appears in melanosomes (Fig. 4c) and occurs only in combination with garnet and/or orthopyroxene. Diatexites are essentially the same as metatexites but due to the higher melt fraction they have lost coherence and layering is disaggregated into a chaotic mass of magma and schollen. Granitic diatexites are porphyritic and contain small (<30 cm long) schollen of meta-psammite and -pelite.

The contact between weakly deformed migmatites and the mylonitic rocks of the PSZ is gradual and marked by an increase in the intensity of foliation towards the SW as rocks become gneissic then protomylonitic (Fig. 5a). The boundary defining the top of the PSZ is placed NE of Anchillo river gorge (Fig. 2) where the
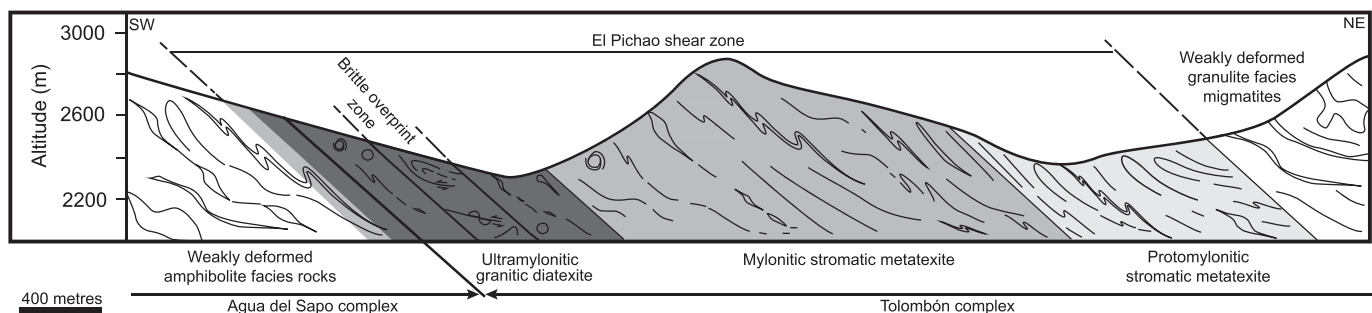
Fig. 3. Schematic cross section showing the layers of the El Pichao shear zone discussed in the main text. Contacts between layers are transitional over 10—20 m and dips of contacts and structures are means.
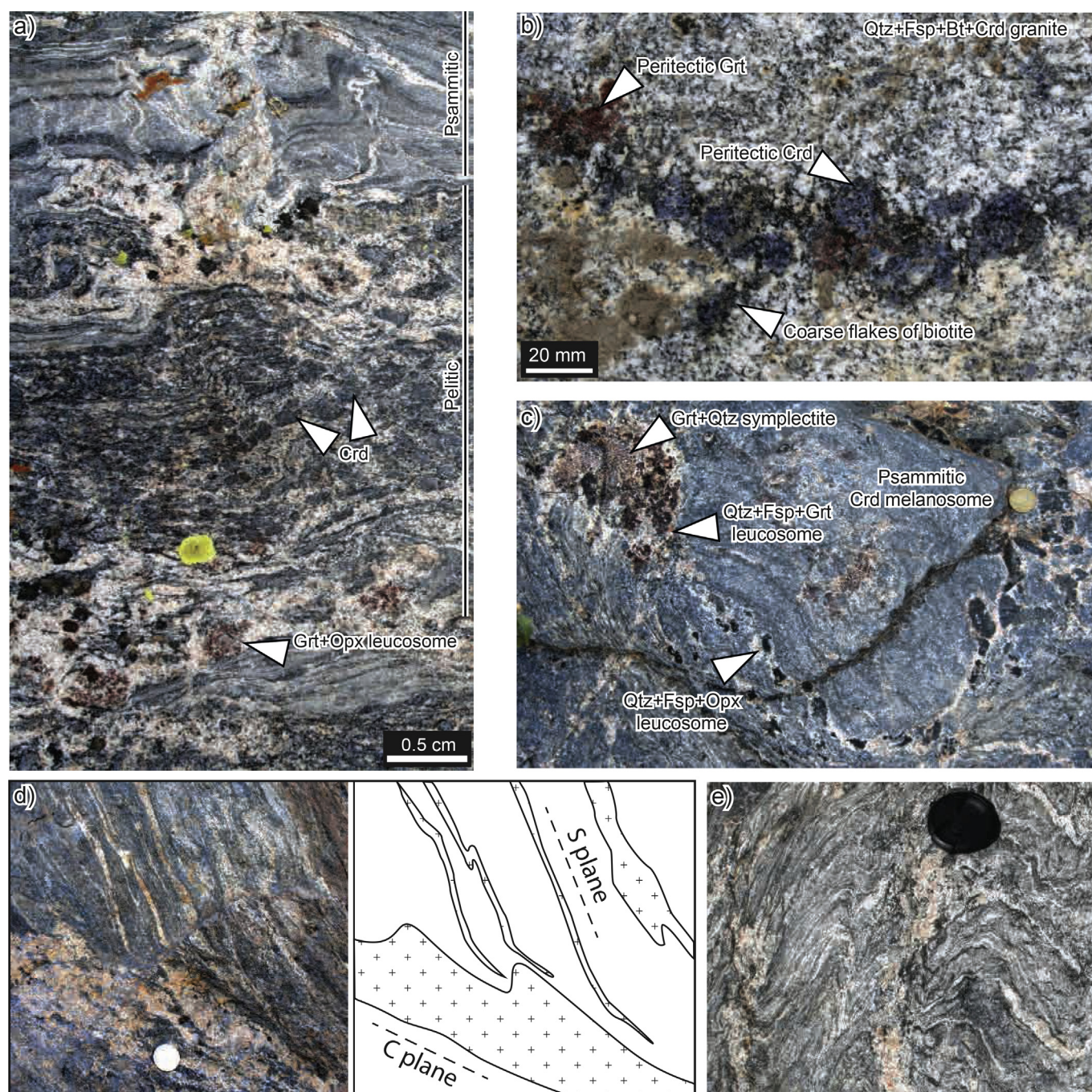
Fig. 4. Primary anatectic structures in weakly deformed Tolombón complex migmatites, protoliths to the PSZ mylonitic rocks. (a) Metatexite with compositional layering inherited from the interbedded protolith which controls leucosome composition and volume. Leucosomes intrude into and cut across foliation in top psammitic layer. (b) Peritectic Crd and Grt porphyroblast aggregates rimmed by biotite inside a Qtz+Kfs+Pl+Bt+Crd granite. Biotite rims are interpreted to result from retrogression due to reaction with crystallizing melt. (c) Patchy Grt—Opx leucosomes with Grt+Qtz symplectite in psammitic Crd—melanosome. (d) Leucosomes in thrust planes indicating possible involvement of melt during thrusting (line drawing shows interpretation of structures). (e) Leucosomes on axial planes of folds formed during shortening related to thrusting event, indicative of syn-kinematic anatexis. (a—d) are vertical planes, parallel to stretching lineation and perpendicular to foliation, (e) is perpendicular to the axial plane of folds.

proportion of protomylonitic metatexite is more than 50% of the total outcrop.

3.2. Protomylonitic metatexite

Protomylonitic metatexites (Fig. 5a) outcrop in Anchillo river gorge and form a 1 km thick-layer at the top of the PSZ. They are differentiated from the weakly deformed rocks NE of the PSZ (Fig. 4) by a higher proportion of dark grey recrystallized matrix and increased foliation intensity. The latter is indicated by an increase in the alignment of micas and the stretching and flattening of quartz and feldspar phenocrysts (Fig. 5a). Quartz and feldspar phenocrysts in the stromatic metatexite become porphyroclasts in the protomylonite and the mica-rich matrix is deflected around them forming S—C fabric. Many porphyroclasts in melanocratic layers are elongate parallel to the foliation or form σ- and δ-clasts with asymmetric tails that thin and recrystallize distal to the clast, but some porphyroclasts retain their euhedral tabular shape.
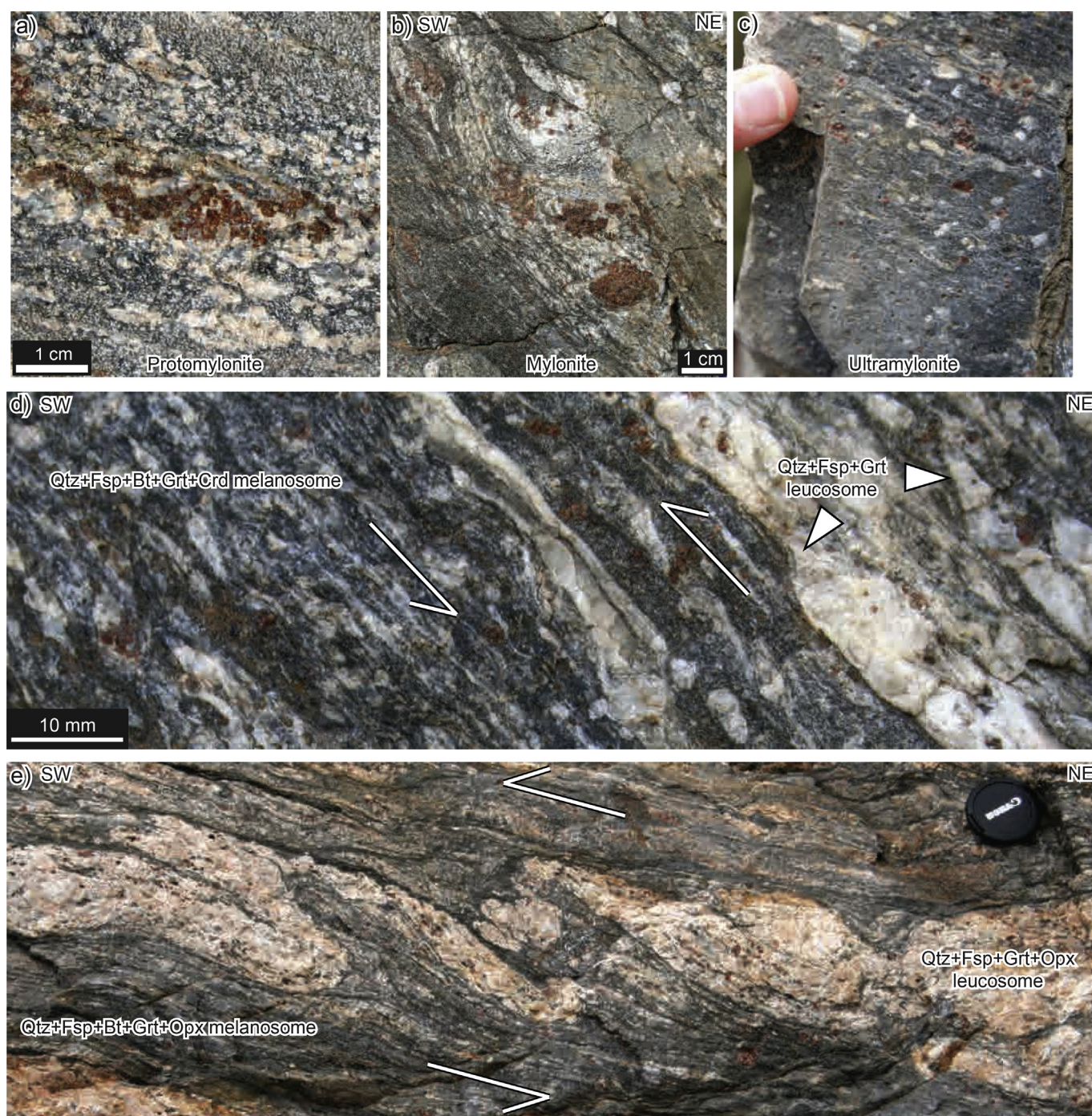
Fig. 5. Features of weakly to highly sheared rocks in metatexite layers of the PSZ. (a) Garnet aggregate in protomylonitic metatexite. (b) Large garnet grains in relict leucosome that has been asymmetrically sheared into a lens indicating top-to-SW shear in a mylonitic metatexite. (c) Ultramylonitic metatexite with naked and rounded clasts of garnet and feldspar. (d) S–C fabric and σ-clasts of feldspar indicating top-to-SW shear in Grt+Crd protomylonitic–mylonitic metatexite. (e) Asymmetric SW-verging folds of Grt+Opx leucosome and melanosome in mylonitic metatexite. All planes are parallel to stretching lineation and perpendicular to foliation.

Leucosomes are generally continuous with their boundaries parallel to S–C fabric but show little obvious internal deformation. Primary anatectic structures described in Section 3.1 are still recognizable. Calc-silicate nodules present in this layer are up to 2 m long and elongate parallel to the foliation.

Within this layer of protomylonitic metatexite there are discontinuous layers of mylonitic metatexite (Fig. 5b,d,e; described in Section 3.3). These increase in proportion to the SW until they form greater than 50% of the total outcrop marking a subjective boundary with the top of the mylonitic metatexite.

3.3. Mylonitic metatexite

The main difference between mylonitic and protomylonitic metatexites is the proportion of mylonitic layers. Mylonites are characterized by a higher proportion of dark grey, fine-grained, recrystallized matrix (Fig. 5b,d,e). Leucosomes and melanosomes are still recognizable and show the same mineralogy and calc-silicate nodules are approximately the same shape and size. Marking the increased strain, leucosomes are sheared into asymmetric, disrupted lenses (Fig. 5b) or folded asymmetrically and
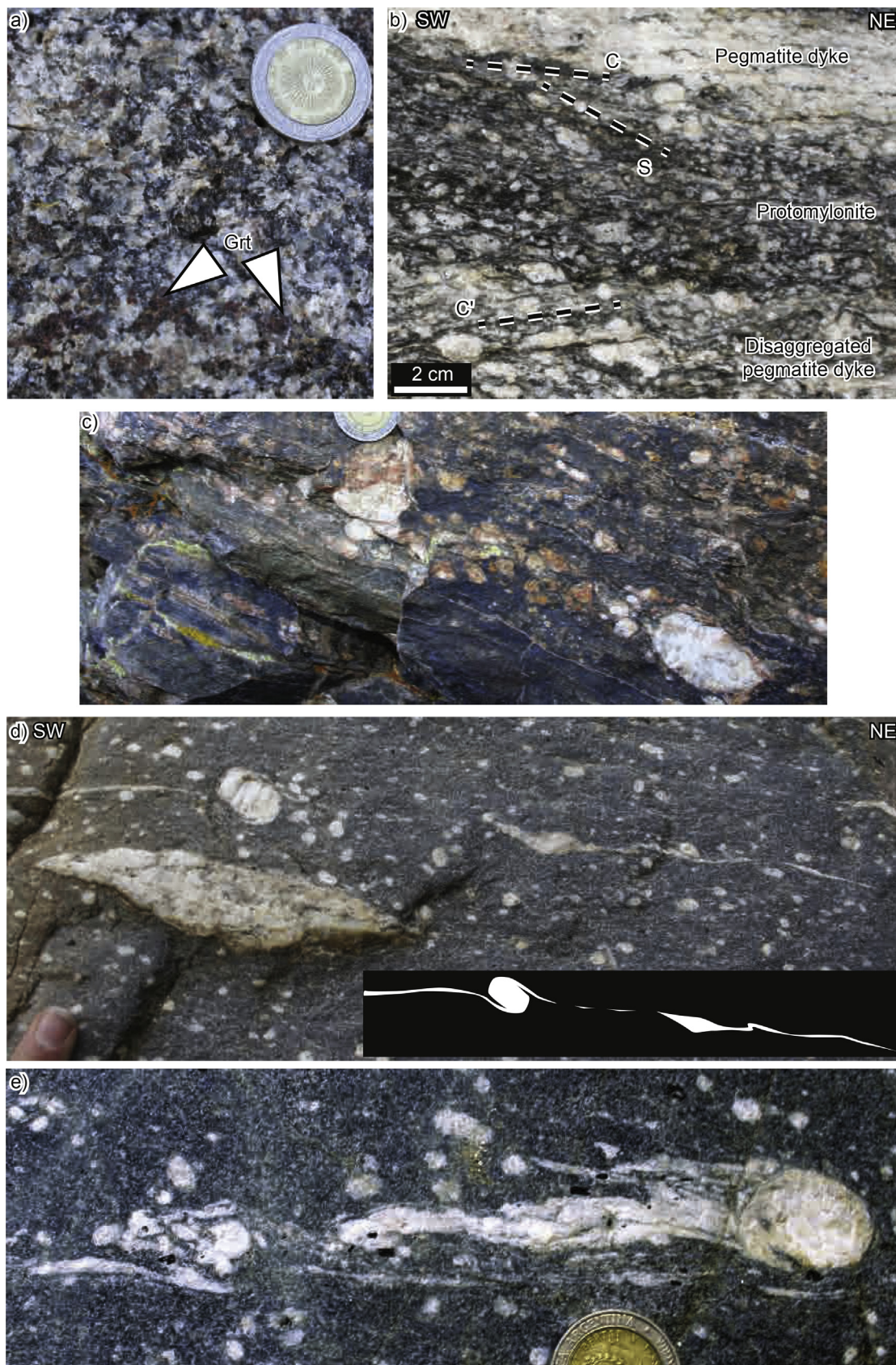
Fig. 6. Features of weakly to highly deformed rocks in the ultramylonitic diatexite layer of the PSZ. (a) Granitic diatexite from a preserved low strain lithon. (b) Progressive disaggregation of pegmatite dyke (top) forms disconnected dykelets and large clasts (bottom) and eventually discrete porphyroclasts (middle) in a protomylonite. (c) Mylonitic pegmatite dyke with large K-feldspar grains. (d) δ-clast (top) and σ-clast resulting from shearing of pegmatite dyke in ultramylonitic diatexite. (e) K-feldspar porphyroclast with "comet" tail and smaller naked porphyroclasts in ultramylonite (view down plunge of stretching lineation). (f) Finely interlayered garnet-bearing gneiss, protomylonite and
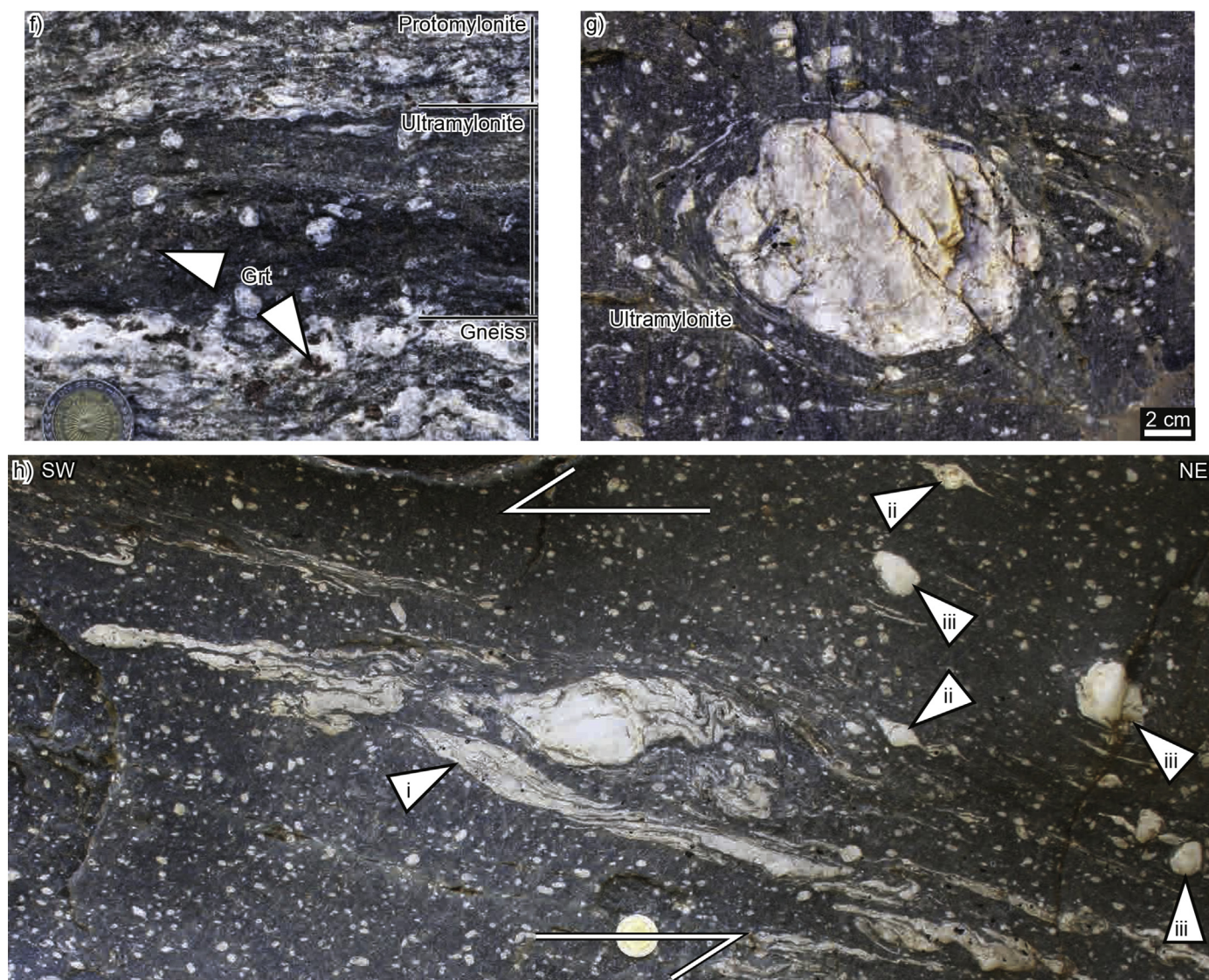
Fig. 6. (*continued*).

intensely (Fig. 5e), indicating their higher viscosity in comparison to melanosome. In melanocratic layers the intensity of the foliation is greater, S—C fabric is well developed, and porphyroclasts of feldspar form σ- and δ-clasts with short asymmetric tails (Fig. 5b,d). Garnet, cordierite, and orthopyroxene in melanocratic layers are surrounded by remnant leucosomes that are asymmetrically sheared (Fig. 5b). Primary anatectic structures are partially preserved, limited to coarse flakes of biotite rimming peritectic minerals, occasional tabular feldspar porphyroclasts, and symplectitic intergrowths of garnet and quartz.

The mylonitic metatexites form a 1.5 km-thick layer that contains occasional and discontinuous layers of protomylonitic (Fig. 5a) and ultramylonitic metatexite (Fig. 5c). Ultramylonitic rocks form melanocratic layers a few cm wide that contain >90% recrystallized matrix and naked, rounded porphyroclasts of feldspar, garnet

(Fig. 5c), cordierite, and orthopyroxene. Below the 1.5 km layer of mylonitic metatexite there is a gradational contact with the underlying layer of much more massive ultramylonitic diatexite (Fig. 6).

3.4. Ultramylonitic diatexite

We first describe the features of this ultramylonitic layer, before describing the transition from the mylonitic metatexites above and these ultramylonites.

The mylonitic metatexite layer grades downward into a massive, homogenous ultramylonitic rock consisting of rounded feldspar porphyroclasts in a black matrix (Fig. 6) that forms a 1 km-thick layer at the base of the PSZ (Fig. 2). Locally the matrix is dark green from retrogression of biotite to chlorite and in some regions the proportion of recrystallized matrix gradually decreases with a

ultramylonite. (g) Large K-feldspar porphyroclast disaggregated from a pegmatite dyke and rotated in ultramylonitic matrix during shearing, causing high rotational strain on its margins and circumcentric ribbons of recrystallized feldspar (view down plunge of stretching lineation). (h) Pegmatite sheared in ultramylonite forming asymmetric lenses (*i*), σ-type clasts (*ii*), and, through prolonged rolling and rotation in the matrix, θ-type clasts (*iii*). View in all photographs except for (e) and (g) is parallel to stretching lineation.

concomitant increase in the proportion of porphyroclasts until a homogenous porphyritic granitic diatexite can be recognised (Fig. 6a). From this association, we interpret that the protolith to the ultramylonites was a granitic diatexite and we call this layer ultramylonitic diatexite.

Within these ultramylonites, there are discontinuous quartz-feldspar layers that contain large feldspar crystals (up to 20 cm in diameter), interpreted as sheared and disaggregated pegmatite dykes. These rocks also document the gradual disaggregation of dykes into σ-clasts (Fig. 6d,h), and then into naked porphyroclasts (Fig. 6g). There are occasional thin (0.5–15 m wide and a few hundred metres long) lenses of protomylonitic diatexite (7% of total width of the 1 km ultramylonitic layer) and mylonitic diatexite (13% of total; Fig. 2) recognized by the lower modal proportion of recrystallized matrix, generally coarser grain size, increased preservation of euhedral feldspars and other primary structures, and less strained, continuous pegmatites. In contrast to the mylonitic metatexites, none of the rocks are layered (Fig. 6) and calc-silicate nodules are absent.

The top of the layer of ultramylonitic diatexite contains porphyroclasts of garnet (Fig. 6f) which reduce in proportion and size downward to the SW, becoming absent 400 m from the base. Immediately below where garnet becomes absent there is a 200 m thick zone where ultramylonites are overprinted by brittle structures (between SQ179 and SQ180; Figs. 2 and 3) described in Section 6. Below the brittle fault zone there is a return to the massive ultramylonitic diatexite for 200 m until the contact with the underlying meta-psammites and -pelites of the Agua del Sapo complex (Fig. 2).

3.5. Transition into ultramylonitic diatexite

The transition from the overlying layer of mylonitic metatexite (Section 3.3) to the ultramylonitic diatexite is described in two regions with complementary information: the southern and northern transects (Fig. 2).

The southern transect is characterized by a gradual transition that is well preserved in a low strain lithon where we recognize many protolith features. Approaching this lithon from the NE to the SW, there is an increase in leucocratic layers in the mylonitic metatexite with a concomitant decrease in the intensity of foliation until melanocratic layers become absent, and the rock becomes a porphyritic granitic diatexite that preserves a granitic texture with psammitic and pelitic schollen (Fig. 6a; at point SQ183 in Fig. 2). Further to the SW this low strain lithon of diatexite transitions into mylonites over a region ~60 m wide where strain intensity increases. This is marked by an increase in the intensity of foliation and definition of S–C fabric and a gradual decrease in the proportion of feldspar porphyroclasts (phenocrysts in the granitic diatexite) and in the size and proportion of garnet.

Within this sequence there is a 20 m-thick layer of a rock that consists mostly of K-feldspar with crystals up to 5 cm in diameter with small garnets (<2 mm diameter), and strongly stretched ribbons of quartz and feldspar. This rock is interpreted to be a mylonitic–ultramylonitic pegmatite and in places the matrix is dark grey and recrystallized and contains few rounded porphyroclasts of K-feldspar (Fig. 6c).

Unlike the southern transect, the northern transect does not include preserved lithons of weakly deformed diatexite. Instead the mylonitic metatexite transitions directly into a massive ultramylonite of the kind described in Section 3.4 and interpreted to have formed after granitic diatexite. As in the southern transect, the northern transect contains garnet 1–6 mm in diameter (Fig. 6f) that occurs in aggregates and decreases in proportion to the SW. The northern transect also contains pegmatite dykes which transition

into a rock with large K-feldspar porphyroclasts sheared into σ- and δ-clasts surrounded by dark grey matrix interpreted as mylonitic–ultramylonitic pegmatite (Fig. 6c). In contrast to the southern transect, here pegmatite dykes are thinner forming only metre-thick bands.

3.6. Contact with the footwall of the PSZ

At the base of the ultramylonitic diatexite layer there is an abrupt change to an interbedded rock that contains layers of meta-sandstone comprised of quartz, K-feldspar, plagioclase, biotite, and garnet that alternate with layers of finer grain size meta-mudstone that contain biotite, K-feldspar, quartz, plagioclase, muscovite, and garnet. This layering is interpreted to be sedimentary in origin indicating a change in rock type from the homogenous, massive ultramylonitic diatexite to sheared interbedded meta-psammite and -pelite. The pelitic layers commonly form well-foliated schists and the sequence contains calc-silicate nodules and layers. There are no primary anatectic structures like those in the Tolombón complex, indicating the rock is part of the amphibolite facies Agua del Sapo complex.

The metasedimentary rocks contain pegmatite dykes that are sheared into discontinuous lenses and large (up to 25 cm diameter) porphyroclasts, similar to dykes in the ultramylonitic diatexites. Within these rocks are layers where the matrix becomes very fine-grained and biotite-rich, and porphyroclasts are rounded and naked. These layers are interpreted as ultramylonitic metasedimentary layers and still part of the PSZ. Further south, garnet–cordierite bearing interbedded meta-psammite and -pelite do not contain mylonitic layers and while pegmatite dykes are sheared, they are generally continuous. These rocks are interpreted to be outside of the high strain zone and accordingly their appearance mark the base of the PSZ (Fig. 2).

4. Structures

In this section we present the full range of structures in the shear zone. We focus first on structures in weakly deformed through to ultramylonitic metatexites (Section 4.1) and then on structures preserved in the 1 km-thick ultramylonitic diatexite layer at the base of the PSZ (Section 4.2).

4.1. Structures in deformed metatexites

This layer shows a gradual transition from weakly deformed and gneissic metatexites into mylonitic rocks. We describe the structures in weakly deformed rocks first and then the changes as strain increases.

Weakly deformed metatexites in the hanging wall of the PSZ show bedding-parallel foliation that dips moderately SE or NE (Fig. 1b; mean = 115/46; measurements in dip direction/dip) with a SE-plunging stretching lineation (mean = 138/34). The foliation, defined by micaceous planes consisting dominantly of biotite, is well-developed in pelitic layers but weak in psammitic layers (Fig. 4a). Leucosomes are generally foliation parallel in pelitic layers but in psammitic layers form isolated patches that are not foliation parallel or intrude from pelitic layers and cross cut foliation (Fig. 4a). Leucosomes are also found in shear planes, commonly sub-parallel to the axial plane of folds and these features are interpreted as indicative of syn-kinematic melting (Fig. 4d,e).

The foliation in the protomylonitic metatexite is defined by the same features as in less deformed metatexites but it is better developed and dips moderately ENE (mean foliation in protomylonitic and mylonitic metatexites = 73/41) with stretching lineations that plunge moderately to the east (mean lineation = 92/

39; Fig. 2). Thrusting with top-to-W transport direction is indicated in protomylonitic metatexites by asymmetric shearing of leucosomes into σ-shaped lenses or σ-shaped porphyroclasts (Fig. 5a), S–C fabric in the melanosome, asymmetrically folded leucosomes, and garnet, cordierite, and orthopyroxene porphyroclasts with asymmetric strain shadows of biotite, quartz and feldspar. Garnet aggregates are occasionally sheared into σ-type shapes. Calcsilicate nodules are flattened parallel to the foliation and may have stair-stepping tails. Leucocratic bands are parallel to both S and C planes and show pervasive internal deformation indicative of solid-state deformation after anatexis ceased. The relationship between anatexis and shearing is discussed further in Section 8.1.

Mylonitic metatexites have more intensely developed foliation (Fig. 5b) with thicker and more continuous layers of biotite defining S–C fabric. Structural features are the same as for protomylonites but leucosomes are less continuous and a greater proportion are sheared into σ-shaped lenses (Fig. 5b) and asymmetrically folded with SW vergence (Fig. 5e). Inside these mylonites there are thin layers of melanocratic ultramylonitic layers characterized by rounded naked clasts of feldspar, garnet, cordierite, and orthopyroxene in a fine and dark matrix. Clasts are generally smaller than those in protomylonites and mylonites (Fig. 5c) with very few σ-clasts, σ-shaped lenses of leucosomes, or asymmetric folds.

4.2. Structures in deformed diatexites

The homogeneity of the diatexite protolith and the intrusion of pegmatite dykes into the layer of ultramylonitic diatexite caused the development of structures that are different to those in the layer of mylonitic metatexite. Within the layer of ultramylonitic diatexite the thin layers of protomylonite and mylonite show similar structures to the ultramylonite so they are discussed together with any differences highlighted.

Similar to the attitude of the foliation in the protomylonitic and mylonitic metatexites, foliation in the layer of ultramylonitic diatexites dips moderately to the east (mean = 83/41) with an east-plunging stretching lineation (mean = 91/39; Fig. 2). In the northern transect (Section 3.5) the foliation rotates gradually from NE to SE dipping defining a broad fold (Fig. 2). The intersection of these planes defines a fold axis which plunges moderately to the east, approximately parallel to the stretching lineation, indicating folding could be a result of large-scale undulations of thrust planes.

The large clasts from sheared pegmatite dykes show a range of structures related to variable amounts of rotation. Porphyroclasts that have experienced little rotation show asymmetric tails and pressure shadows, form σ-type clasts (Fig. 6d,h) and occasionally have comet-like tails (Fig. 6e). With increasing rotation δ-type clasts are produced (Fig. 6d,h) or porphyroclast tails wrap around and mantle the clast (Fig. 6g). These structures are more common in protomylonitic and mylonitic diatexites than ultramylonitic diatexites. The ultimate product of this rotation is naked θ-type clasts characteristic of ultramylonites, possibly because of shearing, thinning, and complete recrystallization of porphyroclast tails (Fig. 6g).

Similar to the mylonitic metatexites, this layer contains occasional tabular porphyroclasts of feldspar, asymmetric shearing of garnet aggregates, and S–C fabric in biotite-rich layers. These features are more pronounced in mylonites than protomylonites but less apparent in ultramylonites which are dominated by naked clasts and strongly sheared pegmatite dykes.

5. Microstructures

Here we start with the description of primary anatectic microstructures (Section 5.1) and then describe the secondary microstructures of mylonitic metatexites (Section 5.2) and diatexites (Section 5.3). The microstructures at each level of the PSZ share a broadly similar set of features characteristic of deformation at amphibolite facies. Grain sizes were determined using digitised maps of 300 grains which were analysed for average grain size using the median Feret diameter (N. Hunter, pers. communication).

5.1. Primary anatectic microstructures

Primary anatectic microstructures are evident in weakly deformed and protomylonitic metatexites in the NE of the PSZ. These microstructures are largely absent in ultramylonitic metatexites but occasionally preserved in mylonitic metatexites.

Leucosomes consist of Qtz+Kfs+Pl+Grt±Crd±Sil±Opx and melanosomes of Bt+Sil±Crd±Ky±Grt±Ilm±Mag±Rt±Ap±Mnz±Ms (Fig. 7a) with increasing proportions of quartz and feldspar closer to leucosomes. In melanosomes anhedral quartz grains are interstitial to biotite and feldspar. Feldspar occasionally forms euhedral tabular crystals that are interpreted as igneous in origin, and plagioclase commonly shows lamellar crystallisation twins, or two sets of twins perpendicular to each other (Fig. 7b).

In weakly deformed metatexites peritectic minerals are found dominantly in leucosomes. There are two types of sillimanite: Sil1 occurs in leucosomes fringing the boundaries of large feldspar crystals (Fig. 7a), and is interpreted to be peritectic. Sil2 and Bt2 replace cordierite (Fig. 7a,b) and garnet, and are interpreted to be a result of the reaction of garnet and cordierite with melt during crystallization (Büttner et al., 2005; Sawyer, 2008). When replacing cordierite, Sil2 is occasionally accompanied by kyanite which forms small subhedral porphyroclasts that show random orientation with respect to the foliation (Fig. 7a) indicating that deformation ceased before the stability field of kyanite was reached, following the interpretation of Büttner et al. (2005).

Garnet is 0.5–30 mm in diameter and commonly poikiloblastic with biotite-filled fractures and inclusions of bulbous quartz, coarse biotite, euhedral zircon, and occasional wormy intergrowths of ilmenite. All inclusions are generally larger than the size of the same mineral in the matrix. In some cases garnet is surrounded by orthopyroxene and in such instances garnet contains wormy intergrowths of quartz forming symplectite (Fig. 7d; Waters, 2001). In areas with a high proportion of biotite and garnet, ilmenite is common and contains exsolved magnetite.

Cordierite is anhedral and up to 5 mm in diameter (Fig. 7a,b). It appears in leucosomes and melanosomes and is the most abundant mineral in some restitic migmatites. It is poikiloblastic with inclusions of quartz, biotite, and zircon and sometimes has an inclusion-free mantle surrounding a poikiloblastic core. Cordierite contains discontinuous lenticular twins and alteration to white mica on microfractures.

Orthopyroxene occurs only in leucosomes and forms large (up to 40 mm), anhedral, occasionally poikiloblastic grains that contain inclusions of quartz, biotite, and ilmenite with magnetite exsolution (Fig. 7c,d). It is replaced at its margins by biotite and occasionally garnet (Fig. 7c). Biotite is partially replaced by chlorite due to a later retrogression.

5.2. Deformation microstructures in sheared metatexites

The deformation microstructures are described for protomylonitic metatexites and differences in mylonitic and ultramylonitic metatexites are then highlighted. Although metatexites show a general decrease in grain size from protomylonites to ultramylonites, grain size estimates are not provided because the variation is too large due to the presence of heterogeneous
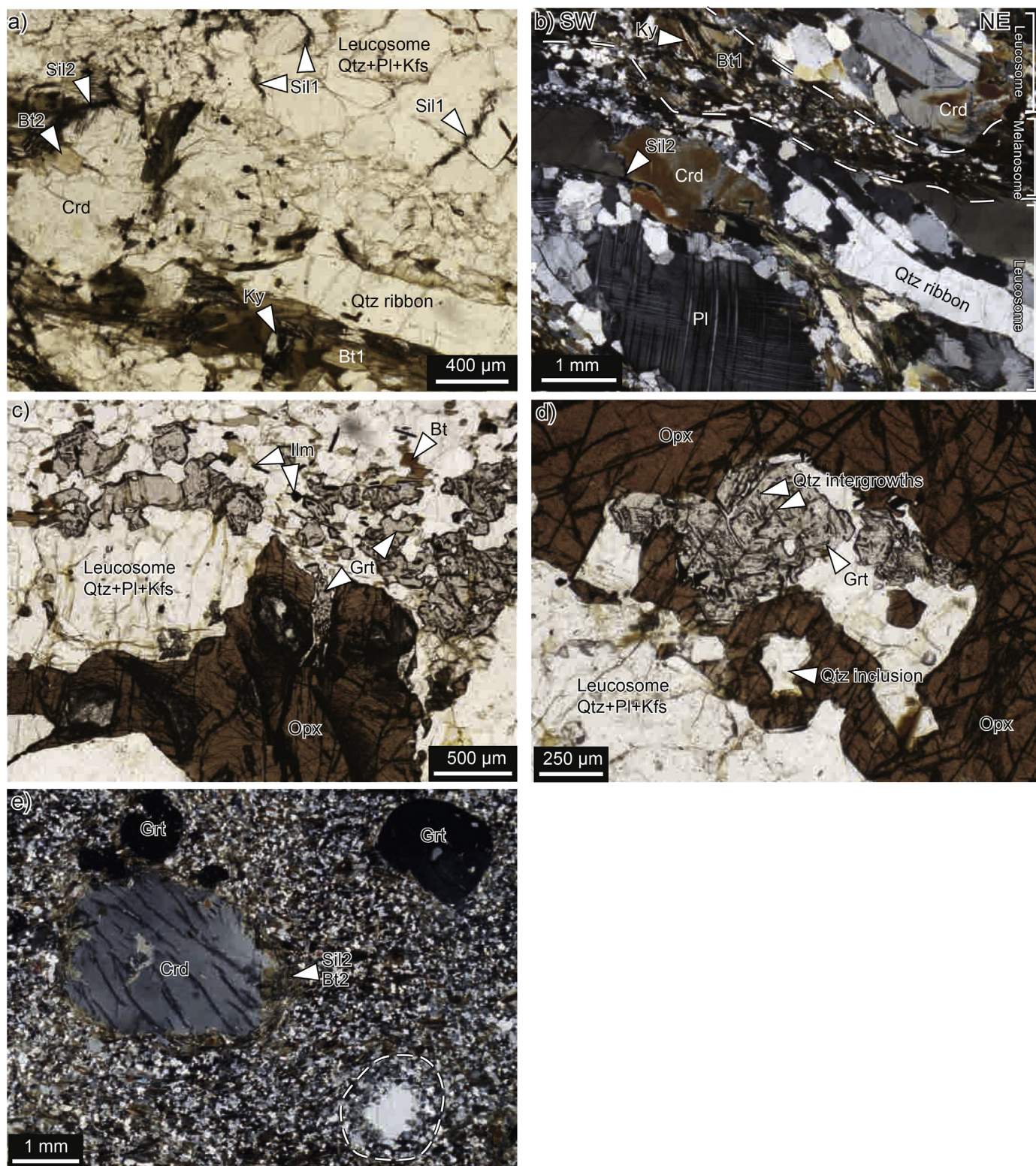
Fig. 7. Metamorphic and microstructural features of deformed rocks after metatexites. (a) Leucosome containing peritectic sillimanite (Sil1) in a Crd-melanosome with kyanite and sillimanite (Sil2; plane polarized light, PPL). (b) Leucosomes and melanosome in metatexite. Quartz in leucosomes is polygonal (top right) or forms ribbons that wrap around peritectic cordierite and plagioclase. Plagioclase contains two sets of twins and shows recrystallization on foliation parallel boundaries. Cordierite is partially replaced at margins by sillimanite (Sil2) and biotite (Bt2). Biotite-rich melanosome contains porphyroblasts of kyanite and interstitial quartz and feldspar (crossed polarised light, XPL). (c) Orthopyroxene–garnet leucosome. Garnet partially replaces orthopyroxene, Bt+Ilm partially replaces garnet (PPL). (d) Orthopyroxene with inclusions of garnet and quartz. Garnet inclusion contains wormy intergrowths of quartz (PPL). (e) Ultramylonite showing fine-grained matrix with poorly-developed foliation and rounded cordierite, garnet, and feldspar porphyroclasts. Cordierite rim is partially replaced by Bt2 and Sil2 and plagioclase has a recrystallised mantle (dashed line; XPL). All thin sections are cut parallel to stretching lineation, perpendicular to foliation.

leucocratic and melanocratic bands and abundant porphyroclasts of garnet, cordierite, and orthopyroxene which do not recrystallize.

Quartz ribbons and leucosomes in protomylonitic metatexites form continuous bands that, together with the micaceous bands, are parallel to S–C fabric and deflect around porphyroclasts (Fig. 7b). Feldspar porphyroclasts occasionally retain crystallization twins (Fig. 7b) and euhedral tabular shape but more commonly show sweeping undulose extinction, recrystallization at margins, and have asymmetric strain shadows with recrystallised quartz and feldspar forming δ- and σ-clasts. Feldspar contains late patchy sericitisation and occasionally microcracks parallel to cleavage planes. Myrmekite is present on some K-feldspar faces parallel to the foliation. Muscovite fish are common and show stair-stepping wings. Quartz in leucosomes has a polygonal shape indicating recrystallization at moderate temperatures, and quartz ribbons are >5 cm long and contain grains of variable sizes with lobate boundaries and pinning structures (Fig. 7b), interpreted to indicate grain boundary migration (GBM) recrystallization indicative of regime 3 of Hirth and Tullis (1992).

In mylonitic metatexites the well-developed S–C fabric is defined by quartz ribbons, biotite and sillimanite, and alignment of leucosome boundaries (Fig. 7a,b). Quartz has the same appearance as in protomylonitic metatexites and it also shows GBM but quartz ribbons are shorter, ~5 mm long, and deflect around porphyroclasts (Fig. 7b).

Ultramylonitic metatexites have a weakly foliated matrix of uniform grain size (Fig. 7e). Unlike protomylonitic and mylonitic metatexites, layers of biotite are ill-defined and instead biotite appears dispersed in the matrix (Fig. 7e). Feldspars have recrystallized margins forming core-and-mantle structure and show late sericitisation (Fig. 7e). Quartz ribbons showing GBM are rare and much shorter than in mylonitic metatexites, crystallization twins in feldspar porphyroclasts are uncommon, and σ- and δ-clasts are absent.

5.3. Deformation microstructures in sheared diatexites

As mentioned in Section 4.2, the homogeneity and presence of pegmatite dykes in the ultramylonitic diatexites gave rise to structures absent in sheared metatexite. Here we focus only on those microstructures which are different. While the layer is dominantly ultramylonitic (as described in Section 3.4) it also contains protomylonitic and mylonitic layers and these are described first, and then compared to ultramylonitic rocks to document the gradual increase in strain. Like for sheared metatexite, these rocks also record deformation at amphibolite facies conditions with late greenschist, possibly static overprint.

Protomylonitic diatexites contain a matrix of Qtz+Kfs+Pl±Bt±Ms±Chl±Sil±Ap with an average quartz grain size of 95 ± 20 μm and an average mica grain size of 170 ± 60 μm. Porphyroclasts of K-feldspar and plagioclase are tabular to rounded with occasional inclusions of coarse flakes of biotite and muscovite and rare monazite (Fig. 8a). Muscovite inclusions are aligned parallel to crystallographic planes of feldspar porphyroclasts (Fig. 8a). Crystallization twins are evident in some feldspar porphyroclasts. Porphyroclasts in protomylonitic diatexite show partial recrystallization, similar to those in the mylonitic rocks of the metatexite but with a higher degree of recrystallization and a progression from core-mantle structure, through to completely recrystallized porphyroclasts (Fig. 8b,c). They also show rotation without internal deformation to form naked clasts although this is rare and most porphyroclasts have strain shadows. The foliation is defined by aligned biotite grains that form connected layers that wrap around the porphyroclasts (Fig. 8a–c). Quartz ribbons show GBM and are a similar length to protomylonitic metatexites (Section 5.2) but also

wrap around porphyroclasts and occasionally form rootless isoclinal folds (Fig. 8a,c). Myrmekite occurs on some porphyroclast grains on foliation-parallel boundaries. Evidence for porphyroclast rolling includes δ-clasts and quartz ribbons that wrap around porphyroclasts (Fig. 8b,c,f) and either thin out or break up close to the porphyroclast (Fig. 8b–d).

Mylonitic diatexites have the same grain size as the protomylonies and contain quartz ribbons that are shorter than in the protomylonites, reaching lengths up to 10 mm but generally ~4 mm long, and are either continuous, parallel to foliation, or wrap around porphyroclasts (Fig. 8d). They do not show evidence for folding, unlike protomylonitic rocks, suggesting transposition. Compared to protomylonites, mylonitic diatexites contain a higher proportion of recrystallized matrix and naked and recrystallized porphyroclasts (Fig. 8d).

Ultramylonitic diatexites have an average quartz grain size of 60 ± 10 μm and average mica grain size of 120 ± 40 μm (Fig. 8e,f) and only a few small remnant porphyroclasts. These porphyroclasts are commonly rounded and have only weakly developed strain shadows or form naked clasts. In some cases they are completely recrystallized but retain the original shape of the porphyroclast (Fig. 8e) and were later partly sericitised and chloritised. Quartz ribbons are mostly absent but occasionally there are few aligned quartz grains that are coarser than the matrix and show remnant lobate boundaries. Unlike less deformed diatexites, connected planes of biotite are missing and instead, biotite is dispersed in the matrix. Consequently the foliation is not well developed (Fig. 8e,f *cf.* 8a–c).

5.4. Interpretation of microstructural data

Irrespective of whether the protolith was metatexite or diatexite, and independent of the intensity of shearing or position in the shear zone, all rocks record partial recrystallization of feldspar, GBM in quartz ribbons, and/or myrmekite on foliation-parallel planes. These features indicate that the temperature of shearing in all rocks and at all structural levels of the PSZ was in the range of 500–700 °C (Passchier and Trouw, 2005) above greenschist facies.

The change from protomylonites to ultramylonites for both protoliths is marked by an increase in the proportion of recrystallized matrix, a decrease in the proportion of porphyroclasts, together with a decrease in the grain size, and length and number of quartz ribbons (nearly absent in the ultramylonites). The foliation intensity increases towards mylonitic rocks but then decreases as rocks become ultramylonitic. In parallel, strain shadows and σ- or δ-clasts grow in importance towards mylonites but then are lost in ultramylonites, dominated by naked clasts.

While there are many microstructural commonalities between all sheared rocks within the PSZ, the increase in intensity of porphyroclast rolling from proto- to ultramylonites leads to some significant differences. Rolling causes folding of the quartz ribbons and tend to destroy them as well as mica layers. This, together with dissolution–precipitation of feldspars that may have been activated in the fine-grained ultramylonites, disperses mica through the matrix where it pins quartz and inhibits its recrystallization and recovery, explaining the origin of the homogenous, weakly foliated matrix in the ultramylonites (Figs. 7e and 8e,f).

6. Late brittle fault zone

The zone of brittle overprint that occurs in the ultramylonitic diatexite layer (Fig. 2) includes brittle faults, breccia, cataclasite and pseudotachylite associated with fault-related folds (Fig. 9). Breccia (>30 vol.% angular fragments of wall rock) and cataclasite (<30 vol.% angular fragments) contain clasts in a brown to black,
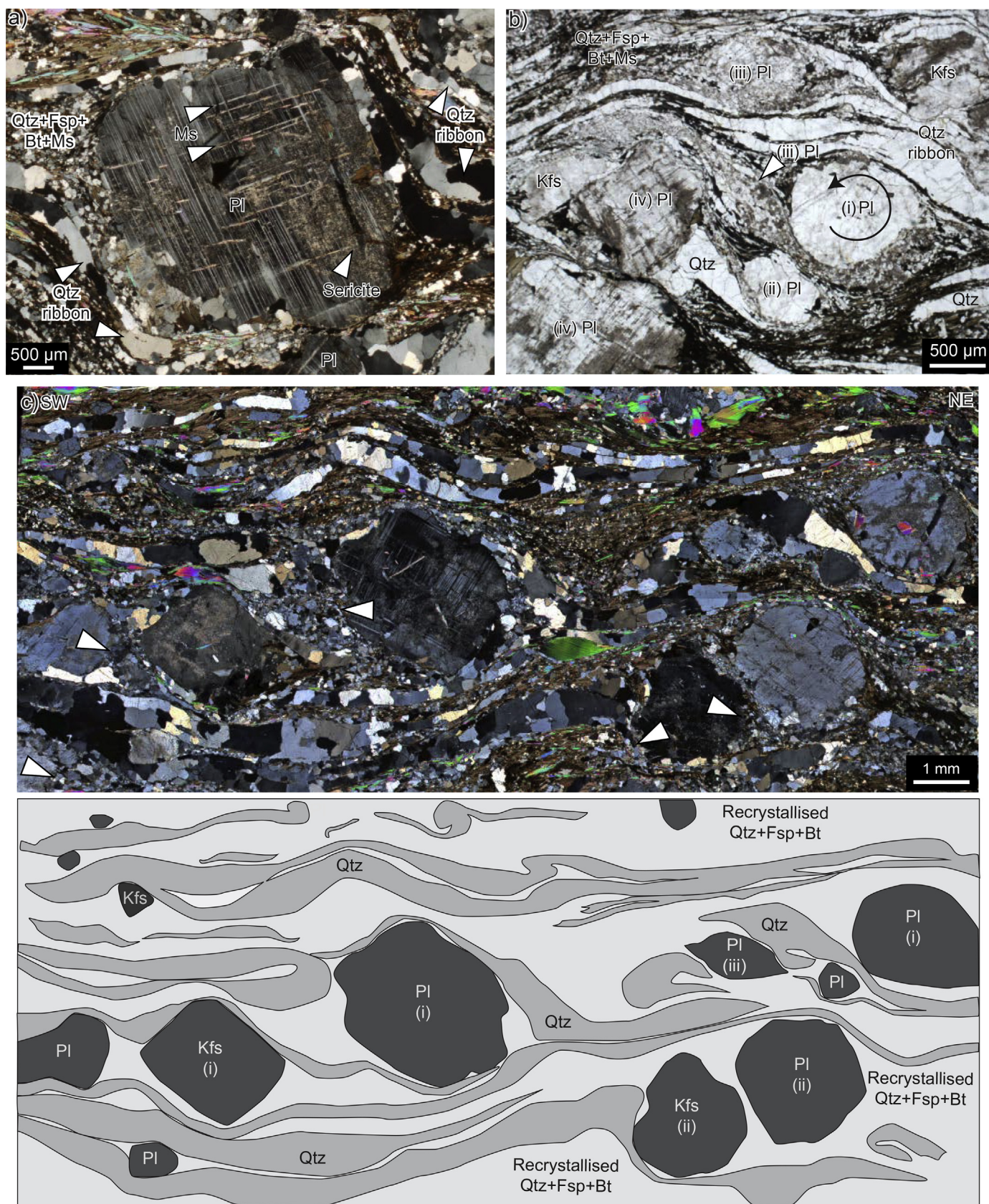
Fig. 8. Microstructures in deformed rocks after diatexites showing differences between protomylonites (a–c), mylonites (d), and ultramylonites (e,f). (a) Rounded plagioclase porphyroclast in protomylonite partially replaced by sericite with inclusions of muscovite parallel to twins. Quartz ribbons are longer than in mylonites and ultramylonites, wrap around the porphyroclast and show lobate boundaries and variable size indicating grain boundary migration (GBM) recrystallisation (XPL). (b) K-feldspar porphyroclasts in protomylonite show four different types of microstructure: rotation (grain *i*, indicated by circular arrow), partial (*ii*) to complete (*iii*) recrystallization, or are subhedral and sericitised
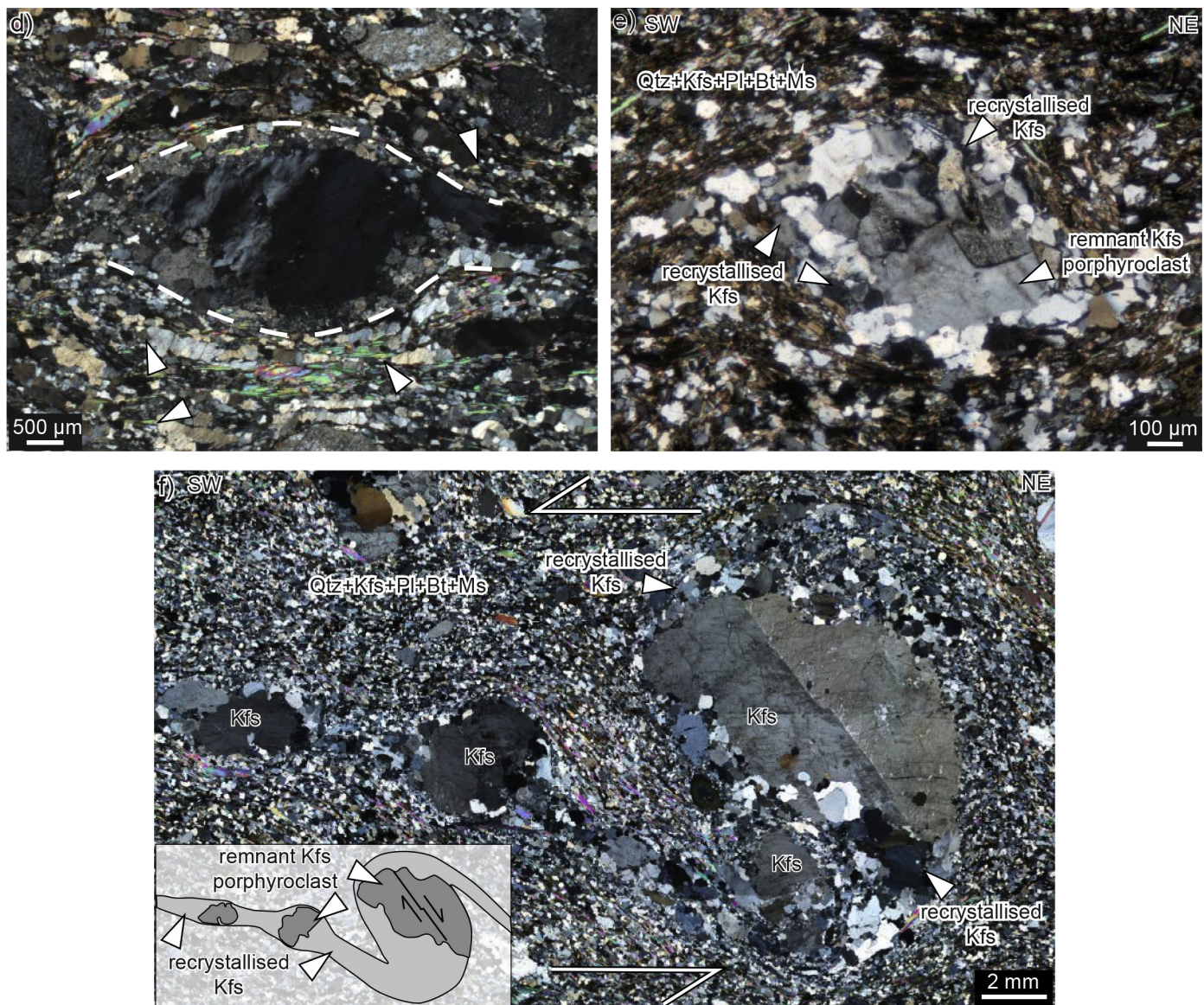
Fig. 8. (*continued*).

finely-comminuted, aphanitic matrix. The fragments contain single grains of quartz, feldspar, and muscovite and quartz ribbons which appear similar to those in the ultramylonitic host rock. Single grains of quartz and feldspar are up to 0.1 mm in diameter. In more altered rocks, feldspar is completely altered to very fine-grained sericite and larger grains are fractured with sericite concentrated on fractures. Biotite is absent from this region of brittle faulting.

Pseudotachylite consists of a black, aphanitic, glassy matrix with few fragments of wall rock or single grains of quartz and feldspar. The main generator vein is either foliation parallel or cross cuts the

foliation, and injection veins are common (Fig. 9b). The matrix in the pseudotachylite, breccia, and cataclasite is similar but in the pseudotachylite, the appearance of generator and injection veins with flow microstructures, suggests the matrix represents rapidly frozen silicate melt formed in the generator planes.

In the region of brittle faulting there are metre-scale folds that commonly occur close to fault planes. Folds are open and asymmetric with a mean fold axis of 162/30 (Fig. 2 inset) and axial planes defined by dissolution cleavage dip moderately south or east. The majority of fault planes dip moderately or steeply to the NE

(*iv*). The matrix is recrystallised and quartz ribbons wrap around porphyroclasts. Notice that a recrystallised ribbon of plagioclase wraps around feldspar clasts (e.g. centre grain, *iii*) showing the bi-modal behaviour of feldspar in protomylonites (PPL). (c) Protomylonite photomicrograph above and interpretative line drawing below: Most quartz ribbons are continuous and wrap around feldspar porphyroclasts which show rotation (*i*), and partial (arrows; *ii*) to complete (*iii*) recrystallisation. Quartz ribbons formed through high-temperature GBM are isoclinally folded in places (XPL). (d) Mylonite containing K-feldspar porphyroclast with recrystallised mantle (dashed lines) and an upper tail with sweeping undulose extinction. Unlike protomylonites, quartz ribbons pinch and swell and may be disaggregated into smaller, discontinuous ribbons (arrows; XPL). (e) Ultramylonite containing remnant K-feldspar porphyroclast core with recrystallised mantle. This mantle is misoriented from the remnant porphyroclast and subgrains are largely free of sericite (XPL). (f) Ultramylonite containing K-feldspar δ-clast showing top-to-SW shear sense. Tails are progressively disaggregated and recrystallised to form individual, isolated porphyroclasts. δ-clast shows brittle fracture along twinning plane, recrystallisation at margins, and rotation (XPL). Inset shows interpretation of microstructure.
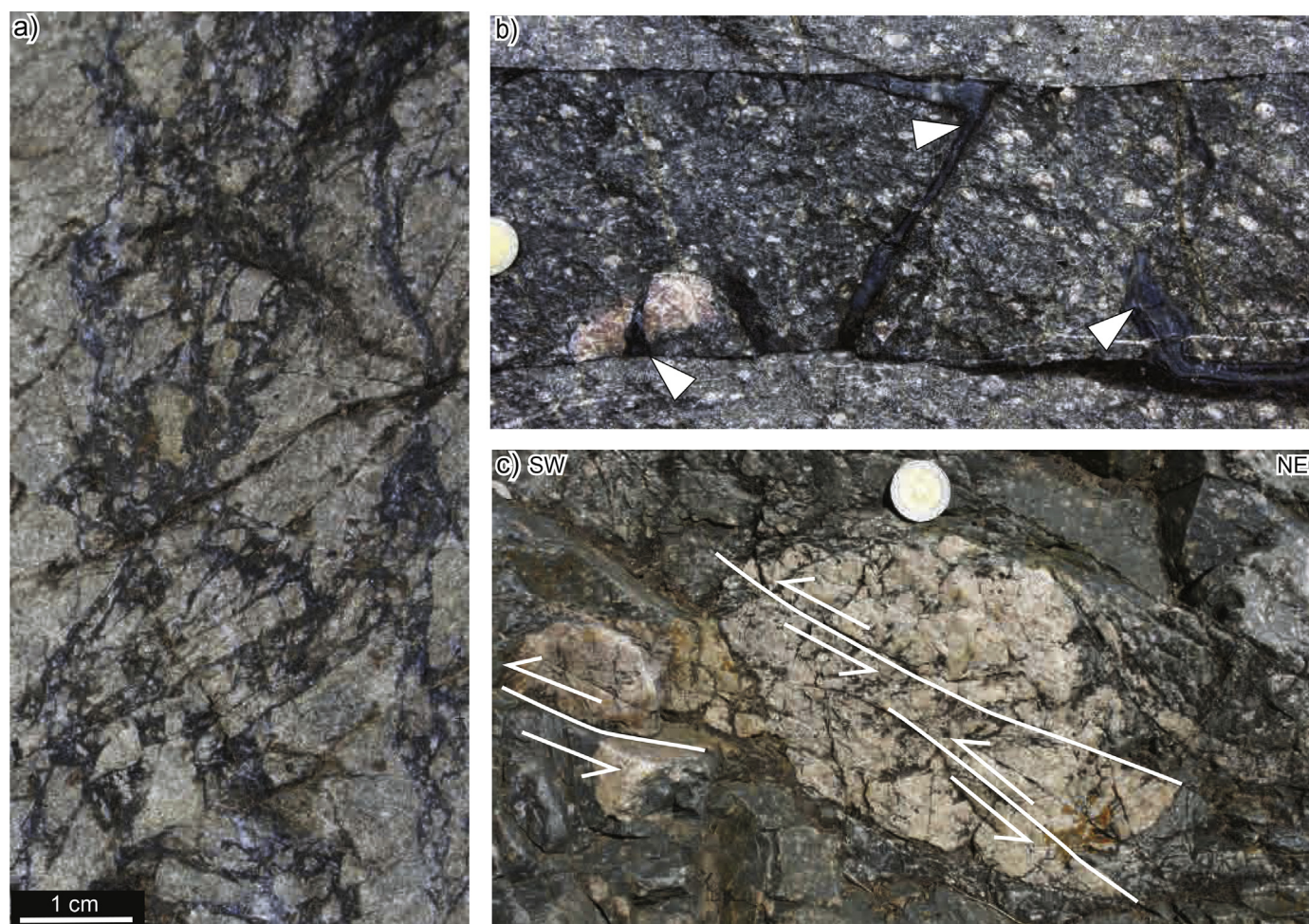
Fig. 9. Brittle overprint of ultramylonitic diatexites. (a) Ultramylonite altered and sericitised (lighter coloured rock), brecciated with cataclasite in fractures (darker rock). (b) Pseudotachylite in mylonitic diatexite. The horizontal planes are interpreted as generation surfaces and cross-cutting, glass-filled planes are injection veins (white arrowheads). In thin section glass, interpreted to represent frozen melt, is isotropic and contains flow structures and small, angular clasts. (c) Large clast from a pegmatite disaggregated during mylonitization and subsequently faulted. Note top-to-SW movement component.

although some dip SE or SW (Fig. 2 inset). While there is no discernible striation on the planes the faults consistently show thrust shear sense indicating thrusting generally to the WSW (Fig. 9c). On the stereonet the poles to the fault planes that are associated with the folds define a great circle indicating a common line of intersection at 140/34, not far from the average orientation of the fold axes. This is interpreted as the intermediate stress axis, σ_2, during faulting (Fig. 2 inset). σ_1 and σ_3 are on the great circle and are poorly defined because of the absence of a striation but we estimate σ_3 as plunging moderately W and σ_1 as moderately NE (Fig. 2 inset) on the basis of the inferred thrust sense on the faults (Fig. 9c). The folds associated physically with these faults may be kinematically related since fold axes are also oriented parallel to the intersections between fault planes, suggesting that they share a similar intermediate stress axis, σ_2 (Fig. 2 inset).

7. Geochemistry

In order to understand the possible role of fluids and element mobility in mylonitization, we analysed the different kinds of mylonitic rocks formed after diatexites and compared them to potential protoliths, including weakly deformed migmatites and granites from the Tolombón complex. Whole-rock major element analyses (Table 1) were conducted on a Bruker-AXS S4 Pioneer X-ray Fluorescence Spectrometer at the Advanced Analytical Centre at

James Cook University, Queensland, Australia. Trace element analyses (Table 1) were conducted on the ICP−MS at Monash University, Victoria, Australia.

Major element and REE analyses of migmatites and granites from the Tolombón complex define a wide field whereas the mylonitic rocks plot in a narrower band within this field (Fig. 10). Major element analyses show that mylonitic rocks are enriched in SiO_2 and TiO_2 relative to the rocks of the Tolombón complex. REE analyses indicate a negative Eu anomaly and a negative REE slope. Mylonitic rocks show a relative LREE enrichment and HREE depletion with La/Lu ratios between 8.05 and 18.13 (Fig. 10b,d). The rocks of the Tolombón complex define a broad field with granites generally enriched in LREE, and migmatites enriched in HREE. For both major element and REE analyses there is no systematic variation within the mylonitic rocks on the basis of degree of mylonitization.

In Section 3.5 we described field observations of weakly deformed granitic diatexite (at point SQ183) transitioning into the layer of ultramylonitic diatexite. We plotted the major element (Fig. 10c) and REE (Fig. 10d) abundances of two weakly deformed but different samples of granitic diatexite from outcrop SQ183 (Fig. 2) and one sample of mylonitic metatexite from outcrop SQ194 with samples of the ultramylonitic diatexites. The two weakly deformed granitic diatexites and the mylonitic metatexite are geochemically almost identical to each other and differ slightly from samples of the ultramylonitic diatexites showing lower HREE and higher LREE.

Table 1
Major and rare earth element analyses of mylonitic rocks and their protoliths from the Tolombón complex.

Description	Ultramylonite						Mylonite				Protomylonite		Granite						
Sample	SQ187c	SQ80a	SQ29b	SQ37b	SQ77c	SQ79a	SQ187a	SQ187d	SQ29a	SQ77b	SQ77a	SQ30a	SQ133	SQ134	SQ130a	SQcrdgr	SQ144	SQ131	SQ70c
Wt.% oxide																			
SiO_2	67.20	71.99	69.48	67.72	69.55	69.09	67.56	67.19	69.07	69.83	68.95	69.47	74.10	72.47	71.90	68.58	65.99	71.52	73.33
TiO	0.74	0.72	0.74	0.95	0.69	0.72	0.73	0.69	0.73	0.66	0.76	0.77	0.04	0.23	0.23	0.64	0.60	0.23	0.36
Al_2O_3	14.14	13.18	14.01	14.79	14.57	14.68	14.59	13.96	14.45	14.46	14.15	14.03	14.10	14.99	15.06	14.85	15.28	15.16	13.85
FeO	5.13	4.70	4.90	5.79	4.46	4.50	4.96	4.57	4.72	4.35	4.93	4.93	0.46	1.98	2.18	4.38	4.73	1.92	1.70
MnO	0.10	0.06	0.09	0.11	0.06	0.07	0.09	0.07	0.07	0.06	0.08	0.08	0.01	0.03	0.09	0.05	0.08	0.04	0.02
MgO	2.13	2.04	1.79	2.86	1.66	1.65	1.99	2.33	1.77	1.56	1.86	2.07	0.06	0.81	0.69	2.31	2.18	0.81	0.66
CaO	1.72	0.85	1.49	1.60	1.33	1.52	1.67	2.71	1.82	0.60	1.58	1.52	0.33	2.28	1.79	1.08	1.52	1.76	1.11
Na_2O	2.46	1.77	2.47	1.98	2.43	2.63	2.30	2.53	2.81	2.69	2.23	2.03	2.70	4.22	3.69	1.77	2.65	3.75	2.65
K_2O	4.09	2.71	3.53	3.53	3.56	3.69	3.60	3.27	3.40	3.63	3.50	3.53	6.72	1.40	3.53	4.44	4.31	3.57	5.50
P_2O_5	0.11	0.13	0.20	0.08	0.23	0.21	0.09	0.31	0.19	0.24	0.23	0.17	0.12	0.14	0.17	0.29	0.29	0.20	0.13
Total	97.82	98.15	98.70	99.41	98.54	98.76	97.58	97.63	99.03	98.08	98.27	98.60	98.64	98.54	99.34	98.38	97.63	98.95	99.31
Chondrite normalised																			
Ce	161.95	139.62					165.67	116.10			140.27	117.90	37.70	111.76	60.82	104.99	109.11	72.26	
Pr	121.69	103.54					123.70	89.75			102.16	89.55	30.68	84.65	47.22	81.24	82.88	55.87	
Nd	93.44	78.12					94.33	70.10			77.80	68.38	23.49	64.57	36.25	64.33	63.63	42.18	
Sm	62.67	50.16					62.18	51.14			52.71	44.79	19.46	43.20	27.33	45.27	44.93	29.22	
Eu	22.16	22.67					23.04	22.14			21.57	19.78	9.57	14.97	13.51	25.88	19.32	13.66	
Gd	43.10	31.48					39.52	35.10			35.06	29.93	14.94	27.12	18.40	30.62	29.30	18.48	
Tb	41.57	27.10					33.08	30.58			32.02	26.64	16.47	23.52	18.24	29.27	26.25	16.69	
Dy	38.82	22.52					27.73	22.86			27.81	22.94	16.15	19.83	16.76	24.43	21.56	13.57	
Ho	39.91	20.94					25.51	17.64			26.14	21.97	16.39	18.33	16.51	19.31	18.96	11.64	
Er	36.73	18.98					20.73	13.02			23.60	19.92	15.10	16.40	16.01	12.40	16.16	9.81	
Tm	30.58	16.97					15.49	9.61			20.47	17.51	12.94	14.26	15.60	6.84	13.73	8.48	
Yb	27.39	16.24					12.89	8.59			19.38	16.43	11.65	13.71	16.18	4.65	12.75	8.03	
Lu	26.07	16.05					11.68	8.38			18.52	15.59	10.83	13.31	16.15	3.97	12.09	7.62	

Description	Granitic diatexite						Stromatic metatexite				Melanosome				Leucosome
Sample	SQ183	SQ183b	SQ132a	SQ120a	SQ114	SQ136c	SQ37a	SQ90c	SQ194a	SQ47a1	SQ50c	SQ65	SQ73a2	SQ136b	SQ70a	SQ132b	SQ50b
Wt.% oxide																	
SiO_2	68.79	66.43	73.11	62.93	67.97	62.63	69.12	74.56	62.75	42.68	61.39	65.31	64.46	67.73	73.38	67.43	71.43
TiO	0.58	0.81	0.58	0.67	0.89	1.17	0.69	0.62	0.89	1.36	0.88	0.90	0.93	0.76	0.72	0.75	0.16
Al_2O_3	13.84	13.83	12.36	17.45	14.58	16.55	13.80	10.43	16.37	28.44	17.30	15.99	16.80	14.74	12.60	15.51	16.53
FeO	5.34	5.77	4.33	6.40	4.94	8.61	4.15	3.81	8.08	11.65	8.86	6.42	5.17	6.78	4.20	6.35	2.31
MnO	0.11	0.06	0.12	0.16	0.07	0.08	0.06	0.08	0.15	0.17	0.14	0.07	0.05	0.07	0.04	0.10	0.03
MgO	2.29	2.65	1.52	2.52	2.23	2.52	1.99	1.56	2.82	5.59	3.10	3.05	2.69	2.43	2.06	2.61	0.61
CaO	2.41	1.38	0.92	1.54	1.96	2.08	2.32	1.24	0.97	0.50	0.77	1.58	1.49	1.57	1.66	1.22	0.68
Na_2O	2.35	1.81	1.96	2.30	3.46	2.46	2.43	2.13	2.21	0.79	1.58	2.32	3.08	2.17	2.17	2.13	2.02
K_2O	2.81	4.27	3.91	4.50	2.53	2.55	3.35	2.98	3.96	5.66	3.80	2.65	3.94	2.89	2.43	2.91	4.77
P_2O_5	0.13	0.07	0.09	0.34	0.09	0.09	0.08	0.08	0.10	0.09	0.08	0.11	0.14	0.09	0.15	0.08	0.08
Total	98.65	97.08	98.89	98.81	98.73	98.73	97.99	97.49	98.30	96.93	97.90	98.39	98.74	99.22	99.40	99.08	98.62
Chondrite normalised																	
Ce	203.48	170.83	136.15	130.35	143.38	287.38	146.36	59.07	149.72		173.63	148.76	160.97	188.14	148.68		
Pr	154.40	127.12	100.90	96.62	103.72	207.88	109.91	43.70	108.66		119.68	113.21	117.78	141.79	109.24		
Nd	119.38	96.85	76.28	74.28	77.87	156.91	82.91	32.55	81.94		88.45	88.90	89.44	108.42	82.61		
Sm	73.51	57.61	49.33	53.36	49.43	93.58	53.97	22.52	52.21		53.62	57.17	55.25	71.11	52.09		
Eu	24.60	22.39	18.01	20.55	14.39	25.26	25.18	10.11	25.26		23.13	27.65	30.27	27.89	22.14		
Gd	44.28	33.66	32.36	40.41	30.75	55.47	33.25	17.89	34.48		33.38	35.54	34.63	44.05	32.36		
Tb	32.38	24.05	28.92	44.72	26.18	39.79	29.36	23.23	29.89		27.55	27.61	27.72	32.49	25.77		
Dy	23.04	17.20	26.30	46.69	20.91	26.28	26.53	29.64	22.94		22.37	19.24	20.91	21.00	18.79		
Ho	18.00	13.20	27.43	52.42	17.84	18.50	28.21	39.74	17.92		20.32	13.84	17.25	13.85	14.66		
Er	13.74	9.96	27.47	55.64	14.58	11.98	29.55	47.04	13.52		18.22	9.57	13.71	8.07	10.93		
Tm	10.76	7.77	27.03	55.10	11.17	7.42	28.27	49.74	10.39		16.15	6.71	10.71	4.47	8.05		
Yb	10.32	7.35	28.95	57.49	9.21	5.85	28.27	52.92	9.11		15.49	5.84	9.60	3.45	7.03		
Lu	10.31	7.34	29.40	59.56	8.14	5.36	27.13	55.72	8.59		15.36	5.62	9.39	3.10	6.66		

8. Discussion

Very few shear zones worldwide contain ultramylonites that are as thick as the PSZ. Here we discuss the geochemistry, shear strain, and tectonic setting of the PSZ to constrain the environment and understand the context in which thick ultramylonites develop.

8.1. Protolith of the mylonitic rocks

The nature of the protolith to the mylonitic rocks can be seen in transition zones between weakly deformed rocks and mylonitic rocks both for metatexites and diatexites. These transitions suggest that the Tolombón complex rocks are the protolith to the mylonitic
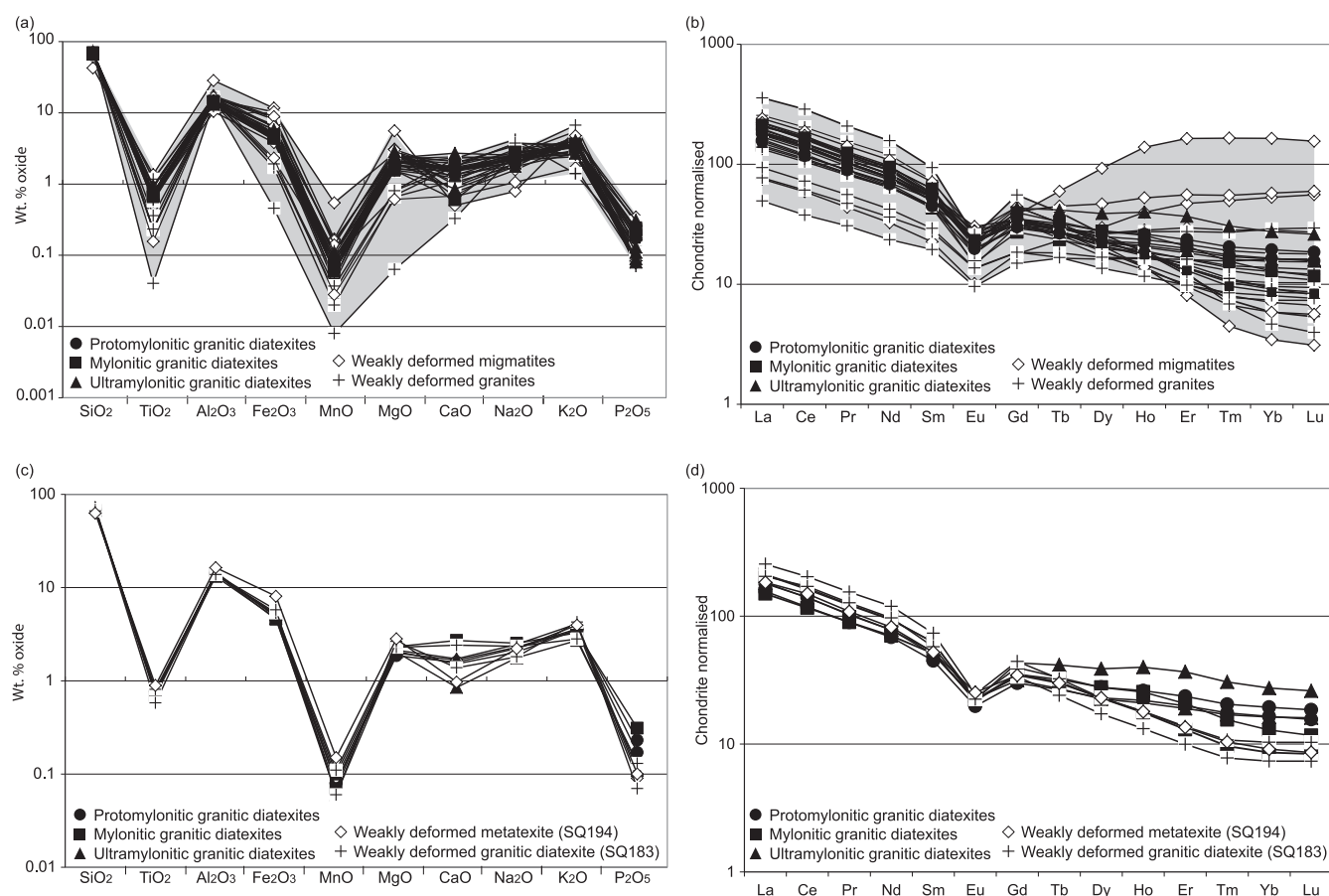
Fig. 10. (a) Major element and (b) chondrite-normalised (Sun and McDonough, 1989) REE abundances of weakly deformed migmatites and granites of the Tolombón complex (white symbols) and of the mylonitic rocks from the ultramylonitic diatexite layer of the El Pichao shear zone (black symbols). Spread of data of weakly deformed migmatites and granites defines a field (shaded in grey) which encompasses the narrower band defined by mylonitic rocks. (c) Major element and (d) chondrite-normalised REE abundances of migmatitic rocks that transition directly into mylonitic rocks.

rocks of the PSZ as further supported by the geochemistry. The fact that the mylonites show less compositional variation than the protoliths (Fig. 10) suggests the possibility of homogenization through shearing, which stretched and folded layering and caused mixing of phases through rotation of porphyroclasts (Fig. 8b,c,f). There is no systematic difference in geochemistry between protomylonites, mylonites, and ultramylonites. Taken together, this indicates that mylonitization was not accompanied by a progressive change in the chemistry of the rock, as has been identified in other shear zones (e.g. Oliot et al., 2010; Goncalves et al., 2012).

Structurally above the PSZ, strain decreases and the migmatites contain structures that indicate that melt was present during and facilitated folding and thrusting to the W, suggesting syn-kinematic anatexis (Fig. 4d,e; see Büttner et al., 2005; Weinberg and Mark, 2008; Weinberg et al., 2013). Deformation within the PSZ overprints and folds these early structures during amphibolite facies solid-state deformation that maintains broadly similar kinematics to the syn-anatectic deformation. This suggests that anatexis began during shearing and ceased with cooling as the rocks were thrust to higher structural levels. This cooling may have caused localization of thrusting to the PSZ where solid-state shearing continued.

8.2. Strain on the PSZ

From weakly deformed to mylonitic metatexites, there is a gradual strain increase described including an increase in the intensity of the foliation and the proportion of recrystallised matrix.

Strain increases further in the ultramylonitic diatexites, characterized by the nearly completely recrystallized matrix and naked clasts. Unlike mylonites, the foliation in ultramylonitic diatexites is poorly developed because mica-rich bands and quartz ribbons are absent. This is likely due to mixing and homogenization of the matrix facilitated by rolling feldspar clasts (Fig. 8a–c,f) and dissolution–precipitation of feldspars.

There is also a general decrease in grain size from protomylonitic to ultramylonitic rocks. Grain size is dependent, among other things, on temperature as well as stress, and it could be argued that the gradual decrease in grain size reflects a decrease in temperature and strain localization to zones of higher stresses. If this occurred, shearing in the PSZ would be at higher temperatures in the protomylonite and mylonite than in ultramylonite. While this is possible, the similarity in microstructures across the width of the shear zone indicates that shearing occurred at amphibolite facies in all rocks and so temperature variations were limited to between 500 and 700 °C. It is also possible that, independent of any temperature variations, stress distribution varied as a function of rock strength. As demonstrated by Regenauer-Lieb et al. (2006), it is possible that the system is controlled by neither constant strain rate nor constant stress (Platt and Behr, 2011) but by maximum energy dissipation. In this case weaker regions are zones of both high stress and high strain rate, and focus energy dissipation of the system. Thus, the decrease in grain size in ultramylonites would be a result of dynamic stress distribution.

The thickness of the ultramylonitic diatexite layer of the PSZ is estimated from its present-day dip and width across strike, disconsidering any possible post-shearing and mylonitization modifications caused by folding and faulting. The intra-mylonite folding is only minor and does not account for significant width modifications. Evidence for some post-mylonitization thickening is seen in the region of brittle overprint (Section 6) where pseudotachylites, breccias and brittle faults with a thrusting component may have caused some stacking of fault slivers. We are unable to ascertain if this brittle zone caused major repetition of fault slivers, however, our field evidence suggests relatively minor movements. If brittle faulting was a significant process and caused stacking of the shear zone, the continuous ultramylonitic layers on the footwall and hanging wall of the fault zone would still be hundreds of metres thick (Fig. 2).

Traditional methods to estimate strain in ductile shear zones use the angle between planes, deflection of markers, and changes in volume and shape of sheared objects (Ramsay and Graham, 1970; Ramsay, 1980). However, these structures are deformed to their maximum extent at shear strains lower than that required to form an ultramylonite because, for example, grains have been recycled several times (Norris and Cooper, 2003) and S planes are parallel to C planes at $\gamma \sim 29$ (using the method of Ramsay and Graham, 1970). Norris and Cooper (2003) estimated shear strain using the statistical change in thickness of pegmatite dykes. They found $\gamma > 120$ in mylonites and $\gamma > 180$ in ultramylonites, an order of magnitude higher than estimates using other methods (e.g. Mawer, 1983; Bailey et al., 1994; Wenk, 1998).

The PSZ ultramylonites show almost complete recrystallization of the matrix and homogenization of layering, destruction of quartz ribbons, and lack well-defined S–C fabric. Accordingly, there is no accurate way to estimate the total amount of movement. Given the current 40° dip of the shear zone, and the relatively small differences in metamorphic conditions between the hanging wall (granulite facies) and footwall (amphibolite facies), we postulate that the thrust had only a relatively small throw. This would imply either a small total movement, that the dip decreases at depth, or that the shear zone has steepened as a result of later (Andean?) crustal tilting.

8.3. Mylonitic shear zones of the Sierras Pampeanas

The Sierras Pampeanas include some very prominent shear zones such as the 16 km-thick Tres Arboles or Guachacorral shear zone in the Sierras de Córdoba (Fig. 1; Whitmeyer and Simpson, 2003) and the 4 km-thick La Chilca shear zone (Larrovere et al., 2008). These shear zones trend N–S, thrust rocks to the west (Le Corre and Rossello, 1994; van Staal et al., 2011), and formed during the Pampean and Famatinian orogenies, between 535 and 450 Ma, with some dating to the Oclóyic tectonic phase between 450 and 430 Ma (Dalla Salda et al., 1992; Rapela et al., 1998a; Astini and Davila, 2004; Collo et al., 2008; Castro de Machuca et al., 2012). Similar to all major shear zones in the Sierras Pampeanas, the PSZ places higher grade rocks (Tolombón complex) on lower grade rocks (Agua del Sapo complex), which is compatible with thrusting, and contradicts the interpretation by Büttner (2009) that this is a tilted extensional terrane.

In Sierra de Quilmes, a terrane undergoing anatexis at 470 Ma, perhaps part of the Famatinian back-arc, was thrust to higher structural levels by generalised ductile shearing, such as recorded by syn-kinematic leucosomes in rocks north of the PSZ, near Laguna (Fig. 1b). These rocks cooled, anatexis ceased, and strain localized into the 3.5 km-wide PSZ. Localization of strain to the PSZ may have caused cessation of shearing north of the PSZ preserving high-temperature magmatic structures. In the PSZ

shearing continued at amphibolite facies producing the ultramylonites and mylonites which obliterated the pre-existing high-temperature structures. Localization during cooling has also been inferred for the Arenosa Creek shear zone in the western Sierras Pampeanas where shearing began at granulite facies conditions (>800 °C) and continued to temperatures of 500–700 °C (Castro de Machuca et al., 2012). This is also similar to the Tres Arboles shear zone (Fig. 1a) which underwent migmatization during the Pampean Orogeny and records deformation temperatures between 540 and 590 °C and pressures of 3–6 kbar (Whitmeyer and Simpson, 2003). Other shear zones of the Sierras Pampeanas show greenschist–amphibolite facies shearing with no evidence of an early higher temperature event. For example, the El Tigre shear zone (Fig. 1a) deformed at temperatures of 300–400 °C (Fig. 1a; Castro de Machuca et al., 2010), the Las Pirquitas thrust formed at amphibolite facies (Fig. 1a; van Staal et al., 2011) and La Chilca shear zone (Fig. 1a) deformed at temperatures of 350–500 °C but also overprints migmatites (Larrovere et al., 2008).

The brittle overprint mapped within the PSZ has also been recorded in other mylonitic shear zones of the Sierras Pampeanas (e.g. Whitmeyer and Simpson, 2003; Delpino et al., 2007). The Sierras Pampeanas have a long history of tectonic activity and such low-temperature deformation could be related to tectonic events in the Mesozoic or Cenozoic (e.g. Delpino et al., 2007).

The length, breadth, and strain documented in the Sierras Pampeanas makes these shear zones of the Pampean and Famatinian orogenies comparable to major shear zones worldwide such as the shear zones of the Pan-African orogeny (Ferkous and Leblanc, 1995; Arthaud et al., 2008), the Mulgandinnah shear zone of the accreted Pilbara terrane in Australia (Zegers et al., 1998), and the Variscan Corredoiras detachment in NW Spain (Díaz García et al., 1999).

8.4. Processes that form thick ultramylonites

Thick ultramylonites are rare and whilst we have a reasonable understanding of the processes that form them (e.g. Poirier, 1980; White et al., 1980; Means, 1995; Kilian et al., 2011; Platt and Behr, 2011; Vauchez et al., 2012), we do not have a good understanding of what controls their final width. Shear zone width is dependent on strain rate, the total amount of strain, and the strength and strength evolution of the shear zone and surrounding rocks during deformation. At upper amphibolite to granulite facies, rock strength is low and strain is distributed producing a thick, low-strain shear zone (Vauchez et al., 2012). At lower temperatures, rock strength increases, which promotes strain localisation enabling formation of thin bands of ultramylonite. However, such variations cannot explain the existence of thick packages of ultramylonites. It has been suggested that the formation of thick shear zones requires shear zone widening which can occur when the rock on the margin of the shear zone becomes easier to deform than the shear zone interior (Means, 1995). This can be due to microstructural changes in the shear zone leading to strain-hardening or changes in the host rock which make it softer and easier to deform (Means, 1984; Hull, 1988; Mitra, 1992; Ingles et al., 1999; Rutter, 1999). Strain-hardening can occur through the accumulation of dislocations and changes in the style or mechanism of deformation (Passchier and Trouw, 2005; Johnson et al., 2011) or reaction-hardening through the growth of new minerals (Groome et al., 2006). The rock is strengthened and more difficult to deform due to the destruction of mica-rich shear planes or an increase in the proportion of dislocation tangles (Passchier and Trouw, 2005). Reaction induced softening can occur in the shear zone or in the host rock and is caused by the growth of new, softer minerals (White and Knipe, 1978; Hippertt and Hongn, 1998).

The thick shear zones formed during the Pampean–Famatinian orogenies suggest that only a few major shear zones accommodated most of the crustal shortening driven by plate convergence. In the absence of significant rheological layering capable of controlling strain localization, the width of a shear zone may be determined by the balance between shear heat generation and diffusion. Small initial perturbations in shear heating localize the initial shear zone, which grows in width as a result of heat diffusion into colder surroundings. A quasi-static state can be reached, where the width of the shear zone (w) is:

$$w \sim \sqrt{\kappa/\dot{\varepsilon}} \tag{1}$$

where $\dot{\varepsilon}$ is the strain rate and the κ is thermal diffusivity (Regenauer-Lieb and Yuen, 2004). For $\kappa = 10^{-6}$ m^2 s^{-1} and strain rate between 10^{-14} s^{-1} and 10^{-12} s^{-1}, equation (1) yields a shear zone between 10 and 1 km thick, bracketing the 3.5 km width of the PSZ. If we assume that the 1 km-thick ultramylonitic section took up most of the strain across the shear zone, and impose a velocity of 30 mm/yr across that part of the shear zone, implying that it accommodates a significant proportion of characteristic plate convergence velocities, the strain rate across the ultramylonite would be 10^{-12} s^{-1}. For these values, a steady-state width balancing heat generation and diffusion would have been reached in only ~0.03 Ma ($t \sim w^2/\kappa$). Thus, we postulate that the dominance of very wide shear zones across the Pampean–Famatinian orogens of NW Argentina is a result of localization of strain into few dominant shear zones whose widths are controlled by the balance between shear heating and thermal diffusion.

9. Conclusions

The El Pichao shear zone is a >3.5 km thick shear zone that thrusts the granulitic migmatites of the Tolombón complex on the amphibolite facies rocks of the Agua del Sapo complex. At its base the shear zone comprises a ~1 km-thick ultramylonitic diatexite with a very fine, intensely recrystallized groundmass, a weak foliation, and naked clasts, generally from disrupted pegmatites. Strain decreases gradually to the NE until weakly deformed metatexites, diatexites, and granites crop out. Geochemistry indicates that the composition of the mylonitic rocks is similar to that of migmatites and granites, but less varied. We interpret this to indicate that the mylonitic rocks have been homogenized by stretching and folding but in an essentially closed system with negligible fluid and element mobility.

The Sierras Pampeanas is a high strain zone that has a discontinuous extent of over 1000 km and a width of 250 km (Larrovere et al., 2011) with a network of wide shear zones comparable in length and breadth to those of major orogens worldwide. Thick bands of mylonites and ultramylonites of the Sierras Pampeanas have accommodated top-to-west thrusting during the Pampean and Famatinian orogenies. In the PSZ anatexis was contemporaneous with the early stages of thrusting and preceded localization into the shear zone, which continued to deform in amphibolite facies eventually thrusting migmatites onto lower grade rocks. The shear zone was later reactivated and overprinted during brittle faulting at greenschist facies.

Thick ultramylonites such as those in the PSZ, although rare, bring up questions regarding the controls on the width of shear zones and strain distribution in an orogeny, together with questions regarding the distribution of stress and strain rate across a deforming mountain belt, and the nature and extent of strain localization. We speculate that in the absence of significant rheological heterogeneities, shear heating localizes crustal strain to a few wide shear zones capable of taking up a large proportion of plate convergence velocity and forming thick mylonite–ultramylonite belts, as is common in the Pampean–Famatinian orogens.

References

Acenolaza, F.G., Miller, H., Toselli, A.J., 1988. The Puncoviscana Formation (Late Precambrian–Early Cambrian) – sedimentology, tectonometamorphic history and age of the oldest rocks of NW Argentina. In: Bahlburg, H., Breitkreuz, C., Giese, P. (Eds.), The Southern Central Andes, Lecture Notes in Earth Sciences, vol. 17. Springer-Verlag, Berlin.

Arthaud, M.H., Caby, R., Fuck, R.A., Dantas, E.L., Parente, C.V., 2008. Geology of the northern Borborema Province, NE Brazil and its correlation with Nigeria, NW Africa. In: Pankhurst, R., Trouw, R.A.J., Brito Neves, B.B., de Wit, M.J. (Eds.), West Gondwana: Pre-Cenozoic Correlations across the South Atlantic Region, vol. 294. Geological Society of London, pp. 49–67.

Astini, R.A., Davila, F.M., 2004. Ordovician back arc foreland and Oclóyic thrust belt development on the western Gondwana margin as a response to Precordillera terrane accretion. Tectonics 23, TC4008.

Bahlburg, H., Herve, F., 1997. Geodynamic evolution and tectonostratigraphic terranes of northwestern Argentina and northern Chile. GSA Bull. 109 (7), 869–884.

Bailey, C.M., Simpson, C., De Paor, D.G., 1994. Volume loss and tectonic flattening strain in granitic mylonites from the Blue Ridge province, central Appalachians. J. Struct. Geol. 16 (10), 1403–1416.

Becchio, R., Lucassen, F., Kasemann, S.F., Franz, G., Viramonte, J., 1999. Geoquimica y sistematica isotopica de rocas metamorficas del Paleozoico inferior: Noroeste de Argentina y Norte de Chile (21°–27°S). Acta Geol. Hisp. 34, 273–299.

Büttner, S.H., 2009. The Ordovician Sierras Pampeanas–Puna basin connection: basement thinning and basin formation in the Proto-Andean back-arc. Tectonophysics 477 (3–4), 278–291.

Büttner, S.H., Glodny, J., Lucassen, F., Wemmer, K., Erdmann, S., Handler, R., Franz, G., 2005. Ordovician metamorphism and plutonism in the Sierra de Quilmes metamorphic complex: implications for the tectonic setting of the northern Sierras Pampeanas (NW Argentina). Lithos 83 (1–2), 143–181.

Castro de Machuca, B., Delpino, S., Previley, L., Mogessie, A., Bjerg, E., 2012. Tectono-metamorphic evolution of a high- to medium-grade ductile deformed meta-gabbro/metadiorite from the Arenosa Creek Shear Zone, Western Sierras Pampeanas, Argentina. J. Struct. Geol. 42, 261–278.

Castro de Machuca, B., Morata, D., Pontoriero, S., Arancibia, G., 2010. Textural variations and chemical mobility during mylonitization: the El Tigre granitoid shear zone, Sierra de Pie de Palo, Western Sierras Pampeanas, San Juan. Rev. Asoc. Geol. Argent. 66 (1), 54–65.

Collo, G., Astini, R.A., Cardona, A., Do Campo, M.D., Cordani, U., 2008. Metamorphic ages of low-grade units in the central region of Famatina: the signature of the Oclóyic Orogeny (Ordovician). Rev. Geol. Chile 35 (2), 191–213.

Dalla Salda, L.H., Cingolani, C.A., Varela, R., 1992. Early Paleozoic orogenic belt of the Andes in southwestern South America: result of Laurentia–Gondwana collision? Geology 20, 617–620.

Delpino, S.H., Bjerg, E.A., Ferracutti, G.R., Mogessie, A., 2007. Counterclockwise tectonometamorphic evolution of the Pringles metamorphic complex, Sierras Pampeanas of San Luis (Argentina). J. South Am. Earth Sci. 23 (2–3), 147–175.

Díaz García, F., Martínez Catalán, J.R., Arenas, R., González Cuadra, P., 1999. Structural and kinematic analysis of the Carredoiras detachment: evidence for early Variscan synconvergent extension in the Ordenes Complex, NW Spain. Int. J. Earth Sci. 88, 337–351.

Ferkous, K., Leblanc, M., 1995. Gold mineralisation in the West Hoggar shear zone, Algeria. Miner. Deposita 30, 211–224.

Fliervoet, T.F., White, S.H., Drury, M.R., 1997. Evidence for dominant grain-boundary sliding deformation in greenschist – and amphibolite-grade polymineralic ultramylonites from the Redbank deformed Zone, Central Australia. J. Struct. Geol. 19 (12), 1495–1520.

Garlick, S.R., Gromet, L.P., 2004. Diffusion creep and partial melting in high temperature mylonitic gneisses, Hope Valley shear zone, New England Appalachians, USA. J. Metamorph. Geol. 22, 45–62.

Goncalves, P., Oliot, E., Marquer, D., Connolly, J.A.D., 2012. Role of chemical processes on shear zone formation: an example from the Grimsel metagranodiorite (Aar massif, Central Alps). J. Metamorph. Geol. 30 (7), 703–722.

Griera, A., Bons, P.D., Jessell, M.W., Lebensohn, R.A., Evans, L., Gomez-Rivas, E., 2011. Strain localisation and porphyroclast rotation. Geology 39 (3), 275–278.

Groome, W.G., Johnson, S.E., Koons, P.O., 2006. The effects of porphyroblast growth on the effective viscosity of metapelitic rocks: implications for the strength of the middle crust. J. Metamorph. Geol. 24 (5), 389—407.

Hanmer, S., Williams, M., Kopf, C., 1995. Modest movements, spectacular fabrics in an intracontinental deep-crustal strike-slip fault: striding-Athabasca mylonite zone, NW Canadian Shield. J. Struct. Geol. 17 (4), 493—507.

Hippertt, J.F., 1998. Breakdown of feldspar, volume gain and lateral mass transfer during mylonitization of granitoid in a low metamorphic grade shear zone. J. Struct. Geol. 20 (2—3), 175—193.

Hippertt, J.F., Hongn, F.D., 1998. Deformation mechanisms in the mylonite/ultramylonite transition. J. Struct. Geol. 20 (11), 1435—1448.

Hirth, G., Tullis, J., 1992. Dislocation creep regimes in quartz aggregates. J. Struct. Geol. 14 (2), 145—159.

Höckenreiner, M., Söllner, F., Miller, H., 2003. Dating the TIPA shear zone: an Early Devonian terrane boundary between the Famatinian and Pampean systems (NW Argentina). J. South Am. Earth Sci. 16 (1), 45—66.

Hongn, F., Becchio, R., 1999. Las fajas miloniticas de Brealito, basamento del Valle Calchaqui, Salta, Argentina. Rev. Asoc. Geol. Argent. 54, 74—87.

Hongn, F.D., Mon, R., Cuevas, J., Tubia, J.M., 1996. Zones de cisaillement calédoniennes à haute température dans la quebrada Barranquilla (Puna Orientale, Argentina): données structurales et cinématiques. Comp. Rend. Acad. Sci. Paris, IIa 323, 809—815.

Hongn, F.D., Riller, U., 2007. Tectonic evolution of the western margin of Gondwana inferred from syntectonic emplacement of Paleozoic granitoid plutons in Northwest Argentina. J. Geol. 115 (2), 163—180.

Hongn, F.D., Tubia, J.M., Aranguren, A., Vegas, N., Mon, R., Dunning, G.R., 2010. Magmatism coeval with lower Paleozoic shelf basins in NW-Argentina (Tastil batholith): constraints on current stratigraphic and tectonic interpretations. J. South Am. Earth Sci. 29 (2), 289—305.

Hull, J., 1988. Thickness—displacement relationships for deformation zones. J. Struct. Geol. 10 (4), 431—435.

Ingles, J., Lamouroux, C., Soula, J.-C., Guerrero, N., Debat, P., 1999. Nucleation of ductile shear zones in a granodiorite under greenschist facies conditions, Neouvielle massif, Pyrenees, France. J. Struct. Geol. 21 (5), 555—576.

Ishii, K., Kanagawa, K., Shigematsu, N., Okudaira, T., 2007. High ductility of K-feldspar and development of granitic banded ultramylonite in the Ryoke metamorphic belt, SW Japan. J. Struct. Geol. 29 (6), 1083—1098.

Jefferies, S.P., Holdsworth, R.E., Wibberley, C.A.J., Shimamoto, T., Spiers, C.J., Niemeijer, A.R., Lloyd, G.E., 2006. The nature and importance of phyllonite development in crustal-scale fault cores: an example from the Median Tectonic Line, Japan. J. Struct. Geol. 28 (2), 220—235.

Jessell, M.W., Siebert, E., Bons, P.D., Evans, L., Piazolo, S., 2005. A new type of numerical experiment on the spatial and temporal patterns of localization of deformation in a material with a coupling of grain size and rheology. Earth Planet. Sci. Lett. 239, 309—326.

Jezek, P., Willner, A.P., Acenolaza, F.G., Miller, H., 1985. The Puncoviscana trough — a large basin of Late Precambrian to Early Cambrian age on the Pacific edge of the Brazilian shield. Geol. Rundsch. 74 (3), 573—584.

Ji, S., Jiang, Z., Rybacki, E., Wirth, R., Prior, D., Xia, B., 2004. Strain softening and microstructural evolution of anorthite aggregates and quartz—anorthite layered composites deformed in torsion. Earth Planet. Sci. Lett. 222 (2), 377—390.

Johnson, S.E., Jin, Z.-H., Naus-Thijssen, F.M.J., Koons, P.O., 2011. Coupled deformation and metamorphism in the roof of a tabular midcrustal igneous complex. GSA Bull. 123 (5—6), 1016—1032.

Jordan, T.E., Allmendinger, R.W., 1986. The Sierras Pampeanas of Argentina: a modern analogue of Rocky Mountain foreland deformation. Am. J. Sci. 286 (10), 737—764.

Kanagawa, K., Shimano, H., Hiroi, Y., 2008. Mylonitic deformation of gabbro in the lower crust: a case study from the Pankenushi gabbro in the Hidaka metamorphic belt of central Hokkaido, Japan. J. Struct. Geol. 30 (9), 1150—1166.

Kilian, R., Heilbronner, R., Stunitz, H., 2011. Quartz grain size reduction in a granitoid rock and the transition from dislocation to diffusion creep. J. Struct. Geol. 33 (8), 1265—1284.

Larrovere, M.A., de los Hoyos, C.R., Toselli, A.J., Rossi, J.N., Basei, M.A.S., Belmar, M.E., 2011. High T/P evolution and metamorphic ages of the migmatitic basement of northern Sierras Pampeanas, Argentina: characterization of a mid-crustal segment of the Famatinian belt. J. South Am. Earth Sci. 31 (2—3), 279—297.

Larrovere, M.A., Toselli, A.J., Rossi De Toselli, J.N., 2008. Petrologia y estructura de la Faja de deformacion La Chilca, Catamarca. Rev. Asoc. Geol. Argent. 63 (2), 254—263.

Le Corre, C.A., Rossello, E.A., 1994. Kinematics of Early Paleozoic ductile deformation in the basement of NW Argentina. J. South Am. Earth Sci. 7 (3—4), 301—308.

Loewy, S.L., Connelly, J.N., Dalziel, I.W.D., 2004. An orphaned basement block: the Arequipa-Antofalla Basement of the central Andean margin of South America. GSA Bull. 116 (1—2), 171—187.

Lopez, J.P., Grosse, P., Toselli, A., 2007. Faja de deformacion La Horqueta, Sierra de Velasco, Sierras Pampeanas, NO de Argentina: petrografia, geoquimica, estructuras y significado tectonico. Estud. Geol. 63 (2), 5—18.

Lopez, J.P., Toselli, A.J., 1993. La faja milonitica TIPA: Faldeo oriental del Sistema de Famatina. In: XII Congreso Geologico Argentino y II Congreso de Exploracion de Hidrocarburos III, Mendoza, pp. 39—42.

Lucassen, F., Becchio, R., 2003. Timing of high-grade metamorphism: Early Palaeozoic U—Pb formation ages of titanite indicate long-standing high-T conditions at the western margin of Gondwana (Argentina, 26—29°S). J. Metamorph. Geol. 21 (7), 649—662.

Lucassen, F., Becchio, R., Franz, G., 2011. The Early Palaeozoic high-grade metamorphism at the active continental margin of West Gondwana in the Andes (NW Argentina/N Chile). Int. J. Earth Sci. 100 (2), 445—463.

Lucassen, F., Becchio, R., Wilke, H.G., Franz, G., Thirlwall, M.F., Viramonte, J., Wemmer, K., 2000. Proterozoic-Paleozoic development of the basement of the Central Andes (18—26°S) — a mobile belt of the South American craton. J. South Am. Earth Sci. 13, 697—715.

Martino, R.D., 2003. Las fajas de deformacion ductil de las Sierras Pampeanas de Cordoba: Una resena general. Rev. Asoc. Geol. Argent. 58 (4), 549—571.

Mawer, C.K., 1983. State of strain in a quartzite mylonite, Central Australia. J. Struct. Geol. 5, 401—409.

Means, W.D., 1984. Shear zones of types I and II and their significance for reconstruction of rock history. Geol. Soc. Am. Abstr. Programs 16, 50.

Means, W.D., 1995. Shear zones and rock history. Tectonophysics 247 (1—4), 157—160.

Mehnert, K.R., 1968. Migmatites and the Origin of Granitic Rocks. Elsevier, Amsterdam, Netherlands.

Mitra, G., 1992. Deformation of granitic basement rocks along fault zones at shallow to intermediate crustal levels. In: Mitra, S., Fisher, G.W. (Eds.), Structural Geology of Fold and Thrust Belts. Johns Hopkins University Press, Baltimore, MD, pp. 123—144.

Montési, L.G.J., Zuber, M.T., 2002. A unified description of localization for application to large-scale tectonics. J. Geophys. Res. 107 (B3), 1—21.

Norris, R.J., Cooper, A.F., 2003. Very high strains recorded in mylonites along the Alpine Fault, New Zealand: implications for the deep structure of plate boundary faults. J. Struct. Geol. 25 (12), 2141—2157.

O'Hara, K., 2007. Reaction weakening and emplacement of crystalline thrusts: diffusion control on reaction rate and strain rate. J. Struct. Geol. 29 (8), 1301—1314.

Oliot, E., Goncalves, P., Marquer, D., 2010. Role of plagioclase and reaction softening in a metagranite shear zone at mid-crustal conditions (Gotthard Massif, Swiss Central Alps). J. Metamorph. Geol. 28 (8), 849—871.

Omarini, R.H., Sureda, R.J., Gotze, H.-J., Seilacher, A., Pfluger, F., 1999. Puncoviscana folded belt in northwestern Argentina: testimony of Late Proterozoic Rodinia fragmentation and pre-Gondwana collisional episodes. Int. J. Earth Sci. 88, 76—97.

Passchier, C.W., Trouw, R.A.J., 2005. Microtectonics. Springer-Verlag, Berlin, Heidelberg.

Pennacchioni, G., Mancktelow, N.S., 2007. Nucleation and initial growth of a shear zone network within compositionally and structurally heterogeneous granitoids under amphibolite facies conditions. J. Struct. Geol. 29 (11), 1757—1780.

Platt, J.P., Behr, W.M., 2011. Lithospheric shear zones as constant stress experiments. Geology 39 (2), 127—130.

Poirier, J.P., 1980. Shear localization and shear instability in materials in the ductile field. J. Struct. Geol. 2 (1—2), 135—142.

Ramos, V.A., 1988. Late-Proterozoic—Early Paleozoic of South America: a collisional history. Episodes 11, 168—175.

Ramsay, J.G., 1980. Shear zone geometry: a review. J. Struct. Geol. 2 (1/2), 83—99.

Ramsay, J.G., Graham, R.H., 1970. Strain variation in shear belts. Can. J. Earth Sci. 7, 786—813.

Rapela, C., 1976. El basamento metamorfico de la region de Cafayate, Provincia de Salta. Aspectos petrologicos y geoquimicos. Rev. Asoc. Geol. Argent. 31, 203—222.

Rapela, C.W., Pankhurst, R.J., Casquet, C., Baldo, E., Saavedra, J., Galindo, C., 1998a. Early evolution of the Proto-Andean margin of South America. Geology 26 (8), 707—710.

Rapela, C.W., Pankhurst, R.J., Casquet, C., Baldo, E., Saavedra, J., Galindo, C., Fanning, C.M., 1998b. The Pampean Orogeny of the southern proto-Andes: Cambrian continental collision in the Sierras de Cordoba. Geol. Soc. Lond. Spec. Publ. 142 (1), 181—217.

Regenauer-Lieb, K., Weinberg, R.F., Rosenbaum, G., 2006. The effect of energy feedbacks on continental strength. Nature 442 (7098), 67—70.

Regenauer-Lieb, K., Weinberg, R.F., Rosenbaum, G., 2012. The role of elastic stored energy in controlling the long term rheological behaviour of the lithosphere. J. Geodyn. 55, 66—75.

Regenauer-Lieb, K., Yuen, D.A., 1998. Rapid conversion of elastic energy into plastic shear heating during incipient necking of the lithosphere. Geophys. Res. Lett. 25 (14), 2737—2740.

Regenauer-Lieb, K., Yuen, D.A., 2004. Positive feedback of interacting ductile faults from coupling of equation of state, rheology and thermal-mechanics. Phys. Earth Planet. Interiors 142, 113—135.

Rossi De Toselli, J.N., Toselli, A., Toselli, G., 1976. Migmatizacion y metamorfismo en el basamento de la Sierra de Quilmes, al oeste de Colalao del Valle, Provincia de Tucuman, Argentina. Rev. Asoc. Geol. Argent. 31 (2), 83—94.

Rutter, E.H., 1999. On the relationship between the formation of shear zones and the form of the flow law for rocks undergoing dynamic recrystallization. Tectonophysics 303 (1—4), 147—158.

Sawyer, E.W., 2008. Atlas of Migmatites. NRC Research Press, Ottawa, Ontario, Canada.

Schwartz, J.J., Gromet, L.P., 2004. Provenance of a late Proterozoic—early Cambrian basin, Sierras de Cordoba, Argentina. Precambrian Res. 129, 1—21.

Sibson, R.H., 1977. Fault rocks and fault mechanisms. J. Geol. Soc. Lond. 133, 191—213.

Sims, J.P., Ireland, T.R., Camacho, A., Lyons, P., Pieters, P.E., Skirrow, R.G., Stuart-Smith, P.G., Miro, R., 1998. U—Pb, Th—Pb and Ar—Ar geochronology from the southern Sierras Pampeanas, Argentina: implications for the Palaeozoic tectonic evolution of the western Gondwana margin. Geol. Soc. Lond. Spec. Publ. 142 (1), 259—281.

Sinha, A.K., Hewitt, D.A., Rimstidt, J.D., 1986. Fluid interaction and element mobility in the development of ultramylonites. Geology 14, 883—886.

Sola, A.M., Becchio, R.A., Pimentel, M., 2010. Leucogranito Pumayaco: anatexis cortical durante el ciclo orogenico Famatiniano en el extremo norte de la Sierra del Molinos, Provincia de Salta. Rev. Asoc. Geol. Argent. 66 (1), 206—224.

Stunitz, H., Gerald, J.D.F., 1993. Deformation of granitoids at low metamorphic grade. II: granular flow in albite-rich mylonites. Tectonophysics 221 (3—4), 299—324.

Sun, S.-s., McDonough, W.F., 1989. Chemical and isotopic systematicsof oceanic basalts: implication for mantle composition and processes. In: Saunders, A.D., Norry, M.J. (Eds.), Magmatism in Ocean Basins, vol. 42. Geological Society London Special Publication, pp. 313—345.

Toselli, A., Rossi De Toselli, J.N., Rapela, C.W., 1978. El basamento metamorfico de la Sierra de Quilmes, Republica Argentina. Rev. Asoc. Geol. Argent. Rev. 33 (2), 105—121.

Trouw, R.A.J., Passchier, C.W., Wiersma, D.J., 2010. Atlas of Mylonites — and Related Structures. Springer, Berlin, Heidelberg.

Tullis, J., Snoke, A.W., Todd, V.R., 1982. Significance and petrogenesis of mylonitic rocks. Geology 10, 227—230.

Tullis, J., Yund, R.A., 1985. Dynamic recrystallization of feldspar: a mechanism for ductile shear zone formation. Geology 13 (4), 238—241.

Turner, J.C., 1960. Estratigrafia de la Sierra de Santa Victoria y adyacencias. Boletin Acad. Nac. Ciencias, Cordoba 41 (2), 163—206.

van Staal, C.R., Vujovich, G.I., Currie, K.L., Naipauer, M., 2011. An Alpine-style Ordovician collision complex in the Sierra de Pie de Palo, Argentina: record of subduction of Cuyania beneath the Famatina arc. J. Struct. Geol. 33 (3), 343—361.

Vauchez, A., Egydio-Silva, M., Babinski, M., Tommasi, A., Uhlein, A., Liu, D., 2007. Deformation of a pervasively molten middle crust: insights from the neo-proterozoic Ribeira-Araçuaí orogen (SE Brazil). Terra Nova 19 (4), 278—286.

Vauchez, A., Tommasi, A., 2003. Wrench faults down to the asthenosphere: geological and geophysical evidence and thermomechanical effects. Geol. Soc. Lond. Spec. Publ. 210 (1), 15—34.

Vauchez, A., Tommasi, A., Mainprice, D., 2012. Faults (shear zones) in the Earth's mantle. Tectonophysics 558—559, 1—27.

Waters, D.J., 2001. The significance of prograde and retrograde quartz-bearing intergrowth microstructures in partially melted granulite-facies rocks. Lithos 56 (1), 97—110.

Weinberg, R.F., Hasalova, P., Ward, L., Fanning, C.M., 2013. Interaction between deformation and magma extraction in migmatites: examples from Kangaroo Island, South Australia. GSA Bull. 125 (7—8), 1282—1300.

Weinberg, R.F., Mark, G., 2008. Magma migration, folding and disaggregation of migmatites in the Karakoram shear zone, Ladakh, NW India. GSA Bull. 120, 994—1009.

Wenk, H.-R., 1998. Deformation of mylonites in Palm Canyon, California, based on xenolith geometry. J. Struct. Geol. 20 (5), 559—571.

White, S.H., Burrows, S.E., Carreras, J., Shaw, N.D., Humphreys, F.J., 1980. On mylonites in ductile shear zones. J. Struct. Geol. 2 (1—2), 175—187.

White, S.H., Knipe, R.J., 1978. Transformation- and reaction-enhanced ductility in rocks. J. Geol. Soc. Lond. 135 (5), 513—516.

Whitmeyer, S.J., Simpson, C., 2003. High strain-rate deformation fabrics charac-terize a kilometers-thick Paleozoic fault zone in the Eastern Sierras Pampeanas, central Argentina. J. Struct. Geol. 25 (6), 909—922.

Whitney, D.L., Evans, B.W., 2010. Abbreviations for names of rock-forming minerals. Am. Mineral. 95, 185—187.

Zegers, T.E., de Keijzer, M., Passchier, C.W., White, S.H., 1998. The Mulgandinnah shear zone; an Archean crustal scale strike-slip zone, eastern Pilbara, Western Australia. Precambrian Res. 88, 233—247.

Comment on "One kilometre-thick ultramylonite, Sierra de Quilmes, Sierras Pampeanas, NW Argentina"

S.H. Büttner

Department of Geology, Rhodes University, Grahamstown 6140 South Africa

Comment and reply

Comment: "One kilometre-thick ultramylonite, Sierra de Quilmes, Sierras Pampeanas, NW Argentina" by M.A. Finch, R.F. Weinberg, M.G. Fuentes, P. Haslova, and R. Becchio, Journal of Structural Geology 72 (2015) 33–54

CrossMark

S.H. Büttner

Department of Geology, Rhodes University, Grahamstown 6140, South Africa

1. Introduction

In their recent publication Finch et al. (2015) present new information on the El Pichao shear zone and, in the context of an assessment of the formation of ultramylonites, interpret the El Pichao shear zone in its significance within the crustal evolution of the Sierras Pampeanas. They hereby particularly address its age, which they associate with the Ordovician "470 Ma Famatinian orogeny". The contractional character of the amphibolite facies shearing along El Pichao shear zone is extrapolated to higher temperature tectonics and metamorphism in other, particularly the northern, parts of the Sierra de Quilmes.

Finch et al. investigate the formation of ultramylonites in the El Pichao shear zone using essentially macro- and microstructural methods. The authors rejected conclusions drawn by Büttner (2009), who used integrated P-T-d-t data sets in order to reconstruct the crustal evolution of the Sierra de Quilmes metamorphic complex (SQMC), including the orientation of Ordovician paleo-isobars. However, Finch et al. neither appropriately discussed these findings nor did they present an alternative data set that would have determined the age of displacement along the El Pichao shear zone or its orientation at the time the shear zone was active.

In addition, Finch et al. did not make effective use of the more than 20 age data available from the Sierra de Quilmes, all of which were produced and interpreted in the context of the P-T-

d evolution of the SQMC in Büttner et al. (2005) and Büttner (2009). This omission led the authors to misinterpret the age of tectonism along the El Pichao shear zone, resulting in misinterpreting the entire Ordovician deformation history of the SQMC and the northern Sierras Pampeanas as *contractional*. Accordingly, Finch et al. see their observations and interpretations in conflict with the model of an Ordovician *extensional* period in a continental back-arc belt, the case for which has been made in Büttner et al. (2005) and Büttner (2009).

Overall, Finch et al. do not present any solid data or argument that would lend robustness or reliability to their estimation of 470 Ma shearing along the El Pichao shear zone, or to any other age related to the Ordovician Famatinian phase. In their defence, Finch et al. are not less untroubled in their time constraints than other authors, who often for the same reasons, the lack of integrated P-T-d-t data, inferred the age of deformation events in the Sierras Pampeanas using data from elsewhere that were not necessarily appropriate for dating the investigated kinematic event.

In this comment I wish to demonstrate that a more rigorous use of the geological information available for the evolution of the Sierra de Quilmes, particularly age data produced for rocks and events in the immediate vicinity of the El-Pichao shear zone, would have allowed Finch et al. a different and arguably more meaningful interpretation of the El Pichao shear zone's significance for the tectono-metamorphic evolution of the northern Sierras Pampeanas. Such an alternative interpretation of Finch et al.'s observations and data reconciles their findings with the data presented in

Büttner et al. (2005), and in particular with the interpretation of a Palaeozoic continental back-arc mobile belt in the northern Sierras Pampeanas with extensional and contractional periods as advocated for by Büttner (2009).

2. Regional geological context

The Sierras Pampeanas are a complex orogen that has formed in several orogenic stages, including the Early to Middle Cambrian Pampean, Ordovician Famatinian, and late Ordovician/early Silurian Oclóyic phases, which show different tectonic patterns at different time and in different parts of the orogen (e.g. Rapela et al., 1998). Particularly during the Ordovician period, the tectonic situation in the Sierras Pampeanas was different in the northern and southern part of the belt. In the southern Sierras Pampeanas the accretion of the Precordillera Terrane caused contractional back-arc tectonics in at least the middle and late Ordovician (e.g., Astini and Davila, 2004; Collo et al., 2008; Castro de Machuca et al., 2012). In the northern Sierras Pampeanas, where the Sierra de Quilmes is located, the tectonic evolution was distinctly different. Lucassen et al. (2000) demonstrated on the basis of comprehensive petrological and geochronological evidence that no terrane accretion occurred in the Ordovician or later in the northern Sierras Pampeanas. Hence we may consider the northern Sierras Pampeanas as a continental back-arc region where contractional, extensional or stable tectonic phases were essentially controlled by movement vectors of the paleo-Pacific and the SW Gondwana plates, and by subduction angles, all of which might have changed over time.

The Ordovician tectonic evolution was preceded by the Cambrian Pampean orogenic phase and followed by the Silurian Oclóyic and the Mesozoic to recent Andean events, creating a highly complex structural situation in the central Andes. Despite of this complexity, Finch et al. attempted to infer the time of displacement along the El Pichao shear zone essentially from literature data that include shear zones in the northern and in the southern Sierras Pampeanas, and shear zones that have formed in the Pampean, Famatinian or the Oclóyic phases of back-arc evolution (their chapter 2 and section 8.3), as if these phases were uniform in their tectonic nature. All that many of these shear zones may have in common is that Andean tectonics have rotated them into mainly east-dipping orientation and that in their present orientation many may show top-to-the west tectonic transport. Arguably, this is an insufficient argument to associate them with the same tectonic setting of origin or to postulate their origin as thrusts at that time.

3. Discussion: the age and significance of the El Pichao shear zone and the tectonic setting of the Sierra de Quilmes metamorphic complex

The SQMC, including the rocks that were tectonised along the El Pichao shear zone, are located in N–S striking basement that in most places dips moderately to the east (Büttner et al., 2005; Büttner, 2009; references therein; Finch et al., 2015). Most macro-structural data and observations made by Finch et al. (2015) in their study area south of Tolombón are near identical to those already published in Büttner (2009; e.g. Fig. 6D), which perhaps would have been fair to mention.

The eastward tilting of the Palaeozoic crust in the Sierra de Quilmes is evident not only from the orientation of the metamorphic layering but also from the distribution of paleo-isotherms and -isobars that correlate with metamorphic zone boundaries, first published in Büttner et al. (2005). Finch et al. do not challenge the position of these zone boundaries; they even show similar ones in their Figure 2b. These zone boundaries represent sets of condensed paleo-isotherms and −isobars that were formed in Ordovician time. Together with the timing at which the condensed nature of these paleo-isotherms/isobars was established, this indicates Ordovician crustal thinning in the SQMC (Büttner, 2009). This view was not challenged by one of Finch's co-authors (R.F. Weinberg), who acted as a particularly thorough and supportive reviewer of the manuscript that was published as Büttner (2009). Since Finch et al. reject the possibility of Ordovician crustal thinning, it is somewhat surprising that this key evidence did not merit further discussion in their paper.

Finch et al. (2015) did also not discuss the attitude of the El Pichao shear zone in the Palaeozoic but appear to assume that it is preserved in its original orientation, which arguably is not the case (Büttner, 2009). The authors, somewhat inconsistently, reject significant post-Ordovician crustal tilting at the end of their chapter 2 but re-introduce it as a possibility at the end of their section 8.2.

South of the El Pichao shear zone follows the lower-grade metamorphic Agua del Sapo complex that, according to the descriptions in Finch et al., shows great similarity with the lower-grade parts of the SQMC west of Cafayate or in the El Divisadero area (Büttner et al., 2005). The rocks in these areas might well be equivalent to each other in their litho- and tectono-stratigraphic position within the SQMC. It is this observation of lower-grade rocks in the tectonic footwall of migmatites and diatexites that led Finch et al. to the interpretation of Famatinian/Ordovician thrusting and crustal contraction. I fully agree with thrusting of high-grade metamorphic parts of the SQMC over the Agua del Sapo complex but I disagree that this could have happened in Famatinian/Ordovician time, and I disagree with the author's conclusion that the Famatinian event was contractional in the northern Sierras Pampeanas.

The tectonic juxtaposition of the SQMC, renamed and referred to as the Tolombón complex in Finch et al., with the Agua del Sapo complex via displacement along the El Pichao shear zone, is not, as the authors state, related to any 470 Ma tectonism, it is very likely younger than ~440 Ma and therefore not of Ordovician/Famatinian age. Several lines of evidence support this.

(i) Time of displacement: The primary age constraint that determines the end of the Ordovician extension in the SQMC is the emplacement of megacrystic type 2 pegmatites that crosscut the extensional shear zones and that are practically undeformed. These pegmatites are common north of the area that was affected by the El Pichao shear zone and were emplaced at the Ordovician-Silurian boundary at ~440 Ma (Büttner et al., 2005). Finch et al. did not report any undeformed pegmatites crosscutting the ultramylonites or other high-strain parts of the El Pichao shear zone, and according to my own notes from the area southwest of Tolombón/west of Colalao del Valle they are indeed absent. By contrast, Finch et al. repeatedly reported mylonitic pegmatites (e.g. their sections 3.4, 3.5, 4.2; Figs. 6 and 9). For a number of these pegmatites the authors reported evidence of very large initial grain size, strongly suggesting that these are sheared type 2 pegmatites that were emplaced at ~440 Ma (Büttner et al., 2005). This strongly suggests that mylonitisation along the El-Pichao shear zone is post-Ordovician.

(ii) Orientation and shape of the El Pichao shear zone: The Ordovician granulite to upper amphibolite facies shear zones along of which crustal thinning was accomplished, are oriented parallel to the migmatitic layering of the anatectic zones of the SQMC (Büttner et al., 2005; Büttner, 2009). This layering strikes NW/NNW and is parallel to the metamorphic zone boundaries, which in turn are parallel to paleo-isotherms and -isobars. The curving El Pichao shear zone cuts across this regional ~ NW-trend at high angle (Fig. 2b in Finch et al., 2015), which suggests its relatively younger and therefore most probably post-Ordovician age.

(iii) Formation temperature of mylonites: Finch et al. estimated the deformation temperatures for the El Pichao mylonites and ultramylonites as amphibolite facies between 500 °C and 700 °C. No pressure estimations were attempted. The reported abundance of muscovite mica fish, the scarcity or absence of syn-kinematic sillimanite, and the fine-grained recrystallization of feldspar may indicate in fact mid-to lower amphibolite facies deformation temperatures. Finch et al.'s observations are well in agreement with mid-amphibolite facies mylonitisation in a tourmaline bearing pegmatite in the temperature interval of 500–660 °C at pressures between 300 and 570 MPa (Büttner, 2005). This sample was collected as a loose block west of Colalao del Valle, an area that has been affected by deformation along the El Pichao shear zone. Its primary mineral assemblage containing tourmaline strongly suggests that the protolith of the mylonite was a ~440 Ma type 2 pegmatite.

However, the Ordovician extension in the migmatites of the SQMC started at granulite facies temperatures and in the presence of melt, and continued towards amphibolite facies temperatures. The bulk of crustal thinning was achieved in the tectono-stratigraphically lowest zones of the SQMC when the crust was at upper amphibolite or granulite facies conditions (~475–464 Ma; Büttner, 2009). With decreasing temperatures extension rates dropped and came to an end between ~450 and ~440 Ma (Büttner, 2009). Only in the vicinity of the El Pichao shear zone synkinematic white mica and the synkinematic breakdown of cordierite forming white mica are seen (Büttner et al., 2005, Fig. 3g; Büttner, 2009, Fig. 5B). This suggests that in the area affected by the El Pichao shear zone the higher temperature Ordovician shearing continued at mid- or lower amphibolite facies temperatures, at P-T conditions well below those of Ordovician shear zones that achieved the early high-temperature and most effective stages of crustal thinning in the SQMC. The shearing of type 2 pegmatites in the stability field of white mica at amphibolite facies conditions demonstrates that this occurred at Silurian time.

(iv) Temperature and time of the El Sapo complex juxtaposition: Along its western boundary the amphibolite facies El Sapo complex is juxtaposed with higher-grade metamorphic SQMC basement along a greenschist facies mylonite zone (Finch et al., 2015). Although the kinematics of this shear zone are not reported this further indicates that juxtaposition of this complex with higher-grade metamorphic layers of the SQMC took place at temperatures that the crust reached only at a post-Ordovician retrograde stage.

All this indicates that the El Pichao shear zone is not of any significance for the Ordovician Famatinian stage of back-arc evolution in the northern Sierras Pampeanas. At Ordovician time the crust of the northern Sierras Pampeanas was hot and exposed to extensional thinning. Particularly during the Arenig, when the middle crust was most effectively thinned out, but probably also for most of the Ordovician period, extensional sedimentary basins formed at the surface (Bahlburg, 1991; see Büttner, 2009; for detailed discussion). Subsequently, the middle and lower crust, now exposed in the SQMC, cooled to temperatures of the middle amphibolite facies, extension rates decreased with increasing crustal shear strength, and post-extensional type 2 pegmatites were emplaced at the Ordovician-Silurian boundary (Büttner et al., 2005; Büttner, 2009).

At this time the extensional Famatinian period converted via tectonic switching (Collins, 2002) into a contractional period. This is indicated by folding of the Ordovician Puna basin sediments during the Oclóyic phase, which lasted until ~430 Ma (Bahlburg, 1991; Bahlburg and Hervé, 1997). The basement, meanwhile at mid/lower amphibolite facies temperatures in levels now exposed in the Sierra de Quilmes, responded to shortening with the

formation of localised high-strain thrusts. The El Pichao shear zone might well be related to this tectonic phase.

Because of the late Ordovician shallow dip angle of the metamorphic layering, the paleo-isotherms and paleo-isobars in the SQMC (Büttner, 2009), the shear zones that controlled Ordovician crustal thinning could easily be reactivated as surfaces of Silurian contractional tectonics. Minor tilting, as it can be expected to occur when subhorizontal layers undergo horizontal contraction, would have been sufficient to convert Ordovician low-angle extensional shear zones into Silurian low-angle thrusts in the then contractional back-arc of the Oclóyic phase. Shear directions of the extensional phase might not have changed significantly during tectonic switching, although in the SQMC the conversion of D3 into D4 displacement (Büttner, 2009) might herald a changing tectonic regime at the end of the Ordovician.

Further contractional shear zone steepening or ramping eventually allowed thrusting to cut through the Ordovician metamorphic zone boundaries, placing higher-grade metamorphic parts of the SQMC on top of lower-grade ones, such as the El Sapo complex. The shape of the El Pichao shear zone, curving from an orientation parallel to the Ordovician zone boundaries into a high-angle discordant orientation (Finch et al., Fig. 2b) might be a corresponding feature. Given sufficient displacement, the formation of thick ultramylonitic thrusts at further crustal cooling through the lower amphibolite and perhaps into the greenschist facies appears unproblematic. In the topical part of their paper Finch et al. have provided abundant information on this.

4. Conclusion

The tectono-metamorphic evolution of the SQMC and the El Pichao shear zone (Büttner, 2009; Finch et al., 2015) fits best with an extensional Ordovician Famatinian phase followed by Silurian contraction related to the Oclóyic orogenic phase in a continental mobile belt that had existed in the central Andes since ~500 Ma (Lucassen et al., 2000). This does not preclude contractional Ordovician tectonics elsewhere in the Sierras Pampeanas, such as in the structural impact zone of the Precordillera Terrane further south, which probably collided in late Ordovician time (e.g. Lucassen et al., 2000).

The deposition of Ordovician deep-water marine sediments at the surface is in perfect time correlation with mid-crustal thinning until the late Ordovician (Büttner, 2009). The increasing shear strength of the cooling crust at late Ordovician time eventually exceeded the differential stresses available in the waning extensional Famatinian phase and extension came to an end between ~450 and ~440 Ma (Büttner, 2009). After ~440 Ma (i.e. in the early Silurian) basin sediments underwent folding (Bahlburg, 1991; Bahlburg and Hervé, 1997). Differential stresses increased again during contraction and the middle crust responded with the formation of localised thrusts, structures like the El Pichao shear zone, which tectonically offset the layers of different Ordovician metamorphic grades. This in itself indicates that they postdate the formation of this layering. The change of the tectonic regime appears also to have correlated with a drastic increase in strain rates to ~10^{-12} s^{-1} (Finch et al., 2015), three to four orders of magnitude faster than strain rates postulated for Ordovician extension (Büttner, 2009). Since the El Pichao shear zone most likely formed in a comparatively short contractional time period in the Silurian Oclóyic phase, in the retrograde metamorphic stage following the Ordovician high temperature phase, and under unusually high strain rates, the process of formation of such ultramylonites might be less typical or representative for the Paleozoic tectonics in the Sierras Pampeanas than Finch et al. postulate in their conclusions.

The present orientation of Palaeozoic shear zones in the Sierras Pampeanas has limited meaning for the kinematic interpretation and even less significance for the interpretation of plate-tectonic settings at the time of their formation. The obscuring impact of the Andean tectonics simply cannot be ignored. Meaningful tectonic studies that aim at contributing knowledge to the understanding of the crustal evolution will always attempt to reconstruct the absolute timing of displacement and the orientation of shear zones at that time, particularly in environments as complex as the poly-tectonic Sierras Pampeanas. Otherwise they easily can be challenged. Field studies with a topical focus, such as the very interesting investigation by Finch et al. on the formation of ultramylonites, perhaps should not venture into commenting on regional geological contexts and processes without thorough assessment and investigation.

Acknowledgements

References

Astini, R.A., Davila, F.M., 2004. Ordovician back arc foreland and Oclóyic thrust belt development on the western Gondwana margin as a response to Precordillera terrane accretion. Tectonics 23, TC4008.

Bahlburg, H., 1991. The Ordovician back-arc to forelands successor basin in the Argentinian-Chilean Puna: tectono-sedimentary trends and sea-level changes. Int. Assoc. Sedimentol. Spec. Publ. 12, 465–484.

Bahlburg, H., Hervé, F., 1997. Geodynamic evolution and tectonostratigraphic terranes of northwestern Argentina and northern Chile. Bull. Geol. Soc. Am. 109, 869–884.

Büttner, S.H., 2005. Deformation-controlled cation diffusion in compositionally zoned tourmaline. Mineral. Mag. 69 (4), 471–489.

Büttner, S.H., 2009. The Ordovician Sierras Pampeanas-Puna connection: basement thinning and basin formation in the Proto-Andean back-arc. Tectonophysics 477, 278–291.

Büttner, S.H., Glodny, J., Lucassen, F., Wemmer, K., Erdmann, S., Handler, R., Franz, G., 2005. Ordovician metamorphism and plutonism in the Sierra de Quilmes metamorphic complex: implications for the tectonic setting of the northern Sierras Pampeanas (NW Argentina). Lithos 83, 143–181.

Castro de Machuca, B., Delpino, S., Previley, L., Mogessie, A., Bjerg, E., 2012. Tectono-metamorphic evolution of a high- to medium-grade ductile deformed meta-gabbro/metadiorite from the Arenosa Creek Shear Zone, Western Sierras Pampeanas, Argentina. J. Struct. Geol. 42, 261–278.

Collins, W.J., 2002. Hot orogens, tectonic switching, and creation of continental crust. Geology 30, 535–538.

Collo, G., Astini, A.R., Cardona, A., Do Campo, M.D., Cordani, U., 2008. Edades de metamorfismo en las unidades con bajo grado de la región central del Famatina: la impronta del ciclo orogénico oclóyico (Ordovícico). Rev. Geol. Chile 35 (2), 191–213.

Finch, M.A., Weinberg, R.F., Fuentes, M.G., Haslova, P., Becchio, R., 2015. One kilometre-thick ultramylonites, Sierra de Quilmes, Sierras Pampeanas, NW Argentina. J. Struct. Geol. 72, 33–54.

Lucassen, F., Becchio, R., Wilke, H.G., Franz, G., Thirlwall, M.F., Viramonte, J., Wemmer, K., 2000. Proterozoic-Paleozoic development of the basement of the Central Andes (18–26°S) — a mobile belt of the South American craton. J. South Am. Earth Sci. 13, 697–715.

Rapela, C.W., Pankhurst, R.J., Casquet, C., Baldo, E., Saavedra, J., Galindo, C., 1998. Early evolution of the Proto-Andean margin of South America. Geology 26, 707–710.

Reply to comment on "One kilometre-thick ultramylonite, Sierra de Quilmes, Sierras Pampeanas, NW Argentina"

M.A. Finch[1], R.F. Weinberg[1], M. G. Fuentes[2], P. Hasalová[1,3], R. Becchio[2]

[1]School of Earth, Atmosphere and Enivronment, Monash University, Clayton, Victoria, 3800, Australia

[2]Instituto Geonorte, National University of Salta, INENCO-CONICET, Av. Bolivia, 5150, 4400 Salta, Argentina

[3]Centre for Lithospheric Research, Czech Geological Survey, Klárov 3, 118 21 Prague 1, Czech Republic

Comment and reply

Reply to comment by S.H. Büttner on: "One kilometre-thick ultramylonite, Sierra de Quilmes, Sierras Pampeanas, NW Argentina"

M.A. Finch [a, *], R.F. Weinberg [a], M.G. Fuentes [b], P. Hasalová [a, c], R. Becchio [b]

[a] School of Earth, Atmosphere and Environment, Monash University, Clayton, VIC, 3800, Australia
[b] Instituto Geonorte, National University of Salta, INENCO-CONICET, Av. Bolivia 5150, 4400, Salta, Argentina
[c] Centre for Lithospheric Research, Czech Geological Survey, Klárov 3, 118 21, Prague 1, Czech Republic

ARTICLE INFO

We thank S.H. Büttner for the opportunity to clarify our work and the evolution we proposed for the shear zones of Sierra de Quilmes. Büttner et al. (2005) was the first comprehensive study of the Tolombón complex. Their map, photographs, and petrography were helpful and although we cited their work more than any other, we apologise that S.H. Büttner felt the work was under referenced.

We have worked throughout the Tolombón complex (as first named in Toselli et al., 1978) covering much of the area described in Büttner et al. (2005) and far beyond, in numerous transects across the Sierra de Quilmes. This was the first of several papers that we aim to publish on the area and our intent was to present our data on the El Pichao shear zone (PSZ). Our next paper is on the high-grade Tolombón complex and makes full use of the comprehensive geochronology data set in Büttner et al. (2005).

The criticisms in Büttner (2015) can be summarised as: (1) we did not appropriately consider the effect of tilting, (2) we did not provide data to indicate that the PSZ formed at the same time as the other shear zones in the Tolombón complex, and (3) we did not provide evidence that the region he studied also underwent thrusting. We will deal with each of Büttner's (2015) concerns in turn below.

(1) Failure to appropriately consider the effect of tilting

We are fully aware of the possibility of tilting of blocks. We know that there are multiple shear zones and brittle faults regionally and throughout Sierra de Quilmes and they could have tilted individual blocks or the entire metamorphic complex. We have seen first-hand tilted Neogene and Quaternary volcanic layers towards the centre of Sierra de Quilmes and tilted (ca. 25°−30°) Cretaceous syn-rift sequences in the north sector of Sierra de Quilmes. We acknowledge the possible effect of tilting in Section 8.2. The important point is not whether the region was tilted because our interpretation that the region was contractional during the Famatinian orogeny is not based on the current geometry of the thrust planes but based on the fact that hot rocks have been placed on top of cooler rocks. The apparent contradiction Büttner (2015) refers to at the end of Section 2 is as follows "Büttner (2009) suggested that shear zones were originally horizontal and extensional, and later rotated by Andean uplift to show apparent thrust shear sense. This interpretation is not consistent with our findings …" It was not our intention to deny that there was any tilting, and we believe the intent behind our sentence is clear: that we find no support for the assertion in Büttner (2009) that shearing occurred during extension and that it is purely as a result of tilting that the shear zones now have an apparent thrust sense.

(2) Failure to provide data to indicate that the PSZ formed at the same time as other shear zones in the Tolómbon complex

Büttner (2015) is quite correct that we have not constrained the absolute timing of motion on the PSZ. We have dated monazite from rocks of the PSZ, and obtained a mean age of ~480 Ma, similar to ages of migmatites of the Tolombón Complex, suggesting that monazites may not have been reset during shearing or that shearing was contemporaneous to migmatization. The ultra-mylonites formed at amphibolite facies (biotite and feldspar are stable) and were later locally retrogressed to greenschist facies with chloritized bands, and subsequently by cataclastic brittle deformation. Timing of retrogression and brittle reactivation remains unconstrained and could have been any time since the Famatinian.

Büttner (2015) suggests that the sheared pegmatites that we documented in the PSZ are type-2 pegmatites from Büttner et al.

(2005), dated to 440 Ma and that therefore shearing took place after 440 Ma. Pegmatites in anatectic terranes are common and may form throughout the anatectic event. There is no reason to suggest that the pegmatites in the PSZ are the same age as the cross-cutting pegmatites from Büttner et al. (2005). Although we have no way of disproving this assertion it is perhaps notable that Büttner et al. (2005) describes type-2 pegmatites as most common in the garnet-cordierite-sillimanite and biotite-muscovite zones whereas the PSZ pegmatites can be traced into voluminous pegmatites within the less-sheared but high temperature orthopyroxene zone.

What we have been able to ascertain is that there is continuity in the kinematics of deformation that took place during partial melting of the Tolombón complex and deformation accommodated by the PSZ. Both accommodate motion of the hanging wall towards the west and place hot rocks on top of cooler rocks (compare Fig. 6 in Büttner, 2009 with stereonets in Fig. 2 of Finch et al., 2015). Our lack of a precise age of movement on the PSZ should not detract from the message that the Famatinian orogeny recorded in Sierra de Quilmes was a result of crustal shortening rather than crustal extension. We summarise the evidence for this below.

(3) Failure to provide evidence that the Divisadero region discussed in Büttner et al. (2005) and Büttner (2009) underwent thrusting.

In Finch et al. (2015) we contend that the shear zones of the Tolombón complex are part of the same shortening event that formed the PSZ. We came to that conclusion by combining the following observations:

a) W-directed movement in high-grade regions was contemporaneous with partial melting, to judge from the relationships between leucosomes and thrust planes and folds (Fig. 4d,e in Finch et al., 2015 and 4c in Büttner et al., 2005).
b) W-directed movement in high-grade and low-grade rocks alike in the Divisadero region is the same as in the mylonitic rocks of PSZ (compare Fig. 6 in Büttner, 2009 with stereonets in Fig. 2 of Finch et al., 2015). From (a) and (b) we conclude movement continuity through time and space and suggested that movement on the PSZ remained constant as it cooled.
c) Most significantly, we find in Divisadero and at the PSZ, thrust planes that place hotter rocks above colder rocks. We will

publish a full description of the major Divisadero shear zone in our next paper.

In summary, we find no support for the interpretation of Büttner et al. (2005) and Büttner (2009) of an extensional terrane. The main argument for extension in Büttner (2009) is evidence for thinning of metamorphic packages in the migmatitic zones so that pressures recorded by the rocks are less than that indicated by the current distance between samples. Although thinned isograds are typical of extensional terranes, they alone should not be used as evidence for extension because the final distribution of isograds depends on the relative timing of paragenesis development and deformation. Furthermore, thinning of layers or metamorphic packages does not require extension. This may also occur during shortening when there is a component of shortening orthogonal or at a high angle to the isograds, bedding or foliation (pure or general shear). Numerous studies (Piñán-Llamas, 2007; Büttner, 2009) have determined that the Tolombón complex underwent general shear, as indicated by symmetric folding with axial surfaces parallel to the shear plane. Therefore, evidence for thinning in the Tolombón complex is not inconsistent with thrusting.

We hope this response provides clarity. Once again, we thank S.H. Büttner for the opportunity to clear up inconsistencies between his work and our own and we acknowledge the rich source of data and inspiration his papers have provided.

References

Büttner, S.H., 2009. The Ordovician Sierras Pampeanas-Puna basin connection: basement thinning and basin formation in the Proto-Andean back-arc. Tectonophysics 477 (3—4), 278—291.

Büttner, S.H., 2015. Comment: "One kilometre-thick ultramylonite, Sierra de Quilmes, Sierras Pampeanas, NW Argentina" by M.A. Finch, R.F. Weinberg, M.G. Fuentes, P. Hasalova, and R. Becchio. J. Struct. Geol. 72, 33—54.

Büttner, S.H., Glodny, J., Lucassen, F., Wemmer, K., Erdmann, S., Handler, R., Franz, G., 2005. Ordovician metamorphism and plutonism in the Sierra de Quilmes metamorphic complex: implications for the tectonic setting of the northern Sierras Pampeanas (NW Argentina). Lithos 83 (1—2), 143—181.

Finch, M.A., Weinberg, R.F., Fuentes, M.G., Hasalova, P., Becchio, R., 2015. One kilometre-thick ultramylonite, Sierra de Quilmes, Sierras Pampeanas, NW Argentina. J. Struct. Geol. 72, 33—54.

Piñán-Llamas, A., 2007. The Early Paleozoic Evolution of the Paleo-Pacific Gondwana Margin: a Structural, Petrographic, and Geochemical Study in the Puncoviscana Formation. Boston University.

Toselli, A., Rossi De Toselli, J.N., Rapela, C.W., 1978. El basamento metamorfico de la Sierra de Quilmes, Republica Argentina. Rev. la Asoc. Geol. Argent. 33 (2), 105—121.

Chapter 3

The role of water in the formation of a thick ultramylonitic shear zone

M.A. Finch, R.F. Weinberg

School of Earth, Atmosphere and Enivronment, Monash University, Clayton, Victoria, 3800, Australia
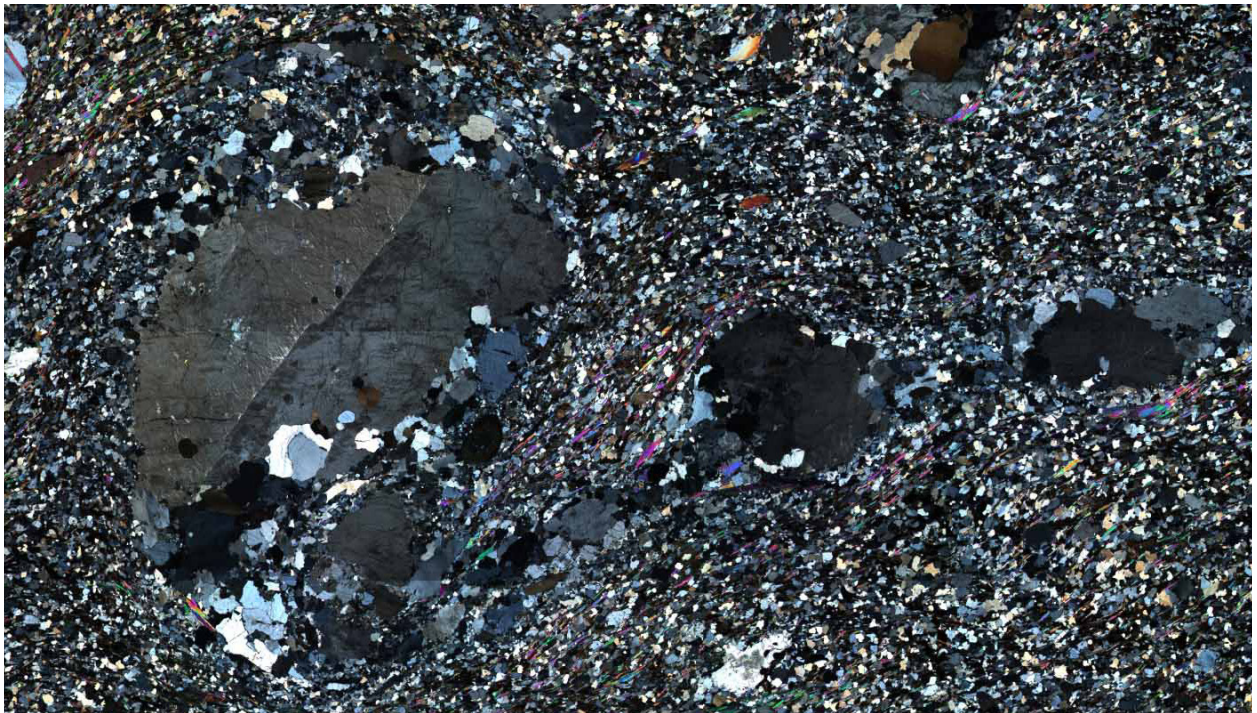
Cover page: Scan of a delta clast from an ultramylonite from the El Pichao shear zone in cross polarised light.

Monash University

Declaration for Thesis Chapter 3

Declaration by candidate

In the case of Chapter 3, the nature and extent of my contribution to the work was the following:

Nature of contribution	Extent of contribution (%)
Sample collection and preparation, FTIR data collection and processing, statistical analyses, interpretation of results, chapter preparation	95%

The following co-authors contributed to the work. If co-authors are students at Monash University, the extent of their contribution in percentage terms must be stated:

Name	Nature of contribution
R. F. Weinberg	Supervisory role

The undersigned hereby certify that the above declaration correctly reflects the nature and extent of the candidate's and co-authors' contributions to this work*.

Candidate's Signature   **Date**

Main Supervisor's Signature   **Date**

Abstract

Shear zone widening is a key process for the generation of thick ultramylonites and is promoted by processes that weaken the host rock or harden the shear zone. Water weakens rocks and minerals and its mobility is determined by pressure gradients that can be dynamic during simple shear, causing movement of water in and around the shear zone and affecting rock strength. We examine the role of water in an unusually thick shear zone: the 1 km-thick ultramylonitic layer of the El Pichao shear zone. We used fourier transform infrared spectroscopy to measure water content in quartz and feldspar, comparing ultramylonitic rocks deformed by diffusion creep to mylonites and weakly-deformed rocks deformed by dislocation creep. We found that quartz and feldspar in ultramylonites contained half the amount of water of weakly-deformed rocks, a result contrary to previous studies of water in shear zones. We propose that the thick ultramylonite formed in three stages: (1) localized deformation and recrystallisation caused release of intracrystalline water to grain boundaries and, once a critical grain size was reached, promoted dissolution-precipitation, which gave rise to an ultramylonite, (2) high pressure in the shear zone compared to the surroundings continuously expelled intercrystalline water, gradually drying the grain boundaries and leading to strain hardening, (3) water migrated to neighbouring, less-deformed rocks causing hydrolytic weakening, initiating diffusion-creep, and repeating the cycle, widening the ultramylonite.

1. Introduction

Localisation of strain within apparently homogenous rocks creates strongly deformed bands and layers known as shear zones (Ramsay and Graham, 1970). Weakening in shear zones is caused by processes that occur during shearing including grain-size decrease, connection of weak phases, shear heating, or development of grain preferred orientation (Ramsay and Graham, 1970, Sibson, 1977, Poirier, 1980). This weakening allows the shear zone to maintain a steady-state width or to narrow as the strain rate increases due to weakening (Platt and Behr, 2011). Alternatively, the strength of shear zones may increase due to strain hardening, which can be caused by the accumulation of dislocations, the growth of new, harder minerals (reaction hardening), dehydration of the shear zone, or changes in the deformation style of the rock (Hull, 1988, Passchier and Trouw, 2005, Groome et al., 2006, Johnson et al., 2011, Oliot et al., 2014). Strain hardening can cause the shear-zone interior to become stronger than the host rock, causing deformation to shift to the margin of the shear zone (Means, 1995). This process causes widening of the shear zone and, if repeated, can form apparently thick zones of high strain as the locus of deformation progressively moves outwards (e.g. Oliot et al., 2014, Finch et al., 2015). Shear zone widening may also occur when the host rock weakens due to the growth of soft minerals (reaction softening), shear heating, or water influx (Sibson, 1977, White and Knipe, 1978, Hippertt and Hongn, 1998, Regenauer-Lieb and Yuen, 1998). Of these weakening mechanisms, water influx has been of particular interest since it weakens rocks and minerals in a multitude of ways and can be a major factor controlling strain localisation in shear zones (e.g. Sibson, 1977, Oliot et al., 2014).

The weakening effect of molecular H_2O and OH species (herein referred to as "water") on quartz was first proposed 50 years ago (Griggs and Blacic, 1964, 1965). Water has multiple effects on rock strength. When it resides on grain boundaries it weakens the intercrystalline rock strength, facilitating dissolution-precipitation and accelerating grain boundary migration (GBM) and grain boundary sliding (GBS; e.g. Chen and Argon, 1979, Urai et al., 1986, Drury and Urai, 1990, Kronenberg, 1994, Mancktelow and Pennacchioni, 2004, Holyoke III and Kronenberg, 2013). When water resides in crystals, it decreases the strength of Si-O bonds through hydrolysis, an effect known as hydrolytic weakening (Griggs and Blacic, 1965, Blacic, 1975). This allows easier glide of dislocations (Kohlstedt, 2006) and diffusion at lower temperatures (Sibson, 1977). Water may also increase the number of cation vacancies since, as a charged species, the introduction of water into the crystal lattice introduces negatively charged point defects (Hobbs, 1981). This increases the rate of diffusion and dislocation climb and at high temperatures is likely to be more important than hydrolysis of Si-O bonds (Hobbs, 1981, Kohlstedt, 2006).

Molecular water was originally thought to be the main cause of hydrolytic weakening, however the equilibrium solubility of water in quartz (<200 H:10^6 Si; Paterson, 1989) is an order of magnitude lower than the amount purported to be required for hydrolytic weakening

(100s–1000s H:10^6 Si; Kronenberg et al., 1990, Nakashima et al., 1995). Additionally, Kekula-wala et al. (1978) found that the only water species common to all easily deformable quartz crystals in their study was gel-type hydroxyl, a non-freezable species distinct from structurally-bound and molecular water. However, their results were restricted to 3 kbar pressure and they suggest that other species of water may be more important at higher pressures. It has also been suggested that water in dislocations and fluid inclusions plays a role in hydrolytic weakening (Gerretsen et al., 1989, Kronenberg et al., 1990). How this occurs is yet to be determined but it may be a result of increasing the water activity and fugacity, which causes molecular water to diffuse more quickly through the crystal lattice (Post and Tullis, 1998) or through the provision of an intracrystalline water reservoir that effectively reduces the diffusion distance through the crystal (Paterson, 1989). Fluid inclusions may also have a more direct role, perhaps allowing increased number of sites for nucleation of dislocations (Gerretsen et al., 1989).

Studies of hydrolytic weakening on experimentally- and naturally- deformed rocks measure the water content in quartz and feldspar using fourier transform infrared spectroscopy (FTIR), with the content measured as the area under a broad peak in the absorbance spectra centred on the wavenumber of approximately 3400 cm^{-1} (Kats, 1962, Aines and Rossman, 1984). Experimental studies compare the strength of wet and dry quartz as single crystals and in polycrystalline aggregates by growing synthetic crystals or drying natural crystals (Griggs and Blacic, 1965, Kekulawala et al., 1978, Kronenberg and Tullis, 1984, Kronenberg and Wolf, 1990, Post and Tullis, 1998). These studies have found that dry quartz is exceptionally strong, it cannot plastically deform at P-T conditions found in nature (Carter et al., 1964, Christie et al., 1964). However, a small proportion of water allows easy plastic deformation of quartz (Griggs and Blacic, 1965, Kekulawala et al., 1978, Kronenberg and Tullis, 1984, Kronenberg and Wolf, 1990, Kronenberg, 1994, Post and Tullis, 1998), provided it is above a critical temperature (Paterson and Kekulawala, 1979). While experimental studies provide well-constrained results, their applicability to nature has been questioned because synthetic crystals are homogenous and are not grown under geological conditions, causing differences in the size, type, and location of fluids compared to natural crystals (Paterson and Kekulawala, 1979, Kronenberg and Wolf, 1990).

Studies on naturally-deformed rocks typically compare shear zone rocks to their less-deformed protoliths and have found that water content increases with degree of deformation. For example, Nakashima et al. (1995) found that water content in quartz was 600–3000 H:10^6 Si in undeformed rocks, and increased dramatically to 10000 – 16000 H:10^6 Si in the most deformed rocks. Kronenberg et al. (1990) also studied samples from a shear-zone traverse and found that water content increased from <2000 H:10^6 Si in the protolith up to 4000 – 11000 H:10^6 Si in the most deformed rocks close to the centre of the shear zone. These studies and others (e.g. Kronenberg and Wolf, 1990, Han et al., 2013) concluded that the high water content caused weakening and strain localisation. Similar results have been found for feldspar with a positive correlation between water content and deformation in naturally-deformed rocks (e.g. Kronenberg et al.,

1990, Han et al., 2013). However, alteration in feldspar affects the water content (Nakashima et al., 1995) and was not described in these studies.

Aside from intracrystalline water, fluids in shear zones may also reside on grain boundaries forming a free-fluid phase. The source of this fluid may be external to the shear zone and have preferentially infiltrated brittle faults or other defects that precede nucleation of the ductile shear zone (e.g. Mancktelow and Pennacchioni, 2005). A free-fluid phase may also develop in situ through the liberation of fluids from hydrous phases including biotite and muscovite (e.g. Mittempergher et al., 2014). These metamorphic fluids are generated during mechanical or chemical breakdown of the minerals. Liberation of intercrystalline water also occurs in quartz and feldspar during recrystallisation (Kerrich, 1976, Faleiros et al., 2010). For example, Faleiros et al. (2010) found that while protoliths contained quartz with abundant fluid inclusions, rocks recrystallised by subgrain rotation contained fewer, and there were even less in rocks with quartz that showed GBM. These studies indicate that recrystallisation and chemical breakdown causes movement of water out of the crystal lattice and into a free fluid phase on grain boundaries. Depending on pressure gradients, water on grain boundaries may be extracted from the shear zone (Mancktelow, 2002, Oliot et al., 2014), which can cause weakening and hydrofracturing of the weakly-deformed rocks at the shear-zone margin (Oliot et al., 2014). If water is liberated during recrystallisation and subsequently extracted from the shear zone, the most deformed and recrystallised rocks should contain less water than their protoliths, a theory at odds with the hydrolytic weakening hypothesis. This issue has important implications for shear-zone width since water migration out of the shear zone may cause weakening of the host rock and shear-zone widening, but water that remains may cause hydrolytic weakening and shear-zone narrowing (Means, 1984).

We investigate the role of water in a 1 km-thick layer of ultramylonite that forms the base of the 3.5 km-thick El Pichao shear zone (PSZ) in NW Argentina. The ultramylonite contains less-deformed lithons of mylonites, protomylonites, and homogenous porphyritic diatexites, which we interpret to be the protolith (Finch et al., 2015). As in previous chapters, we follow Sibson's (1977) classification for mylonitic rocks with protomylonites consisting of <50% recrystallised matrix, mylonites 50–90%, and ultramylonites >90%. We use the term 'mylonitic rocks' as a collective term referring to all sheared rocks within the range from protomylonites to ultramylonites, and the term 'mylonite' according to Sibson's definition. First we describe the differences in microstructure between weakly-deformed and mylonitic rocks of the PSZ. Then we present and discuss the differences in water content in weakly-deformed and mylonitic rocks and propose a model for shear-zone widening based on movement of water through the deforming zone.

2. Geologic setting and rock description

The protolith to the ultramylonite is a homogenous porphyritic diatexite that consists of phenocrysts of feldspar, quartz, and garnet in a matrix of Qtz+Kfs+Pl+Bt±Ms±Chl±Sil±Ap (Finch et al., 2015). Shearing of the diatexite led to compositional layering consisting of layers of Qtz+Fsp alternating with layers of Bt+Ms+Qtz+Fsp and monominerallic quartz ribbons. The latter are laterally continuous and show GBM recrystallization (Finch et al., 2015). Plagioclase and K-feldspar contain growth twins and form tabular to rounded phenocrysts that are partially sericitised. Biotite and muscovite show strong preferred orientation parallel to the foliation.

Finch et al. (2015) showed that the transition from weakly-deformed protolith through protomylonites, mylonites and to ultramylonites is defined by an increase in the proportion of recrystallised matrix and a concomitant decrease in the proportion of quartz ribbons and porphyroclasts. Hunter et al. (submitted) determined that porphyroclast rotation in protomylonites and mylonites caused the gradual disruption of quartz ribbons and compositional layering. They also showed that mylonites showed stronger Crystallographic Preferred Orientation (CPO) of quartz than protomylonites and both rock types deformed by dislocation creep and underwent grain-size reduction through recrystallisation. In contrast, ultramylonites showed evidence of grain-size sensitive processes, including GBS, which caused phase mixing and weakened the CPO of quartz. The recrystallization of feldspar and GBM in quartz indicates that rocks deformed at amphibolite facies (Finch et al., 2015). A later greenschist facies overprint is recorded by retrogression of biotite to chlorite and sericitization of feldspars. For a detailed description of these rocks see chapter 2, sections 3 and 5.

3. Method

We measured the water concentration in quartz and feldspars in ultramylonites and their less-deformed equivalents by means of FTIR. One double-polished XZ thin section was made of each sample. The final thickness (Table 1) was consistent over the area of the thin section and measured using a Mitutoyo digimatic micrometer with a resolution of 1 μm. Thin sections were ~50 μm thick except for one more fragile sample that was 75 μm thick (Table 1). Thin sections were scanned and photo-mosaic maps created in crossed-polarised light to assist in identification of grains for analysis.

A Varian FTS 7000 FTIR spectrometer with a Varian 600 UMA microscope was used at the Molecular Spectroscopy Centre, School of Chemistry, Monash University. The sample was placed on the microscope stage and the aperture adjusted to 50 μm square. Although a plastic guard was lowered to reduce atmospheric influence, sharp spikes in the absorption spectra indicate the presence of a small amount of atmospheric H_2O but this does not affect measurement of the broadband absorption for liquid water (Post and Tullis, 1998). Once the microscope was focussed and aligned the sample was moved out of the beam path and a background spectrum was taken. Water content was measured in individual grains in the matrix, quartz ribbons, and

Table 1.

Samples, thicknesses, means, and standard deviations for quartz and feldspar water content in the three mylonitisation categories.

Quartz

Mylonitisation category	Sample	Thickness (cm)	n	Mean ppm	Std. Dev.	Mean H:10^6 Si
Weakly-deformed rocks	SQ183a	0.0051	18	552	307	3684
	SQ183b	0.0050	20	548	229	3657
	SQ77a	0.0057	18	604	367	4030
	Overall		56	537	298	3790
Mylonites	SQ32a	0.0055	21	495	251	3305
	SQ30a	0.0051	20	290	134	1931
	SQ187d	0.0049	16	350	160	2335
	SQ187e	0.0050	15	298	160	1986
	SQ26a	0.0051	19	478	207	3186
	Overall		91	383	205	2549
Ultramylonites	SQ80a	0.0050	18	255	190	1700
	SQ8d	0.0055	31	294	191	1963
	SQ29b	0.0076	15	145	100	970
	SQ83	0.0052	15	236	122	1576
	SQ77c	0.0050	16	317	171	2113
	Overall		95	258	172	1664

Feldspar

Mylonitisation category	Sample	Thickness (cm)	n	Mean ppm	Std. Dev.	Mean H:10^6 Si,Al
Weakly-deformed rocks	SQ183a	0.0051	19	310	172	2499
	SQ183b	0.0050	21	362	82	2794
	SQ77a	0.0057	14	519	338	4638
	Overall		54	384	218	3310
Mylonites	SQ32a	0.0055	19	185	91	1481
	SQ30a	0.0051	21	184	128	1420
	SQ187d	0.0049	26	278	186	2177
	SQ187e	0.0050	16	271	213	2088
	SQ26a	0.0051	16	251	110	1937
	Overall		98	234	157	1821
Ultramylonites	SQ80a	0.0050	16	117	94	903
	SQ8d	0.0055	14	294	189	2268
	SQ29b	0.0076	16	67	62	516
	SQ83	0.0052	17	131	82	1014
	SQ77c	0.0050	17	219	120	1688
	Overall		80	163	137	1278

feldspar porphyroclasts. Optically-clear regions were identified using a reflected-light microscope with the aid of photo-mosaic maps. No grain or subgrain boundaries, microcracks, altered or retrogressed regions were sampled. Spectra were obtained over a wavenumber of 700 to 4000 cm^{-1} at room temperature and were normalized to the background spectra. Between 14 and 31 spectra were collected for quartz and feldspar from each sample depending on the number of optically-clear areas available.

O-H stretching bonds in OH and H_2O cause a broad absorbance peak from 2800–3800 cm^{-1} (Kats, 1962) and the height of the peak increases with greater water content and is associated with hydrolytic weakening (Kekulawala et al., 1978). The concentration of water in quartz was calculated as the integral area under the broad peak between 2800 to 3800 cm^{-1} using the integral absorbance version of the Beer-Lambert law:

$$A = k \cdot C \cdot t \tag{1}$$

Where A is the integrated absorbance (cm^{-1}), k is the integral molar absorption coefficient of the molecule absorbing the radiation (mol^{-1} cm^{-2}), C is the water concentration in the sample (H:10^6 Si), and t is the thickness of the sample (cm). The calibration factor, k was taken from Kats (1962) for consistency with previously published work (e.g., Kronenberg et al., 1990, Kronenberg and Wolf, 1990, Gleason and DeSisto, 2008). Water concentrations in H:10^6 Si were divided by 6.67 to obtain concentrations in ppm by weight (Gleason and DeSisto, 2008).

To calculate water concentration in feldspar a modified version of the Beer-Lambert law in (1) was used as follows:

$$A = k \cdot c \cdot t \tag{2}$$

where c is the water content in ppm H_2O to $KAlSi_3O_8$ by weight and the value of k is 15.3±0.7 ppm^{-1} cm^{-2} (Johnson and Rossman, 2003). Water concentration in ppm was multiplied by 7.72 to obtain concentrations in H:10^6 Si, Al. The data for quartz and feldspar are reported in ppm by weight and molar concentration (H:10^6 Si or H:10^6 Si,Al) in Table 1 to assist comparisons to other work. Example spectra from a quartz grain and a feldspar grain are shown in Fig. 1.

4. FTIR results

Samples were separated into three categories: (1) weakly-deformed rocks, (2) mylonites, and (3) ultramylonites. Protomylonites contained only a few percent more recrystallised matrix than the weakly-deformed granitic diatexite so they were grouped together in the weakly-deformed category. The sample thicknesses, mean water concentrations and standard deviations for each sample and category are shown in Table 1 (see Appendix A for full data set).

There is a slight tendency for water concentrations to be higher in the quartz ribbons than in the matrix quartz, and higher in matrix feldspar than porphyroclast feldspar (see Appendix A for details). However, these differences are small and inconsistent so the different observations for each mineral are combined for further analysis.

Fig. 1. Infrared spectra for optically clear regions of grains of (a) quartz and (b) feldspar with insets zoomed on broad absorbance peak of interest.

The data show that the mean water content is lowest in ultramylonites and higher in mylonites and weakly-deformed rocks (Fig. 2). The three rock groups show large standard deviations that vary systematically (see size of the error bars in Fig. 2). Large ranges of values and high standard deviations are common (Fig. 3; e.g. Post and Tullis, 1998, Gleason and DeSisto, 2008, Han et al., 2013) and reflect the multitude of sites water can reside within crystals beyond the equilibrium amount of molecular water, including within dislocations and fluid inclusions (Post and Tullis, 1998).

We performed statistical tests to investigate if the differences between the three groups were significant. To test the differences in molar water concentration between three levels of the independent variable (mylonitisation intensity), a one-way analysis of variance (ANOVA) would typically be employed. However, the standard version of ANOVA assumes that data are normally distributed and homoscedastic and preliminary tests indicated that these assumptions were violated (discussed in section 5.2). Consequently Welch's one-way ANOVA (Welch, 1951) was employed as it is robust to violations of these assumptions and widely considered to be the best alternative (e.g. Lix et al., 1996, Grissom, 2000). This test determines whether there is a difference between any of the groups in mylonitisation intensity (main effect of the independent variable) but does not determine the locus of the effect (i.e., which groups are statistically different from each other). ANOVAs determine the ratio of the variance between groups to the variance within groups (the F statistic), which is close to one if groups are not statistically different from one another. The test weights the variance by the degrees of freedom (number of observations in each group minus 1) and, based on the value of the F-statistic, determines the likelihood that the differences between groups occurred by chance (p value), with values less than 5% ($p < 0.05$) usually taken to indicate statistical significance. If a significant main effect is determined, post-hoc tests are then employed to determine which of the three groups are significantly different from each other. This approach
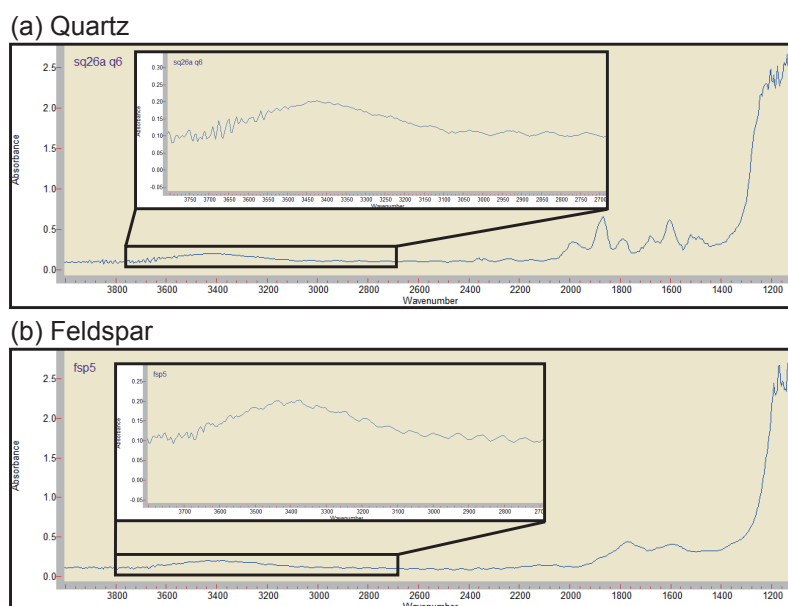
is taken to reduce the type-1 error rate (the chance of falsely rejecting the null hypothesis), which increases when multiple tests are performed instead of one omnibus test.

Analysis indicates that there is a significant main effect of mylonitisation intensity for quartz (F = 25.96 (degrees of freedom between groups= 2, within groups= 122.20), $p < 0.05$) and feldspar (F (2, 118.51) = 21.33, $p < 0.05$). Post-hoc comparisons using the Games-Howell test indicated that quartz in ultramylonites (mean water content (mean = 1721 H:10^6 Si contained significantly less water than quartz in weakly-deformed rocks (mean = 3786 H:10^6 Si) and

Fig. 2. (a) Mean molar water concentration in quartz and feldspar for weakly-deformed rocks, mylonites, and ultramylonites. Error bars are one standard deviation from the mean.

mylonites (mean = 2590 H:10^6 Si; Fig. 2). Similarly there was significantly less water in feldspar in ultramylonites (mean = 1255 H:10^6 Si, Al) than weakly-deformed rocks (mean = 3168 H:10^6 Si, Al) and mylonites (mean = 1826 H:10^6 Si, Al; Fig. 2). Quartz and feldspar in mylonites also contained significantly less water than the same minerals in weakly-deformed rocks.

5. Discussion

In the PSZ, water content in quartz and feldspar reduces with increasing deformation intensity (Fig. 2). This is inconsistent with research on hydrolytic weakening that has found the opposite (Fig. 3). However, it is consistent with studies that have shown that water is liberated from minerals during recrystallization. We first discuss the mechanism for liberation of water from rocks in a shear zone and then the meaning of this result for the evolution of the PSZ, before discussing the differences between this study and others and proposing a model for shear zone widening.

5.1. Water extraction from minerals and shear zones

In the PSZ, quartz and feldspar show a statistically significant decrease in water content from weakly-deformed rocks to ultramylonites. This is concomitant with an increase in recrystallisation, consistent with the results of Kerrich (1976) and Faleiros et al. (2010) who determined that recrystallisation liberated intracrystalline water, which could be extracted from the actively deforming zone. The pressure gradient between shear zone and surroundings will then control the fate of this water. Casey (1980), Mancktelow (1993), and Mancktelow (2002) found that the weakest part of a shear zone has higher

Fig. 3. Mean molar water concentration in (a) quartz and (b) feldspar compared to previous studies. Kronenberg et al. (1990) and Nakashima et al. (1995) did not categorise rocks on the degree of deformation but rather the distance from a central fault surface. We designated the samples closest to the fault surface as most deformed and separated the remainder of the data evenly into the two less deformed groups on the basis of distance from the fault surface. Han et al. (2013) described the degree of deformation for their samples and we split their data into three groups using their descriptions.

mean pressure than the stronger surroundings. Consequently, they argued that fluids are expelled from the shear zone outwards (Mancktelow, 2002).

Fusseis et al. (2009) suggested that GBS in the middle crust provided a mechanism for fluid flow through deformed rocks in their 'dynamic granular fluid pump' model. The model is based on the movement of grains during GBS, which causes opening and closure of vacancies in the matrix of the rock (Fusseis et al., 2009). Fusseis et al. (2009) suggested that when a cavity opens, water moves from the grain boundaries to the vacant site and then, as grains move again, the site closes and the fluid is pumped from the vacancy onto the next grain boundary. This motion creates a type of dynamic porosity that pumps fluids laterally through the rock.

Oliot et al. (2014) combined the 'dynamic granular fluid pump' model and the pressure gradient model of Mancktelow (2002) to explain widening of a shear zone. They determined that weak rocks in the centre of the shear zone experienced grain-size decrease and began deforming by 'fluid-assisted granular flow', a combination of GBS and dissolution-precipitation enhanced by the presence of water. This gave rise to a pressure gradient that expelled fluids to the shear zone margins by means of dynamic 'pumping'. The addition of water to the host rock caused hydraulic microfracturing and metasomatism, which caused weakening and shear zone widening (Oliot et al., 2010, Oliot et al., 2014). We propose a variation on this model to explain the development of the thick layer of ultramylonite in the PSZ.

5.2. Widening of the PSZ

Based on the evidence presented here and in Hunter et al. (submitted) we propose that generation of the 1 km-thick ultramylonite occurred through shear-zone widening by water loss to the surroundings. Strain localisation began in a narrow, propitious site, perhaps slightly more micaceous, or previously fractured (Fig. 4a). The first stages of shearing gave rise to a mylonite through grain-size insensitive mechanisms (Hunter et al., submitted). These processes generated heat, reduced the grain size, and caused liberation of water to the grain boundaries (Fig. 4b; Kerrich, 1976, Faleiros et al., 2010). High pressure in the weak shear zone (Mancktelow, 2002) caused gradual expulsion of water to the surroundings. The diffusion of water and heat caused weakening of the surroundings, widening the shear zone. Although not investigated here, biotite and muscovite recrystallization may also have provided water to the system. As deformation progressed, the presence of fluids on grain boundaries in the main shear zone promoted diffusion creep, including GBS when a critical grain size was reached (Fig. 4b; Chen and Argon, 1979, Mainprice and Paterson, 1984) and dissolution-precipitation, allowing fluid-assisted granular flow (Oliot et al., 2014). These processes caused phase mixing and decreased the connectivity of weak phases, homogenising the rock matrix, giving rise to the ultramylonite (Oliot et al., 2014, Hunter et al., submitted). While the rate of water expulsion from the shear zone was roughly balanced with the rate of intracrystalline water liberation by recrystallization, a weak rheology was maintained in the shear zone (Fig. 4b). As the rate of intracrystalline water liberation slowed due to continued water loss, the ultramylonite hardened, eventually becoming stronger than the weakened shear zone margins (Fig. 4c). This refocused deformation to the margins and caused repetition of the cycle, gradually building up the 1 km-thick layer of ultramylonite preserved today (Fig. 4). We refer to this cycle of recrystallisation, water liberation and expulsion, weakening of the neighbouring rocks, and hardening of the ultramylonite as the water expulsion cycle.

5.3 Hydrolytic weakening in natural shear zones

There are two possible explanations for the contrast between our results and previous

(a) Protolith: granitic diatexite

Bt

Qtz

Pl

Kfs
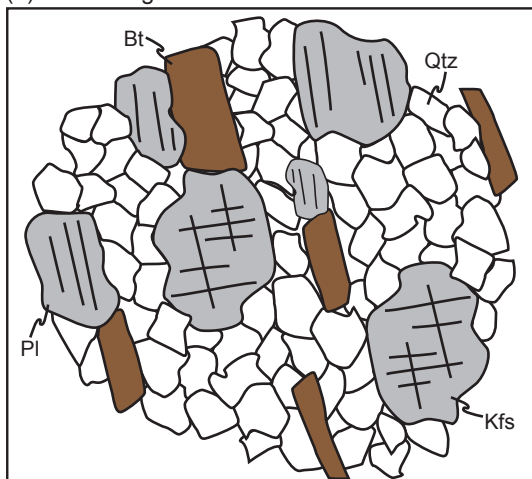
(b) Localisation to weak zone

Water liberated from crystals to grain boundaries
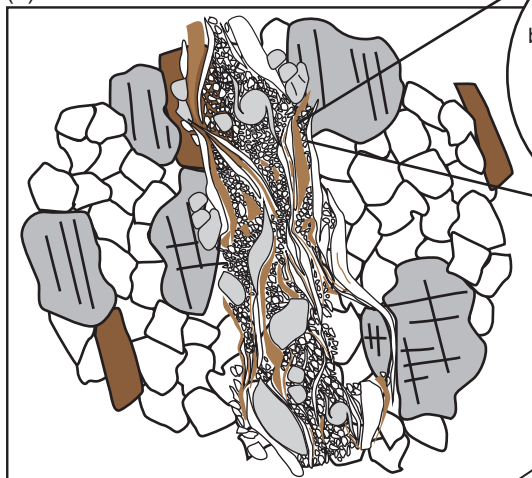
Water

(c) Ultramylonitisation and water expulsion

Water expulsion to ultramylonite margin

Water

Hardened
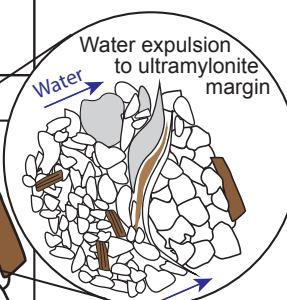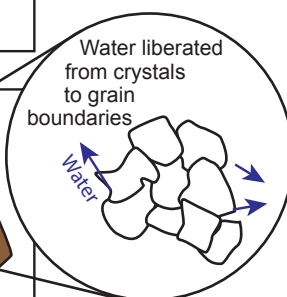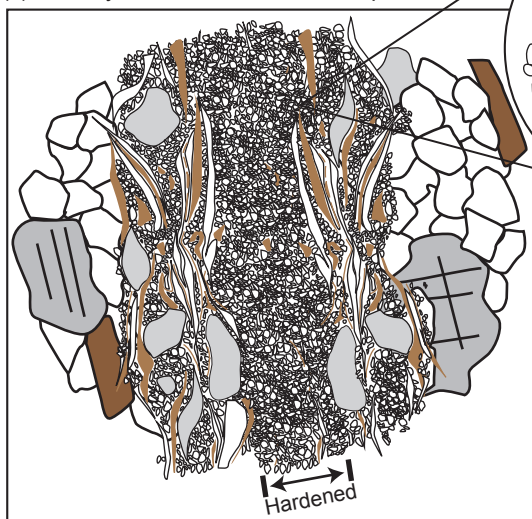
studies. High water content in sheared rocks could be a result of: (1) limited water loss during deformation, or (2) water infiltration after deformation with more efficient diffusion into the rocks of high strain zones than the surroundings (Gleason and DeSisto, 2008).

In order to establish whether hydrolytic weakening has occurred, the relative timing of water infiltration and shearing must be determined. One study that demonstrated this is Kronenberg et al. (1990) who suggested that the source of water was fluid inclusions in microfractures and overprinting relationships indicated the fractures formed before ductile shearing. The contribution fluid inclusions make to hydrolytic weakening is uncertain and is likely to remain unresolved until the mechanism for hydro-

Fig. 4. Model for shear zone widening: the water expulsion cycle. (a) Granitic diatexite protolith begins shearing (b) A mylonitic band forms and shear heat diffuses out to shear zone margins. Recrystallisation causes liberation of intracrystalline water to grain boundaries (inset) and towards the margins of the shear zone, in response to pressure gradients. (c) Water on grain boundaries accelerates diffusion, GBS and dissolution-precipitation which causes ultramylonitisation and mixing of phases. During steps (b) and (c) the outward flux of water may be aided by pumping due to dynamic porosity created during GBS. At this stage, the balance between water liberation by recrystallisation and water fluxing outwards is lost and the ultramylonites begin to dry and harden, while the shear zones shoulders weaken. This process causes the locus of maximum strain rate to move outwards, where the cycle begins again.

lytic weakening is understood. Nevertheless, the direction of causation implied in Kronenberg et al. (1990) appears reasonable and suggests that hydrolytic weakening caused strain localisation. The question then remains of why water in the rocks of Kronenberg et al. (1990) was not liberated during recrystallisation and ductile deformation. In the microstructural description of the shear zone rocks in Kronenberg et al. (1990) they state that quartz grains show undulatory extinction and are recrystallised at their margins while feldspar does not show ductile deformation, only microcracks. This description suggests that while these rocks are deformed, they are not mylonitic and have not undergone substantial recrystallisation and accompanying water liberation.

The same cannot be concluded for studies of mylonitic rocks (e.g. Gleason and DeSisto, 2008; Han et al., 2013; Nakashima et al., 1995), where substantial recrystallization makes it unlikely minerals would have retained their original water content. It is possible that the positive correlation between water content and deformation in these studies was due to post-tectonic diffusion of water that was more efficient in more deformed rocks, as suggested by Gleason and DeSisto (2008). Alternatively, these shear zones may not have experienced higher mean stress than the matrix, which would prevent the expulsion of fluids from the shear zone. Shear zones that initiate parallel to the shear direction will not undergo extension or shortening during simple shear, so they will remain at the same mean stress as the matrix (Mancktelow, 2002). Conversely, shear zones that initiate or rotate into the field of instantaneous shortening during progressive simple shear will thicken, reducing the mean stress within the shear zone and attracting water from the surroundings (Mancktelow, 2002). It is only shear zones that rotate to the extension direction and undergo stretching and thinning that will experience higher mean stress than the matrix, leading to water expulsion from the shear zone (Mancktelow, 2002) and shear zone hardening.

6. Conclusions

Rocks in the 1 km-thick ultramylonitic layer of the PSZ contain less water than their weakly-deformed protoliths, consistent with studies that have found that recrystallisation liberates intracrystalline water, but inconsistent with many studies of natural shear zones that have found a positive correlation between water content and deformation. We suggest that some of those shear zones may have not undergone substantial recrystallisation minimizing water loss, while others may have been hydrated due to shear zone thickening or post-tectonic fluid infiltration that was more efficient in more deformed rocks.

We proposed here a variation and expansion on the model of Oliot et al. (2014) who found that shear-zone widening was caused by expulsion of an externally-derived fluid out of the shear zone due to a gradient in mean pressure. We propose this also occurred in the PSZ but fluids were derived from grain interiors and liberated during recrystallisation. In contrast to the

cms-wide ultramylonite in Oliot et al. (2014), we find that this water expulsion cycle may have repeated many times, gradually building up the 1km-thick ultramylonite of the PSZ.

References

Aines, R. D. and Rossman, G. R., 1984. Water in minerals? A peak in the infrared. Journal of Geophysical Research: Solid Earth 89(B6), 4059-4071.

Blacic, J. D., 1975. Plastic-deformation mechanisms in quartz: The effect of water. Tectonophysics 27(3), 271-294.

Carter, N. L., Christie, J. M. and Griggs, D. T., 1964. Experimental Deformation and Recrystallization of Quartz. The Journal of Geology 72(6), 687-733.

Casey, M., 1980. Mechanics of shear zones in isotropic dilatant materials. Journal of Structural Geology 2(1-2), 143-147.

Chen, I. W. and Argon, A. S., 1979. Grain boundary and interphase boundary sliding in power law creep. Acta Metallurgica 27(5), 749-754.

Christie, J. M., Griggs, D. T. and Carter, N. L., 1964. Experimental Evidence of Basal Slip in Quartz. The Journal of Geology 72(6), 734-756.

Drury, M. R. and Urai, J. L., 1990. Deformation-related recrystallization processes. Tectonophysics 172(3–4), 235-253.

Faleiros, F. M., Campanha, G. A. d. C., Bello, R. M. d. S. and Fuzikawa, K., 2010. Quartz recystallization regimes, c-axis tecture transitons and fluid inclusion reequilibration in a prograde greenschist to amphibolite facies mylonite zone (Ribeira Shear Zone, SE Brazil). Tectonophysics 485, 193-214.

Finch, M. A., Weinberg, R. F., Fuentes, M. G., Hasalova, P. and Becchio, R., 2015. One kilometre-thick ultramylonite, Sierra de Quilmes, Sierras Pampeanas, NW Argentina. Journal of Structural Geology 72, 33-54.

Fusseis, F., Regenauer-Lieb, K., Liu, J., Hough, R. M. and De Carlo, F., 2009. Creep cavitation can establish a dynamic granular fluid pump in ductile shear zones. Nature 459, 974-977.

Gerretsen, J., Paterson, M. S. and McLaren, A. C., 1989. The uptake and solubility of water in quartz at elevated pressure and temperature. Physics and Chemistry of Minerals 16(4), 334-342.

Gleason, G. C. and DeSisto, S., 2008. A natural example of crystal-plastic deformation enhancing the incorporation of water into quartz. Tectonophysics 446(16-30).

Griggs, D. T. and Blacic, J. D., 1964. The strength of quartz in the ductile regime. Eos Transactions 45, 102-103.

Griggs, D. T. and Blacic, J. D., 1965. Quartz: Anomalous Weakness of Synthetic Crystals. Science 147(3655), 292-295.

Grissom, R. J., 2000. Heterogeneity of Variance in Clinical Data. Journal of Consulting & Clinical Psychology 68(1), 155-165.

Groome, W. G., Johnson, S. E. and Koons, P. O., 2006. The effects of porphyroblast growth on the effective viscosity of metapelitic rocks: implications for the strength of the middle crust. Journal of Metamorphic Geology 24(5), 389-407.

Han, L., Zhou, Y. S. and He, C. R., 2013. Water enhanced plastic deformation in felsic rocks. Science in China Earth Series 56(2), 203-216.

Hippertt, J. F. and Hongn, F. D., 1998. Deformation mechanisms in the mylonite/ultramylonite transition. Journal of Structural Geology 20(11), 1435-1448.

Hobbs, B. E., 1981. The influence of metamorphic environment upon the deformation of minerals. Tectonophysics 78(1-4), 335-383.

Holyoke III, C. W. and Kronenberg, A. K., 2013. Reversible water weakening of quartz. Earth and Planetary Science Letters 374, 185-190.

Hull, J., 1988. Thickness-displacement relationships for deformation zones. Journal of Structural Geology 10(4), 431-435.

Hunter, N. J., Hasalova, P., Weinberg, R. F., Finch, M. A. and Becchio, R., submitted. Clast rotation and strain localisation in thick ultramylonites: The El Pichao shear zone, NW Argentina. GSA Bulletin Submitted.

Johnson, E. A. and Rossman, G. R., 2003. The concentation and speciation of hydrogen in feldspars using FTIR and 1H MAS NMR spectroscopy. American Mineralogist 88, 901-911.

Johnson, S. E., Jin, Z.-H., Naus-Thijssen, F. M. J. and Koons, P. O., 2011. Coupled deformation and metamorphism in the roof of a tabular midcrustal igneous complex. GSA Bulletin 123(5-6), 1016-1032.

Kats, A., 1962. Hydrogen in alpha-quartz. Philips Research Reports 17, 1-31, 133-195.

Kekulawala, K. R. S. S., Paterson, M. S. and Boland, J. N., 1978. Hydrolytic weakening in quartz. Tectonophysics 46(1–2), T1-T6.

Kerrich, R., 1976. Some effects of tectonic recrystallisation on fluid inclusions in vein quartz. Contributions to Mineralogy and Petrology 59(2), 195-202.

Kohlstedt, D. L., 2006. The role of water in high-temperature rock deformation. In: Water in Nominally Anhydrous Minerals (edited by Keppler, H. & Smyth, J. R.). Reviews in Mineralogy & Geochemistry 62, 377-396.

Kronenberg, A. K., 1994. Hydrogen speciation and chemical weakening of quartz. In: Silica: Physical behavior, geochemistry and materials applications (edited by Heaney, P. J., Prewitt, C. T. & Gibbs, G. V.). Mineralogical Society of America, Washington, DC, 123-176.

Kronenberg, A. K., Segall, P. and Wolf, G. H., 1990. Hydrolytic weakening and penetrative deformation within a natural shear zone. In: The Brittle-Ductile Transition in Rocks: the Heard volume (edited by Duba, A. G., Durham, W. B., Handin, J. W. & Wang, H. F.) 56. American Geophysical Union Monograph, 21-36.

Kronenberg, A. K. and Tullis, J., 1984. Flow strengths of quartz aggregates: Grain size and pressure effects due to hydrolytic weakening. Journal of Geophysical Research 89(B6), 4281-4297.

Kronenberg, A. K. and Wolf, G. H., 1990. Fourier transform infrared spectroscopy determinations of intragranular water content in quartz-bearing rocks: implications for hydrolytic weakening in the laboratory and within the earth. Tectonophysics 172(3–4), 255-271.

Lix, L. M., Keselman, J. C. and Keselman, H. J., 1996. Consequences of assumption violations revisited: A quantitative review of alternatives to the one-way analysis of variance F test. Review of Educational Research 66(4), 579-619.

Mainprice, D. H. and Paterson, M. S., 1984. Experimental studies of the role of water in the plasticity of quartzites. Journal of Geophysical Research 89(NB6), 4257-4269.

Mancktelow, N. S., 1993. Tectonic overpressure in competent mafic layers and the development of isolated eclogites. Journal of Metamorphic Geology 11(6), 801-812.

Mancktelow, N. S., 2002. Finite-element modelling of shear zone development in viscoelastic materials and its implications for localisation of partial melting. Journal of Structural Geology 24(6–7), 1045-1053.

Mancktelow, N. S. and Pennacchioni, G., 2004. The influence of grain boundary fluids on the microstructure of quartz-feldspar mylonites. Journal of Structural Geology 26(1), 47-69.

Mancktelow, N. S. and Pennacchioni, G., 2005. The control of precursor brittle fracture and fluid–rock interaction on the development of single and paired ductile shear zones. Journal of Structural Geology 27(4), 645-661.

Means, W. D., 1984. Shear zones of types I and II and their significance for reconstruction of rock history. Geological Society of America Abstracts with Programs 16, 50.

Means, W. D., 1995. Shear zones and rock history. Tectonophysics 247(1–4), 157-160.

Mittempergher, S., Dallai, L., Pennacchioni, G., Renard, F. and Di Toro, G., 2014. Origin of hydrous fluids at seismogenic depth: Constraints from natural and experimental fault rocks. Earth and Planetary Science Letters 385(0), 97-109.

Nakashima, S., Matayoshi, H., Yuko, T., Michibayashi, K., Masuda, T., Kuroki, N., Yamagishi, H., Ito, Y. and Nakamura, A., 1995. Infrared microspectroscopy analysis of water distribution in deformed and metamorphosed rocks. Tectonophysics 245(3–4), 263-276.

Oliot, E., Goncalves, P. and Marquer, D., 2010. Role of plagioclase and reaction softening in a metagranite shear zone at mid-crustal conditions (Gotthard Massif, Swiss Central Alps). Journal of Metamorphic Geology 28(8), 849-871.

Oliot, E., Goncalves, P., Schulmann, K., Marquer, D. and Lexa, O., 2014. Mid-crustal shear zone formation in granitic rocks: Constraints from quantitative textural and crystallographic preferred orientations analyses. Tectonophysics 612-613, 63-80.

Passchier, C. W. and Trouw, R. A. J., 2005. Microtectonics. Springer-Verlag Berlin, Heidelberg.

Paterson, M. S., 1989. The interaction of water with quartz and its influence in dislocation flow - an overview. In: Rheology of Solids and of the Earth (edited by Karato, S. I. & Toriumi, M.). Oxford University Press, London, 107-142.

Paterson, M. S. and Kekulawala, K. R. S. S., 1979. The role of water in quartz deformation. Bulletin Mineralogie 102, 92-98.

Platt, J. P. and Behr, W. M., 2011. Lithospheric shear zones as constant stress experiments. Geology 39(2), 127-130.

Poirier, J. P., 1980. Shear localization and shear instability in materials in the ductile field. Journal of Structural Geology 2(1–2), 135-142.

Post, A. D. and Tullis, J., 1998. The rate of water penetration in experimentally deformed quartzite: implications for hydrolytic weakening. Tectonophysics 295, 117-137.

Ramsay, J. G. and Graham, R. H., 1970. Strain variation in shear belts. Canadian Journal of Earth Science 7, 786 - 813.

Regenauer-Lieb, K. and Yuen, D. A., 1998. Rapid conversion of elastic energy into plastic shear heating during incipient necking of the lithosphere. Geophysical Research Letters 25(14), 2737-2740.

Sibson, R. H., 1977. Fault rocks and fault mechanisms. Journal of the Geological Society of London 133, 191-213.

Urai, J. L., Means, W. D. and Lister, G. S., 1986. Dynamic Recrystallization of Minerals. In: Mineral and Rock Deformation: Laboratory Studies: The Paterson Volume (edited by Hobbs, B. E. & Heard, H. C.). American Geophysical Union, Washington, DC, 161-199.

Welch, B. L., 1951. On the comparison of several mean values: An alternative approach. Biometrika 38, 330-336.

White, S. H. and Knipe, R. J., 1978. Transformation- and reaction-enhanced ductility in rocks. Journal of the Geological Society London 135(5), 513-516.

Chapter 4

The tectono-metamorphic evolution of the Famatinian Sierra de Quilmes, Sierras Pampeanas, NW Argentina

M.A. Finch[1], R.F. Weinberg[1], P. Hasalová[2], R. Becchio[3], A. Kennedy[4]

[1]School of Earth, Atmosphere and Enivronment, Monash University, Clayton, Victoria, 3800, Australia

[2]Centre for Lithospheric Research, Czech Geological Survey, Klárov 3, 118 21 Prague 1, Czech Republic

[3]Instituto Geonorte, National University of Salta, INENCO-CONICET, Av. Bolivia, 5150, 4400 Salta, Argentina

[4]Department of Applied Physics, Curtain University, Bentley, Western Australia, 6102, Australia

Previous page: Restitic Bt-Grt-Crd layer in migmatite from the Tolombón complex, Sierra de Quilmes

Monash University

Declaration for Thesis Chapter 4

Declaration by candidate

In the case of Chapter 4, the nature and extent of my contribution to the work was the following:

Nature of contribution	Extent of contribution (%) for student co-authors only
Fieldwork, structural analysis, petrography, thermodynamic modelling, geochronological analysis, preparation of the chapter	90%

The following co-authors contributed to the work. If co-authors are students at Monash University, the extent of their contribution in percentage terms must be stated:

Name	Nature of contribution
R.F. Weinberg	Supervisory role
P. Hasalová	Supervisory role
R. Becchio	Assistance with field work
A. Kennedy	Assistance with geochronology data acquisition

The undersigned hereby certify that the above declaration correctly reflects the nature and extent of the candidate's and co-authors' contributions to this work*.

Candidate's Signature   **Date**

Main Supervisor's Signature   **Date**

Abstract

The Sierras Pampeanas reveal a rich record of the impact of subduction on the western margin of Gondwana during the Paleozoic. The magmatic arc and back-arc region of the Late Cambrian - Silurian Famatinian orogeny are preserved discontinuously over 1000 km in the Sierras Pampeanas, a series of mountain blocks uplifted in the foreland of the Andean orogeny. One of these mountain blocks, the Sierra de Quilmes, consists of a tilted metamorphic terrane that has been displaced by a number of Ordovician shear zones, making it a valuable orogen for unravelling the events of the Famatinian orogeny. We present new metamorphic, structural, geochronological, and geothermobarometric data on Sierra de Quilmes, which places it within its regional tectono-metamorphic context. Metamorphism was high temperature, low pressure and peak metamorphism occurred between 485 and 465 Ma. Metamorphic isograds, from greenschist to granulite facies, increase in grade from NE to SW in the northern section of Sierra de Quilmes and are repeated on either side of two major shear zones: the Tolombón thrust and the El Pichao shear zone. These are E or NE dipping and have top-to-W or -NW shear sense and this, combined with the emplacement of hot rocks on top of cooler rocks, indicates ductile thrusting. Shortening was coincident with peak metamorphism, a result of either contact metamorphism, increased rates of shallow convection of the asthenosphere, or inheritance of elevated geotherms due to early extension. We find no evidence to support previous models that suggest shearing in the Sierra de Quilmes occurred during extension.

1. Introduction

The rocks of NW Argentina record deformation and metamorphism related to sub-duction and terrane accretion on the paleo-Pacific margin of Gondwana. Three major orogenic events are recognised from the Paleozoic: the Cambrian Pampean orogeny (540 – 520 Ma; Rapela et al., 1998a,b), the late Cambrian to Silurian Famatinian orogeny (490 – 430 Ma; Rapela et al., 1998a, Sims et al., 1998) including the Oclóyic tectonic phase (470–430 Ma; Bahlburg and Herve, 1997, Rapela et al., 1998a), and the Devonian to Carboniferous Achalian orogeny (400 – 350 Ma; Rapela et al., 1998a, Steenken et al., 2011). These periods of subduction accreted, then deformed and metamorphosed rocks in the region between the Río de la Plata craton to the west, and the Chilenia terrane to the east (Fig. 1b in chapter 1; Aceñolaza et al., 2002). This region is known as the Sierras Pampeanas and was uplifted in the foreland of the Andean orogeny to form twelve N-S trending mountain blocks in northwest and central Argentina (Jordan and All-mendinger, 1986). Each of the three orogenies produced intrusive rocks and west-directed ductile shear zones, which occur discontinuously in the Sierras Pampeanas, over 1000 km along strike and over a width of >250 km (Höckenreiner et al., 2003).

While the subduction-terrane accretion model is reasonably well-delineated for the southern Sierras Pampeanas, there is very little evidence for the model in the northern section. For example, the northern Sierras Pampeanas lacks ophiolites (Mon and Hongn, 1991, Bahlburg and Herve, 1997, Bock et al., 2000), suture zones (Franz and Lucassen, 2001), high P/low T met-amorphism, and geochronological and petrological breaks or anomalies (Lucassen et al., 2000). Instead, it is proposed the region formed a mobile belt that accommodated periods of extension and shortening during contiguous Pampean and Famatinian orogenies (Lucassen et al., 2000, Becchio and Lucassen, 2002). The mobile belt consists of sedimentary rocks that were deposited on the southwest margin of Gondwana between 670 and 530 Ma, forming an interbedded psam-mite and pelite turbidite sequence, the Puncoviscana formation (Turner, 1960, Aceñolaza et al., 1988). The onset of subduction in the Pampean orogeny accreted the Puncoviscana Formation onto the Río de la Plata craton (Piñán-Llamas and Simpson, 2006). In the southern Sierras Pam-peanas a magmatic arc formed on the craton, and the Puncoviscana Formation accretionary prism deformed and underwent granulite facies metamorphism (Piñán-Llamas and Simpson, 2006). Collision of the MARA block at ~520 Ma in the southern Sierras Pampeanas signalled the end of the Pampean orogeny. In the northern Sierras Pampeanas magmatism is continuous from 510 Ma to the middle of the Ordovician, which has been interpreted as evidence for contiguous Pampean and Famatinian orogenies (Becchio and Lucassen, 2002). However, many Cambrian granitoids originally thought to be a product of the Pampean orogeny have been reassigned to the Famatin-ian orogeny on the basis of their field relationships with structures developed during Famatinian extension, implying that the Famatinian orogeny may have started earlier in the northern Sierras Pampeanas (Hongn et al., 2010). Commencement of the Famatinian orogeny formed the Famati-

nian magmatic arc on the Puncoviscana Formation accretionary prism (Aceñolaza and Toselli, 1973). The arc is exposed in the Sierras Pampeanas in an area 200 km wide at ~67° W between 22° and 33° S (Fig. 1 in chapter 1; Pankhurst et al., 1998, Tibaldi et al., 2011) and produced S-type granites, voluminous I-type granites, and intrusions of tonalite-trondhjemite-granodiorite sequences (Pankhurst et al., 2000). East of the Famatinian arc, high T/low P metamorphism and anatexis (Grissom et al., 1998, Hauzenberger et al., 2001, Otamendi et al., 2008, Larrovere et al., 2011) and bi-modal volcanism (Coira et al., 2009) suggest the development of a back-arc basin behind the magmatic arc (Fig. 1 in chapter 1). In Puna and the Cordillera Oriental (Fig. 1 in chapter 1), Ordovician sedimentary rocks record a period of extension early in the Ordovician, followed by a switch to thrusting and folding in the Late Ordovician, during the Oclóyic tectonic phase (Bahlburg and Hervé, 1997). Evidence for the back-arc basin is longitudinally continuous from the northern Sierras Pampeanas to the south (22° and 33° S; Chernicoff et al., 2009, Coira et al., 2009). In some areas close to the magmatic arc, metamorphism is a result of contact with arc-related intrusions (Alasino et al., 2014).

Collision of the Laurentia-derived Precordillera terrane with the continent margin (e.g. Pankhurst et al., 1998) or accelerated approach of the terrane prior to collision (Rapela et al., 1998a) in the southern Sierras Pampeanas, began the Oclóyic tectonic phase (Rapela et al., 1998a), with ductile thrusting throughout the back-arc. Mylonitic shear zones, active between 470 and 430 Ma, are pervasive in the Sierras Pampeanas, including, for example, the Tres Arboles shear zone (32° S; Simpson et al., 2003), Arenosa Creek shear zone (31° S; Castro de Machuca et al., 2012), shear zones in the Sierra de Pie de Palo (31° S; Ramos et al., 1998), the Tinogasta-Pituil-Anti-
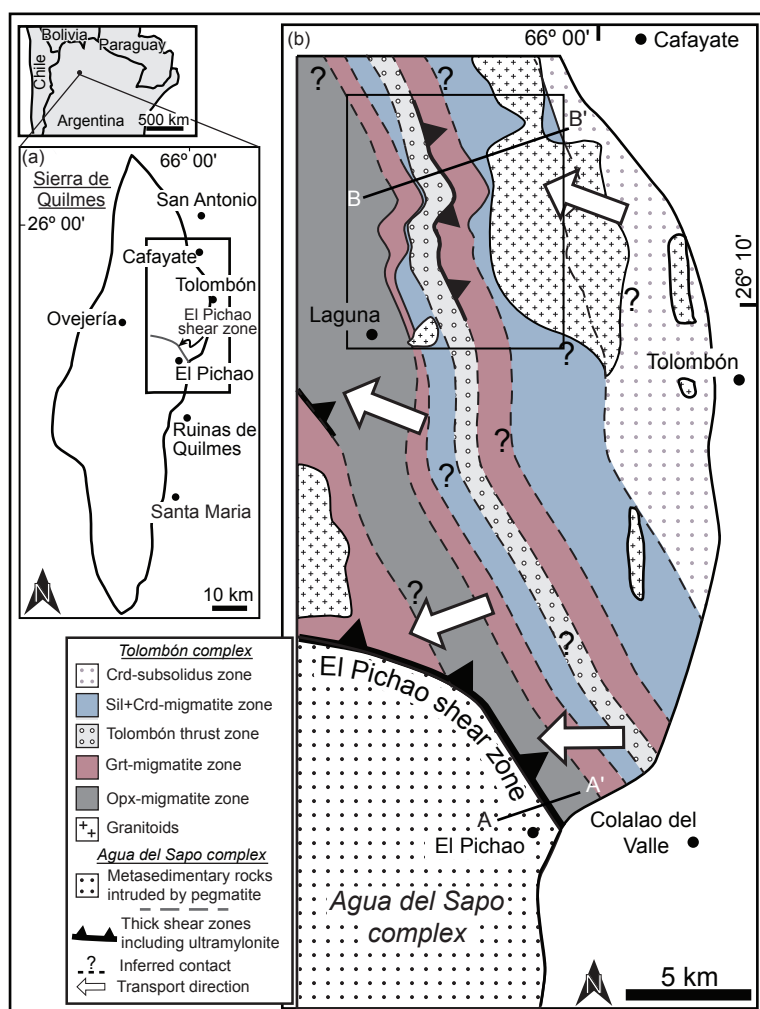
Fig. 1. (a) Outline of the Sierra de Quilmes mountain block with the region shown in (b) boxed. (b) The metamorphic zones of the Tolombón complex and its contact with the Agua del Sapo complex. For a detailed map of the region near El Pichao shear zone see Fig . 2 in chapter 2. In (b) the area shown in Fig. 3 is boxed and the line for the cross section in Fig. 4 is indicated A-A', B-B'.

naco (TIPA) shear zone (27–28° S; Höckenreiner et al., 2003), and the Agua Rosada shear zone (25–26° S; Wegmann et al., 2008; Fig. 1). This has led to the suggestion that the Oclóyic tectonic phase caused shortening and closure of the Famatinian back-arc (Rapela et al., 1998a, Astini and Davila, 2004, Otamendi et al., 2004). Outboard of the western Sierras Pampeanas MARA block, collision of the Precordillera terrane (Fig. 1) south of 29 °S ended the Famatinian orogeny (Thomas and Astini, 2003 and references therein, Varela et al., 2011).

Büttner et al. (2005) and Büttner (2009) found support for the mobile-belt model in the Sierra de Quilmes, northern Sierras Pampeanas (Figs. 1, 2). These mountains expose a sheared and tilted metamorphic terrane varying from greenschist to granulite facies, making it an important region for studying Famatinian orogenesis and metamorphism in the northern Sierras Pampeanas. They found that the shearing in Sierra de Quilmes was a result of extension, not thrusting as is generally interpreted for shear zones in the Sierras Pampeanas. Contrary to this, Finch et al. (2015) reported a Famatinian-age, kilometre-thick, ultramylonitic shear zone in Sierra de Quilmes, the El Pichao shear zone, which thrusts granulite-facies migmatites onto amphibolite-facies metasedimentary rocks and therefore is not a result of extension. The El Pichao shear zone is part of the migmatite terrane studied by Büttner (2009) and Finch et al. (2015) suggested that shearing there also resulted from shortening rather than extension.

In this paper, we first describe the metamorphic paragenesis and structures of the Tolombón complex, followed by thermodynamic and geochronologic analyses. This data, combined with that of previous studies, allows determination of a regionally-consistent tectono-metamorphic model for the Sierra de Quilmes, as part of the Famatinian back-arc. The basin was inverted during the Famatinian, in the Oclóyic tectonic phase, causing crustal shortening and mylonitisation in the thermally-weakened rocks.

2. Geologic setting

The Sierra de Quilmes is a 140 km-long mountain range located in the northern Sierras Pampeanas, west of the town Cafayate (Fig. 1; Rossi De Toselli et al., 1976). The protolith to the mountain range, the Puncoviscana Formation, was described in chapter 1 (section 3.2).

Puncoviscana Formation rocks show a high degree of compositional variability (Fig. 2). Major element data for the entire Sierras Pampeanas from 161 samples of Puncoviscana Formation rocks were compiled, from our own analyses (Table 1) as well as published data (see figure caption for references). The samples plot in the greywacke and lithic arenite fields based on cation ratios (Fig. 2; Pettijohn et al., 1972), consistent with other samples of Puncoviscana Formation in Jezek et al. (1985). Samples are divided into two grain-size dependant end-members: psammites (low-grade sandstones) and pelites (low-grade mudstones; Pettijohn et al., 1972). For samples from the literature this information is not always available. Zimmermann (2005) describe the general appearance of rocks but do not classify single samples as psammites

or pelites. We use their descriptions where possible but where ambiguous, we classify them on the basis of silica content where pelites contain <70% SiO_2 and psammites >70% SiO_2, after Boggs (2006). Do Campo and Guevara (2005) Lucassen et al. (2000), Lucassen et al. (2001), and Sola et al. (2013) classified their samples into psammites and pelites, presumably on the basis of texture and mineralogy as their lithological descriptions suggest. Harker diagrams in Fig. 2 show that Puncoviscana Formation rocks cover a broad compositional range and samples collected in
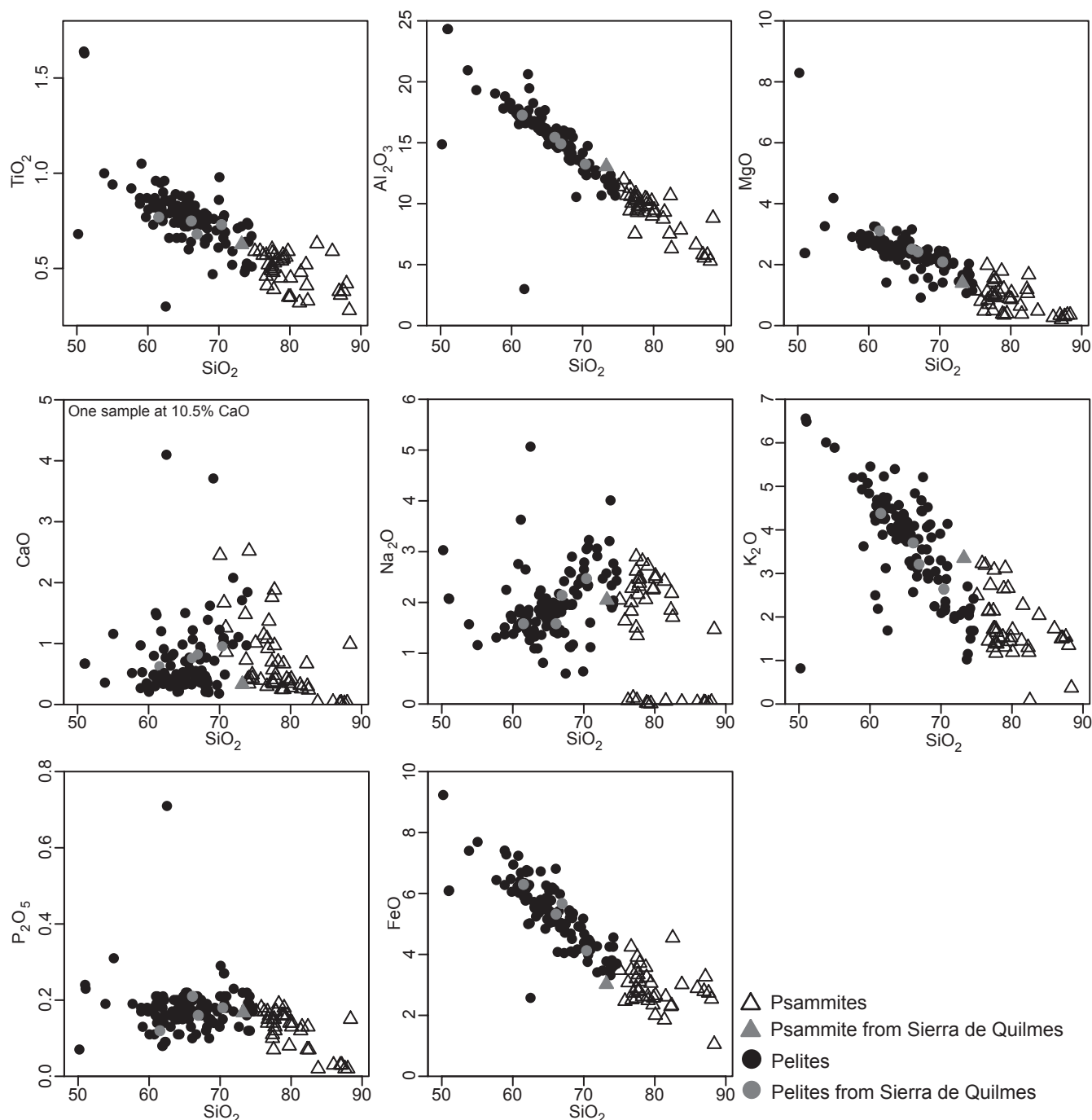
Fig. 2. Harker diagrams for 161 samples of Puncoviscana Formation rocks from the Sierras Pampeanas. Triangles indicate psammites, circles indicate pelites and grey symbols indicate samples (n=5) from Sierra de Quilmes. Data sources are Zimmermann (2005), Do Campo and Guevara (2005), Lucassen et al. (2000), Lucassen et al. (2001), and Sola et al. (2013).

Table 1.
Whole rock major element data for Puncoviscana Formation samples.

Sample	Location	Rock type	SiO$_2$	TiO$_2$	Al$_2$O$_3$	Fe$_2$O$_3$T	MnO	MgO	CaO	Na$_2$O	K$_2$O	P$_2$O$_5$	LOI	Total
Punco1	50 km N of Sierra de Quilmes	Psammite	73.23	0.63	13.06	3.40	0.01	1.38	0.32	2.06	3.36	0.17	2.47	100.10
Punco2a	16 km E of Sierra de Quilmes	Pelite	61.51	0.77	17.26	7.00	0.13	3.11	0.63	1.58	4.38	0.12	2.98	99.49
Punco2b	16 km E of Sierra de Quilmes	Pelite	70.39	0.73	13.25	4.58	0.08	2.09	0.94	2.47	2.64	0.18	1.96	99.31

Sierra de Quilmes plot within the range at the high silica end of the pelite spectrum. Linear trends in TiO$_2$, Al$_2$O$_3$, MgO, K$_2$O, and FeO are attributable to compositional maturity where quartz proportion increases at the expense of clay minerals (Pettijohn et al., 1972). Psammites show a weak, positive linear trend between SiO$_2$ and Na$_2$O reflecting increase in albite content.

The Sierra de Quilmes consists of the metamorphic equivalents of the Puncoviscana Formation divided in two complexes according to metamorphic facies: the amphibolite facies Agua del Sapo complex in the south-east of the range, separated by shear zones from the granulite facies Tolombón complex surrounding it to the north and west (Toselli et al., 1978). The Agua del Sapo complex is thrust under the Tolombón complex by the El Pichao-Overjería shear zone (Fig. 2 in chapter 1). The eastern strand of this shear zone, the El Pichao shear zone (PSZ), is a NW trending 3.5 km-thick mylonitic – ultramylonitic shear zone located west of the village Colalao del Valle (Finch et al., 2015).

The Agua del Sapo complex consists of garnet- and cordierite- bearing gneisses and schists that are intruded by pegmatite dykes (Toselli et al., 1978). The Tolombón complex is a tilted metamorphic sequence and Büttner et al. (2005) described four major metamorphic zones that increase in grade from northeast to southwest, with the lowest grade, chlorite zone in the northeast, which grades into the biotite-muscovite zone, then into the garnet-cordierite-sillimanite zone, and finally the orthopyroxene zone in the southwest. Evidence for anatexis is first apparent in the biotite-muscovite zone with Ms-dehydration melting. This is followed by Bt-dehydration melting in the higher-grade zones (Büttner et al., 2005). Migmatites are mainly stromatic metatexites with diatexites more common in the higher-grade zones in the high mountains to the southwest. The Cafayate pluton intruded into sillimanite-cordierite migmatites and consists of granitoids that grade in composition from granitic in the east to tonalitic in the west (Rapela and Shaw, 1979).

Büttner et al. (2005) dated migmatites from the Tolombón complex and found that monazite growth occurred between 485 and 450 Ma (U/Pb TIMS), better constraining earlier Rb-Sr ages (Rapela et al., 1982, Miller et al., 1991). They also dated muscovite

by Ar/Ar in one of the migmatites to 450±7 Ma, indicating the time of cooling. Lucassen et al. (2000) dated garnet from a deformed gneiss from Anchillo gorge (in the Tolombón complex and immediate hanging wall of the El Pichao shear zone) to 442±9 Ma (Sm-Nd mineral isochrons). Büttner et al's (2005) data suggest a high-temperature regime between 485 and 450 Ma with cooling through muscovite closure by ~ 443 Ma. Using the mean of the high temperature age range, Büttner et al. (2005) suggested peak metamorphism occurred at 470 Ma. Peak metamorphism was accompanied by ductile shearing, which continued as cooling proceeded to amphibolite facies and localized to major shear zones (Finch et al., 2015). Ductile shearing ended with the thrusting of migmatites onto lower-grade rocks (Finch et al., 2015), which Büttner et al. (2005) determined was at ~440 Ma from the dating of undeformed pegmatites that cross-cut ductile shear zones. Büttner et al. (2005) suggest an additional period of localised ductile shearing to explain muscovite (K-Ar) ages between 420 and 370 Ma in low-grade rocks from northern Sierra de Quilmes.

Büttner (2009) described a zone of intense shearing in the Tolombón complex separating the biotite-muscovite zone in the hanging wall and the garnet-cordierite-sillimanite zone in the footwall. He interpreted this as a detachment that allowed the lower-grade rocks to deform differently to the migmatites. Based on the current distance between the detachment and samples of estimated metamorphic pressure in the migmatite terrane, he inferred that the terrane had undergone substantial thinning. He estimated the paleo-pressure of key samples using multi-equilibrium methods and found that the current distance between samples was less than the vertical distance that should separate them based on pressure determinations. From this he inferred that the package as a whole had been thinned, interpreted by Büttner (2009) as indicative of crustal extension. The shear sense throughout the Sierra de Quilmes is top-to-west thrusting, but Büttner (2009) suggested that the shear zones were originally horizontal and accommodated crustal extension and rotated to their current dip during the Andean orogeny. Finch et al. (2015) studied the PSZ, where the granulite facies migmatites of the Tolombón complex studied by Büttner (2009) are on the hanging wall, and lower grade rocks of the Agua del Sapo complex are on the footwall. They interpreted this hot-over-cold sequence as a result of the regional top-to-west thrusting rather than extension. Büttner (2015) argued that Finch et al. (2015) did not date movement on the PSZ. However, Finch et al. (2015) found that that the amphibolite facies PSZ recorded the same kinematics as high-grade shearing in the migmatites, suggesting a continuity of movement and metamorphism, supporting the interpretation of thrusting. We return to this question in later sections in light of new structural and metamorphic data.

3. Metamorphism in the Tolombón complex

In this section we describe the macroscopic and microscopic features in rocks of the Tolombón complex and its overall increase in metamorphic grade to the SW. We use the term

migmatite to describe any partially melted rock with leucosomes, metatexite for migmatites that retain their stromatic layering, diatexite for rocks that have lost coherence due to high melt fraction, neosome for the part of the rock that has undergone partial melting, leucosome for the light-coloured, crystallised product of the melting reaction, and melanosome for the solid or residual part of the neosome left behind after the leucosome was extracted (Mehnert, 1968). The melanosome usually has a high concentration of biotite commonly accompanied by peritectic minerals.

3.1. Analytical procedures and abbreviations

Whole-rock major-element analyses (Tables 1, 2) were carried out at the Advanced Analytical Centre at James Cook University, Townsville, Australia. Minerals were analysed using the HyperProbe field-emission gun electron probe microanalyser at the Microbeam Laboratory at CSIRO in Clayton, Victoria, Australia in point beam mode and the Tescan Vega scanning electron microscope equipped with an X-Max 50 EDS detector at Charles University in Prague, Czech Republic (Table 2). Isopleth notations used are: Almandine (Alm) = $Fe/(Ca+Fe+Mg+Mn)$, Grossular (Grs) = $Ca/(Ca+Fe+Mg+Mn)$, Spessartine (Sps) = $Mn/(Ca+Fe+Mg+Mn)$, Pyrope (Prp)= $Mg/(Ca+Fe+Mg+Mn)$, X_{Fe} = $Fe/(Fe+Mg)$, Ca(Pl) = $Ca/(Ca+Na+K)$. Mineral abbreviations are after Kretz (1983).

3.2. Metamorphic zones in the Tolombón complex

We describe metamorphic rocks from a region that extends 20 km west into the mountain range between Cafayate town and Colalao del Valle village (Fig. 1). Similar to Büttner et al. (2005), we find metamorphic zones that are marked by the appearance of index minerals. We define five zones oriented ~NNW-SSE that generally increase in metamorphic facies to the west from Crd → Sill → Grt → Opx, although there are notable exceptions where zones are repeated by shear zones (Figs. 3, 4). The zones were divided into: (1) Crd-subsolidus zone, (2) Sil+Crd-migmatite zone, (3) Grt-migmatite zone, (4) Tolombón thrust zone, and (5) Opx-migmatite zone. These are simplified zone names based on their most significant characteristic. We begin with a description of the greenschist facies rocks that crop out north of this region (Büttner et al., 2005) and then progress to the metamorphic zones that are the focus of this study, from NE to SW.

3.2.1. Greenschist facies metasedimentary rocks

Low-grade Puncoviscana formation metasedimentary rocks are exposed north and east of San Antonio (Fig. 1). They comprise two interbedded end-member lithologies: pelite

forms brown to green layers that consist of clay- to silt-sized grains, and psammite forms brown to grey layers that consist of fine-to-medium sand-sized grains. Pelite layers contain Qtz+Chl+Ill+Bt+Ms+Kfs+Pl and psammites Qtz+Kfs+Pl+Bt+Chl+lithic fragments. The presence of chlorite and biotite in the pelite indicates greenschist facies metamorphism. These rocks retain primary structures preserved in the Puncoviscana Formation protolith (Büttner et al., 2005), discussed in chapter 1, section 2. A bedding parallel cleavage, S1, is defined by aligned micas and more pronounced in pelitic layers.

3.2.2. Crd-subsolidus zone

The easternmost part of the Tolombón complex consists of a >1.5 km-thick section of rocks metamorphosed at lower amphibolite facies (<650 °C). The paragenesis in metapelites is Bt (45%)+Qtz (15%)+Pl (15%)±Crd (10%)±Ms (5%)±Kfs (<5%) with accessory amounts of zircon, apatite, monazite and ilmenite. In metapelites, the matrix grain size of quartz, plagioclase and K-feldspar is <0.1 mm and contains porphyroblasts of biotite up to 0.5 mm and cordierite up to 2 cm (Fig. 5a). Biotite porphyroblasts are asymmetrically sheared forming mica fish or coarse flakes and contain radiation damage haloes around zircon inclusions. Cordierite is poikiloblastic and up to 2 cm in diameter. Metapsammites consist of Qtz(65%)+Pl(15%)+Bt(10%)± Kfs(5%) ±Ms(5%) with accessory amounts of zircon, apatite and monazite. In the matrix, the minerals have a grain size up to 1 mm with occasional monominerallic quartz layers that show dynamic recrystallization by bulging and undulose extinction.

These rocks are intruded by Ms+Tur±Grt pegmatite, tonalitic and two-mica granitic dykes that are parallel to bedding. Magma intrusion is more voluminous in pelitic layers where it occasionally disaggregates the country rock. In these regions, pelite rafts and biotite-rich schlieren are evident within "dirty" granites, which form mappable units.

3.2.3. Sil+Crd-migmatite zone

This 4 km-thick zone is marked by the first appearance of in situ melting indicated by leucosomes (1–5 cm width) and the first appearance of fibrous sillimanite in leucosomes. Typically leucosomes contain occasional grains of cordierite, and sparse grains of muscovite (Fig. 6a). Migmatites are intruded by leucogranites, which are differentiated from in situ leucosomes by the absence of sillimanite and melanocratic selvedges, as well as their greater width (up to 50 cm).

Leucosomes contain Qtz+Pl+Ksp+Sil±Crd±Bt±Ms (Fig. 6a), comprise about 10–20% of the total rock, and are mostly parallel to S0/S1. Sillimanite (<10%) is fibrolite and forms individual grains or continuous layers (Fig. 6a). Cordierite (<3 mm) is occasionally retrogressed to pinite or replaced by muscovite and is rare (<1%; Fig. 6a). Compared to cordierite in the previ-

Table 2.

Whole-rock and mean electron microprobe analyses for samples used in thermodynamic modelling.

Sample	SQ49					SQ55			
Metamorphic zone	Grt-migmatite zone Hanging wall of Tolombón thrust					High strain zone Tolombón thrust			
Mineral	bulk	wr(m) b	Crd a	Bt a	Pl a	bulk	wr(m) b	Bt a	Pl a
SiO$_2$	59.82	65.82	45.72	34.15	61.05	64.05	67.58	32.36	57.31
TiO$_2$	1.04	0.97	0.00	2.88	0.00	0.76	0.58	2.35	0.00
Al$_2$O$_3$	19.22	13.35	32.22	19.04	23.94	15.98	14.09	17.04	22.88
Fe$_2$O$_3$T	8.43	5.58	8.46	19.72	0.05	6.11	3.81	19.29	0.02
MnO	0.15	0.10	0.61	0.27	0.02	0.08	0.06	0.33	0.01
MgO	3.74	2.20	8.29	10.42	0.00	2.77	1.65	10.09	0.00
CaO	1.44	1.55	0.02	0.00	5.37	1.54	1.46	0.00	5.28
Na$_2$O	2.30	2.63	0.28	0.18	8.77	2.58	2.67	0.13	8.65
K$_2$O	3.12	2.62	0.00	10.06	0.15	3.59	3.08	9.71	0.17
P$_2$O$_5$	0.18	0.10	0.01	0.00	0.14	0.22	0.16	0.01	0.18
Total	99.44	94.92	95.61	96.72	99.49	97.68	95.15	91.32	94.50
Cations/charges									
Si			4.87	2.59	2.73			2.61	2.70
Ti			4.06	1.70	1.26			1.62	1.28
Al			0.00	0.16	0.00			0.14	0.00
Fe			0.76	1.25	0.00			1.30	0.00
Mn			0.06	0.02	0.00			0.02	0.00
Mg			1.33	1.18	0.00			1.21	0.00
Ca			0.00	0.00	0.26			0.00	0.27
Na			0.06	0.03	0.76			0.02	0.80
K			0.00	0.97	0.01			1.01	0.01
Total			11.13	7.90	5.02			7.95	5.06
X$_{Fe}$			0.36	0.51				0.52	
Alm									
Prp									
Grs									
Sps									
Ca(Pl)					0.25				0.25

Notes:

a Electron microprobe analysis at CSIRO, Clayton

b Electron microprobe analysis at Charles University, Prague

Table 2. (continued)

Sample	SQ58a				SQ62b			
Metamorphic zone	Grt-migmatite zone Footwall of Tolombón thrust				Grt-migmatite zone Footwall of Tolombón thrust			
Mineral	bulk	Grt a	Crd a	Bt a	wr(m) b	Grt b	Bt b	Pl b
SiO_2	57.14	35.42	46.21	33.35	71.37	37.22	35.15	61.24
TiO_2	1.16	0.00	0.00	3.57	0.65	0.00	3.46	0.00
Al_2O_3	19.89	21.52	32.44	18.28	11.33	20.88	18.15	24.26
Fe_2O_3T	9.45	37.74	9.92	21.64	4.94	30.49	20.09	0.00
MnO	0.09	2.82	0.26	0.11	0.33	6.84	0.24	0.00
MgO	4.75	3.93	7.98	9.43	1.47	3.64	8.45	0.00
CaO	0.58	1.02	0.01	0.00	2.34	0.95	0.07	5.72
Na_2O	0.97	0.00	0.17	0.16	2.71	0.00	0.07	8.16
K_2O	4.31	0.00	0.05	9.75	1.90	0.00	9.96	0.22
P_2O_5	0.17	0.00	0.00	0.00	0.47	0.00	0.00	0.16
Total	98.51	102.44	97.03	96.28	97.51	100.02	95.65	99.77
Cations/charges								
Si		2.84	4.89	2.57		3.00	2.69	2.73
Ti		2.03	4.03	1.66		0.00	0.20	0.00
Al		0.00	0.00	0.21		1.98	1.64	1.27
Fe		2.53	0.87	1.39		2.05	1.29	0.00
Mn		0.19	0.02	0.01		0.47	0.02	0.00
Mg		0.47	1.26	1.08		0.44	0.96	0.00
Ca		0.09	0.00	0.00		0.08	0.01	0.27
Na		0.00	0.03	0.02		0.00	0.01	0.70
K		0.00	0.01	0.96		0.00	0.97	0.01
Total		8.15	11.11	7.89		8.01	7.78	4.99
X_{Fe}			0.41	0.56			0.57	
Alm		0.77				0.68		
Prp		0.14				0.14		
Grs		0.03				0.03		
Sps		0.25				0.47		
Ca(Pl)								0.28

Table 2. (continued)

Sample	SQ65					SQ72				
Metamorphic zone	Grt-migmatite zone Footwall of Tolombón thrust					Opx-migmatite zone Hanging wall of PSZ				
Mineral	wr(m) b	Crd b	Bt b	Pl b	bulk	wr(m) b	Grt a	Crd a	Bt a	Pl a
SiO_2	63.46	48.28	34.99	61.60	62.56	67.19	36.56	46.94	34.20	57.76
TiO_2	0.87	0.00	3.59	0.00	0.88	0.84	0.00	0.00	4.13	0.00
Al_2O_3	16.21	32.71	17.92	24.23	15.66	13.38	21.76	32.46	17.13	24.35
Fe_2O_3T	5.57	8.23	18.86	0.00	6.19	4.58	32.80	7.17	19.61	0.04
MnO	0.09	0.32	0.16	0.00	0.10	0.15	4.26	0.45	0.22	0.02
MgO	2.81	8.19	9.38	0.00	2.90	2.17	6.07	9.20	10.92	0.00
CaO	1.55	0.00	0.05	5.60	1.03	2.59	1.16	0.02	0.00	6.63
Na_2O	2.46	0.18	0.12	8.34	1.83	3.14	0.01	0.15	0.09	7.92
K_2O	3.04	0.00	9.91	0.20	7.43	2.09	0.01	0.01	10.03	0.23
P_2O_5	0.10	0.00	0.00	0.17	0.20	0.20	0.07	0.02	0.06	0.14
Total	96.16	97.90	94.97	100.13	98.78	96.32	102.70	96.42	96.40	97.09
Cations/charges										
Si		5.00	2.68	2.73			2.87	4.92	2.61	2.66
Ti		0.00	0.21	0.00			2.01	4.01	1.54	1.32
Al		3.99	1.62	1.27			0.00	0.00	0.24	0.00
Fe		0.71	1.21	0.00			2.15	0.63	1.25	0.00
Mn		0.03	0.01	0.00			0.28	0.04	0.01	0.00
Mg		1.26	1.07	0.00			0.71	1.44	1.24	0.00
Ca		0.00	0.00	0.27			0.10	0.00	0.00	0.33
Na		0.04	0.02	0.72			0.00	0.03	0.01	0.71
K		0.00	0.97	0.01			0.00	0.00	0.98	0.01
Total		11.03	7.78	5.00			8.13	11.08	7.88	5.04
X_{Fe}		0.36	0.53					0.30	0.50	
Alm							0.66			
Prp							0.22			
Grs							0.03			
Sps							0.26			
Ca(Pl)				0.27						0.31

Table 2. (continued)

Sample			SQ73a						SQ106	
Metamorphic zone			Opx-migmatite zone Hanging wall of PSZ						Agua del Sapo complex Footwall of PSZ	
Mineral	bulk	wr(m) b	Opx a	Grt a	Crd a	Bt a	Pl a	bulk	Grt a	Bt a
SiO$_2$	64.54	61.18	46.19	36.46	47.84	34.16	61.29	66.24	38.05	36.99
TiO$_2$	1.03	0.74	0.14	0.01	0.00	4.73	0.01	0.77	0.10	2.59
Al$_2$O$_3$	16.05	14.95	5.25	21.59	33.04	16.47	23.38	15.43	21.82	19.76
Fe$_2$O$_3$T	6.48	7.41	33.31	33.84	8.17	20.42	0.03	5.91	32.88	16.58
MnO	0.10	0.23	0.96	2.06	0.19	0.12	0.03	0.07	4.49	0.07
MgO	2.88	2.68	15.19	6.93	8.75	10.52	0.00	2.45	3.38	9.42
CaO	1.60	1.35	0.09	0.82	0.01	0.00	4.71	1.23	0.93	0.01
Na$_2$O	3.10	2.97	0.01	0.02	0.08	0.09	9.12	2.69	0.03	0.16
K$_2$O	2.98	4.04	0.01	0.00	0.01	9.86	0.24	3.23	0.00	10.02
P$_2$O$_5$	0.15	0.19	0.03	0.06	0.00	0.06	0.21	0.23	0.04	0.00
Total	98.91	95.74	101.18	101.78	98.09	96.44	99.01	98.25	101.72	95.60
Cations/charges										
Si			1.81	2.87	4.94	2.61	2.75		3.00	2.76
Ti			0.24	2.00	4.02	1.49	1.24		2.03	1.74
Al			0.00	0.00	0.00	0.27	0.00		0.01	0.15
Fe			1.09	2.23	0.71	1.31	0.00		2.17	1.04
Mn			0.03	0.14	0.02	0.01	0.00		0.30	0.00
Mg			0.89	0.81	1.35	1.20	0.00		0.40	1.05
Ca			0.00	0.07	0.00	0.00	0.23		0.08	0.00
Na			0.00	0.00	0.02	0.01	0.80		0.00	0.02
K			0.00	0.00	0.00	0.96	0.01		0.00	0.95
Total			4.07	8.13	11.06	7.86	5.03		7.98	7.71
X_{Fe}			0.55		0.34	0.52				0.50
Alm				0.69					0.74	
Prp				0.25					0.14	
Grs				0.02					0.03	
Sps				0.13					0.38	
Ca(Pl)							0.22			

ous zone, here it is not poikiloblastic, has a smaller diameter, and is only seen in the neosome. Plagioclase has lamellar crystallization twins and forms myrmekite with quartz around K-feldspar grains (Fig. 6b), K-feldspar has tartan twinning, and quartz shows chessboard extinction. Quartz and feldspars have cuspate, indented grain boundaries perhaps indicative of simultaneous crystallisation at the solidus (Vernon, 2004).

Melanosomes contain Bt+Sil+Ms with minor Qtz+Pl+Ksp+Crd+Chl+Ilm+Rt (Fig. 6b). Layers and agglomerates of sillimanite (up to 5 mm length, 10% of rock) occur as both fibrolite and blocky crystals that appear adjacent to biotite (Fig. 6b). Coarse flakes of muscovite (up to 3 mm length, <5% of melanosome) are euhedral and appear with ilmenite and rutile overgrowing biotite (Fig. 6b). Coarse flakes of dark-brown biotite (up to 3 mm length, ~85% of melanosome) contain zircon radiation haloes and are partially replaced on grain boundaries by Sil+Ilm+Rt, Ms+Ilm+Rt, or chlorite (Fig. 6b). Occasional films of Pl+Qtz on the edges of biotite grains close to leucosomes are interpreted as crystallised interstitial melt.

The relatively large modal proportion of sillimanite indicates that melting occurred due to dehydration of muscovite, the minor presence of cordierite in neosomes (Fig. 6a) indicates possible incipient dehydration melting of biotite. Muscovite in melanosomes is interpreted to be a result of the retrogression of biotite. The absence of a phase of muscovite interpreted as predating melting suggests that the Ms-dehydration melting reaction went to completion.

The NE-SW trending, 4 km-wide, leucogranitic - tonalitic Cafayate pluton intrudes the the Sil+Crd-migmatite zone. The pluton was described in detail by Rapela (1976), Rapela and Shaw (1979), and Büttner et al. (2005). Approaching the pluton from the east, the proportion of intrusions increases until metasedimentary rocks form rafts up to a metre long, marking the start of the pluton. The Cafayate pluton grades in composition from granite, through granodiorite, to tonalite from east to west (Rapela and Shaw 1979). On the western side of the pluton, the contact with the Sil+Crd migmatites is sharp and layer-parallel dykes intrude into the migmatite. This marks a return to the Sil+Crd-migmatite zone.

3.2.4. Grt-migmatite zone

The first appearance of garnet signals the beginning of this ~1.5 km-thick zone. In contrast to the previous zone, the proportion of cordierite is greater (>10%) and sillimanite generally lower (<2%), and metatexites have a higher proportion of leucosomes (~30% of rock).

Fig. 3. (Left) Geological map of the El Divisadero-Laguna transect including isograds and metamorphic mineral parageneses. See Fig. 1 for location. Black circles are waypoints and indicate outcrop locations. Contacts extrapolated beyond waypoints are uncertain and based on Google Earth imagery and Fig. 2 in Büttner et al. (2005). Diatexites are separated into different metamorphic zones on the basis of mineralogy, consistent with other zones. However, magma may have been mobile and carried peritectic minerals, which would lead to error in these boundaries. Inset: stereonets for foliation (top), intersection lineation (left), and stretching lineation (right). Stereonets are lower hemisphere, equal area.

Pelitic layers contain foliation-parallel leucosomes, whereas those in psammitic layers cross-cut the weakly-developed foliation and form large patches. Toward the west, the proportion of melt increases and metatexites transition into diatexites over 300 m (Fig. 3). Diatexites contain preserved pelitic layers with >70% cordierite (Fig. 5c) surrounded by thin leucosomes, psammitic layers that are intruded by melt, and granitic layers.

While garnet is mostly restricted to leucosomes, cordierite appears in both melanosomes and leucosomes. Leucosomes contain Qtz+Pl+Ksp+Crd+Sil±Grt, the presence of peritectic Crd+Grt+Sil+Ksp indicates Bt- and Ms- dehydration melting (Spear, 1993). Quartz and plagioclase in the leucosome have the same appearance as in the previous zone. Beyond tartan twinning, K-feldspar is also perthitic. Although the proportion of sillimanite is generally lower in leucosomes, in some pelitic rocks it forms thin, continuous bands of fibrolite. Cordierite is up to 3 mm in diameter, commonly occurring in aggregates up to 5 cm in diameter, and partially replaced by sillimanite or pinite (Fig. 6c). Toward the west, still within the Grt-migmatite zone, the size of garnet increases until it forms poikiloblasts up to 3 cm diameter partially replaced by biotite, interpreted as resulting from a retrograde reaction. Leucosomes can be traced from pelitic layers, through psammitic layers, into granites (Fig. 5c). Cordierite (< 5%) appears in the granite but the high proportion (~50%) in pelitic layers suggests that most cordierite remained in
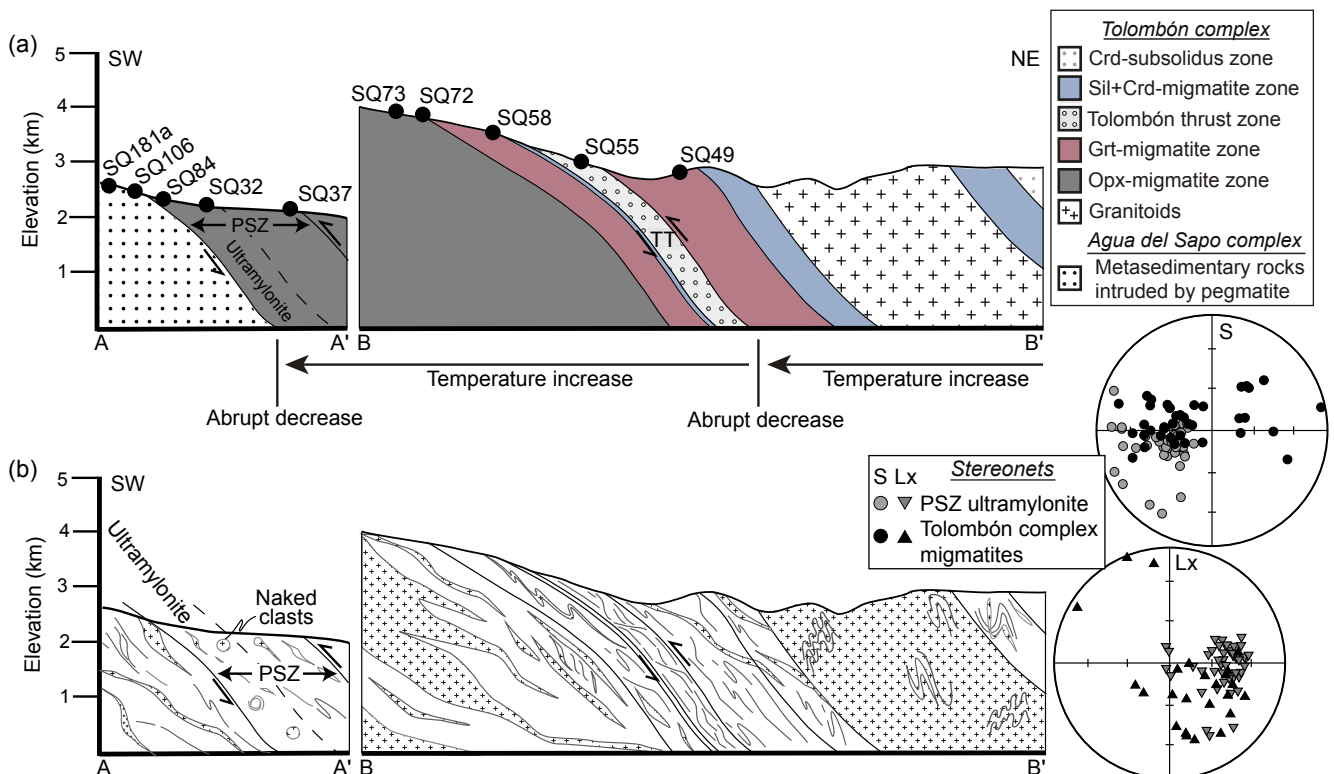
Fig. 4. (a) Schematic cross-section of the Tolombón complex showing repetition of metamorphic zones after thrust planes and the location of samples for thermodynamic modelling and geochronology. (b) Schematic representation of the structures and their intensity in the metamorphic zones of the Tolombón complex. The line of the section is shown in Fig. 1. Insets: stereonets of thrust C-plane and stretching lineation for the ultramylonitic granitic diatexite layer of the PSZ (Finch et al., 2015) and the Tolombón complex between Laguna and Cafayate.

the restitic pelite when the melt was extracted (Figs. 5c,d, 6c). Occasionally garnet leucosomes contain only one kind of feldspar, that is, they contain either Ksp+Qtz+Grt or Pl+Qtz+Grt. This suggests fractionation or remelting and is explored further in section 5.

Melanosomes contain Bt+Sil with minor Ms+Qtz+Pl+Ksp+Crd+Ilm+Rt+Sp. Biotite (<1 mm long) is partially replaced by Ilm+Ms+Rt. When replacing biotite, muscovite forms a corona around Ilm+Rt, or the three minerals are intergrown. Biotite and quartz intergrowths occur on the edges of leucosomes at the expense of K-feldspar, indicating retrogression due to reaction with crystallising melt (Waters, 2001). The appearance of garnet in this zone and increased volume of leucosomes indicates an increase in metamorphic grade to the west, away from Cafayate pluton, which suggests that metamorphism was not a result of contact with the pluton, but rather part of the regional trend.

3.2.5. Tolombón thrust

West of the Grt-migmatite zone there is a zone of mylonitic rocks that contain Qtz (30%)+Bt(30%)+Pl(20%)+Ms(15%)+Ap(<5%) and accessory Mnz and Fe- and Ti-oxides. Rocks are finely-laminated Bt+Ms schists that are strongly sheared with top-to-west, thrust shear sense (Fig. 6d,e), and form a 1.5 km-thick zone, named here the Tolombón thrust. Within the intensely-foliated, recrystallised, micaceous matrix there are bands Pl±Qtz up to 1.5 cm-length where plagioclase shows simple concentric zoning and quartz shows chessboard extinction. Zoning in plagioclase may be igneous or metamorphic (Vernon, 2004) and the zoning pattern is truncated by deformation indicating that zoning developed prior to deformation. Typical markers of in situ melting present in other zones, such as peritectic minerals, former melt films around melanocratic minerals, biotite and quartz intergrowths, clear melanosomes with a high proportion of restitic minerals, and melanosome-leucosome banding, are absent from this zone, suggesting it did not undergo anatexis. The absence of K-feldspar and high proportion of plagioclase suggests this rock may have been igneous and tonalitic in composition, similar to the western tonalitic section of the Cafayate pluton. However, the intensity of the deformation makes petrogenesis uncertain. The contact between the rocks of the mylonitic Tolombón thrust and the migmatites either side of this zone is abrupt.

3.2.6. Footwall of the Tolombón thrust

In the footwall of the Tolombón thrust, to the west, there is a return to the Sil+Crd- migmatite zone (Figs. 3,4). The contact between the shear zone and these migmatites is characterised by a decrease in the proportion of primary muscovite, an increase in the proportion of sillimanite, and the appearance of thin Sil+Crd-bearing leucosomes surrounded by melanosomes over a short distance. This layer is only ~200 m thick and to the west of it millimetre-sized garnet and centi-
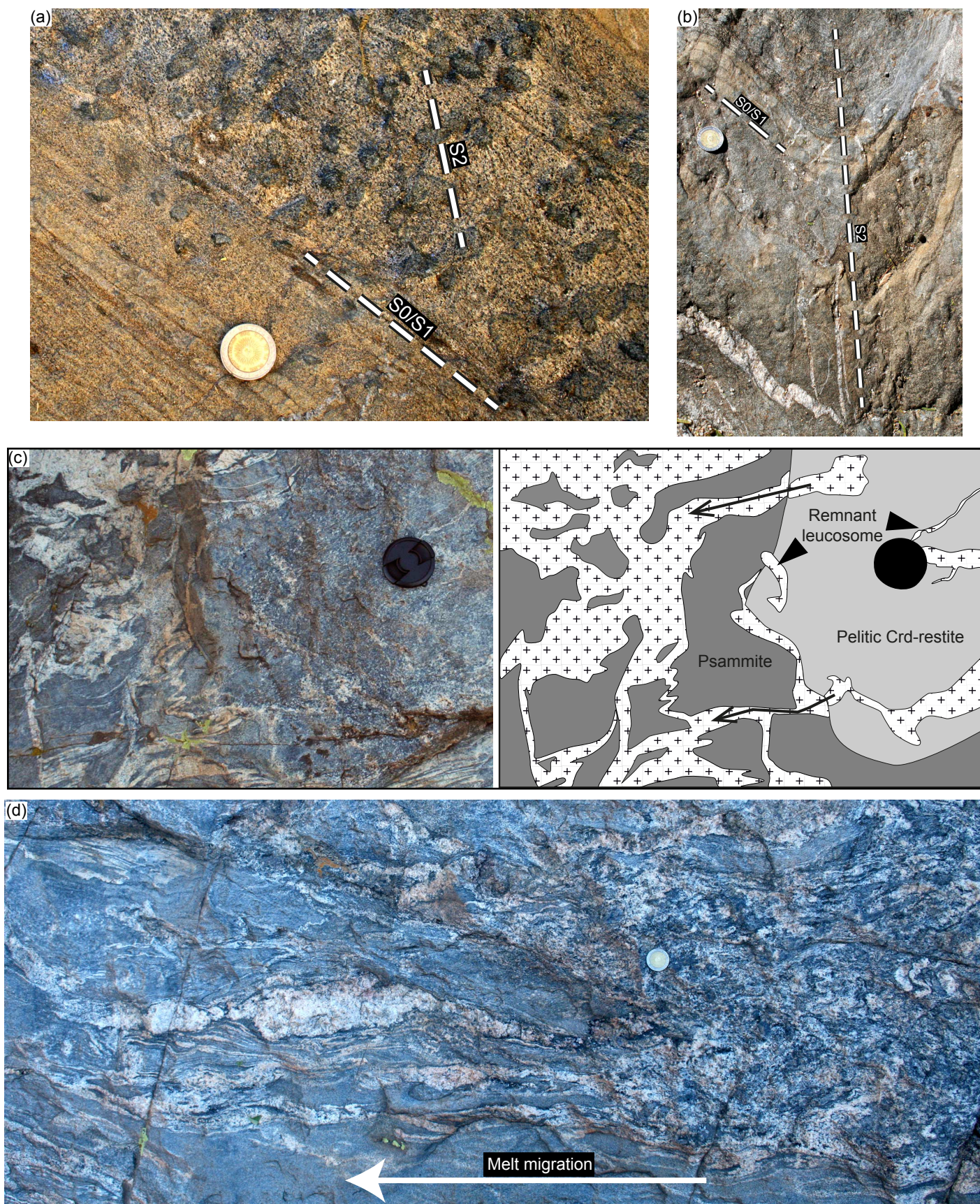
Fig. 5. Photographs of outcrops in the subsolidus and migmatitic zones of the Tolombón complex. (a) Contact between psammite and pelite layers in Crd-subsolidus zone. Pelitic layers contain large porphyroblasts of Crd and show two well-developed dissolution cleavages, S1 and S2. S1 is parallel to S0 and is also seen in psammitic layers. (b) Upright F2 fold in psammo-pelite in Crd-subsolidus zone. S0 and S1 are folded and S2 is a dissolution cleavage

metre-sized cordierite appear, accompanied by a small proportion of partial melting, indicating the return of the Grt-migmatite zone. This zone is ~ 1 km thick and becomes diatexitic toward the west, until the first appearance of orthopyroxene signals the beginning of the Opx-migmatite zone.

3.2.7. Opx-migmatite zone

This >3 km-thick zone is characterized by the appearance of orthopyroxene accompanied by the disappearance of sillimanite from the leucosome. Orthopyroxene is not present in every outcrop, but its presence in rocks with appropriate compositions, typically more psammitic layers, characterizes this zone. Metatexites have a similar appearance to those in the previous zone except the proportion of melt is 30–50% and in places greater than 50%, causing loss of coherence and forming diatexites.

Leucosomes contain Qtz+Pl+Kfs±Grt±Crd±Opx (Fig. 6f), and the presence of peritectic Grt, Crd, and Opx indicates Bt-dehydration melting (Spear, 1993). Peritectic minerals are larger and more voluminous than in the previous zone. Leucosomes contain peritectic minerals in different combinations depending on the composition of the protolith. Orthopyroxene is more common in leucosomes in psammitic layers (Fig. 6f), cordierite in pelitic layers, and garnet is common to both. Quartz and feldspar in leucosomes have the same appearance as in previous anatectic zones. Myrmekite is common in K-feldspar at the margins of porphyroblasts of garnet. Garnet is up to 3 cm in diameter and commonly poikiloblastic with inclusions of quartz or wormy inclusions of ilmenite and partially replaced at its edges by biotite and chlorite. Cordierite is up to 2 cm in diameter and contains inclusions of zircon, biotite, and quartz, and is partially replaced by biotite. Orthopyroxene forms strongly pleochroic porphyroblasts up to 3 cm diameter that include and are replaced by garnet, indicating a decrease in the stable modal proportion of orthopyroxene late in the metamorphic history (see Fig. 7d in chapter 2). Orthopyroxene is also partially replaced by Bt+Il or Bt+Qtz intergrowths, interpreted to be a result of retrogression (Fig. 6f). As in the Grt-migmatite zone, here there are occasional leucosomes that contain only one feldspar comprising either Ksp+Qtz+Grt or Pl+Qtz+Grt.

Melanosomes contain Bt±Crd with minor Ilm±Qtz±Pl±Ksp±Sil±Ky±Mag±Grt±Opx

Fig. 5 (cont.) that defines the axial plane. Thin granitic dykes are on the limb and axial plane of the fold. (c) Photograph and interpretative sketch of anatectic, layered sequence of psammite and pelite from the Grt-migmatite zone. Pelitic layer contains >70% residual Crd, suggesting melt loss. Melt pooled in the psammite layer, which has only undergone minor partial melting, evident from the lack of peritectic minerals in this layer. (d) Photograph of in situ leucosomes (right) that coalesce into networks and larger dykes that migrate out of the system (left). While it is possible to interpret the opposite migration direction, we suggest magma migrated from right to left because the neosome on the right side shows melanocratic selvedges that surround and have diffuse margins with leucosomes, suggesting in situ melting. Photograph in (a) is parallel to stretching lineation, (b) is perpendicular to S2 and to the fold axis.
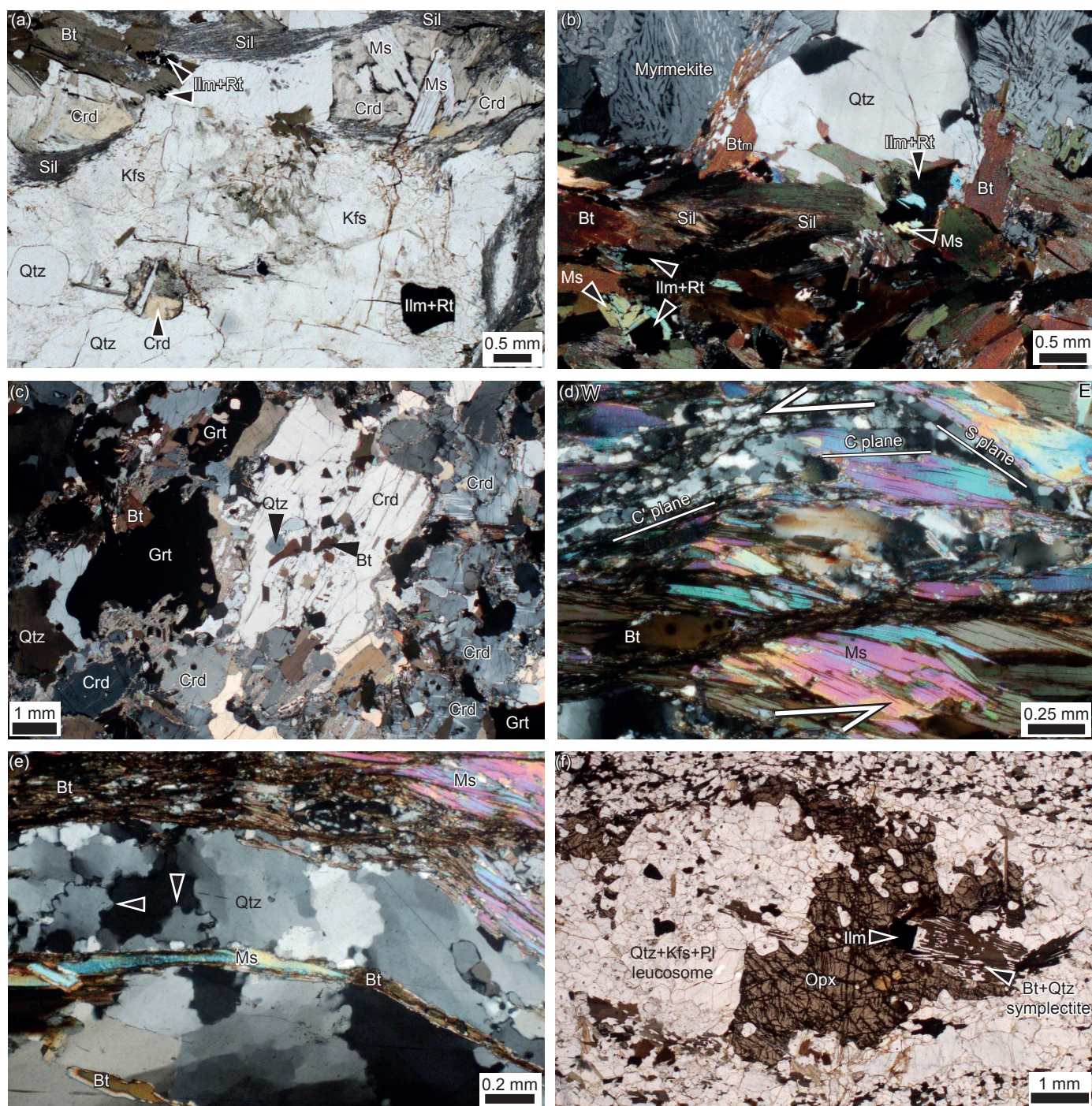
Fig. 6. Photomicrographs showing relationships between metamorphic minerals in the Tolombón complex. (a) Leucosome from the Sil+Crd-migmatite zone. Biotite is partially replaced by Ilm+Rt and Crd is partially replaced by Ms+Sil. (b) Migmatite from the Sil+Crd-migmatite zone. Leucosome contains myrmekite close to the boundary with melanosome. Ms forms coronas around Ilm+Rt and they replace biotite. (c) Restitic rock from the Grt-migmatite zone with >80% Crd and occasional porphyroblasts of garnet and remnant biotite. (d) Rock from the Tolombón thrust zone showing top-to-W, thrust shear sense. Flakes of muscovite define S-C fabric and very fine grained layers of Bt+Qtz+Fsp define C′ planes. (e) Rock from the Tolombón thrust zone. Quartz in monomineralic layer shows bulging recrystallization (arrows). (f) Opx-bearing leucosome from the Opx-migmatite zone. Edges of orthopyroxene grain have reacted with melt to form Bt+Qtz symplectite. All thin sections are oriented parallel to stretching lineation, perpendicular to foliation. (a) and (f) are plane-polarised light, (b-e) are cross-polarised light.

and have the same appearance as those in previous zones. Kyanite appears for the first time here and forms small subhedral porphyroblasts that are randomly oriented with respect to the foliation indicating that deformation ceased before the stability field of kyanite was reached, as interpreted by Büttner et al. (2005).

Within this zone there are voluminous layers of garnet diatexite (Fig. 6a in chapter 2) containing Qtz+Kfs+Pl+Bt+Grt±Ms±Chl±Sil±Ap with schollen of garnet-bearing psammite and pelite. The proportion of leucosome varies between 70 and 90% and contains phenocrysts of garnet up to 1 cm in diameter and tabular feldspar up to 3 cm in length. These rocks are described in more detail in section 3.4 of chapter 2.

3.3. Restitic rocks

A marked feature of all suprasolidus zones is the relatively common occurrence of rocks rich in residual minerals and interpreted to represent restitic rocks (Fig. 5c, 6c). They form metre-wide layers (Fig. 5c) and can comprise up to 5% of the total outcrop. Restitic rocks contain dominantly Crd+Bt±Opx (Fig. 6c), Grt+Bt±Opx, or Grt+Crd+Bt±Opx, except in the Sil+Crd zone where they contain Bt+Sil. Small grains of interstitial quartz and feldspar comprise <20% of the mineralogy. Biotite commonly forms coarse, euhedral flakes up to 3 mm in length, and other minerals have the same appearance as in the leucosome of metatexites in their respective zones. Occasionally, over the distance of a few metres, there are restitic rocks with different modal contents of residual minerals (e.g., Grt+Bt restite metres away from Crd+Opx+Bt restite). The former peritectic minerals in restitic layers comprise up to 80% of the rock (Fig. 6c) with only mm–cm-wide films of remnant leucosome (Fig. 5c) indicating they have undergone significant and efficient melt loss.

3.4. Summary and interpretation of metamorphic zones

The Tolombón complex shows a gradual increase in metamorphic grade from the lowest temperature Crd-subsolidus zone, through the Sil+Crd-migmatite zone, the Grt-migmatite zone, and to the highest temperature Opx-migmatite zone. This increase is indicated by the first appearance of key minerals, the decrease or disappearance of lower temperature minerals (e.g., absence of prograde muscovite in migmatites and absence of peritectic sillimanite in the Opx-migmatite zone), and the change in the dominant melt producing reaction from Ms-dehydration melting in the Sil+Crd-migmatite zone, to Bt-dehydration melting in the Grt-migmatite and Opx-migmatite zones. In the Opx-migmatite zone the presence of cordierite, orthopyroxene, and absence of sillimanite indicates that metamorphism was high T/low P.

A number of features within the migmatites of the Tolombón complex indicate that melt was mobile. The high proportion of restitic rocks in all migmatitic zones implies that leucosomes

formed melt networks and migrated out of the source rock (Fig. 5c,d). The presence of leuco-somes that with only one type of feldspar (i.e., either Kfs or Pl) suggests leucosomes have under-gone fractionation, with the Kfs-leucosomes representing the mobile fraction and Pl-leucosomes representing the residuum (Sawyer, 1998). This suggests that migmatites form an open system where the addition and subtraction of melt has modified rocks from their protolith compositions.

4. Structural geology

4.1. Structural features of the Tolombón complex

In the easternmost part of the studied area, in subsolidus rocks, bedding-parallel folia-tion, S1, and a cross-cutting foliation, S2, are well-developed in pelitic layers (Fig. 5a). S0 and S1 dip moderately SE and S1 is defined by the alignment of micas and dissolution cleavage (Fig. 3). S2 dips steeply west or occasionally moderately east (Figs. 3 and 4a) and is defined by disso-lution cleavage. S2 can be traced into folded regions where it is the axial plane of F2 folds (Figs. 3, 4b). Folds are upright and isoclinal to open with fold axes that plunge gently SSE, subparallel to the S0/S2 intersection lineation and coincident with the stretching lineation (Fig. 3). Grt-Tur leucogranite intrusions are dominantly foliation parallel in pelitic layers and cross-cut or pool underneath and above psammitic layers.

Down-sequence and to the west, the migmatites in the Sil+Crd-migmatite zone show cm-scale ptygmatic folds, S-C fabric, leucosomes sheared into σ-shapes, and metre-scale, upright folds in the same orientation as subsolidus rocks. Leucosomes are parallel to the main foliation (S0/S1) and are linked continuously with leucosomes on the axial planes of folds (S2), which cut through fold hinges. Toward the west of this zone there are fewer folds and asymmetrical struc-tures become more pervasive (Fig. 4). In the Grt-migmatite zone, no upright folds are seen, in-stead simple shearing is dominant, indicated by asymmetrically-sheared leucosomes, west-verg-ing asymmetrical folds, and S-C fabric defined by biotite-rich planes (Fig.4). The dominant orientation of the stretching lineation is E- or SE- plunging, indicating top-to-W and top-to-NW, thrust shear sense. The stretching lineation is defined by elongate grains of biotite and feldspar and is parallel to the intersection lineation. Leucosomes appear on thrust planes, suggesting possible involvement of melt during thrusting (Fig. 5d in chapter 2). In the immediate hanging wall of the Tolombón thrust, there is the upper limb and hinge of a recumbent fold with a hinge ~ 10 metres in width. Leucogranite intruded and pooled in the hinge and granitic dykes are sheared and boudinaged with asymmetry that indicates top-to-west, thrust shear sense.

The Tolombón thrust is a region of increased foliation intensity where rocks form mylonites with well-developed S-C-C` fabric defined by thin planes (<0.1 mm) of fine-grained, recrystallised quartz, biotite, feldspar and muscovite (Fig. 6d). Quartz ribbons show bulging recrystallization (Fig. 6e arrows) and are parallel to S-C fabric and thin or pinch-out

on C` planes. Bands and σ-shaped porphyroclasts of Pl±Qtz have strain shadows containing Qtz±Pl±Ms±Bt. C planes dip on average moderately to the ENE, with an E- or SE-plunging stretching lineation defined by the alignment of muscovite, biotite, and plagioclase grains. S planes dip moderately to the east and the shear sense is top-to-W or -NW thrusting, indicated by the asymmetry of σ-clasts, mica fish and S-C-C` fabric. The C plane orientation coincides with the slope of the ridge indicating the shear zone partially controls the topography.

In the footwall of the Tolombón thrust, the metamorphic grade increases as strain decreases until there is a return to the Sil+Crd-migmatite zone and then the Grt-migmatite zone (Fig. 4). Like the anatectic zones in the hanging wall, these have lineations and S-C fabric that indicate thrusting to the W or NW and leucosomes folded into asymmetric, W- and NW-verging folds (Fig. 4).

The Opx-migmatite zone also shows thrusting to the NW, indicated by the SE-plunging stretching lineation, S-C fabric and asymmetric, NW-verging folds (Fig. 4). In some areas the thrust plane steepens (dip ~60°) concomitant with a decrease in the foliation intensity (Fig. 7). These regions alternate with more common areas where the dip is moderate (30–45°) and the foliation more intense (Fig. 7). Steeply dipping areas show only S-C fabric, whereas more shallowly dipping regions show asymmetric, recumbent, isoclinal folds with west vergence, leucosomes sheared into σ shapes, C′ planes, and a higher proportion of leucosome and granitic dykes than steeper regions (Fig. 7).

Occasionally there are small lithons that show S-C fabric indicating top-to-SE, normal shearing. In one region in the Opx-migmatite zone (at 26°10'46.70"S, 66°05'20.40"W), the normal shear plane bends into the C-plane of the thrust shear zone, indicating that normal shearing is overprinted by thrust shearing. Within the Grt-migmatite zone, there is another region that shows west-dipping C and S planes with a NW-plunging stretching lineation, defining thrusting to the SE, which may represent preserved lithons of an earlier normal shearing that were rotated during thrusting. Some sparse diatexitic regions show little deformation and have a massive texture except for in melanocratic areas where minor shearing is evident.

In thin section, sheared rocks contain feldspar σ-clasts, which have core-mantle structure with myrmekite on foliation-parallel edges and quartz ribbons that show grain boundary migration recrystallization and chessboard extinction. S-C-C′ fabric is well-developed and defined by layers of biotite, with a small proportion of muscovite. Biotite in C′ planes is very fine-grained (<0.10 mm).

In the south of the Tolombón complex, the Opx-migmatite zone is overprinted by the 3.5 km-thick PSZ (Finch et al., 2015). The PSZ comprises a 2.5 km-thick section of protomylonitic to mylonitic stromatic metatexite on top of a 1 km-thick ultramylonitic base that overprints granitic Grt-diatexite. The shear zone thrusts the granulite-facies migmatites to the west onto amphibolite-facies metasedimentary rocks of the Agua del Sapo complex (Finch et al., 2015). The shear zone dips moderately to the NE, with an east-plunging stretching lineation, and de-

fines similar to the kinematics of the Tolombón complex in general and the Tolombón thrust in particular (Fig. 4).

4.2. Interpretation of structural data

In subsolidus rocks the parallelism of fold axes and stretching lineations suggests that folds may have been modified during simple shear, interpreted as a two-stage process involving: (1) fold generation with axial planes perpendicular to the Z axis of the finite strain ellipsoid and fold axes close to the Y axis, followed by (2) rotation of the fold axis during prolonged non-co-axial shearing, which progressively rotated the fold axis into parallelism with the X axis and the axial plane into parallelism with the shear plane (e.g. Ramsay and Graham, 1970).

The structural features of the zones are tied to their metamorphic grade and crustal position at the time of deformation. The lower grade rocks to the NE were at a higher structural level than the other zones during shearing, and show upright folding and passive rotation of folds into parallelism with the shear plane. In the Sil+Crd-migmatite zone, upright folds in the east of the zone become rarer to the west and ductile shear structures increase in intensity (Fig. 4). Below this, at lower-crustal depths, migmatites show pervasive S-C-C′ structures, asymmetric folds, and sigma-shaped leucosomes reflecting a strong thrusting component verging to the NW (Fig. 4). The presence of upright folds in lower-grade rocks and asymmetric shear structures in higher-grade zones, indicates that rocks underwent general shear.

The presence of leucosomes on axial planes of folds formed during shortening and thrusting, and leucosomes on S-C planes (Fig. 5d, e in chapter 2), suggests top-to-W or –NW thrusting and anatexis were coeval. This is consistent with the interpretation of Büttner et al. (2005) that shearing began during the metamorphic peak coincident with anatexis. Evidence for solid-state deformation in the PSZ (Figs. 5, 6 in chapter 2), as well as in the migmatites described here, indicates that thrusting continued to lower temperatures after the cessation of anatexis.

Shear plane orientations define a relatively narrow field, dipping approximately east with stretching lineations that dip shallowly to steeply. Occasional west-dipping shear planes in the Grt-migmatite zone may represent back-thrusts or else relate to an earlier shearing event. However, these overprinting relationships are rare and do not provide sufficient information for determination of the number of deformation events or their meaning.

The alternation of steeply and shallowly dipping thrust planes in the Opx-migmatite zone is interpreted as a thrust duplex comprising steeper "horses", which bend into the shallower roof and floor thrusts forming an S-shaped geometry in cross section (Fig. 7).

4.2.1. Major thrust planes

Our mapping revealed two major thrust planes, which placed hot rocks on cooler rocks:
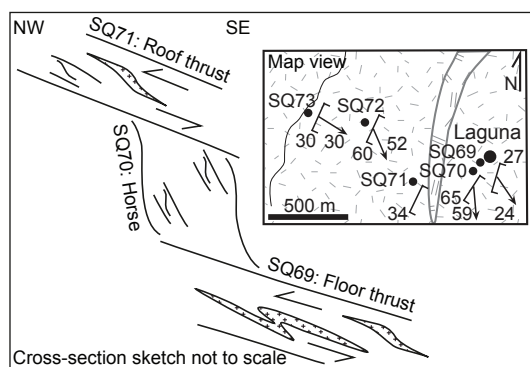
Fig. 7. Schematic cross section of duplex structure in the Opx-migmatite zone with inset map showing location.

the Tolombón thrust and the PSZ. The Tolombón thrust placed rocks of the Grt-migmatite zone onto rocks of the Sil+Crd-migmatite zone (Figs. 3, 4). The hanging wall is a ~7 km-thick sequence ranging from rocks of the Crd-subsolidus zone in the east to rocks of the Grt-migmatite zone in the west. The Tolombón thrust overprints a rock that is tonalitic in composition and may be a repeat of the tonalitic section of the Cafayate pluton. Immediately below the shear zone there is a drop in metamorphic facies to the Sil+Crd-migmatite zone, a band only 200 m thick, before returning to higher-temperature metamorphic rocks of the Grt-migmatite-zone. Structurally below the Tolombón thrust, the amphibolite facies PSZ placed a ~10 km-thick sequence, ranging from lower-amphibolite facies rocks in the east to granulite facies rocks in the west (Fig. 1b), onto amphibolite facies rocks of the Agua del Sapo complex. While subsequent block rotation during the Andean orogeny may have changed the orientation of the rocks, the emplacement of hot rocks onto cooler rocks indicates thrusting, consistent with the present-day orientation of the shear sense. Structures which formed during anatexis show the same kinematics as solid state shearing in the PSZ, suggesting that shearing began during peak metamorphism and anatexis, and continued to lower temperatures as rocks were thrust and cooled.

5. Thermodynamic modelling

In order to support our field observations that hot rocks were thrust onto cold rocks, we attempted to determine the peak P-T conditions for the metamorphic zones above and below the PSZ and Tolombón thrust. We constructed P-T pseudosections for different protolith rocks and migmatites and used them to determine the P-T path and peak metamorphic conditions. Modelling was not straightforward and in this section we detail the steps taken to model and understand the equilibration of these rocks.

5.1. Calculation methods

The software used for calculating the phase diagrams was THERMOCALC 3.33 (Powell et al., 1998, 2009 upgrade) and the internally consistent thermodynamic data set 5.5 (Holland and Powell, 1998, 2003 update). The pseudosections were calculated in the system MnO-Na$_2$O-CaO- K$_2$O-FeO-MgO-Al$_2$O$_3$-SiO$_2$-H$_2$O-TiO$_2$-O (MnNCKFMASH-TO). The protolith to the migmatites is the metasedimentary Puncoviscana Formation but, as demonstrated in Fig. 2, the

formation consists of a compositionally diverse package of rocks with two major end-members, pelite and psammite. We used the data in Fig. 2 to determine the mean composition of each oxide for psammites and pelites. These mean compositions were used as the bulk composition for modelling with the molar amounts of the oxides normalised to 100%. The amount of H_2O used in the calculations for suprasolidus conditions was the amount needed to saturate the rock at the solidus and preserve the observed mineral assemblage and composition. The activity-composition models used were as follows: melt from White et al. (2007), cordierite and staurolite from a combination of Mahar et al. (1997) and Holland and Powell (1998), garnet, ilmenite and biotite from White et al. (2005), orthopyroxene from White et al. (2002), muscovite from Coggon and Holland (2002), and plagioclase and K-feldspar from Holland and Powell (2003).

5.2. Comparison of the pelite and psammite pseudosections

The two pseudosections in Fig. 8 depict the stability fields for different paragenesis for the average pelite and psammite. They contain the same reactions and mineral equilibria, however, they differ slightly in the stability of the equilibria over P-T space, particularly the Bt-dehydration reactions. In the psammitic pseudosection, orthopyroxene is stable to ~ 6.2 kbar, whereas in the pelite pseudosection it is only stable to ~ 5.2 kbar. At low pressures both pseudosections start Bt-dehydration melting at ~750–760 °C, but at moderate pressures (6–7 kbar), biotite is stable to temperatures about 30 °C higher in the psammitic section than in the pelitic.

The peak equilibrium mineral assemblage of each metamorphic zone (section 3) corresponds to an area in P-T space in the pseudosections (Fig. 8). The mineral assemblage in the Sil+Crd-migmatite zone is stable in a narrow region in P-T space between 650 and 700 °C, at pressures between 3.2 and 4.5 kbar (blue in Fig. 8). The mineral assemblage in the Grt-migmatite zone is stable at temperatures between 700 and 800 °C below 6.5 kbar in the pelite and below 7.2 kbar in the psammite (pink in Fig. 8). The Opx-migmatite zone occupies a narrow region in P-T space between 750 and 800 °C and pressures below 5.2 kbar in the pelite and 6.2 kbar in the psammite (purple in Fig. 8). These broad constraints suggest 100–150 °C increase across these three fields and a relatively low pressure, typical of high T/low P metamorphism.

5.3. Isopleth thermobarometry

The P-T conditions of equilibration of the metamorphic zones can be further constrained by determining the P-T position of the composition of end-member minerals from rocks within each zone. Six rocks from different structural positions were selected including rocks from the Grt-migmatite zone in the hanging wall of the Tolombón thrust (SQ49), the Tolombón thrust zone (SQ55), the Grt-migmatite zone from the footwall of the Tolombón thrust (SQ58a), the Opx-migmatite zone in the hanging wall of the PSZ (two samples: SQ72 and SQ73a1), and the
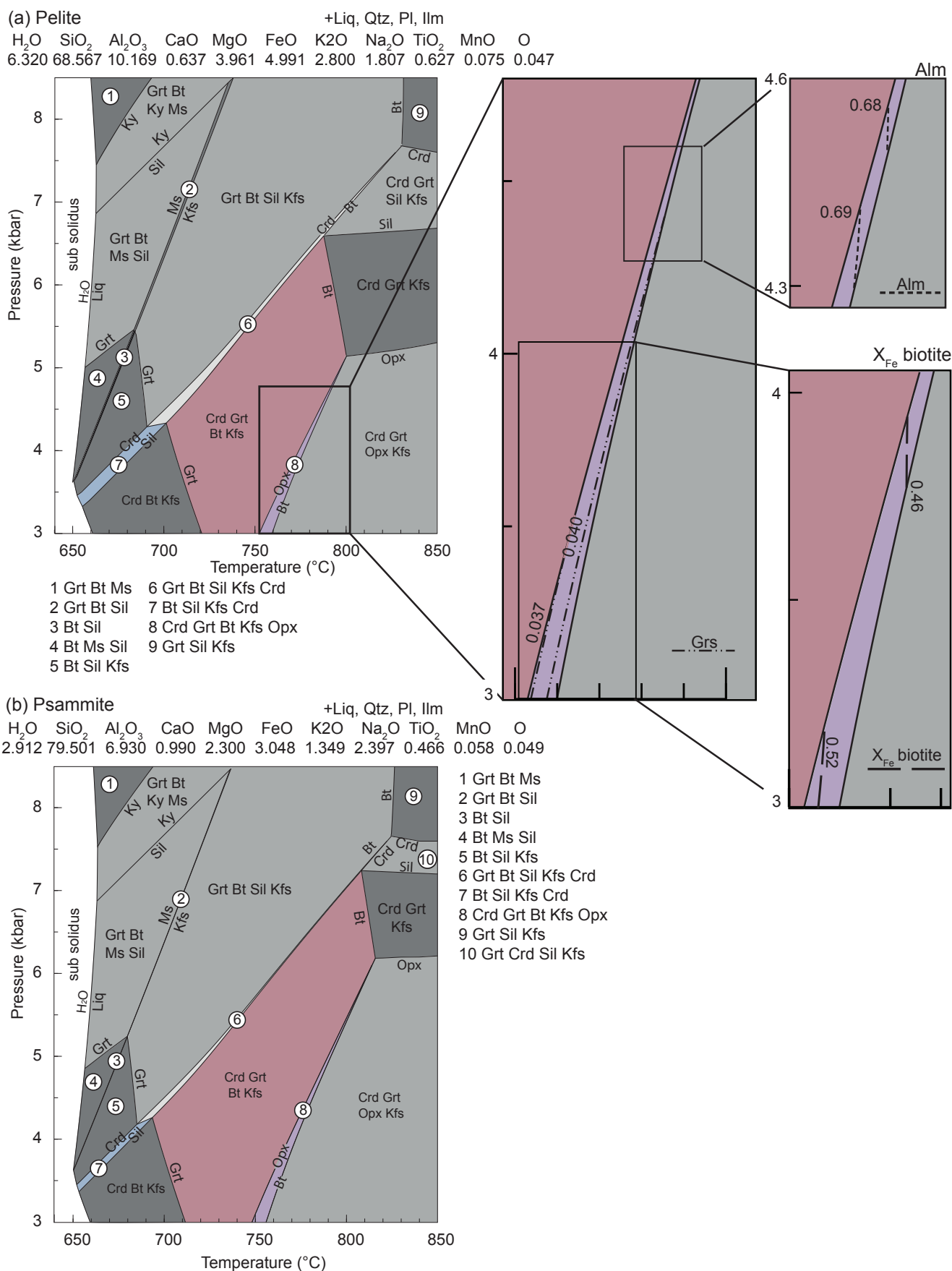
Fig. 8. H_2O-undersaturated MnNCKFMASHTO P-T pseudosection for the average composition of (a) a pelite and (b) a psammite determined from the data in Fig. 2.

Agua del Sapo complex in the footwall of the PSZ (SQ106; see Fig. 4 for sample locations). Sample SQ49 contains Qtz+Pl+Kfs+Crd±Grt in the leucosome and Bt+Crd+Qtz+Pl+Kfs±Sil in the melanosome. Cordierite is partially replaced by sillimanite and pinite and while sillimanite is found elsewhere in the melanosome, pinite is not so is not included in the peak assemblage. While neighbouring rocks contained garnet, it is not present in the thin section studied. Sample SQ55 contains Bt+Ms+Qtz+Pl+Ap+Mnz+oxides with leucocratic lenses and layers of Pl+Qtz. Sample SQ58a contains Qtz+Pl+Kfs+Crd+Grt in the leucosome and Bt+Crd+Qtz+Pl+Kfs±Sil in the melanosome. Cordierite is partially replaced by sillimanite and pinite and, while sillimanite appears elsewhere in the melanosome, pinite doesn't so is interpreted as a retrograde phase and not included in the peak assemblage. Cordierite and has inclusions of biotite, garnet has inclusions of Zrn. Sample SQ72 contains Qtz+Pl+Kfs+Crd+Grt in the leucosome and Bt+Crd+Qtz+Pl+Kfs±Crd±Grt in the melanosome. Biotite is partially replaced by chlorite and ilmenite and, while ilmenite appears elsewhere in the melanosome, chlorite is interpreted as a retrograde phase and not included in the peak assemblage. Cordierite has inclusions of biotite and quartz. Sample SQ73a is described in section 5.5. Sample SQ106 contains Qtz+Bt+Pl+Kfs with rounded clasts of K-feldspar and garnet in a homogenous matrix. Garnet is partially replaced by biotite and cordierite contains inclusions of quartz.

The minerals from each sample were measured by electron microprobe (Table 2) in a variety of structural and textural positions to control for local differences in Fe-Mg exchange. Minerals were also checked for zoning by measuring compositional profiles through grains, and were not zoned. The relevant isopleths were calculated for the two pseudosections (Fig. 8) and we found that in both pseudosections the isopleths of at least one mineral did not plot within the field of mineral stability on the suprasolidus part of the pseudosection. For example, isopleths measured in SQ72 and SQ73a from the Opx-migmatite zone have a stable mineral assemblage that corresponds to the Opx+Bt field (Opx+Bt+Liq+Crd+Grt+Kfs+Pl+Ilm+Qtz). Within that field in the pelitic pseudosection garnet has the composition of Alm>66 and Grs>3. However the actual composition of garnet in the rocks is $Alm_{64-69}Grs_{2-3}Prp_{18-25}Sps_{4-9}$. In the same rocks the composition of prograde biotite is X_{Fe}= 0.45–0.59 but biotite in the Opx+Bt field in the pelitic pseudosection has X_{Fe} <0.53. Similar disparities are found for all six rocks in both pseudosections.

We developed new pseudosections and, instead of using the sedimentary protoliths as the bulk composition, we used the whole-rock composition of the six rock samples listed above, producing six different pseudosections. Whole-rock analyses (Table 2) were used for the bulk composition with the molar amounts of the oxides normalised to 100%. The migmatites contain 57–66% SiO_2, ~1% TiO_2, 15–20% Al_2O_3, 6–10% Fe_2O_3, <0.2% MnO, 2–5% MgO, and <0.25% P_2O_5. There was a marked variation in CaO, with sample SQ58a containing only 0.58% while the other samples contained double or triple the proportion (~1–1.5%). Sample SQ58a also contained about half Na_2O (~1%) of the other samples (~2–3%). There was also a high degree of variation in the K_2O content, with SQ72 containing double the amount (7.43%) of the other

samples (~3–4%).

For each pseudosection, we calculated relevant isopleths in key minerals to constrain peak pressure and temperature and compared them to the actual composition of the minerals in the rock. Isopleths were calculated within the field that contains the stable peak mineral assemblage. However, we found that in all pseudosections the actual composition of the end-member minerals did not correspond to the composition of minerals stable within that field. This may occur when the different minerals in the rock equilibrate under different P-T conditions or when Fe-Mg exchange occurs during cooling. We tested this by plotting isopleths for minerals over the entire P-T space, above and below the solidus, but found isopleths did not correspond to the mineral compositions anywhere in the pseudosection. The minerals that were inconsistent with the calculated isopleths varied between pseudosections, there was no consistent pattern. For example, in sample SQ73a Alm and Sps in garnet were consistent with the isopleths calculated for Alm and Sps in the pseudosection but Grs in garnet and X_{Fe} of biotite were not. In sample SQ58a, Alm, Sps, Grs in garnet and X_{Fe} of biotite were only partially consistent with the isopleths for the same minerals in the pseudosection. In the next section we detail the attempts made to understand and address this problem and demonstrate that the migmatites do not represent an equilibrium assemblage (even at thin section scale), and therefore their peak P-T conditions and P-T path cannot be modelled without understanding the processes that cause such strong disequilibrium (e.g. movement of magma through the rocks).

5.4. Methods to correct the bulk composition of migmatites

The differences between the calculated composition of the minerals and the measured end-member minerals may be due heterogeneity of the rock. Migmatites are heterogeneous at various scales by definition. Moreover, the rock composition evolves through time as a result of melt loss or gain and possible remelting. We do not know the size of the equilibration volume, it may be smaller than the whole rock. Accordingly, we determined a new rock composition for each sample by measuring a representative area within the thin section using an electron microprobe. The measured area was split into sections, allowing more control over the relative proportion of leucosome, melanosome, and key minerals, such as garnet and orthopyroxene. New rock compositions were determined for all samples except for SQ58a since it was particularly heterogeneous and problematic to model. This sample was replaced by two samples from the Grt-migmatite zone, SQ62b and SQ65. The new rock compositions did not differ greatly from the original bulk rock compositions (Table 2). In order to see if these small differences changed the composition of the minerals we created new pseudosections but found they were not substantially different from the original pseudosections that used the bulk composition.

Having ruled out measurement error, we then investigated processes within the rock that may have caused disequilibrium. As described in section 3, individual migmatite samples con-

tain different leucosomes. In extreme cases, some do not contain plagioclase (Kfs+Qtz+Grt) and some do not contain K-feldspar (Pl+Qtz+Grt). There are a number of possibilities for why this may occur including remelting, fractionation, and loss or gain of melt. We explored each of these possibilities for each sample and since the outcome was the same for each case, we describe the process only for sample, SQ73a, below (pseudosections for other samples are presented in appendix B). We begin with a description of the rock and the pseudosection, before describing the attempts made to alter the bulk composition of the rock.

5.5. Opx-migmatite, sample SQ73a

Sample SQ73a is a metatexite from the Opx-migmatite zone that contains two types of leucosomes: Qtz+Pl+Ksp+Crd+Opx and Ksp+Qtz+Grt+Crd. Melanosome surrounds both types of leucosomes and consists of Bt+Qtz+Ksp+Pl+Crd+Sil. Plagioclase is oligoclase with compositions $Ab_{77}An_{22}Or_1$ and X_{Fe} of biotite ranging from 0.47 to 0.57. Garnet is almandine with compositions $Alm_{68-69}Grs_2Prp_{24-25}Sps_4$ and is not zoned. Cordierite has X_{Fe} ranging between 0.33 and 0.35 and orthopyroxene has X_{Fe} ranging from 0.54 to 0.56. Sillimanite only appears on the edges of cordierite, interpreted to be a result of retrogression of cordierite and not part of the peak equilibrium assemblage.

The pseudosection for this sample (Fig. 9) shows that the mineral assemblage Bt+Qtz+Ksp+Pl+Crd+Grt+Opx defines a narrow triangular field (bold lines in Fig. 9) at temperatures of ~760–825 °C, spanning the complete pressure range. Within this field, isopleths for X_{Fe} of cordierite, X_{Fe} of orthopyroxene, and Sps and Alm in garnet indicate pressures between 3.5 and 5 kbar (box in Fig. 9). However, the measured compositions of X_{Fe} of biotite, Ca(Pl), and Grs in garnet do not plot in this field. Ca(Pl) plots in a lower temperature field, below the stability of orthopyroxene, suggesting that it may have equilibrated at lower temperatures during retrograde metamorphism instead of during the peak indicated by the other minerals. However, the compositions for X_{Fe} of biotite and Grs do not plot anywhere on the pseudosection (Fig. 9), including in the subsolidus area.

As mentioned earlier, one of the leucosomes in this rock contains no plagioclase (Ksp+Qtz+Grt+Crd). We investigated whether a leucosome of this composition was a possible result of melting SQ73a by determining the composition of the liquid (melt) in the pseudosection and found that the melt composition is granitic, inconsistent with the abundance of K-feldspar and absence of plagioclase in these leucosomes. There are two possibilities to explain the absence of plagioclase: (1) the leucosome was generated from a different protolith and is not in situ, and/or (2) fractionation. If the leucosome is not in situ, it is possible that subtracting it from the bulk-rock composition may correct the composition of the bulk rock. Using the rock composition determined by microprobe, we calculated a new whole-rock composition that included only areas from the melanosome and the Qtz+Pl+Ksp+Crd+Opx leucosome. The resultant com-
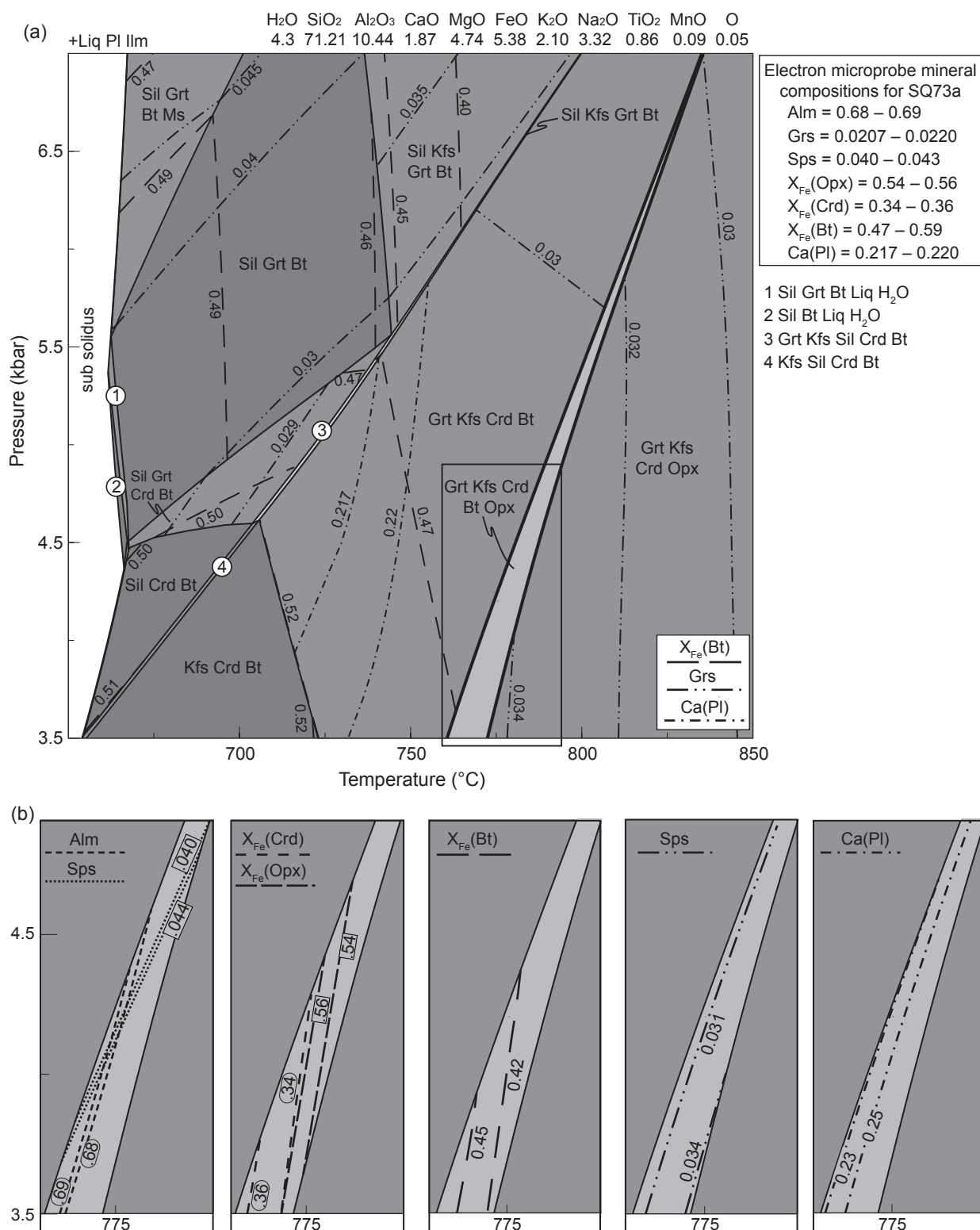
Fig. 9. (a) H_2O-undersaturated MnNCKFMASHTO P-T pseudosection for sample SQ73a from the Opx-migmatite zone. (b) Isopleths for key minerals in the region boxed in (a).

position did not produce isopleths different to the original pseudosection in Fig. 9.

     An alternative explanation is that the Ksp-rich leucosome is in-source and represents an early melt fraction. This is supported by the presence of Pl-rich leucosomes that could represent

the complementary residual fraction. Melt fractionation is a geochemical problem and could be modelled in the future using geochemical tools, but is beyond the scope of this project. Therefore, having rejected more straightforward solutions, this issue remains unresolved. Regardless of the reason, this work demonstrates that the migmatites are not equilibrium assemblages, but complicated packages of rocks within an open system.

5.6. Summary of results

As detailed above, these results suggest that the mineral assemblages in migmatitic rocks are not in equilibrium, even on a small scale. It is possible that the preserved leucosomes did not originate at the same P-T conditions and/or by similar melting processes. Some leucosomes preserved in migmatites reflect peak anatexis while others are fractionated or are not in situ. The other pseudosections calculated are presented in Appendix B and, like sample SQ73a, almost all (exception, SQ49, described in next paragraph) show isopleth compositions inconsistent with the bulk rock composition.

The pseudosection for sample SQ49 of a migmatite from the Sil+Crd-migmatite zone (SQ49), showed isopleth compositions consistent with those measured in the end-member minerals. However, only two sets of isopleths plotted in the field defined by the stable mineral assemblage: X_{Fe} of biotite and X_{Fe} of cordierite. Ca(Pl) plotted in a lower temperature field, which is typical for feldspars since they equilibrate at lower temperatures than biotite and cordierite. Two sets of contours are insufficient for isopleth thermobarometry, at least one other set is required for accuracy. This is particularly the case for Tolombón complex migmatites since we have already shown most do not contain equilibrium assemblages. Therefore, we include this pseudosection in Appendix B and do not discuss it further here.

Sample SQ73a was the only sample investigated that showed plagioclase-absent leucosomes in thin section. As mentioned previously, other samples contained tonalitic leucosomes with no K-feldspar (Pl+Qtz+Grt), but most leucosomes are granitic, containing two feldspars in addition to quartz. While melt migration or fractionation in these samples is not obvious, we see evidence in the field for the complexity of this process. Migmatites are open systems where magma is produced in situ and segregates into leucosomes that become linked to a network that allows migration of magma through the system (Fig. 5c,d). Mobile magma may carry peritectic minerals or it may leave them behind in the restite, and we see evidence for both processes in the field. The high proportion of restitic rocks in the Tolombón complex suggests that magma migration was pervasive throughout the system. Magma intrusion and migration may lead to the preservation of leucosomes generated from several different rock compositions within just one rock. Additionally, melt may be extracted from a migmatite and the new bulk composition of the rock may be remelted. While there is not direct evidence for magma migration in all thin sections, it is a complex process which may be cryptic in some rocks.

6. Geochronology

Büttner et al. (2005) provided age data on the rocks between Cafayate and Anchillo river gorge (Fig. 2 in chapter 1). To complement this data and relate the rest of the Tolombón complex to the PSZ, we dated rocks close to and within the PSZ. Two samples were from the PSZ in the Tolombón complex, one mylonitic stromatic migmatite (SQ37d: 26° 18' 59.3" S, 66° 01' 07.1" W) and one ultramylonitic granitic diatexite (SQ32c: 26° 18' 37.2" S, 66° 04' 05.7" W). The third sample was an intensely sheared Grt-schist (SQ84a: 26° 20' 20.3" S, 66° 02' 18.3" W) from the base of the PSZ at the top of the Agua del Sapo complex, lacking evidence for anatexis and intruded by pegmatite dykes that were mylonitised. We also dated one rock from the foot-wall of the PSZ in the Agua del Sapo complex, an amphibolite facies Ms-Grt schist (SQ181a: 26° 23' 37.2" S, 66° 01' 27.4" W).

6.1. Analytical method

Each sample was crushed and milled and monazite was separated using a magnetic separator and heavy liquids. Grains of a variety of appearances were hand-picked under a binocular microscope and mounted in 25 mm epoxy disks along with the monazite standard IND-1 (509 Ma, $^{206}Pb/^{238}U$ = 0.082133; Korhonen et al., 2011). The mount was polished and prior to analysis all monazite grains were photographed in transmitted light and, after gold coating, imaged using backscattered electrons on the scanning electron microscope, which revealed that grains did not exhibit any zoning so photomicrographs were not taken. For each sample three grains were reanalysed at the end of the run using a different spot to ensure accuracy was maintained over the run. Monazites were dated using the SHRIMP-II at the Department of Applied Physics at Curtin University in Western Australia. The procedure for monazite dating followed the method described in Korhonen et al. (2011).

6.2. Results

Isotopic age data are presented in Table 3 and Fig. 10. Common Pb was corrected assuming $^{206}Pb/^{238}U$-$^{207}Pb/^{235}U$ age-concordance. The mean ages are weighted and the error shown for each mean age incorporates the error in the standard.

Fifteen grains in sample SQ32c were analysed using 18 spots and revealed a range of ages between 423–510 Ma with a weighted mean of 478±12 Ma (all errors reported are 2σ unless otherwise stated). Ten of the analyses were >10% discordant. Without these points the range was 460–510 Ma with a weighted mean of 483±15 Ma (Fig. 11; MWSD of concordance =24, probability of concordance (*p*) =0.00). Twenty-three monazites (26 spots) from SQ37d were analysed and they had a range of ages between 452 and 501 Ma with a mean of 477±5 Ma (Fig.

Table 3.
U-Pb analytical data.

Spot name	U (ppm)	Th (ppm)	Th/U	$^{207}Pb/^{235}U$	±%	$^{206}Pb/^{238}U$	±%	$^{238}U/^{206}Pb$	±%	$^{207}Pb/^{206}Pb$	±%	Age (Ma)		Discord %
Mylonitic Grt-schist from PSZ														
SQ84a														
84.1	2888	34317	12	0.607	1.3	0.0781	1.1	12.81	1.1	0.05637	0.73	485	±5	-4
n=14														
84.2	2292	37066	16	0.596	1.7	0.0784	1.1	12.75	1.1	0.05517	1.31	487	±5	-17
84.3	2414	37160	15	0.579	1.8	0.0748	1.7	13.37	1.7	0.05614	0.72	465	±8	-2
84.4	2155	32214	15	0.589	2.0	0.0742	1.9	13.48	1.9	0.05755	0.73	461	±8	+10
84.5	3630	39369	11	0.570	1.5	0.0741	1.2	13.50	1.2	0.05583	0.75	461	±6	-4
84.7	2310	29184	13	0.605	1.4	0.0780	1.1	12.83	1.1	0.05629	0.77	484	±5	-5
84.8	2235	37562	17	0.576	1.5	0.0750	1.3	13.33	1.3	0.05565	0.78	466	±6	-7
84.9	2086	35404	17	0.583	1.6	0.0777	1.1	12.87	1.1	0.05442	1.16	482	±5	-26
84.10	4375	31347	7	0.566	1.5	0.0734	1.4	13.63	1.4	0.05598	0.53	457	±6	-2
84.11	2873	33094	12	0.605	1.3	0.0778	1.1	12.86	1.1	0.05644	0.67	483	±5	-3
84.13	1927	37240	19	0.609	1.4	0.0785	1.1	12.75	1.1	0.05630	0.88	487	±5	-6
84.2R	2170	35617	16	0.567	1.5	0.0743	1.3	13.45	1.3	0.05534	0.90	462	±6	-9
84.9R	2095	36082	17	0.587	1.5	0.0749	1.3	13.35	1.3	0.05687	0.71	466	±6	+4
84.7R	2359	32528	14	0.586	1.4	0.0755	1.3	13.24	1.3	0.05625	0.70	470	±6	-2
Weighted mean												475	±7	
Mylonitic stromatic metatexite from PSZ														
SQ37d														
37.1	3951	43253	11	0.621	1.3	0.0798	1.1	12.53	1.1	0.05642	0.78	495	±5	-6
n=25														
37.2	7346	39783	5	0.590	1.3	0.0764	1.1	13.09	1.1	0.05597	0.64	475	±5	-6
37.3	2533	38833	15	0.616	1.3	0.0785	1.1	12.74	1.1	0.05690	0.69	487	±5	-0
37.4	5334	43594	8	0.598	1.7	0.0766	1.7	13.05	1.7	0.05660	0.46	476	±8	-1
37.5	3534	44492	13	0.588	1.4	0.0754	1.2	13.25	1.2	0.05650	0.62	469	±5	+0
37.6	4094	47642	12	0.614	1.2	0.0784	1.1	12.76	1.1	0.05684	0.51	487	±5	-1
37.7	2973	45934	15	0.596	2.2	0.0761	2.1	13.13	2.1	0.05674	0.67	473	±9	+1
37.8	2809	46166	16	0.597	1.3	0.0772	1.1	12.96	1.1	0.05616	0.72	479	±5	-5
37.9	2867	46349	16	0.596	1.9	0.0765	1.8	13.07	1.8	0.05650	0.64	475	±8	-1
37.11	4228	42598	10	0.592	1.8	0.0758	1.8	13.20	1.8	0.05664	0.54	471	±8	+1
37.12	2763	56726	21	0.584	1.3	0.0746	1.1	13.40	1.1	0.05679	0.71	464	±5	+4
37.13	3654	42813	12	0.593	1.3	0.0768	1.2	13.02	1.2	0.05601	0.59	477	±5	-6
37.14	1277	50887	40	0.603	1.8	0.0789	1.1	12.67	1.1	0.05545	1.40	490	±5	-15
37.15	3412	47232	14	0.582	1.4	0.0765	1.2	13.07	1.2	0.05513	0.67	475	±5	-15
37.16	6054	48305	8	0.570	1.7	0.0738	1.7	13.54	1.7	0.05602	0.49	459	±7	-2
37.17	4025	43115	11	0.602	1.2	0.0781	1.1	12.81	1.1	0.05594	0.58	485	±5	-9
37.18	3659	32798	9	0.614	1.6	0.0796	1.4	12.56	1.4	0.05598	0.64	494	±7	-10
37.19	1289	57095	44	0.606	2.3	0.0768	2.1	13.01	2.1	0.05724	0.97	477	±10	+4
37.21	656	53718	82	0.596	2.2	0.0776	1.2	12.89	1.2	0.05576	1.84	482	±6	-10
37.22	2161	45386	21	0.583	1.6	0.0747	1.3	13.39	1.3	0.05659	0.89	464	±6	+2
37.23	5319	45340	9	0.592	1.4	0.0764	1.3	13.08	1.3	0.05621	0.49	475	±6	-4
37.24	2165	50640	23	0.585	1.5	0.0756	1.3	13.22	1.3	0.05606	0.82	470	±6	-4

Table 3. (continued)

	Spot name	U (ppm)	Th (ppm)	Th/ U	$^{207}Pb/$ ^{235}U	± %	$^{206}Pb/$ ^{238}U	± %	$^{238}U/$ ^{206}Pb	± %	$^{207}Pb/$ ^{206}Pb	± %	Age (Ma)		Dis-cord %
														Radiogenic ratios	
	37.1R	4733	37937	8	0.593	1.8	0.0762	1.8	13.13	1.8	0.05642	0.47	473	±8	-2
	37.19R	1030	56717	55	0.599	2.0	0.0774	1.5	12.91	1.5	0.05612	1.33	481	±7	-6
	37.23R	4218	52617	12	0.596	1.3	0.0772	1.1	12.95	1.1	0.05597	0.61	479	±5	-7
	Weighted mean												477	±5	
Ultramylonitic granitic diatexite from PSZ															
SQ32c	32.1	1667	33252	20	0.576	2.4	0.0763	2.0	13.11	2.0	0.05477	1.17	474	±9	-19
n=17	32.2	2199	34395	16	0.614	1.6	0.0809	1.3	12.36	1.3	0.05501	0.91	501	±6	-23
	32.5	1887	35004	19	0.589	1.6	0.0760	1.3	13.15	1.3	0.05617	0.92	472	±6	-4
	32.6	1981	36910	19	0.626	1.4	0.0816	1.1	12.26	1.1	0.05568	0.82	505	±6	-16
	32.7	894	35083	39	0.588	2.9	0.0789	1.2	12.67	1.2	0.05401	2.58	490	±6	-34
	32.8	941	34190	36	0.566	4.2	0.0754	2.9	13.26	2.9	0.05442	3.01	469	±13	-22
	32.11	4920	47649	10	0.643	1.2	0.0815	1.1	12.27	1.1	0.05724	0.46	505	±5	-1
	32.3	3705	30874	8	0.617	1.3	0.0788	1.2	12.70	1.2	0.05679	0.58	489	±6	-2
	32.4	1461	35661	24	0.618	1.7	0.0782	1.4	12.79	1.4	0.05731	0.90	485	±7	+3
	32.12	832	35607	43	0.632	2.1	0.0769	1.6	13.01	1.6	0.05961	1.38	477	±7	+19
	32.13	1037	34095	33	0.527	3.7	0.0740	3.0	13.52	3.0	0.05171	2.18	460	±13	-73
	32.14	2055	33884	16	0.560	2.4	0.0730	2.2	13.69	2.2	0.05567	0.81	454	±10	-4
	32.15	1389	34529	25	0.577	2.2	0.0754	1.9	13.27	1.9	0.05556	1.12	468	±9	-9
	32.16	2460	32169	13	0.500	2.0	0.0688	1.5	14.53	1.5	0.05263	1.22	429	±6	-39
	32.7R	1046	36912	35	0.589	1.9	0.0758	1.5	13.19	1.5	0.05629	1.20	471	±7	-2
	32.9R	2508	33401	13	0.558	1.4	0.0736	1.1	13.58	1.1	0.05500	0.88	458	±5	-12
	32.1R	937	36120	39	0.574	2.1	0.0754	1.5	13.25	1.5	0.05522	1.47	469	±7	-12
	Weighted mean												478	±12	
Ms-Grt schist from Agua del Sapo complex															
SQ181a	181.1	4920	26203	6	14.29	1.1	0.05570	0.49	0.537	1.2	0.0700	1.1	436	±5	+1
n=15	181.2	4621	27999	6	14.38	1.1	0.05561	0.52	0.533	1.2	0.0695	1.1	433	±5	+0
	181.3	3843	20208	5	14.64	1.2	0.05445	0.78	0.513	1.4	0.0683	1.2	426	±5	-10
	181.4	3103	30649	10	14.99	1.5	0.05501	0.80	0.506	1.7	0.0667	1.5	416	±6	-1
	181.5	3557	23526	7	15.01	1.5	0.05536	0.68	0.509	1.6	0.0666	1.5	416	±6	+2
	181.6	3881	28225	8	14.74	1.2	0.05496	0.73	0.514	1.4	0.0678	1.2	423	±5	-4
	181.7	3147	19565	6	14.93	1.2	0.05625	0.66	0.519	1.4	0.0670	1.2	418	±5	+9
	181.8	4583	26434	6	14.47	1.1	0.05493	0.60	0.523	1.2	0.0691	1.1	431	±5	-6
	181.9	2428	29437	13	14.04	1.1	0.05513	0.82	0.541	1.4	0.0712	1.1	443	±5	-7
	181.10	3954	11996	3	14.32	1.2	0.05479	0.69	0.527	1.4	0.0698	1.2	435	±5	-9
	181.11	4781	23851	5	14.65	1.4	0.05528	0.57	0.520	1.5	0.0682	1.4	426	±6	-1
	181.12	5265	26722	5	14.96	1.6	0.05545	0.54	0.511	1.6	0.0669	1.6	417	±6	+3
	181.1R	4767	27913	6	14.38	1.1	0.05492	0.61	0.527	1.3	0.0696	1.1	433	±5	-7
	181.3R	3422	10409	3	14.69	1.2	0.05525	0.68	0.518	1.4	0.0681	1.2	424	±5	-1
	181.7R	4847	27588	6	15.05	1.6	0.05523	0.56	0.506	1.7	0.0664	1.6	415	±7	+1
	Weighted mean												428	±5	

11; MWSD=9.3, *p*=0.00). Two of the analyses were >10% discordant but their exclusion did not change the mean age. Thirteen monazites (16 spots) were analysed from SQ84a and they showed a spread of ages between 451 and 492 Ma with a weighted mean age of 474.5±7 Ma. Three analyses were >10% discordant and without these the range was the same but the mean age was slightly lower, 472.3±7.2 Ma (Fig. 11; MSWD=15, *p*=0.00). Twelve monazites (15 spots) were analysed from sample SQ181a, the Agua del Sapo schist, and they showed a range of ages between 410 and 441 Ma, with a mean age of 428±5 Ma (Fig. 11; MSWD=11.2, *p*=0.00). None of the analyses were >10% discordant.

   The data show low probability of concordance and high MSWD values. This indicates that the line calculated to fit the data is not a good fit, suggesting that the mean age is not representative of the range of age determinations and their errors. This may be a result of multiple age populations within the data set, which can be distinguished using the mixture modelling approach of Sambridge and Compston (1994). Each dataset was re-analysed using the unmix
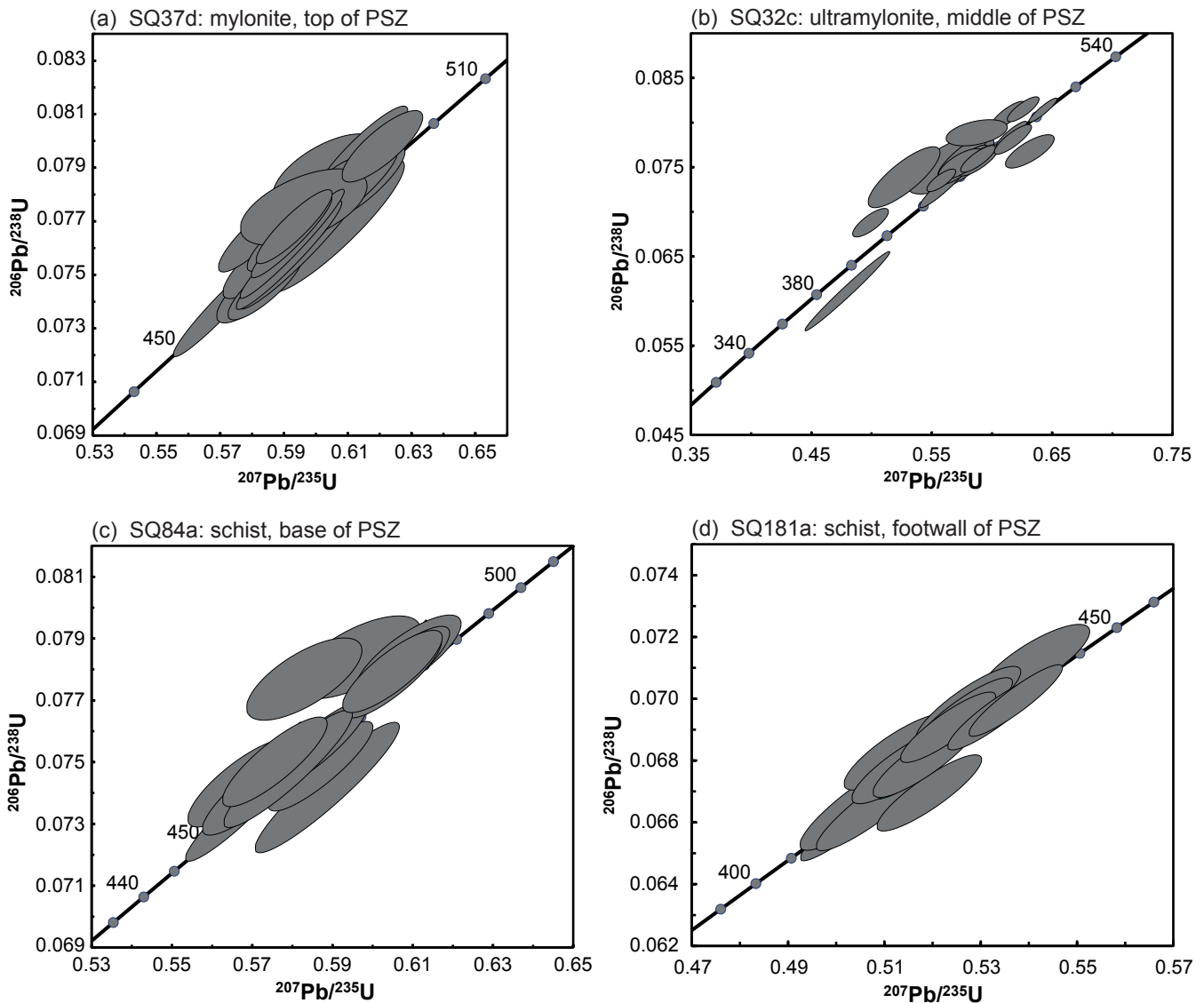
Fig. 10. Monazite geochronology concordia diagrams for the four samples analysed in this study. Error ellipses are 1σ (68.3% confidence level) and sample locations are indicated in Fig. 4.
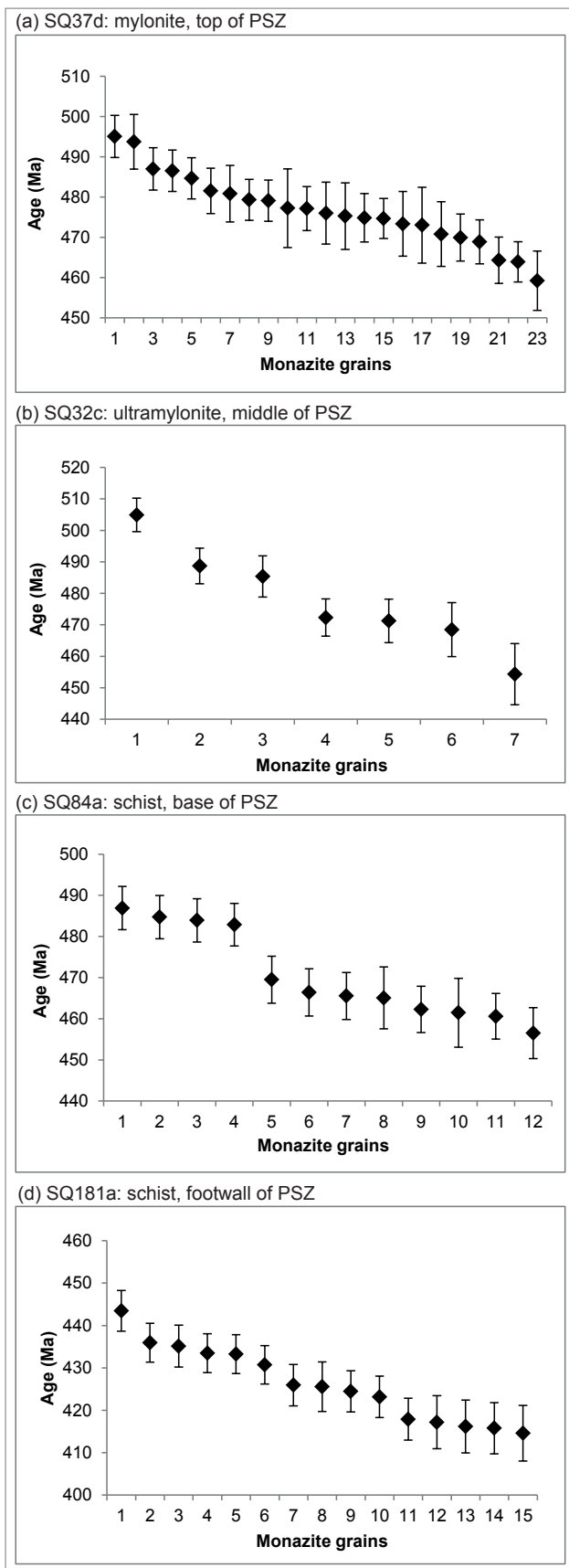
Fig. 11. U-Pb monazite age of each spot (concordant samples only) with 1σ error bars.
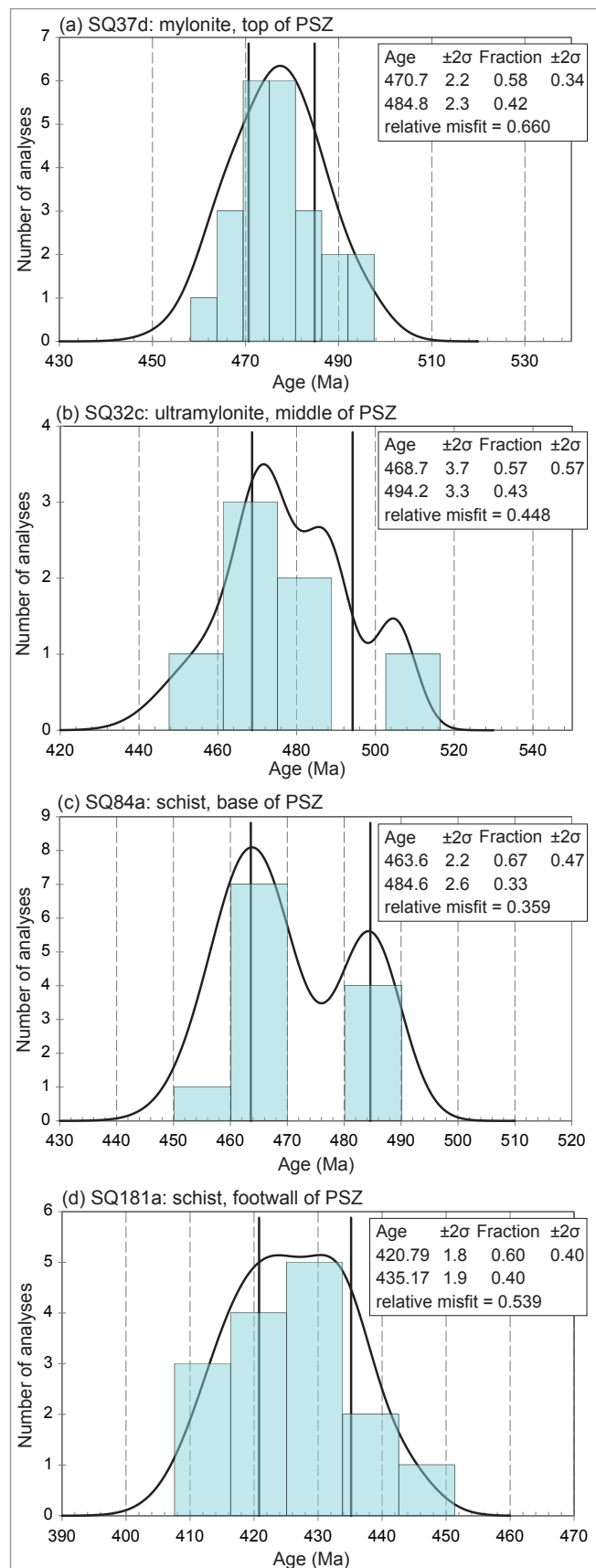
Fig. 12. U-Pb monazite age probability density plots of the mixture modelling analysis for the four samples analysed in this study.

127

function of isoplot (Ludwig, 2008). Two age components were determined for each sample. Models with further components were calculated but found to be redundant since they resulted in at least two almost identical ages. The three samples from the PSZ showed similar age groups with peaks for SQ37d at 470.7±2.2 Ma and 484.8±2.3 Ma (Fig. 12a), for SQ32c at 468.7±3.7 Ma and 494.2±3.3 Ma (Fig. 12b), and SQ84 at 463.6±2.2 and 484.6±2.6 (Fig. 12c). Sample SQ181a also showed two peaks but the ages were younger, at 420.79±1.8 Ma and 435.17±1.9 Ma (Fig. 12d). The meaning of these results is interpreted in section 7.2.

7. Discussion

The Sierra de Quilmes comprises two metamorphic terranes separated by the PSZ: the granulite facies Tolombón complex, and the amphibolite facies Agua del Sapo complex. Within the Tolombón complex there are a number of major shear zones. Conflicting theories for their development suggest they may have accommodated either crustal shortening (Finch et al., 2015) or extension (Büttner et al., 2005, Büttner, 2009). We find evidence to support the shortening model and we summarise this below, beginning with a discussion of the two major shear zones described here and their timing, before comparing the two structural models explicitly.

7.1. Major thrust shear zones of Sierra de Quilmes

The Tolombón thrust is a 1.5 km-thick zone marked by mylonites indicating a sudden increase in the intensity of shearing and the repetition of metamorphic zones. The exposed hanging wall of the Tolombón thrust is a ~10 km-thick zone that grades from Crd-metasedimentary rocks through Sil+Crd-migmatites, to Grt-migmatites. The footwall of the Tolombón thrust repeats this sequence from the Sil+Crd-migmatite zone, into the Grt-migmatite zone, and then into higher-grade rocks. This repetition of units and emplacement of hotter on cooler rocks is consistent with the top-to-west, thrust shear sense given by S-C-C′ fabric and asymmetric strain shadows on porphyroclasts in rocks of both the Tolombón thrust and the migmatitic zones.

Like the Tolombón thrust, the PSZ is marked by an increase in the intensity of shearing but here the shear zone is wider, 3.5 km thick, and shows a gradient from protomylonite at the top of the shear zone, through to ultramylonite at the base. The PSZ also places hotter rocks on cooler rocks, thrusting Opx-migmatites onto lower amphibolite-facies metasedimentary rocks (Finch et al., 2015). The PSZ and the Tolombón thrust show the same kinematics (Fig. 4), shear sense, and time of peak metamorphism and cooling (Fig. 13), suggesting they are part of the same system that thrusts rocks to the W or NW. Questions regarding the exact timing and duration of thrusting, and whether the hanging wall was still hot at the time of thrusting, are discussed in the next section.

7.2. Geochronology and peak metamorphism

Of the four samples dated, three were from the PSZ, situated at the top (SQ37d), middle (SQ32c), and base (SQ84) of the shear zone (Fig. 4). The three samples from the PSZ show two age groups, one between 498 and 482 Ma and the other between 472 and 461 Ma. The older age group contains two samples with almost identical ages and errors, SQ37d and SQ84a at ~485±2.5 Ma. SQ32c is ~10 Ma older than these samples, but the age is constrained by only three data points, so it is less reliable. Accordingly, we take the average of the other two samples, ~485 Ma, as representing the mean age of the group. Further geochronological work is necessary
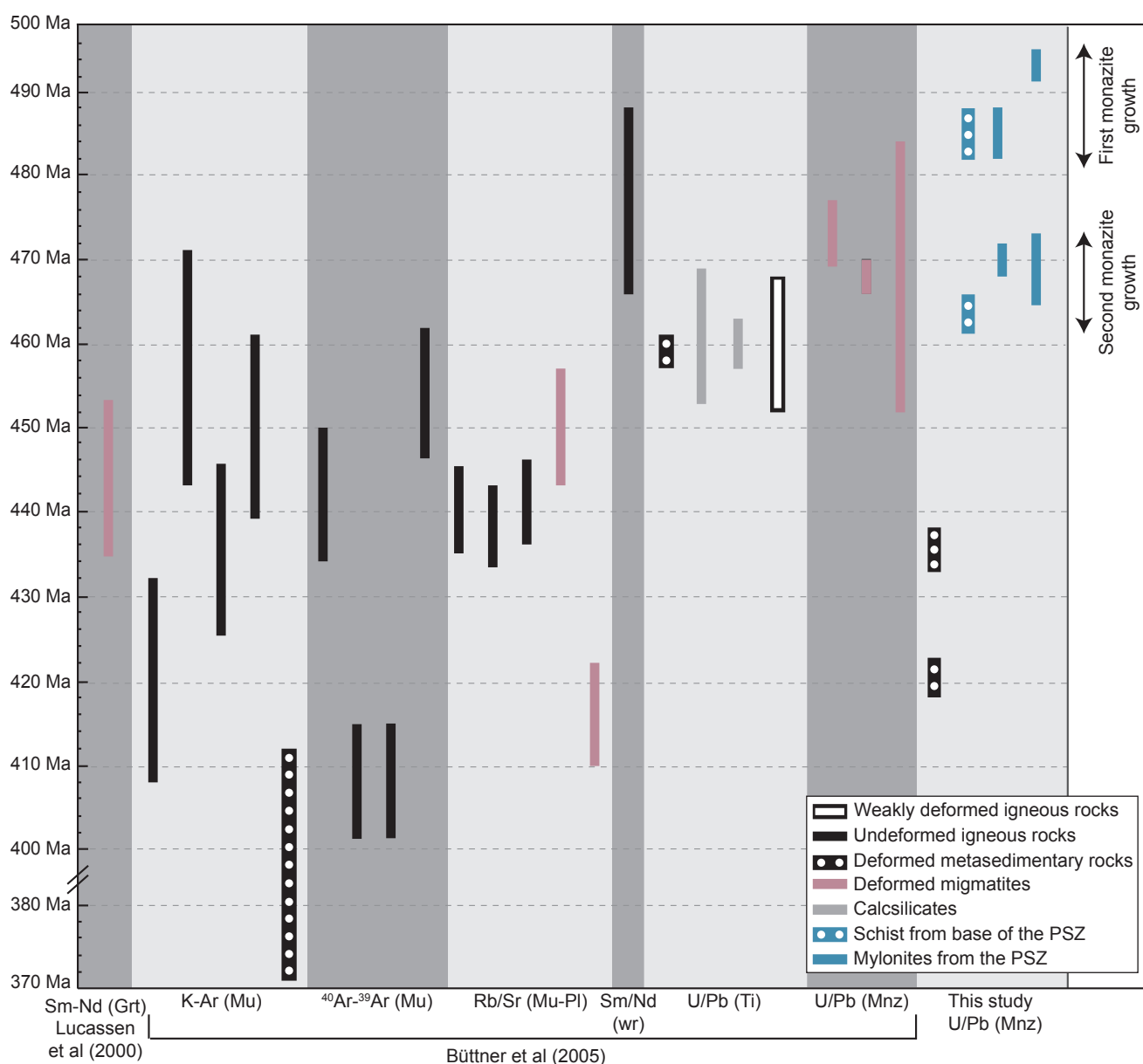
Fig. 13. Summary of geochronology data for Sierra de Quilmes. Peak metamorphism in Sierra de Quilmes occurred during or between the two periods of monazite growth determined in this study, at the same time as ductile thrusting. wr = whole rock.

to establish this group more precisely.

Monazite ages that form the younger group show an increase in mean age toward the hanging wall from 463.6±2.2 Ma (SQ84) at the base of the shear zone, to 470.7±2.2 Ma (SQ37d) at the top with the mean age of sample in the middle, SQ32c, within error of the other two samples. The age trend suggests that the ultramylonitic base of the PSZ was active longer, or that only monazite in the ultramylonitic base of the shear zone was reset by shearing whereas monazite in less-sheared rocks preserved their magma crystallization age. However, without further geochronological investigation we cannot be certain of this progression, so we take the conservative view that they all represent the same age, broadly centred on ~465 Ma. We explore the meaning of this age below.

There are a number of possible causes for these two periods of monazite growth at ~485 Ma and 465 Ma, including two thermal peaks, the first in the prograde path (at upper amphibolite facies; Copeland et al., 1988, Parrish, 1990) and the second during crystallisation of the magma in migmatites and granites. We cannot determine this with any certainty without monazite geochemistry, textural controls, and perhaps more samples to confirm the two age brackets. Regardless, the ages suggest that the metamorphic peak occurred sometime between 485 and 465 Ma.

Although the closure temperature of monazite can be as high as 900 °C (Cherniak et al., 2004), in the presence of a fluid it may be lower than 450 °C (Williams et al., 2011). Chapter 3 demonstrated that during shearing in the PSZ, water was liberated from within crystals due to recrystallisation and migrated through the shear zone to the margins, causing shear zone widening. The availability of water during shearing, and the amphibolite facies conditions of mylonitisation (chapter 2), suggests that the youngest stage of monazite growth (~465 Ma) may be coincident with the time of mylonitisation on the PSZ. Büttner et al. (2005) dated retrograde muscovite growth in a migmatite using Rb/Sr to 450 ±7 Ma (Fig. 13). Muscovite has closure temperatures between 500 and 350 °C, within lower amphibolite to upper greenschist facies. Combined, the monazite ages presented here and the cooling ages in Büttner et al. (2005) suggest an approximate temperature-time path for the Tolombón complex, with cooling through upper amphibolite facies and then upper greenschist facies from ~465–450 Ma (Fig. 13). This supports our suggestion that thrusting of the Tolombón complex and activation of the amphibolite facies PSZ was coincident with the younger generation of monazite growth. However, until there are further constraints this remains speculative and we interpret the 465 Ma age group as indicative of melt crystallisation at upper amphibolite facies conditions.

The Agua del Sapo schist sample from the footwall, SQ181a, showed two younger age groups at ~435 and 420 Ma. This may the result of two thermal pulses or the second group of ages may be a result of partial resetting of monazite due to shearing and/or fluid infiltration. This suggests that the footwall underwent a first peak metamorphism ~30 m.y. after the hanging wall. A time gap between peak metamorphism in hanging wall and footwall is typical of thrust zones. Peak is reached earlier in the thrusted hanging wall, and later in the footwall (Le Fort, 1975).

However, age gaps between hanging wall and footwall are usually on the order of 5–10 m.y. (e.g. Kohn et al., 2001, Mottram et al., 2014), not >30 m.y. as is the case here. This implies that the final stage of thrusting and emplacement of the hanging wall on the footwall may have occurred later, sometime between the 465 Ma peak in the hanging wall and the 435 Ma peak in the footwall. Accordingly, we suggest that shearing began in the Tolombón complex during the hanging wall peak between 485 and 465 Ma, and localised to the PSZ once the hanging wall reached amphibolite facies after 465 Ma. The PSZ thrust the hanging wall onto the footwall between 465 and 435 Ma.

Final emplacement of the hanging wall on the footwall occurred at around the same time as the final stage of movement on other shear zones in the Sierra de Quilmes back-arc. For example, the Agua Rosada shear zone (located ~50 km NW of Sierra de Quilmes) was active during granitioid emplacement, dated to 480–455 Ma (Hongn and Riller, 2007), and continued shearing to greenschist faces at 441–424 Ma (Rb-Sr syn-tectonic white mica, Wegmann et al., 2008). Similarly, the Arenosa Creek shear zone (~500 km S of Sierra de Quilmes) also began as a high T shear zone and cooled to upper greenschist facies by ~445–435 Ma ($^{40}Ar/^{39}Ar$ hornblende, Castro de Machuca et al., 2012). This suggests a similar evolution for shear zones in the Famatinian back-arc with high temperature shearing at the start of the Ordovician followed by thrusting of rocks to greenschist facies at 440–430 Ma. This may be coincident with the end of the Famatinian orogeny and collision of the Precordillera terrane in the southern Sierras Pampeanas.

Büttner et al. (2005) dated migmatites of the Tolombón complex using U/Pb in monazite using TIMS and found only one group of ages centred around 465–480 Ma (Fig. 13). While three analyses were performed on single large grains, the others consisted of three or four grains dissolved together. If individual grains had different ages, corresponding to the two groups identified here by means of SHRIMP spot analyses, the result would be a mixed age.

7.3. Thermodynamic modelling

Field and thin section observations in migmatites documented here suggest disequilibrium assemblages at various scales. This is likely a result of modification of the bulk composition due to, for example, the addition or subtraction of melt and solids. Disequilibrium has meant that we were unable to estimate precise peak P-T conditions using pseudosection modelling.

Büttner et al. (2005) used the average P-T technique to determine P-T equilibrium for these migmatites. Instead of modelling a pseudosection based on the bulk composition of the rock and comparing this to the end-member minerals, average P-T approaches use only the end-member minerals and calculate the reactions between them to derive a best-fit pressure and temperature. Each reaction is calculated as a line in P-T space and the location of their intersection is the average P-T. Each reaction and its P-T position have a degree of uncertainty and, because end-members overlap between reactions, the positions of the independent reactions are

correlated. To determine an average P-T from the set of independent reactions, many approaches (e.g., Powell and Holland, 1994) employ a least-squares method where the positions of the reactions are varied in proportion to their uncertainty and correlations with other reactions. Reactions with the least uncertainty are moved the least and have the greatest effect on the average P-T result. This is complicated by the correlations between reactions when, for example, a reaction with a high uncertainty is correlated with two others with low uncertainties. Moving one reaction in P-T space must move the other two that share its end-members but this movement must be balanced with the uncertainty of each reaction, ensuring that the least uncertain reactions have the greatest effect on the calculated average P-T. Most methods for average P-T consider this and compute an optimised result. In contrast to these approaches, the method used by Büttner et al. (2005), called TWEEQU (Berman, 1991), does not consider uncertainties or correlations between reactions (Powell and Holland, 2008). This allows each reaction to have equal weighting regardless of its uncertainty. Additionally, the position of any reaction can be shifted in P-T space without affecting the placement of the correlated reactions. Failure to consider uncertainties and their correlations increases the uncertainty in P-T determinations. Additionally, in TWEEQU the average P-T is estimated visually from a plot of the equilibria rather than statistically, so the uncertainty of the P-T is indeterminable (Powell and Holland, 2008). Furthermore, because there is no uncertainty data on the average P-T plot, the user cannot take uncertainty into account and calibrate their P-T determination (Powell and Holland, 2008).

Also in contrast to the approach used in this chapter, Büttner et al. (2005) used only the average composition of minerals, so their results are not sensitive to variation in chemical composition of a single phase. As described in section 5.5 and Appendix B, minerals within a single sample showed a range of compositions, which led to a range in cation ratios for each mineral. We found examples where the mean chemical composition plotted within the pseudosection but parts of the full range did not. For example, in the pseudosection for SQ106, X_{Fe} of muscovite has a range of 0.47 to 0.53 and Alm has a range of 0.72–0.77 and while the mean of both ranges was in equilibrium with the field of mineral stability in the pseudosection, values of X_{Fe} of muscovite > 0.52 and Alm>0.76 were not (Appendix B). This suggests that at least some of the muscovite and garnet were not in equilibrium with the bulk composition. Büttner et al. (2005) compared the results from single grains to the average compositions and the results did not vary greatly, which is why they typically only report average compositions. This suggests that the average P-T method used was not sensitive to small changes in mineral composition, or else that the number of single grains tested did not cover the full spectrum of variation.

In summary, while Büttner et al. (2005) constrained the average P-T of migmatites from the Tolombón complex, their results may have a high degree of uncertainty implicit in the method. TWEEQU has been superseded by other methods of calculating average P-T, which account for the uncertainties of reactions and correlations between reactions (Powell and Holland, 2008). Finally, variations in mineral composition in a single sample may not have been fully account-

ed for in Büttner et al. (2005). These differences were found to be significant in pseudosection modelling as they revealed that the bulk composition was not consistent with the composition of the end-member minerals.

7.4. Comparison to the tectono-metamorphic history of Büttner (2009)

In the first comprehensive studies of the tectono-metamorphic evolution of the Tolombón complex, Buttner et al. (2005) and Büttner (2009) proposed the region recorded an extensional phase of the Famatinian orogeny. They suggested that shear zones were originally horizontal and rotated to their current dip during the Andean orogeny. They argued for a detachment between subsolidus rocks and migmatites, which allowed the two regions to deform differently. They purport that subsolidus rocks show only minor kinking and small-scale localised shear zones, while migmatites show more pervasive, although non-penetrative, deformation with regions that underwent localised ductile shearing that alternate with undeformed migmatites. Based on determinations of paleo-pressures of key samples, they determined that the migmatitic terrane had undergone thinning and attributed this to extension. We examine each of these suggestions in turn below.

Contrary to Büttner (2009) but consistent with Piñán-Llamas (2007), we found that subsolidus rocks underwent pervasive folding (section 4). From subsolidus rocks to migmatites, we see a gradual change in deformation style with a higher proportion of ductile shear zones and concomitant decrease in the inclination and asymmetry of folds. The gradual increase in asymmetric structures with increasing structural depth suggests that the change in structural style is attributable to the increased ductility of rocks at higher temperatures. We find that the intensity of the deformation varies throughout the migmatitic Tolombón complex, but undeformed regions are rare. Less-deformed regions are diatexitic, suggesting that shearing that occurred after the crystallisation of migmatites localised to less-competent zones, such as more micaceous melanocratic regions.

Büttner (2009) suggested that there was an interface between subsolidus and migmatitic zones which was marked by a detachment characterized by a 300–500 m-thick band of intensely deformed migmatites. We found that contact ~1 km east of the location in Büttner et al. (2005) and found no indication of an increase in deformation intensity marking a possible detachment. We did find the Tolombón thrust located further west of the location of Büttner's (2009) detachment. However, the emplacement of hotter rocks on cooler rocks indicates that this was a major thrust rather than an extensional shear zone.

Büttner (2009) used estimates for thinning of the migmatitic zones as evidence for extension. Using estimates of paleo-pressure from Büttner et al. (2005), they calculated the thickness of crust separating metamorphic isograds from the detachment at the time of formation and compared it to the present-day thickness. They determined that the crust had been thinned by up

to ~50% and attributed this to extensional shearing. However, it is also possible to decrease the space between isograds during crustal shortening. This requires a component of shortening at a high angle to the isograds that can be generated, for example, by simple shear during thrusting, with a component of pure shear (i.e., general shear), which causes the layers between isograds to thin and elongate parallel to the shear plane. We also see evidence for a high proportion of melt removal in the form of abundant restitic rocks, indicating volume loss. Thinning of isograds during shortening is also reported in the Agua Rosada shear zone (50 km NW of Sierra de Quilmes), which emplaces hotter rocks on cooler and shows evidence for general shear (Wegmann et al., 2008). While we have not constrained the effects of later tilting in the current geometry of the Sierra de Quilmes, our results suggest that peak metamorphism occurred during shortening and thrusting in the Tolombón complex. We discuss this model in the next section.

7.5. Sierra de Quilmes: tectonic context

In this section, we discuss the possible tectonic settings that can explain the high T/low P metamorphism during crustal shortening. The high heat flux in the crust could be a result of: (a) arc magmatism and regional contact metamorphism (e.g. Alasino et al., 2014), (b) shallow convection of the asthenosphere in a back-arc region undergoing shortening or extension (Hyndman et al., 2005), or (c) elevated geotherms inherited from an early stage of extension (e.g. Forbes et al., 2008). We explore each of these in turn.

Sierra de Quilmes is directly east of granitoids of the Famatinian arc (see Fig. 1 in chapter 1). Other regions close to arc rocks in the Sierras Pampeanas show kilometre-thick high T/low P aureoles surrounding intrusions of arc magmas. For example, the Cerro Toro thermal aureole developed in Puncoviscana formation metasedimentary rocks adjacent to the tonalites of the Sierra de Famatina. The aureole is characterised by metamorphic zones analogous to the Sil+Crd-migmatite zone and Grt-migmatite zone of the Tolombón complex (Alasino et al., 2014). Unlike the Cerro Toro thermal aureole, Sierra de Quilmes does not record evidence of arc rocks, there are no mafic dykes or tonalite-trondhjemite-granodiorite intrusions. However, it is possible that arc rocks underlie the range, and the high T/low P metamorphism in Sierra de Quilmes may be a result of contact with an intrusive body that does not outcrop.

The back-arc region of the Famatinian arc is recognised from Puna (22° S) to San Luis (33° S; Otamendi et al., 2008, Coira et al., 2009, Larrovere et al., 2011) and incorporates the Sierras of Ancasti, Ambato, Aconquija and Velasco (~27°–30° S, 66°–67° W) all with peak metamorphism at ~ 470–477 Ma (de los Hoyos et al., 2011, Larrovere et al., 2011). Back-arc regions are characterised by high T/low P metamorphism, often thought to be a result of extension, which causes thinning and underplating of the crust by the mantle. However, some back-arcs are convergent and still show high T/low P metamorphism, suggesting crustal underplating cannot be the sole cause of the high heat flux in back-arc regions. Instead it has been proposed that hot

back-arcs are the result of increased rates of shallow convection of the asthenosphere underneath the back-arc region, independent of whether it is undergoing shortening or extension (Hyndman et al., 2005). This can be caused by the introduction of volatiles into the overriding plate by dehydration of the subducting slab (Hyndman et al., 2005).

Within the Famatinian back arc, several mountain ranges show evidence for shortening (e.g. Lucassen and Becchio, 2003, Castro de Machuca et al., 2012, Pearson et al., 2012, Hongn et al., 2014, Finch et al., 2015), and in some ranges it has been demonstrated that shortening was coincident with peak metamorphism (e.g. Castro de Machuca et al., 2012). Some of these mountain ranges also show evidence for a period of extension early in the Famatinian, prior to peak metamorphism and shortening. For example, in Sierra de San Luis, mafic intrusive rocks with a back-arc geochemical signature are recorded (Chernicoff et al., 2009). Similar rocks are seen in Puna (22°–24° S), which also records bi-modal magmatism dated to 475–480 Ma (Coira et al., 2009). Extension is also suggested by outcrops in Puna and the Cordillera Oriental of km-thick packages of sediment, deposited in the Ordovician (Zimmermann and Bahlburg, 2003). In Puna, deposition began between 478 and 468 Ma and finished around 475–460 Ma (graptolites; Bahlburg, 1990, 1991), and consists of the Tolar Chico, Tolillar, and Diablo Formations overlain by the Puna Turbidite Complex, which was deposited into a tectonically subsiding basin (described in section 3.2 of chapter 1; Bahlburg, 1990, Zimmerman et al., 2002, Aceñolaza et al., 2013). The sedimentary packages record progressively deeper marine rocks, indicative of basin subsidence. This suggests a period of extension in the early stages of the Famatinian orogeny in some areas within the back-arc. Extension may have caused lithospheric thinning and increased heat flux in the back-arc, causing thermal weakening and subsequent inversion of the basin during shortening. This model is similar to that proposed in other high T/low P convergent terranes, for example, the Broken Hill block in Australia (Forbes et al., 2008).

8. Conclusion

We have recognized two significant shear zones in the Tolombón complex in the eastern side of the Sierra de Quilmes: the Tolombón thrust and the El Pichao shear zone. These shear zones are marked by an abrupt increase in deformation intensity and emplace hotter rocks above cooler rocks. Top-to-W or NW shearing was continuous from anatexis during peak metamorphism, through to amphibolite facies when shearing became localised to these major thrust zones. This runs counter to the model of Büttner (2009) that the shear zones record extension.

Magmas migrated throughout the Tolombón complex and leucosomes formed magma networks where they fractionated during migration. These networks drained some rocks of almost all their melt leaving highly residual rocks behind. The high proportion of restitic rocks attests to the ubiquity of this process. The influx and extraction of magma through the system

prevented pseudosection modelling and peak P-T determination. However, Opx+Grt+Crd in the migmatites indicate the metamorphism occurred at high temperatures and low pressures.

Two periods of monazite crystallisation were recorded in the PSZ mylonites at ~485 and 465 Ma. This indicates two periods of monazite growth, suggesting two thermal peaks or one period of growth in the prograde path and a second upon crystallisation of melt. While we cannot differentiate between these alternatives, these ages suggest that peak metamorphism occurred in the time interval between 485 and 465 Ma. Thrusting with a top-to-W or –NW shear sense began in the Tolombón complex during peak metamorphism as evidenced by the relationship between leucosomes and structures (chapter 2). The Sierra de Quilmes is included within the Famatinian back-arc because they share a high geothermal gradient and position inboard of the magmatic arc. There are a number of models that can explain high T/low P metamorphism during short-ening, including contact metamorphism, increased rates of shallow convection of the astheno-sphere in a back-arc environment, and high heat flux during an early extension event followed by shortening. While other regions in the back-arc show evidence for an early extensional event, we are reluctant to generalise this to Sierra de Quilmes since we found no evidence for extension. Therefore, we are unable to differentiate between models for syn-shortening, high T/low P meta-morphism in the early Famatinian.

Thrusting of the Tolombón complex caused cooling of the hanging wall to amphibolite facies, and localisation of shearing to the PSZ. The delayed timing of peak metamorphism in the Agua del Sapo complex suggests that the PSZ thrust the Tolombón complex onto the Agua del Sapo complex between ~465 and 435 Ma. The PSZ shows the same foliation, stretching linea-tion, and shear sense as the rest of the Tolombón complex, including the Tolombón thrust. This suggests that shearing maintained the same kinematics from the start of shearing during anatexis at 485 Ma, to final emplacement of the PSZ hanging wall on the footwall between 465 and 435 Ma. This event coincided with the activation of other shear zones in the region, suggesting an ex-tensive shortening event throughout the Sierras Pampeanas at this time, perhaps coincident with collision of the Precordillera terrane in the southern Sierras Pampeanas (e.g. Pankhurst et al., 1998). The Famatinian orogeny ended with collision of this terrane in the southern Sierras Pam-peanas and the cessation of shearing and metamorphism for 30 million years, before the onset of the Achalian orogeny at 400 Ma.

References

Aceñolaza, F. G., Miller, H. and Toselli, A. J., 1988. The Puncoviscana Formation (Late Precambrian - Early Cambrian) - Sedimentology, tectonometamorphic history and age of the oldest rocks of NW Argentina. In: Lecture Notes in Earth Sciences, The Southern Central Andes (edited by Bahlburg, H., Breitkreuz, C. & Giese, P.) 17. Springer-Verlag, Berlin.

Aceñolaza, F. G., Miller, H. and Toselli, A. J., 2002. Proterozoic–Early Paleozoic evolution in western South America—a discussion. Tectonophysics 354, 121-137.

Aceñolaza, F. G. and Toselli, A., 1973. Stratigraphic and tectonic considerations concerning the Lower Paleozoic of northwestern Argentina. Il Congreso Latinoamericano de Geologia, Memorias 2(755-763).

Aceñolaza, G., Bayetgoll, A., Nieva, S. and Aráoz, L., 2013. Environmental constraints of a Middle Ordovician trace fossil association from the Lina Formation (Puna of Jujuy province, NW Argentina). In: Second Latin American Symposium on Ichnology (edited by Bedatou, E., Sostillo, R. & Varela, J. A.), Universidad Nacional de La Pampa, 23.

Alasino, P. H., Casquet, C., Larrovere, M. A., Pankhurst, R., Galindo, C., Dahlquist, J., Baldo, E. and Rapela, C. W., 2014. The evolution of a mid-crustal thermal aureole at Cerro Toro, Sierra de Famatina, NW Argentina. Lithos 190-191, 154-172.

Astini, R. A. and Davila, F. M., 2004. Ordovician back arc foreland and Oclóyic thrust belt development on the western Gondwana margin as a response to Precordillera terrane accretion. Tectonics 23, TC4008.

Bahlburg, H., 1990. The Ordovician basin in the Puna of NW Argentina and N Chile: Geodynamic evolution from back-arc to foreland basin. Geotektonische Forschungen 75, 1-107.

Bahlburg, H., 1991. The Ordovician back-arc to foreland successor basin in the Argentinian-Chilean Puna: tectono-sedimentary trends and sea-level changes. Special Publication, International Association of Sedimentologists 12, 465-484.

Bahlburg, H. and Herve, F., 1997. Geodynamic evolution and tectonostratigraphic terranes of northwestern Argentina and nothern Chile. Geological Society of America Bulletin 109(7), 869-884.

Becchio, R. and Lucassen, F., 2002. Concordant titanite U-Pb ages of Cambrian to Silurian high T metamorphism at the western edge of Gondwana (Southern Puna and western Sierras Pampeanas, Argentina, 26-29°). In: 5th International Symposium on Andean Geodynamics, Toulouse.

Berman, R. G., 1991. Thermobarometry using multiequilibrium calculations: a new technique, with petrological applications. Canadian Mineralogist 29, 833-855.

Bock, B., Bahlburg, H., Worner, G. and Zimmermann, U., 2000. Tracing crustal evolution in the Southern Central Andes from Late Precambrian to Permian with Geochemical and Nd and Pb isotope data. The Journal of Geology 108, 515-535.

Boggs, S., 2006. Principles of Sedimentology and Stratigraphy. Pearson Prentice Hall, New Jersey.

Büttner, S. H., 2009. The Ordovician Sierras Pampeanas-Puna basin connection: Basement thinning and basin formation in the Proto-Andean back-arc. Tectonophysics 477(3-4), 278-291.

Büttner, S. H., 2015. Comment: "One kilometre-thick ultramylonite, Sierra de Quilmes, Sierras Pampeanas, NW Argentina" by M.A. Finch, R.F. Weinberg, M.G. Fuentes, P. Hasalova, and R. Becchio, Journal of Structural Geology 72 (2015) 33-54. Journal of Structural Geology 76, 80-83.

Büttner, S. H., Glodny, J., Lucassen, F., Wemmer, K., Erdmann, S., Handler, R. and Franz, G.,

2005. Ordovician metamorphism and plutonism in the Sierra de Quilmes metamorphic complex: Implications for the tectonic setting of the northern Sierras Pampeanas (NW Argentina). Lithos 83(1-2), 143-181.

Castro de Machuca, B., Delpino, S., Previley, L., Mogessie, A. and Bjerg, E., 2012. Tectono-metamorphic evolution of a high- to medium-grade ductile deformed metagabbro/metadiorite from the Arenosa Creek Shear Zone, Western Sierras Pampeanas, Argentina. Journal of Structural Geology 42, 261-278.

Cherniak, D. J., Watson, E. B., Grove, M. and Harrison, T. M., 2004. Pb diffusion in monazite: A combined RBS/SIMS study. Geochimica et Cosmochimica Acta 68(4), 829-840.

Chernicoff, C. J., Zappettini, E. O., Villar, L. M., Chemale Jr, F. and Hernández, L., 2009. The belt of metagabbros of La Pampa: Lower Paleozoic back-arc magmatism in south-central Argentina. Journal of South American Earth Sciences 28(4), 383-397.

Coggon, R. and Holland, T. J. B., 2002. Mixing properties of phengitic micas and revised garnet-phengite thermobarometers. Journal of Metamorphic Geology 20, 683-696.

Coira, B., Kirschbaum, A., Hongn, F., Pérez, B. and Menegatti, N., 2009. Basic magmatism in northeastern Puna, Argentina: Chemical composition and tectonic setting in the Ordovician back-arc. Journal of South American Earth Sciences 28(4), 374-382.

Copeland, P., Parrish, R. R. and Harrison, T. M., 1988. Identification of inherited radiogenic Pb in monazite and its implications for U-Pb systematics. Nature 333(6175), 760-763.

de los Hoyos, C. R., Willner, A. P., Larrovere, M. A., Rossi, J. N., Toselli, A. J. and Basei, M. A. S., 2011. Tectonothermal evolution and exhumation history of the Paleozoic Proto-Andean Gondwana margin crust: The Famatinian Belt in NW Argentina. Gondwana Research 20(2–3), 309-324.

Do Campo, M. D. and Guevara, S. R., 2005. Provenance analysis and tectonic setting of late Neoproterozoic metasedimentary successions in NW Argentina. Journal of South American Earth Sciences 19, 143-153.

Finch, M. A., Weinberg, R. F., Fuentes, M. G., Hasalova, P. and Becchio, R., 2015. One kilometre-thick ultramylonite, Sierra de Quilmes, Sierras Pampeanas, NW Argentina. Journal of Structural Geology 72, 33-54.

Forbes, C. J., Betts, P. G., Giles, D. and Weinberg, R. F., 2008. Reinterpretation of the tectonic context of high-temperature metamorphism in the Broken Hill Block, NSW, and implication on the Palaeo- to Meso-Proterozoic evolution. Precambrian Research 166, 338-349.

Franz, G. and Lucassen, F., 2001. Comment on the paper "Puncoviscana folded belt in northwestern Argentina: testimony of Late Proterozoic Rodinia fragmentation and pre-Gondwana collisional episodes" by Omarini et al. International Journal of Earth Sciences 90, 890-893.

Grissom, G. C., Debari, S. M. and Snee, L. W., 1998. Geology of the Sierra de Fiambala, northwestern Argentina: implications for Early Palaeozoic Andean tectonics. Geological Society, London, Special Publications 142(1), 297-323.

Hauzenberger, C. A., Mogessie, A., Hoinkes, G., Felfernig, A., Bjerg, E. A., Kostadinoff, J., Delpino, S. and Dimieri, L., 2001. Metamorphic evolution of the Sierras de San Luis, Argentina: granulite facies metamorphism related to mafic intrusions. Mineralogy and Petrology 71(1-2), 95-126.

Höckenreiner, M., Söllner, F. and Miller, H., 2003. Dating the TIPA shear zone: an Early Devonian terrane boundary between the Famatinian and Pampean systems (NW Argentina). Journal of South American Earth Sciences 16(1), 45-66.

Holland, T. J. B. and Powell, R., 1998. An internally consistent thermodynamic dataset for phas-

es of petrological interest. Journal of Metamorphic Geology 16, 309-343.

Holland, T. J. B. and Powell, R., 2003. Activity-composition relations for phases in petrological calculations: an asymmetric multicomponent formulation. Contributions to Mineralogy and Petrology 145, 492-501.

Hongn, F. D., Tubia, J. M., Esteban, J. J., Aranguren, A., Vegas, N., Sergeev, S., Larionov, A. and Basei, M., 2014. The Sierra de Cachi (Salta, NW Argentina): geological evidence about a Famatinian retro-arc at mid crustal levels. Journal of Iberian Geology 40(2), 225-240.

Hyndman, R. D., Currie, C. A. and Mazzotti, S. P., 2005. Subduction zone backarcs, mobile belts, and orogenic heat. GSA today 15(2), 4-10.

Jezek, P., Willner, A. P., Acenolaza, F. G. and Miller, H., 1985. The Puncoviscana trough - a large basin of Late Precambrian to Early Cambrian age on the Pacific edge of the Brazilian shield. Geologische Rundschau 74(3), 573-584.

Jordan, T. E. and Allmendinger, R. W., 1986. The Sierras Pampeanas of Argentina; a modern analogue of Rocky Mountain foreland deformation. American Journal of Science 286(10), 737-764.

Kohn, M. J., Catlos, E. J., Ryerson, F. J. and Harrison, T. M., 2001. Pressure-temperature-time path discontinuity in the Main Central thrust zone, central Nepal. Geology 29(7), 571-574.

Korhonen, F. J., Saw, A. K., Clark, C., Brown, M. and Bhattacharya, S., 2011. New constraints on UHT metamorphism in the Eastern Ghats Province through the application of phase equilibria modelling and in situ geochronology. Gondwana Research 20(4), 764-781.

Kretz, R., 1983. Symbols for rock-forming minerals. American Mineralogist 68, 277 - 279.

Larrovere, M. A., de los Hoyos, C. R., Toselli, A. J., Rossi, J. N., Basei, M. A. S. and Belmar, M. E., 2011. High T/P evolution and metamorphic ages of the migmatitic basement of northern Sierras Pampeanas, Argentina: Characterization of a mid-crustal segment of the Famatinian belt. Journal of South American Earth Sciences 31(2-3), 279-297.

Le Fort, P., 1975. Himalayas: The collided range. Present knowledge of the continental arc. American Journal of Science 275-A, 1-44.

Lucassen, F. and Becchio, R., 2003. Timing of high-grade metamorphism: Early Palaeozoic U–Pb formation ages of titanite indicate long-standing high-T conditions at the western margin of Gondwana (Argentina, 26–29°S). Journal of Metamorphic Geology 21(7), 649-662.

Lucassen, F., Becchio, R., Harmon, R., Kasemann, S. A., Franz, G., Trumbull, R., Wilke, H. G., Romer, R. L. and Dulski, P., 2001. Composition and density model of the continental crust at an active continental margin - the Central Andes between 21 and 27°S. Tectonophysics 341, 195-223.

Lucassen, F., Becchio, R., Wilke, H. G., Franz, G., Thirlwall, M. F., Viramonte, J. and Wemmer, K., 2000. Proterozoic-Paleozoic development of the basement of the Central Andes (18-26°S)-a mobile belt of the South American craton. Journal of South American Earth Sciences 13, 697-715.

Ludwig, K. R., 2008. Isoplot/Ex version 4.0: A geochronological toolkit for Microsoft Excel. Berkeley Geochronology Center, Berkeley, CA.

Mahar, E. M., Baker, J. M., Powell, R., Holland, T. J. B. and Howell, N., 1997. The effect of Mn on mineral stability in metapelites. Journal of Metamorphic Geology 15, 223-238.

Mehnert, K. R., 1968. Migmatites and the Origin of Granitic Rocks. Elsevier, Amsterdam, Netherlands.

Miller, C., Pankhurst, R., Rapela, C., Saavedra, J. and Toselli, A., 1991. Genesis de los granitoides Paleozoicos peraluminoses areas Tafi del Valle y Cafayate, Sierras Pampeanas, Argentina. Actas 6th Congreso Geologico Chileno 1, 36-39.

Mon, R. and Hongn, F., 1991. The structure of the Precambrian and Lower Paleozoic basement of the Central Andes between 22° and 32°S. Lat. Geologische Rundschau 80(3), 745-758.

Mottram, C. M., Warren, C. J., Regis, D., Roberts, N. M. W., Harris, N. B. W., Argles, T. W. and Parrish, R. R., 2014. Developing an inverted Barrovian sequence; insights from monazite petrochronology. Earth and Planetary Science Letters 403, 418-431.

Otamendi, J. E., Castellarini, P. A., Fagiano, M. R., Demichelis, A. H. and Tibaldi, A. M., 2004. Cambrian to Devonian geologic evolution of the Sierra de Comechingones, eastern Sierras Pampeanas, Argentina: evidence for the development and exhumation of continental crust on the proto-Pacific margin of Gondwana. Gondwana Research 7(4), 1143-1155.

Otamendi, J. E., Tibaldi, A. M., Vujovich, G. I. and Viñao, G. A., 2008. Metamorphic evolution of migmatites from the deep Famatinian arc crust exposed in Sierras Valle Fértil–La Huerta, San Juan, Argentina. Journal of South American Earth Sciences 25(3), 313-335.

Pankhurst, R. J., Rapela, C. W. and Fanning, C. M., 2000. Age and origin of coeval TTG, I- and S-type granites in the Famatinian belt of NW Argentina. Earth and Environmental Science Transactions of the Royal Society of Edinburgh 91(1-2), 151-168.

Pankhurst, R. J., Rapela, C. W., Saavedra, J., Baldo, E., Dahlquist, J., Pascua, I. and Fanning, C. M., 1998. The Famatinian magmatic arc in the central Sierras Pampeanas: an Early to Mid-Ordovician continental arc on the Gondwana margin. Geological Society, London, Special Publications 142(1), 343-367.

Parrish, R. R., 1990. U–Pb dating of monazite and its application to geological problems. Canadian Journal of Earth Sciences 27(11), 1431-1450.

Pearson, D. M., Kapp, P., Reiners, P. W., Gehrels, G. E., Ducea, M. N., Pullen, A., Otamendi, J. E. and Alonso, R. N., 2012. Major Miocene exhumation by fault-propagation folding within a metamorphosed, early Paleozoic thrust belt: Northwestern Argentina. Tectonics 31, TC4023.

Pettijohn, F. J., Potter, P. E., and Siever, R., 1972. Sand and sandstone. Springer-Verlag, Heidelberg.

Piñán-Llamas, A., 2007. The early Paleozoic evolution of the paleo-Pacific Gondwana margin: A structural, petrographic, and geochemical study in the Puncoviscana Formation. Unpublished PhD thesis, Boston University, 1-286.

Piñán-Llamas, A. and Simpson, C., 2006. Deformation of Gondwana margin turbidites during the Pampean orogeny, north-central Argentina. Geological Society of America Bulletin 118(9-10), 1270-1279.

Powell, R. and Holland, J. B., 2008. On thermobarometry. Journal of Metamorphic Geology 26, 155-179.

Powell, R. and Holland, T., 1994. Optimal geothermometry and geobarometry. American Mineralogist 79, 120-133.

Powell, R., Holland, T. and Worley, B., 1998. Calculating phase diagrams involving solid solutions via non-linear equations, with examples using THERMOCALC. Journal of Metamorphic Petrology 16, 577-588.

Ramos, V. A., Dallmeyer, R. D. and Vujovich, G., 1998. Time constraints on the Early Palaeozoic docking of the Precordillera, central Argentina. Geological Society, London, Special Publications 142(1), 143-158.

Ramsay, J. G. and Graham, R. H., 1970. Strain variation in shear belts. Canadian Journal of

Earth Science 7, 786 - 813.

Rapela, C., 1976. El basamento metamorfico de la region de Cafayate, Provincia de Salta. Aspectos petrologicos y geoquimicos. Revista de la Asociación Geológica Argentina 31, 203-222.

Rapela, C. W., Heaman, L. M. and McNutt, R. H., 1982. Rb-Sr geochronology of granitoid rocks from the Pampean Ranges, Argentina. The Journal of Geology 90(5), 574-582.

Rapela, C. W., Pankhurst, R. J., Casquet, C., Baldo, E., Saavedra, J. and Galindo, C., 1998a. Early evolution of the Proto-Andean margin of South America. Geology 26(8), 707-710.

Rapela, C. W., Pankhurst, R. J., Casquet, C., Baldo, E., Saavedra, J., Galindo, C. and Fanning, C. M., 1998b. The Pampean Orogeny of the southern proto-Andes: Cambrian continental collision in the Sierras de Cordoba. Geological Society, London, Special Publications 142(1), 181-217.

Rapela, C. W. and Shaw, D. M., 1979. Trace and major element models of granitoid genesis in the Pampean Ranges, Argentina. Geochimica et Cosmochimica Acta 43(7), 1117-1129.

Rossi De Toselli, J. N., Toselli, A. and Toselli, G., 1976. Migmatizacion y metamorfismo en el basamento de la Sierra de Quilmes, al oeste de Colalao del Valle, Provincia de Tucuman, Argentina. Revista de la Asociación Geológica Argentina 31(2), 83-94.

Sambridge, M. S. and Compston, W., 1994. Mixture modeling of multi-component data sets with application to ion-probe zircon ages. Earth and Planetary Science Letters 128, 373-390.

Sawyer, E. W., 1998. Formation and evolution of granite magmas during crustal reworking: the significant of diatexites. Journal of Petrology 39(6), 1147-1167.

Schwartz, J. J. and Gromet, L. P., 2004. Provenance of a late Proterozoic-early Cambrian basin, Sierras de Cordoba, Argentina. Precambrian Research 129, 1-21.

Simpson, C., Law, R. D., Gromet, L. P., Miro, R. and Northrup, C. J., 2003. Paleozoic deformation in the Sierras de Cordoba and Sierra de Las Minas, eastern Sierras Pampeanas, Argentina. Journal of South American Earth Sciences 15(7), 749-764.

Sims, J. P., Ireland, T. R., Camacho, A., Lyons, P., Pieters, P. E., Skirrow, R. G., Stuart-Smith, P. G. and Miro, R., 1998. U-Pb, Th-Pb and Ar-Ar geochronology from the southern Sierras Pampeanas, Argentina: implications for the Palaeozoic tectonic evolution of the western Gondwana margin. Geological Society, London, Special Publications 142(1), 259-281.

Sola, A. M., Becchio, R. A. and Pimentel, M., 2013. Petrogenesis of migmatites and leucogranites from Sierra de Molinos, Salta, Northwest Argentina: A petrologic and geochemical study. Lithos 177(1), 470-491.

Spear, F. S., 1993. Metamorphic phase equilibria and pressure-temperature-time paths. Mineralogical Society of America, Washington DC.

Steenken, A., López de Luchi, M., Martínez Dopico, C., Drobe, M., Wemmer, K. and Siegesmund, S., 2011. The Neoproterozoic-early Paleozoic metamorphic and magmatic evolution of the Eastern Sierras Pampeanas: an overview. International Journal of Earth Sciences 100(2), 465-488.

Thomas, W. A. and Astini, R. A., 2003. Ordovician accretion of the Argentine Precordillera terrane to Gondwana: a review. Journal of South American Earth Sciences 16(1), 67-79.

Tibaldi, A. M., Álvarez-Valero, A. M., Otamendi, J. E. and Cristofollini, E. A., 2011. Formation of paired pelitic and gabbroic migmatites: An empirical investigation of the consistency of geothermometers, geobarometers, and pseudosections. Lithos 122(1–2), 57-75.

Toselli, A., Rossi De Toselli, J. N. and Rapela, C. W., 1978. El basamento metamorfico de la

Sierra de Quilmes, Republica Argentina. Revista de la Asociación Geológica Argentina 33(2), 105-121.

Turner, J. C., 1960. Estratigrafia de la Sierra de Santa Victoria y adyacencias. Boletin de la Academia Nacional de Ciencias, Cordoba 41(2), 163-206.

Varela, R., Basei, M. S., González, P., Sato, A., Naipauer, M., Campos Neto, M., Cingolani, C. and Meira, V., 2011. Accretion of Grenvillian terranes to the southwestern border of the Río de la Plata craton, western Argentina. International Journal of Earth Sciences 100(2-3), 243-272.

Vernon, R. H., 2004. A practical guide to rock microstructure. Cambridge University Press, New York.

Waters, D. J., 2001. The significance of prograde and retrograde quartz-bearing intergrowth microstructures in partially melted granulite-facies rocks. Lithos 56(1), 97-110.

Wegmann, M. I., Riller, U., Hongn, F. D., Glodny, J. and Oncken, O., 2008. Age and kinematics of ductile deformation in the Cerro Durazno area, NW Argentina: Significance for orogenic processes operating at the western margin of Gondwana during Ordovician-Silurian times. Journal of South American Earth Sciences 26(1), 78-90.

White, R. W., Pomroy, N. E. and Powell, R., 2005. An in-situ metatexite-diatexite transition in upper amphibolite facies rocks from Broken Hill, Australia. Journal of Metamorphic Geology 23, 579-602.

White, R. W., Powell, R. and Clarke, G. L., 2002. The interpretation of reaction textures in Fe-rich metapelitic granulites of the Musgrave Block, central Australia: constraints from mineral equilibria calculations in the system $K_2O-FeO-MgO-Al_2O_3-SiO_2-H_2O-TiO_2-Fe_2O_3$. Journal of Metamorphic Geology 20, 41-55.

White, R. W., Powell, R. and Holland, T. J. B., 2007. Progress relating to calculation of partial melting equilibria for metapelites. Journal of Metamorphic Geology 25, 511-527.

Williams, M. L., Jercinovic, M. J., Harlov, D. E., Budzyń, B. and Hetherington, C. J., 2011. Resetting monazite ages during fluid-related alteration. Chemical Geology 283(3–4), 218-225.

Zimmerman, U., Luna Tula, G., Marchioli, A., Narvaez, G., Olima, H. and Ramirez, A., 2002. Analisis de procedencia de la Formacion Falda Cienaga (Ordovicico Medio, Puna Argentina) por petrografia sedimentaria, elementos trazas e isotopia de Nd. Revista de la Asociación Argentina de Sedimentologia 9(2), 165-188.

Zimmermann, U., 2005. Provenance studies of very low- to low-grade metasedimentary rocks of the Puncoviscana complex, northwest Argentina. Geological Society, London, Special Publications 246(1), 381-416.

Zimmermann, U. and Bahlburg, H., 2003. Provenance analysis and tectonic setting of the Ordovician clastic deposits in the southern Puna Basin, NW Argentina. Sedimentology 50, 1079-1104.

Chapter 5

Summary, discussion, and conclusions

Previous page: Quilmes beer at a bar in La Boca, Argentina

1. Introduction

This thesis investigated the evolution of the Tolombón complex including its bounding shear zone, the El Pichao-Ovejería shear zone with its thick ultramylonite. The aims were (1) to characterise the structural and metamorphic evolution of the Tolombón complex and its significance for understanding the western margin of Gondwana during the Famatinian orogeny, and (2) to determine the processes that formed the thick ultramylonitic layer in the El Pichao shear zone. In the preceding chapters, these aims were addressed using field observations, mapping, petrographical analysis, geochemistry, geochronology, thermodynamic modelling, and FTIR. This chapter draws general conclusions about the evolution of the Sierra de Quilmes and Sierras Pampeanas based on the findings in the preceding chapters. Problems and questions that require further research are also highlighted.

2. Thickness of the ultramylonitic layer of the PSZ

Chapter 2 suggested that the 1 km thickness of the ultramylonitic layer of the PSZ is a result of the balance between shear heating and thermal diffusion, if the ultramylonitic layer took up a high proportion of the plate convergence velocity. We suggested that the ultramylonitic layer widened as shear heat diffused outwards, causing weakening of the shear zone margins. In this case the shear zone width is established by a balance between heat generation and heat loss to the surroundings. In chapter 3, we built on this theory and explored the possibility that in addition to heat, water may have also diffused outwards from the ultramylonite, weakening the surroundings. We showed by means of FTIR measurement of the water content in quartz and feldspar, that ultramylonites contained significantly less water than mylonites and weakly-deformed rocks, in contrast to several other studies that have found the opposite. We suggest that the PSZ differs from rocks investigated in previous studies because in previous studies either (1) water infiltration was post-tectonic and the relative timing of water infiltration and deformation was not determined, or (2) hydrolytic weakening focused deformation to water-rich bands, but unlike the case reported here, water loss to the surroundings was relatively unimportant (chapter 3). The latter category likely includes studies which focus on weakly-deformed rocks since they may not have undergone sufficient recrystallisation to liberate water from grains, therefore preventing the commencement of the ultramylonitisation-water expulsion cycle. As outlined in chapter 3 (section 5.3), it is only shear zones that experience thinning during shearing that are at a higher mean stress than the surrounding matrix. Shear zones that do not experience thinning are either at the same mean stress as the matrix (those that initiate parallel to the shear direction), or at a lower mean stress (thickening shear zones). In such shear zones water is either not expelled, or is attracted to the shear zone from the surrounds, respectively.

Together, heat and water diffusion into the neighbouring rocks may have caused harden-
ing of the ultramylonite, weakening of its surroundings, and movement of the locus of maximum
strain outwards. We propose that the final thickness of the ultramylonite built up gradually, start-
ing with strain localisation in a narrow, propitious site, perhaps slightly more micaceous or pre-
viously fractured. As described in chapter 3 (section 5.2), recrystallisation freed intragrain water,
and heat and water diffused into rocks on the shoulder of the ultramylonite. Shearing refocused to
the newly-weakened rocks, which then underwent the same water expulsion cycle. Repetition of
this cycle widened the ultramylonitic layer, until it reached its present-day thickness of ~1 km.

3. Tectonic implications of structural and metamorphic data

Chapters 2 and 4 demonstrated that metamorphism and anatexis occurred at high T/
low P conditions during shortening. In chapter 4 we outlined three possible mechanisms to
account for the high heat flux: contact metamorphism, increased rates of shallow convection of
the asthenosphere, and elevated geotherms inherited from an earlier stage of extension. It has
been suggested that the Sierra de Quilmes was part of the Famatinian back-arc, a longitudinal-
ly-continuous region in the Sierras Pampeanas between 65° and 66° W characterised by high T/
low P metamorphism and anatexis. In some areas, the early evolution of the Famatinian back-arc
involved extension, evidenced by the deposition of thick packages of sediment into subsiding
basins between ~480 and 465 Ma and bimodal volcanism dated to 480–475 Ma (see chapter 1,
section 3.3.2.2.2 for review). Evidence for these processes is preserved in Puna and the Cordil-
lera Oriental, but is sparse in other regions in the Famatinian back-arc, such as Sierra de Quilm-
es, which does not show evidence of bi-modal volcanism, mafic igneous rocks, or Ordovician
sedimentary basins. However, the high geothermal gradient of Sierra de Quilmes, and its location
behind the magmatic arc suggests it was part of the Famatinian back-arc.

Considering the relatively sparse evidence for extension in the back-arc, we are reluctant
to generalise extension to the entire region since it may have been a localised event. Even if the
extensional event was widespread through the back-arc, in Sierra de Quilmes it finished before
peak metamorphism in the Tolombón complex, which, as we demonstrated, is associated with
folding with leucosomes in planes parallel to the axial planar orientation, and thrusting of hotter
over colder rocks (between 485 and 465 Ma; chapters 2 and 4). This has also been demonstrated
in previous studies in other areas of the Famatinian back-arc, which determined shearing in-
volved emplacement of hotter rocks on cooler rocks, with thrusting during peak metamorphism
(e.g. Larrovere et al., 2008, Wegmann et al., 2008, Castro de Machuca et al., 2012). The com-
mencement of thrust shearing signals the beginning of the Oclóyic tectonic phase, previously
suggested to have initiated at 470 Ma. Our results allow for this, but they also suggest that it may
have started as early as 485 Ma.

Tectonic switching between extension and shortening may occur in back-arcs when

there is, for example, a change in the buoyancy of the subducting plate (Collins, 2002a). Trench retreat or rollback causes extension in the overriding plate (Forsyth and Uyeda, 1975, Royden, 1993), but the arrival of an oceanic plateau at the subduction zone may cause a period of flat subduction, leading to shortening in the back-arc, inverting it into a fold and thrust belt (Collins, 2002a). The high heat flux in the back-arc during extension results in granulite facies metamorphism, but it is not until inversion that the back-arc experiences peak metamorphism when the hot crust is buried and shortened (Collins, 2002b).

Evidence for tectonic switching in a back-arc is found in the Lachlan orogen, eastern Australia (Collins, 2002a, b). An overall extensional back-arc regime in the Lachlan orogen is indicated by extensive and long-lasting rift basins, with primitive mafic rocks, pre- and early- rift volcanics and volcaniclastic turbidites (Collins, 2002b). The high heat flux in the back-arc generated voluminous granites and granulite facies metamorphism (Collins, 2002b). However, the structures in the Lachlan orogen preserve only shortening and crustal thickening, which obliterated earlier extensional structures (Collins, 2002b). Peak metamorphism in the Lachlan orogen occurred during shortening as the hot crust was inverted into a fold and thrust belt (Collins, 2002a). Lack of evidence for terrane accretion distinguishes the Lachlan orogen from other accretionary orogens and suggests that tectonic switching was a result of increased buoyancy of the subducting slab due to the arrival of an oceanic plateau at the trench (Collins, 2002a). Like the Lachlan orogen, evidence for exotic terranes is lacking in the northern Sierras Pampeanas, suggesting that tectonic switching in the Famatinian back-arc may have resulted from a similar process. This is in contrast to the southern Sierras Pampeanas, where exotic terranes and ophiolites are preserved and models of terrane collision have wide acceptance.

Back-arc regions are often the focus of deformation when the overriding plate experiences convergence because the high heat flux causes thermal weakening. Many back-arcs develop into mobile belts, that is, zones <1000 km-wide located in the back-arc of subduction zones (Stein and Freymueller, 2002). These belts accommodate 10–20% of the plate convergence velocity and, despite changes in the configuration of the tectonic setting over time, can remain the focus for lithospheric deformation over >200 m.y., suggesting that they are intrinsically weaker than the neighbouring regions (Hyndman et al., 2005). The ubiquity of mylonitic shear zones in the Famatinian back-arc region of the Sierras Pampeanas suggests that it was the focus of ductile deformation when the overriding plate went into convergence during the Oclóyic tectonic phase, consistent with the suggestion of Lucassen et al. (2000) that this region represents a mobile belt.

The Sierra de Quilmes represents a classic thrust belt, with high grade rocks emplaced on lower grade rocks, and a decrease in metamorphic grade in the hanging wall away from the thrust shear zone. These "right-way-up" metamorphic isograds contrast with orogenic belts where isograds are inverted, so that in the hanging wall metamorphic grade increases towards the structurally higher levels, away from the shear zone, as seen above the Main Central Thrust in the Himalaya. Inversion of isograds may be a result of folding and overturning, shear heating,

or lower crustal flow (Searle and Rex, 1989, England and Molnar, 1993, Jamieson et al., 1996). Thrust belts that include "right-way-up" metamorphic isograds are relatively common in mountain ranges in overriding plates, including the Rocky Mountains in Canada (Bally et al., 1966), the Alps (Boyer and Elliot, 1982), the Appalachians in North America (Gwinn, 1964), the Scottish Highlands (Elliot and Johnson, 1980), and the Taiwan thrust belt (Suppe, 1983).

4. Implications of the geochronology data

P-T-t paths of rocks in thrust belts record the emplacement of hot rocks on cold rocks. The hot rocks at the base of the hanging wall are cooled from below by contact with the lower-grade rocks in the footwall (England and Molnar, 1993), so there may be a decrease in cooling age in the hanging wall upwards, away from the cooler footwall. Alternatively, peak metamorphism may be reached in the high-grade hanging wall prior to the final stage of thrusting onto the footwall, so minerals with high blocking temperatures (zircon, monazite) may record older ages than minerals with lower blocking temperatures that do not equilibrate until the final stage of thrusting. This may be the case in Sierra de Quilmes, where peak metamorphism occurred at granulite facies at the start of shearing, but final emplacement of the Tolombón complex on the Agua del Sapo complex occurred at amphibolite facies (chapter 2, section 5.4).

In contrast to the P-T-t evolution of the hanging wall, footwall rocks do not reach peak metamorphism until after the hanging wall is thrust onto the footwall, and they experience a consequent increase in pressure (Mottram et al., 2014). This is evident in the rocks of Sierra de Quilmes, where footwall rocks are younger than hanging wall rocks.

5. Implications of the thermodynamic modelling

In chapter 4, we modelled pseudosections of a pelite and psammite using their mean composition determined from a database of Puncoviscana Formation samples. We found that the two pseudosections were quite similar, in contrast to our field observations that indicate that the bulk composition controlled the appearance of peritectic minerals: orthopyroxene was more common in psammite layers and cordierite was more common in pelite layers. This suggests that the difference between the composition of pelites and psammites in Sierra de Quilmes was greater than the difference between the mean psammite and pelite of the Puncoviscana Formation rocks. However, as demonstrated in chapter 4, melting and melt migration was complex, so we cannot rule out that their effects may at least partly explain some of these differences.

The petrographic investigation of the migmatites and thermodynamic modelling suggested that they did not contain equilibrium assemblages, perhaps a result of magma migration and fractionation of leucosomes. Melt removal is a common feature of anatectic terranes and thermodynamic modelling of migmatites has been successfully applied to such rocks elsewhere.

While it is possible that successful attempts are more commonly published, there may be other factors which distinguish the Tolombón complex migmatites from other anatectic terranes. For example, it is possible that melt mobility in the Tolombón complex exceeds that common in other terranes. This is a cryptic process where it is difficult to differentiate between in situ and intrusive leucosomes in an interconnected network of leucosomes. Also important is the composition of the material added and subtracted from the system. In the Tolombón complex we observe examples where melt has migrated and left behind peritectic and early crystallized igneous minerals, and other examples where intrusive granites have retained some peritectic minerals. Differences such as these may cause the composition of the rock to deviate more substantially from the original composition than is typical, and may distinguish the Tolombón complex from other anatectic terranes.

6. Reply to Büttner (2015)

The end of chapter 2 included a comment by Büttner (2015) where he makes some valid observations on the limitations of the data published in Finch et al. (2015a). The main criticisms put forward by Büttner (2015) were: (1) we did not appropriately consider the effect of tilting, (2) we did not provide data to indicate the timing of movement on the PSZ in relation to peak metamorphism and that therefore thrusting could overprint the extension that he interpreted for the Tolombón Complex, and (3) we did not provide evidence that the Tolombón complex underwent thrusting. In this section, we add to the reply given in Finch et al. (2015b; chapter 2) on the basis of new data presented in chapters 3 and 4.

The Tolombón complex records top-to-NW and top-to-W shearing, an observation also recorded by Büttner et al. (2005) and not debated by Büttner (2015). However, he argues that shear zones were originally horizontal and extensional, and were tilted to their current orientation during Andean orogenesis. Büttner et al. (2005) and Büttner (2009) did not observe the emplacement of hotter on colder rocks at major thrust shear zones and this observation is not consistent with Büttner's (2009) extensional hypothesis. Finch et al. (2015a) demonstrated a continuity of movement through time and space, from thrusting during peak metamorphism in the Tolombón complex, to localisation of shearing to the PSZ, as the complex was thrust upwards and rocks cooled. Localisation of strain to the PSZ at amphibolite facies is associated with solid-state shear structures, and may have caused cessation of shearing north of the PSZ, where high-temperature, syn-anatectic structures are preserved. Combined, the evidence suggests that top-to-NW and -W thrusting was continuous from the time of anatexis in the Tolombon Complex, to subsequent solid-state localisation of shearing into the shear zones, leading to the thrusting of hotter over cooler rocks.

Büttner also contended that shearing on the PSZ post-dated shearing in the Tolombón complex. He argued that 440 Ma pegmatite dykes that cross-cut ductile shear zones in the

Tolombón complex (Büttner et al., 2005) were the same as mylonitic pegmatites in the PSZ, indicating movement was post-Ordovician. Given that multiple generations of pegmatites are common in migmatite terranes, it remains to be seen whether the pegmatites in the PSZ intruded at 440 Ma. However, even if they are this young, this does not constrain the start of shearing, it demonstrates only that shearing was active after 440 Ma, a possibility that is supported by our young monazite ages in the PSZ footwall.

Büttner's (2009, 2015) arguments for extension in the Tolombón complex rely in part on arguments for thinning of layers between metamorphic isograds. In chapter 4, we discussed how extension is not required for layer thinning, since it is possible to thin rocks during crustal shortening when there is a component of pure or general shear. Evidence for a component for pure shear is suggested by strongly folded veins and symmetrical folds with axial planes parallel to shear planes in the Crd-subsolidus and Sil+Crd-migmatite zones of the Tolombón complex, described in chapter 4, and in subsolidus rocks described by Piñán-Llamas (2007) and Büttner (2009). Isograds that were thinned during shortening are also reported in the Agua Rosada shear zone (50 km NW of Sierra de Quilmes), which emplaces hotter rocks on cooler and shows evidence for general shear (Wegmann et al., 2008). Aside from thinning, there are other mechanisms in thrust shear zones that can cause the distance between isograds to be less than that assuming lithostatic pressures. Ductile shear zones and their ductile hanging wall may have velocity gradients during exhumation that allow rocks from deeper levels to exhume faster than those from shallower levels, leading to apparent thinning of the isograds (Visona et al., 2012). This could result in, for example, a decrease in the distance between rocks that equilibrated at 5 kbar with shallower rocks, say 4.5 kbar. We find no evidence to suggest that telescoping of the isograds in the Tolombón complex was a result of extension.

Despite these differences, we agree with many aspects of Büttner (2015), including his suggestion of a tectonic switching event, where the back-arc went from extension to contraction. We differ in the timing of the switch, where Büttner (2015) claims it occurred post-Ordovician, we find evidence for Ordovician shortening and thrusting, so we place the switch in the early Famatinian. We also differ in how to interpret the structural record. However, we find that many of our observations are consistent with those in Büttner et al. (2005) and we suggest that together our work provides a better understanding of Sierra de Quilmes during the Famatinian orogeny.

7. Further research

Our geochronology work revealed an earlier age group of monazites at ~485 Ma. This age group may record growth during prograde metamorphism, a thermal pulse, or during a prolonged period of high-temperature metamorphism continuous with younger age groups at 465 Ma. Establishing this age further with more data points and monazite geochemistry may help constrain the thermal evolution of these rocks and determine the nature of these two age groups.

Furthermore, we have dated only one sample of the footwall of the PSZ, located ~ 5 km south of the shear zone (map view). In order to better understand the timing of PSZ movement and metamorphism of the footwall, samples from different structural levels of the footwall could be dated.

To determine the time of thrust shearing in the Tolombón complex, we dated syn-kinematic anatectic monazite. However, we did not date structures or minerals that bracketed the start and end of shearing. Future research could date cooling in the PSZ using biotite, muscovite, feldspar and/or pseudotachylites that cross-cut the foliation in the ultramylonite layer, although some of these could yield Andean ages that would not help much in bracketing. Our geochronology data suggests that shearing in the Tolombón complex localised to the PSZ at amphibolite facies after 465 Ma and emplaced the hanging wall on the footwall at sometime between 465 and 435 Ma. Further geochronology work, as described above, will help determine the duration of any break in thrusting more precisely.

At the easternmost extent of the PSZ, the foliation changes from NW-SE to N-S trending, suggesting that the shear zone turns to the south. This orientation is not unlike the Tapado shear zone (Fig. 2 in chapter 1), where the ultramylonites of the PSZ are overprinted and rotated by sinistral shearing (R. Weinberg, pers. comm.). In the course of our field work south of the PSZ in rocks of the Agua del Sapo complex, we found that while rocks are sheared, the intensity of shearing is difficult to determine because of the micaceous or quartzitic nature of these rocks with many areas lacking phenocrysts or dykes that could form clasts. In regions where dykes are present, they are isoclinally folded, thinned and occasionally sheared apart, suggesting that the rocks are strongly deformed. Piñán-Llamas (2007) reports a 1 km-thick shear zone near the Ruinas de Quilmes (Fig. 1b in chapter 1), but how it relates to the El Pichao shear zone remains unexplored. Recognising mylonites in metasedimentary rocks is difficult and could be an interesting and useful avenue for future research using microstructural investigation, such as the crystallographic preferred orientation of key minerals, since it is presently difficult to determine the degree of deformation and strain these rocks accommodate.

In the Tolombón complex we found two regions that record a possible pre-thrusting stage of shearing, detailed in chapter 4. The scarcity of these outcrops meant we were unable to interpret their meaning, but more detailed mapping may provide the data required.

In chapter 3, we find that water content in ultramylonites was significantly less than mylonites or weakly-deformed rocks of the PSZ, contrary to previous studies which investigated water in shear zones and found the opposite. We speculate that one reason our results differ from those previous is that the PSZ may be a thinning shear zone, whereas others may undergo thickening or no modification. A thinning shear zone is one that rotated into the extension direction and underwent stretching, which caused an increase in mean stress to levels higher than the surrounding rock. Future research in natural shear zones may indicate the conditions necessary for shear zones to expel water: do thinning shear zones expel, and thickening shear zones attract water? It may be that this is an underlying principle for the behaviour of water in shear zones

and, if so, this would have important implications for understanding shear zone weakening and controls on their steady-state width.

In chapter 4, we describe evidence for fractionated garnet-bearing leucosomes and speculate that fractionation and melt migration may contribute to the lack of a clear match between the mineral chemical composition in nature, and those predicted through mineral equilibria modelling. Understanding fractionation in these rocks and the movement of leucosomes within the complex is vital before any thermodynamic modelling can be undertaken.

8. Conclusion

The Sierra de Quilmes exposes a tilted cross-section of Famatinian high temperature, low pressure metamorphism. The high-grade Tolombón complex consists of metamorphic zones that grade from greenschist facies rocks to granulite facies Opx-diatexites (chapters 2, 4). Mapping revealed that the structures in the Tolombón complex show top-to- W or -NW thrust shear sense and shearing intensifies close to the El Pichao shear zone and the Tolombón thrust (chapter 2). These thrust planes interrupt and repeat metamorphic zones, placing hotter rocks on cooler rocks. U-Pb dating of monazite in the El Pichao shear zone indicated two periods of monazite growth at ~485 Ma and 465 Ma, suggesting that peak metamorphism occurred in the Tolombón complex within this range (chapter 4). Shearing in the Tolombón complex began during peak metamorphism, as rocks were thrust upwards they cooled, and eventually shearing localised to the amphibolite facies El Pichao shear zone (chapter 2). We suggest that the high heat flux during shortening may be a result of: a) contact metamorphism, b) increased shallow convection of the asthenosphere, or c) inheritance of a high geothermal gradient from an earlier period of shearing.

The Sierra de Quilmes may be part of the Famatinian back-arc, a region characterised by a high geothermal gradient and mylonitic thrust shear zones. Previous models for the evolution of the Sierra de Quilmes have suggested it records an extensional phase. We argue that there may have been a brief period of extension before peak metamorphism in the Famatinian back-arc but there is no evidence preserved in Sierra de Quilmes to support this. Shortening in the back-arc may be due to flat slab subduction, perhaps a result of the arrival of an oceanic plateau at the trench in the northern Sierras Pampeanas (chapter 5).

The ultramylonitic layer of the El Pichao shear zone is unusually thick, suggesting that it may have widened over time. Water weakens minerals and is mobile within and around shear zones, so we investigated whether it played a role in the development of the ultramylonite. FTIR analysis of minerals in samples from within the ultramylonitic layer of the PSZ showed that quartz and feldspar from the most deformed rocks contained the least water, contrary to most previous studies that showed the opposite (chapter 3). We suggest that water was extracted from minerals during recrystallization and development of ultramylonites and infiltrated rocks on the margin of the ultramylonitic layer. This hardened the ultramylonite, weakened the neighbouring rocks, and caused shearing to re-focus to the newly weakened rocks. These rocks underwent

the same processes of ultramylonitisation and water extraction, repeating the same cycle. This process was repeated many times, gradually building up the 1 km-thickness of the ultramylonite layer (chapter 3). The thick ultramylonitic layer at the base of the El Pichao shear zone provides an important insight into the role of water and heat diffusion in widening shear zones. Thick shear zones such as these can accommodate a significant proportion of the plate convergence velocity.

This work identifies Sierra de Quilmes as a key site for understanding shortening during the Famatinian orogeny, the development of the Sierras Pampeanas during the Ordovician, and the processes that lead to mylonitisation during thrust shearing in back-arcs.

References

Bally, A. W., Gordy, P. L. and Stewart, G. A., 1966. Structure, seismic data, and orogenic evolution of southern Canadian Rocky Mountains. Bulletin of Canadian Petroleum Geology 14, 337-381.

Boyer, S. E. and Elliot, D., 1982. Thrust systems. AAPG Bulletin 66, 1196-1230.

Büttner, S. H., 2009. The Ordovician Sierras Pampeanas-Puna basin connection: Basement thinning and basin formation in the Proto-Andean back-arc. Tectonophysics 477(3-4), 278-291.

Büttner, S. H., 2015. Comment: "One kilometre-thick ultramylonite, Sierra de Quilmes, Sierras Pampeanas, NW Argentina" by M.A. Finch, R.F. Weinberg, M.G. Fuentes, P. Hasalova, and R. Becchio, Journal of Structural Geology 72 (2015) 33-54. Journal of Structural Geology 76, 80-83.

Büttner, S. H., Glodny, J., Lucassen, F., Wemmer, K., Erdmann, S., Handler, R. and Franz, G., 2005. Ordovician metamorphism and plutonism in the Sierra de Quilmes metamorphic complex: Implications for the tectonic setting of the northern Sierras Pampeanas (NW Argentina). Lithos 83(1-2), 143-181.

Castro de Machuca, B., Delpino, S., Previley, L., Mogessie, A. and Bjerg, E., 2012. Tectono-metamorphic evolution of a high- to medium-grade ductile deformed metagabbro/metadiorite from the Arenosa Creek Shear Zone, Western Sierras Pampeanas, Argentina. Journal of Structural Geology 42, 261-278.

Collins, W. J., 2002a. Hot orogens, tectonic switching, and creation of continental crust. Geology 30, 535-538.

Collins, W. J., 2002b. Nature of extensional accretionary orogens. Tectonics 21(4), 1024.

Elliot, D. and Johnson, M. R. W., 1980. Structural evolution in the northern part of the Moine thrust belt, NW Scotland. Royal Society of Edinburgh Transactions 71(2), 69-96.

England, P. and Molnar, P., 1993. The interpretation of inverted metamorphic isograds using simple physical calculations. Tectonics 12(1), 145-157.

Finch, M. A., Weinberg, R. F., Fuentes, M. G., Hasalova, P. and Becchio, R., 2015a. One kilometre-thick ultramylonite, Sierra de Quilmes, Sierras Pampeanas, NW Argentina. Journal of Structural Geology 72, 33-54.

Finch, M. A., Weinberg, R. F., Fuentes, M. G., Hasalova, P. and Becchio, R., 2015b. Reply to comment by S.H. Büttner on: "One kilometre-thick ultramylonite, Sierra de Quilmes, Sierras Pampeanas, NW Argentina". Journal of Structural Geology 76, 84-85.

Forsyth, D. and Uyeda, S., 1975. On the relative importance of the driving forces of plate motion. Geophysical Journal of the Royal Astronomical Society 43, 163-200.

Gwinn, V. E., 1964. Thin-Skinned Tectonics in the Plateau and Northwestern Valley and Ridge Provinces of the Central Appalachians. Geological Society of America Bulletin 75(9), 863-900.

Hyndman, R. D., Currie, C. A. and Mazzotti, S. P., 2005. Subduction zone backarcs, mobile belts, and orogenic heat. GSA today 15(2), 4-10.

Jamieson, R. A., Beaumont, C., Hamilton, J. and Fullsack, P., 1996. Tectonic assembly of inverted metamorphic sequences. Geology 24(9), 839-842.

Larrovere, M. A., Toselli, A. J. and Rossi De Toselli, J. N., 2008. Petrologia y estructura de la Faja de deformation La Chilca, Catamarca. Revista de la Asociación Geológica Argentina 63(2), 254-263.

Lucassen, F., Becchio, R., Wilke, H. G., Franz, G., Thirlwall, M. F., Viramonte, J. and Wemmer, K., 2000. Proterozoic-Paleozoic development of the basement of the Central Andes

(18-26°S)-a mobile belt of the South American craton. Journal of South American Earth Sciences 13, 697-715.

Mottram, C. M., Warren, C. J., Regis, D., Roberts, N. M. W., Harris, N. B. W., Argles, T. W. and Parrish, R. R., 2014. Developing an inverted Barrovian sequence; insights from monazite petrochronology. Earth and Planetary Science Letters 403, 418-431.

Piñán-Llamas, A., 2007. The early Paleozoic evolution of the paleo-Pacific Gondwana margin: A structural, petrographic, and geochemical study in the Puncoviscana Formation. Unpublished PhD thesis, Boston University, 1-286.

Royden, L. H., 1993. The tectonic expression of slab pull at continental convergent boundaries. Tectonics 12, 303-325.

Searle, M. P. and Rex, A. J., 1989. Thermal model for the Zanskar Himalaya. Journal of Metamorphic Geology 7(1), 127-134.

Stein, S. and Freymueller, J., 2002. Plate Boundary Zones. American Geophysical Union Monograph 30, 425.

Suppe, J., 1983. Geometry and kinematics of fault-bend faulting. American Journal of Science 283, 684-721.

Visona, D., Carosi, R., Montomoli, C., Tiepolo, M. and Peruzzo, L., 2012. Miocene andalusite leucogranite in central-east Himalaya (Everest-Masang Kang area): Low-pressure melting during heating. Lithos 144-145, 194-208.

Wegmann, M. I., Riller, U., Hongn, F. D., Glodny, J. and Oncken, O., 2008. Age and kinematics of ductile deformation in the Cerro Durazno area, NW Argentina: Significance for orogenic processes operating at the western margin of Gondwana during Ordovician-Silurian times. Journal of South American Earth Sciences 26(1), 78-90.

Appendices

Cacti in tributary off Managua river gorge, Sierra de Quilmes

Appendix A

Table A1
Water content for each grain analysed by FTIR

Category	Sample number	ID	H:10^6 Si or Si,Al	Position
Weakly deformed	SQ183 Weakly deformed granitic diatexite	q1	1276	Quartz ribbon
		q2	1580	Quartz ribbon
		q3	2301	Quartz ribbon
		q4	1495	Matrix
		q5	2957	Matrix
		q6	7300	Matrix
		q7	7790	Disaggregated quartz ribbon
		q8	7649	Disaggregated quartz ribbon
		q9	4147	Quartz ribbon
		q10	6254	Quartz ribbon
		q11	3543	Quartz ribbon
		q12	3544	Quartz ribbon
		q13	3387	Quartz ribbon
		q14	1302	Quartz ribbon
		q15	3031	Quartz ribbon
		q16	3088	Quartz ribbon
		q17	1527	Quartz ribbon
		q18	4151	Quartz ribbon
	SQ77a Protomylonite	q1	581	Matrix
		q2	6250	Quartz ribbon
		q3	2140	Matrix
		q4	3796	Matrix
		q5	1095	Matrix
		q6	1764	Quartz ribbon
		q7	1880	Matrix
		q8	1363	Quartz ribbon
		q9	7134	Strain shadow of porphyroclast
		q10	7347	Strain shadow of porphyroclast
		q11	10306	Quartz ribbon
		q12	7706	Quartz ribbon
		q13	6322	Matrix
		q14	5736	Quartz ribbon
		q15	2104	Quartz ribbon
		q16	1108	Quartz ribbon
		q17	2320	Quartz ribbon
		q18	3598	Quartz ribbon

Category	Sample number	ID	H:10^6 Si or Si,Al	Position
Weakly deformed	SQ183b Weakly deformed granitic diatexite	q1	4794	Quartz porphyroclast
		q2	3504	Quartz ribbon
		q3	3645	Quartz ribbon
		q4	4907	Quartz ribbon
		q5	3478	Quartz ribbon
		q6	3730	Quartz ribbon
		q7	3999	Quartz ribbon
		q8	3993	Quartz ribbon
		q9	3649	Quartz ribbon
		q10	3606	Quartz ribbon
		q11	5593	Quartz ribbon
		q12	3919	Quartz ribbon
		q13	3805	Quartz ribbon
		q14	3754	Quartz ribbon
		q15	6432	Matrix
		q16	5734	Matrix
		q17	1157	Matrix
		q18	1330	Matrix
		q19	971	Matrix
		q20	1144	Matrix
Mylonitic	SQ30a	q1	1873	Quartz ribbon
		q2	2936	Quartz ribbon
		q3	1473	Quartz ribbon
		q4	2721	Quartz ribbon
		q5	1741	Quartz ribbon
		q6	1235	Quartz ribbon
		q7	1470	Quartz ribbon
		q8	1958	Quartz ribbon
		q9	2245	Quartz ribbon
		q10	943	Quartz ribbon
		q11	1579	Matrix
		q12	743	Matrix
		q13	3795	Matrix
		q14	1009	Quartz ribbon
		q15	895	Quartz ribbon
		q16	841	Quartz ribbon
		q17	2778	Quartz ribbon
		q18	2866	Quartz ribbon
		q19	3220	Matrix
		q20	2302	Matrix
	SQ32a	q1	4098	Quartz ribbon
		q2	2708	Quartz ribbon

Category	Sample number	ID	H:10^6 Si or Si,Al	Position
Mylonitic	SQ32a	q3	2730	Quartz ribbon
		q4	2876	Quartz ribbon
		q5	2718	Quartz ribbon
		q6	5547	Quartz ribbon near porphyroclast
		q7	2795	Quartz ribbon near porphyroclast
		q8	2590	Quartz ribbon near porphyroclast
		q9	3322	Quartz ribbon near porphyroclast
		q10	7763	Quartz ribbon near porphyroclast
		q11	3905	Quartz ribbon near porphyroclast
		q12	5676	Quartz ribbon near porphyroclast
		q13	5527	Quartz ribbon near porphyroclast
		q14	1135	Matrix
		q15	2889	Matrix
		q16	4639	Matrix
		q17	1000	Matrix
		q18	1433	Matrix
		q19	1134	Matrix
		q20	1642	Matrix
		q21	3286	Matrix
	SQ187d	q1	917	Quartz ribbon near porphyroclast
		q2	1431	Quartz ribbon near porphyroclast
		q3	1367	Matrix in strain shadow of porphyroclast
		q4	1400	Matrix in strain shadow of porphyroclast
		q5	1667	Matrix in strain shadow of porphyroclast
		q6	2303	Matrix
		q7	2910	Matrix
		q8	1546	Disaggregated qtz ribbon
		q9	1920	Disaggregated qtz ribbon
		q10	2539	Quartz ribbon
		q11	2263	Quartz ribbon

Category	Sample number	ID	H:10^6 Si or Si,Al	Position
Mylonitic	SQ187d	q12	2765	Quartz ribbon
		q13	2695	Quartz ribbon
		q14	5037	Quartz ribbon
		q15	2591	Quartz ribbon
		q16	4022	Quartz ribbon
	SQ187e	q1	1013	Quartz ribbon
		q2	1165	Quartz ribbon
		q3	1603	Quartz ribbon near porphyro-clast
		q4	778	Quartz ribbon near porphyro-clast
		q5	1951	Quartz ribbon near porphyro-clast
		q6	1279	Quartz ribbon near porphyro-clast strain shadow
		q7	1074	Quartz ribbon near porphyro-clast strain shadow
		q8	1665	Quartz ribbon near porphyro-clast
		q9	1518	Quartz ribbon near porphyro-clast strain shadow
		q10	1633	Matrix
		q11	2905	Matrix
		q12	3405	Matrix
		q13	2766	Matrix
		q14	2321	Quartz ribbon
		q15	4715	Quartz ribbon
	SQ26a	q1	1505	Quartz ribbon
		q2	2881	Quartz ribbon
		q3	2731	Quartz ribbon
		q4	4378	Matrix
		q5	2186	Matrix
		q6	5769	Quartz ribbon
		q7	1942	Matrix
		q8	1657	Quartz ribbon
		q9	2887	Matrix
		q10	3133	Quartz ribbon
		q11	3621	Matrix
		q12	3519	Matrix
		q13	5404	Matrix
		q14	2495	Matrix
		q15	2041	Quartz ribbon

Category	Sample number	ID	H:10⁶ Si or Si,Al	Position
Mylonitic	SQ26a	q16	2166	Quartz ribbon
		q17	2246	Quartz ribbon
		q18	6162	Quartz ribbon
		q19	3823	Quartz ribbon
Ultramylonitic	SQ80a	q1	621	Quartz ribbon near porphyroclast
		q2	712	Quartz ribbon near porphyroclast
		q3	758	Quartz ribbon
		q4	690	Quartz ribbon
		q5	725	Quartz ribbon near porphyroclast
		q6	1090	Quartz ribbon near porphyroclast
		q7	2832	Quartz ribbon near porphyroclast
		q8	3439	Matrix
		q9	3523	Matrix
		q10	3645	Matrix
		q11	4433	Matrix in strain shadow of porphyroclast
		q12	848	Quartz ribbon
		q13	1881	Quartz ribbon
		q14	1046	Matrix
		q15	1066	Matrix
		q16	1450	Matrix
		q17	743	Matrix
		q18	1107	Matrix
	SQ8d	q1	1336	Disaggregated quartz ribbon
		q2	1530	Matrix
		q3	777	Disaggregated quartz ribbon
		q4	1565	Disaggregated quartz ribbon
		q5	964	Disaggregated quartz ribbon
		q6	2003	Disaggregated quartz ribbon
		q7	431	Disaggregated quartz ribbon
		q8	1937	Disaggregated quartz ribbon
		q9	798	Disaggregated quartz ribbon
		q10	1098	Disaggregated quartz ribbon
		q11	1769	Matrix
		q12	2648	Matrix
		q13	1381	Matrix
		q14	3439	Matrix

Category	Sample number	ID	H:10⁶ Si or Si,Al	Position
Ultramylonitic	SQ8d	q15	1050	Matrix
		q16	1432	Quartz ribbon
		q17	847	Quartz ribbon
		q18	876	Quartz ribbon
		q19	1509	Quartz ribbon
		q20	814	Quartz ribbon
		q21	767	Quartz ribbon
		q22	663	Quartz ribbon
		q23	1138	Quartz ribbon
		q24	4236	Quartz ribbon
		q25	3649	Quartz ribbon
		q26	3914	Quartz ribbon
		q27	3800	Quartz ribbon
		q28	3894	Quartz ribbon
		q29	4896	Quartz ribbon
		q30	3259	Quartz ribbon
		q31	2452	Quartz ribbon
	SQ29b	q1	576	Matrix
		q2	500	Disaggregated quartz ribbon near porphyroclast
		q3	642	Matrix near porphyroclast
		q4	363	Matrix near porphyroclast
		q5	1634	Matrix
		q6	834	Matrix
		q7	320	Matrix
		q8	532	Matrix near porphyroclast
		q9	756	Matrix near porphyroclast
		q10	545	Matrix near porphyroclast
		q11	1158	Matrix
		q12	945	Matrix
		q13	1098	Matrix
		q14	1930	Matrix
		q15	2720	Matrix
	SQ83	q1	1152	Quartz ribbon
		q2	1116	Quartz ribbon
		q3	1448	Disaggregated quartz ribbon
		q4	883	Quartz ribbon
		q5	2461	Quartz ribbon
		q6	911	Quartz ribbon
		q7	977	Quartz ribbon
		q8	990	Quartz ribbon

Category	Sample number	ID	H:10⁶ Si or Si,Al	Position
Ultramylonitic	SQ83	q9	456	Quartz ribbon
		q10	1509	Quartz ribbon
		q11	2108	Matrix
		q12	2156	Matrix
		q13	2537	Matrix
		q14	3498	Matrix
		q15	1440	Matrix
	SQ77c	q1	1448	Strain shadow of porphyroclast
		q2	3487	Strain shadow of porphyroclast
		q3	1829	Strain shadow of porphyroclast
		q4	3134	Strain shadow of porphyroclast
		q5	1264	Matrix
		q6	1136	Matrix
		q7	1502	Quartz ribbon
		q8	1414	Matrix
		q9	972	Matrix
		q10	1142	Matrix
		q11	494	Quartz ribbon
		q12	3585	Quartz ribbon
		q13	3327	Quartz ribbon
		q14	2627	Quartz ribbon
		q15	2176	Quartz ribbon
		q16	4287	Quartz ribbon
Weakly deformed	SQ183 Weakly deformed granitic diatexite	f1	1333	Porphyroclast edge
		f2	1513	Porphyroclast edge
		f3	1626	Matrix strain shadow
		f4	1355	Matrix strain shadow
		f5	1580	Porphyroclast edge
		f6	4930	Matrix strain shadow
		f7	4619	Matrix strain shadow
		f8	5840	Matrix strain shadow
		f9	4395	Matrix strain shadow
		f10	2418	Porphyroclast edge
		f11	2390	Porphyroclast core
		f12	2840	Porphyroclast edge
		f13	2804	Porphyroclast core
		f14	2870	Porphyroclast edge
		f15	930	Porphyroclast core
		f16	1195	Porphyroclast edge
		f17	1733	Porphyroclast core
		f18	1342	Porphyroclast core

Category	Sample number	ID	H:10^6 Si or Si,Al	Position
		f19	1778	Porphyroclast core
	SQ77a Protomylonite	f1	6095	Porphyroclast core
		f2	2965	Porphyroclast edge
		f3	6145	Porphyroclast core
		f4	7419	Porphyroclast core
		f5	7780	Recrystallised porphyroclast edge
		f6	8387	Recrystallised porphyroclast edge
		f7	9026	Porphyroclast core
		f8	8472	Matrix
		f9	1598	Matrix
		f10	1563	Matrix
		f11	1626	Matrix
		f12	1408	Porphyroclast edge
		f13	1642	Porphyroclast edge
		f14	819	Porphyroclast edge
Weakly deformed	SQ183b Weakly deformed granitic diatexite	f1	2469	Porphyroclast edge
		f2	3608	Porphyroclast core
		f3	3190	Porphyroclast edge
		f4	2195	Porphyroclast core
		f5	2750	Porphyroclast edge
		f6	1769	Porphyroclast edge
		f7	1940	Porphyroclast edge
		f8	2195	Porphyroclast edge
		f9	2148	Porphyroclast core
		f10	3420	Porphyroclast edge
		f11	3309	Porphyroclast core
		f12	2504	Porphyroclast edge
		f13	3405	Porphyroclast core
		f14	2711	Porphyroclast edge
		f15	2520	Porphyroclast core
		f16	3175	Porphyroclast edge
		f17	3050	Porphyroclast core
		f18	4324	Porphyroclast core
		f19	3120	Recrystallised porphyroclast
		f20	2235	Recrystallised porphyroclast
		f21	2653	Recrystallised porphyroclast
Mylonitic	SQ30a	f1	840	Porphyroclast core
		f2	927	Porphyroclast core
		f3	2132	Porphyroclast core
		f4	704	Porphyroclast edge
		f5	804	Porphyroclast edge

Category	Sample number	ID	H:10^6 Si or Si,Al	Position
Mylonitic	SQ30a	f6	1094	Porphyroclast core
		f7	722	Porphyroclast core
		f8	1166	Porphyroclast edge
		f9	845	Porphyroclast edge
		f10	1644	Porphyroclast core
		f11	2715	Porphyroclast core
		f12	2553	Porphyroclast core
		f13	543	Porphyroclast core
		f14	219	Porphyroclast edge
		f15	844	Porphyroclast edge
		f16	1326	Porphyroclast edge
		f17	4463	Porphyroclast edge
		f18	1076	Porphyroclast core
		f19	2056	Porphyroclast core
		f20	2321	Porphyroclast core
		f21	840	Porphyroclast core
	SQ32a	f1	1518	Porphyroclast core
		f2	1910	Porphyroclast core
		f3	1789	Porphyroclast edge
		f4	1842	Porphyroclast edge
		f5	3447	Recrystallised porphyroclast
		f6	983	Recrystallised porphyroclast
		f7	1612	Matrix near porphyroclast
		f8	307	Matrix near porphyroclast
		f9	660	Porphyroclast edge
		f10	1358	Recrystallised porphyroclast
		f11	882	Recrystallised porphyroclast
		f12	2315	Porphyroclast edge
		f13	1135	Porphyroclast core
		f14	1203	Porphyroclast core
		f15	1152	Porphyroclast core
		f16	1364	Porphyroclast core
		f17	1025	Porphyroclast edge
		f18	987	Porphyroclast edge
		f19	2662	Porphyroclast edge
	SQ187d	f1	1078	Porphyroclast core
		f2	715	Porphyroclast edge
		f3	1185	Porphyroclast core
		f4	1370	Matrix in strain shadow of porphyroclast

Category	Sample number	ID	H:10^6 Si or Si,Al	Position
Mylonitic	SQ187d	f5	1324	Matrix in strain shadow of por-phyroclast
		f6	1228	Matrix in strain shadow of por-phyroclast
		f7	1726	Matrix
		f8	2341	Matrix
		f9	873	Porphyroclast edge
		f10	983	Porphyroclast core
		f11	3081	Porphyroclast edge
		f12	4848	Matrix in strain shadow of por-phyroclast
		f13	7085	Matrix in strain shadow of por-phyroclast
		f14	2394	Matrix between porphyroclasts
		f15	603	Matrix between porphyroclasts
		f16	858	Matrix between porphyroclasts
		f17	2700	Porphyroclast edge
		f18	922	Matrix
		f19	2939	Porphyroclast edge
		f20	2126	Porphyroclast core
		f21	1862	Porphyroclast core
		f22	2383	Porphyroclast core
		f23	3921	Porphyroclast edge
		f24	2564	Porphyroclast edge
		f25	3268	Porphyroclast core
		f26	2225	Matrix
	SQ187e	f1	581	Porphyroclast core
		f2	730	Porphyroclast core
		f3	1353	Porphyroclast edge
		f4	1378	Porphyroclast edge
		f5	1082	Porphyroclast edge
		f6	4210	Porphyroclast edge
		f7	854	Porphyroclast core
		f8	965	Porphyroclast edge
		f9	931	Porphyroclast edge
		f10	2480	Matrix
		f11	1135	Porphyroclast edge
		f12	2306	Porphyroclast core
		f13	2186	Porphyroclast edge
		f14	5984	Porphyroclast core
		f15	5146	Porphyroclast edge
		f16	2095	Porphyroclast core

Category	Sample number	ID	H:10^6 Si or Si,Al	Position
Mylonitic	SQ26a	f1	1397	Porphyroclast core
		f2	1373	Porphyroclast core
		f3	1411	Porphyroclast core
		f4	2215	Porphyroclast edge
		f5	1608	Porphyroclast edge
		f6	4430	Porphyroclast edge
		f8	1599	Matrix
		f9	1130	Matrix
		f10	2288	Matrix
		f11	1505	Matrix
		f12	2462	Matrix
		f13	1432	Matrix
		f14	1373	Porphyroclast core
		f15	1832	Porphyroclast core
		f16	3191	Porphyroclast core
		f17	1758	Porphyroclast core
Ultramylonitic	SQ80a	f1	340	Porphyroclast core
		f2	429	Porphyroclast core
		f3	774	Porphyroclast edge
		f4	265	Porphyroclast edge
		f5	306	Porphyroclast core
		f6	464	Porphyroclast edge
		f7	544	Porphyroclast edge
		f8	428	Porphyroclast edge
		f9	2502	Porphyroclast core
		f10	1608	Porphyroclast edge
		f11	639	Porphyroclast edge
		f12	2485	Porphyroclast edge
		f13	1205	Porphyroclast edge
		f14	1236	Porphyroclast core
		f15	630	Porphyroclast core
		f16	595	Porphyroclast core
	SQ8d	f1	1189	Porphyroclast edge
		f2	1083	Porphyroclast edge
		f3	757	Porphyroclast edge
		f4	953	Matrix
		f5	881	Matrix
		f6	1266	Matrix
		f7	2460	Matrix
		f8	956	Porphyroclast core
		f9	2973	Porphyroclast core

Category	Sample number	ID	H:10^6 Si or Si,Al	Position
Ultramylonitic	SQ8d	f10	5134	Porphyroclast core
		f11	3884	Porphyroclast edge
		f12	3049	Porphyroclast edge
		f13	4301	Porphyroclast core
		f14	2877	Porphyroclast core
	SQ29b	f1	153	Porphyroclast core
		f2	280	Porphyroclast core
		f3	861	Porphyroclast core
		f4	541	Porphyroclast edge
		f5	688	Porphyroclast edge
		f6	145	Porphyroclast edge
		f7	124	Porphyroclast edge
		f8	87	Porphyroclast edge
		f9	339	Porphyroclast edge
		f10	392	Porphyroclast core
		f11	453	Porphyroclast core
		f12	2107	Matrix
		f13	533	Matrix
		f14	509	Matrix
		f15	543	Matrix
		f16	503	Matrix
	SQ83	f1	415	Porphyroclast core
		f2	820	Porphyroclast core
		f3	923	Porphyroclast core
		f4	411	Porphyroclast edge
		f5	677	Porphyroclast edge
		f6	650	Porphyroclast core
		f7	990	Porphyroclast edge
		f8	1796	Porphyroclast core
		f9	307	Porphyroclast edge
		f10	276	Recrystallised porphyroclast
		f11	624	Matrix
		f12	869	Matrix
		f13	2449	Matrix
		f14	926	Matrix
		f15	1855	Matrix
		f16	1637	Porphyroclast core
		f17	1622	Porphyroclast core
	SQ77c	f1	794	Porphyroclast core
		f2	1070	Porphyroclast edge
		f3	957	Porphyroclast edge

Category	Sample number	ID	H:10^6 Si or Si,Al	Position
Ultramylonitic	SQ77c	f4	1760	Recrystallised porphyroclast
		f5	2113	Porphyroclast edge
		f6	1684	Porphyroclast edge
		f7	2110	Porphyroclast core
		f8	959	Porphyroclast edge
		f9	720	Porphyroclast edge
		f10	470	Porphyroclast core
		f11	377	Porphyroclast core
		f12	2670	Matrix
		f13	2485	Matrix
		f14	2607	Matrix
		f15	1856	Matrix
		f16	3684	Matrix
		f17	2398	Matrix

Appendix B

Pseudosections for thermodynamic modelling

In order to determine the P-T conditions of equilibration of the metamorphic zones, pseudosections of rocks from key metamorphic zones were constructed. The method and interpretation of this data is presented in section 6 of chapter 4 along with the pseudosection for one of the samples, SQ73a. This section describes the remaining five pseudosections and the problems encountered in each case. The minerals that were measured in the rock are referred to as end-member minerals, the field in the pseudosection that corresponds to the stable mineral assemblage preserved in the rock is referred to as the field of the stable mineral assemblage.

B1. Crd+Sil metatexite from the hanging wall of the Tolombón thrust (SQ49)

Sample SQ49 is a metatexite from the Grt-migmatite zone with the mineral assemblage Qtz+Ksp+Pl+Bt+Sil+Crd+Ilm±Grt. While other rocks in this zone contain peritectic sillimanite, in this sample sillimanite replaces cordierite and biotite suggesting it is a product of retrogression. Plagioclase is oligoclase with compositions $Ab_{73-75}An_{24-25}Or_{0.2-1}$, biotite has X_{Fe} ranging from 0.51 to 0.53 and cordierite has X_{Fe} from 0.35 to 0.39. While this sample contains garnet, there were none in the thin section.

A pseudosection of SQ49 was constructed (Fig. B1a) and isopleths of the end-member minerals plotted in the equilibrium field (highlighted in grey in Fig. B1a). X_{Fe} in cordierite indicates a temperature range of 730–775 °C and pressure of <5.5 kbar. X_{Fe} in biotite suggests a narrower temperature range between 725–750 °C and pressure of <5 kbar. Plagioclase gives a broad temperature range 675–775 °C and pressure <6.5 kbar. These ranges suggest that cordierite equilibrated at higher temperatures than the other minerals, with a maximum temperature given by X_{Fe} = 0.35, up to 750–775°C. In the field that contains the stable mineral assemblage isopleths for XFe in biotite and cordierite (X_{Fe}=0.39) do not exceed 5 kbar, suggesting this may reflect the maximum pressure. Taken together, this pseudosection suggests that peak metamorphism occurred at 750–775°C and 5 kbar with equilibration of plagioclase and retrogression of cordierite to sillimanite at lower temperatures.

B2. Bt-Ms schist from the Tolombón thrust (SQ55)

Sample SQ55 is a Bt-Ms schist from the Tolombón thrust high strain zone with the mineral assemblage Bt+Ms+Qtz+Pl+Ap+Mnz+oxides. The rock contains leucocratic lenses of Pl+Qtz and shows no evidence for in situ melting. Plagioclase is oligoclase and in the matrix has the composition $Ab_{70-72}An_{27-28}Or_{<1}$, and in the leucocratic lenses is slightly more albitic with the composition $Ab_{76-77}An_{22}Or_{<1}$. Biotite has X_{Fe} ranging from 0.50 to 0.53.

A pseudosection of SQ55 was constructed (Fig. B1b) and it was determined that the composition of the end-member minerals did not correspond to the calculated composition of those minerals in the field of the stable mineral assemblage. The isopleths for Ca(Pl) = 0.22 plot in the field Chl+Ms+Bt+Qtz+Pl+H$_2$O in the subsolidus part of the pseudosection (not shown in Fig. A2). The isopleths for Ca(Pl) = 0.27–0.28 and X$_{Fe}$ of biotite = 0.50–0.52 plotted in the Liq+Grt+Kfs+Sil+Bt+Crd field (Fig. A1b). X$_{Fe}$ of biotite = 0.53 did not plot anywhere on the pseudosection.

There field that the isopleths for the end-member minerals plot in does not reflect the stable mineral assemblage of the rock. This may be due to alteration, the rock has been strongly modified during shearing on the Tolombón thrust. However, we were unable to discipher the processes that took place.

B3. Grt+Crd metatexite from the footwall of the Tolombón thrust (SQ58a)

Sample SQ58a is a metatexite from the Grt-migmatite zone with Qtz+Pl+Kfs+Crd+Grt in the leucosome and Bt+Crd+Qtz+Pl+Kfs+Ilm±Sil in the melanosome. Biotite has X$_{Fe}$ ranging from 0.51 to 0.60 and cordierite has X$_{Fe}$ ranging from 0.39 to 0.43. Garnet has the composition Alm$_{76-79}$Grs$_{2-3}$Prp$_{12-15}$Sps$_{5-6}$ and is not zoned.

A pseudosection of SQ58a was constructed (Fig. B1c) and isopleths of the end-member minerals plotted in the equilibrium field (highlighted in grey in Fig. A1c). Of the end-member mineral compositions only X$_{Fe}$ of biotite = 0.52–0.53, X$_{Fe}$ of cordierite = 0.39–0.40, and Sps = 5–6 plotted in the field of the stable mineral assemblage. We attempted to plot the remaining isopleths in any field above and below the solidus and found that the composition of the end-member minerals did not correspond to any field.

B4. Grt+Crd metatexite from the footwall of the Tolombón thrust (SQ72a)

Sample SQ72a is a metatexite from the Opx-migmatite zone with Qtz+Pl+Kfs+Crd+Grt in the leucosome and Bt+Crd+Qtz+Pl+Kfs±Crd±Grt in the melanosome. Biotite has X$_{Fe}$ ranging from 0.49 to 0.51 and cordierite has X$_{Fe}$ ranging from 0.29 to 0.32. Garnet has the composition Alm$_{64–68}$Grs$_{2.8–3.2}$Prp$_{18-24}$Sps$_{7–10}$ and is not zoned.

A pseudosection of SQ72a was constructed (Fig. B1d) and isopleths of the end-member minerals plotted in the equilibrium field (highlighted in grey in Fig. B1d). Of the end-member mineral compositions isopleths for Alm, Sps, and X$_{Fe}$ of cordierite plotted in the field of the stable mineral assemblage. The isopleths for Grs and X$_{Fe}$ of biotite did not plot in the field of the stable mineral assemblage. We attempted to plot the remaining isopleths in any field above and below the solidus and found that the composition of the end-member minerals did not correspond to any field.

B5. Grt-schist from the footwall of the PSZ (SQ106)

Sample SQ106 is a metapsammite from the Agua del Sapo complex with the mineral assemblage Qtz+Bt+Ms+Ksp+Grt+Pl. Biotite has X_{Fe} ranging from 0.47 to 0.51, muscovite has X_{Fe} of 0.47 to 0.52, garnet is almandine with compositions $Alm_{72-76}Grs_{2-3}Prp_{11-15}Sps_{9-12}$.

A pseudosection of SQ106 was constructed (Fig. B1e) and isopleths of the end-member minerals plotted in the equilibrium field (highlighted in grey in Fig. B1e). Of the end-member mineral compositions, isopleths for X_{Fe} in biotite and Sps in garnet plot within the field of the stable mineral assemblage. However, isopleths for Alm>0.76, X_{Fe} of muscovite >0.52 and all isopleths for Grs do not plot on the subsolidus pseudosection.

This sample shows no evidence for partial melting so is not susceptible to the effects of fractionation and melt removal or addition, as described for sample SQ73a in chapter 4, section 6. However, this rock contains large K-feldspar porphyroblasts and has been strongly sheared, perhaps suggesting that it was intruded by melt which was subsequently sheared into porphyroblasts. Pegmatite intrusions in neighbouring rocks are strongly sheared and may also be the source of the garnet and muscovite in this rock.
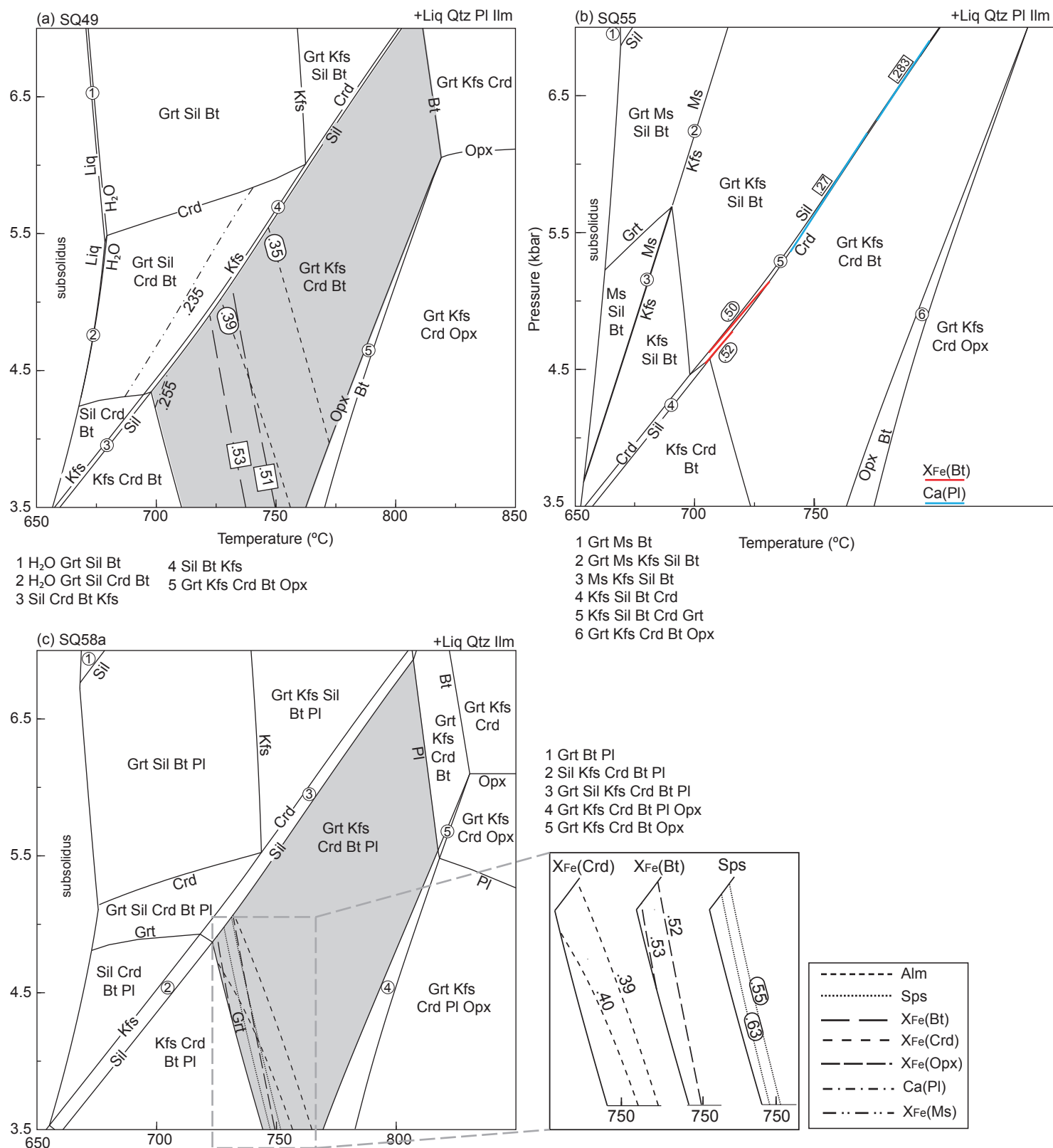
Fig. B1. H₂O-undersaturated MnNCKFMASHTO P-T pseudosections for five samples in key structural positions above and below major thrust planes (see chapter 4, Fig. 4 for sample locations).
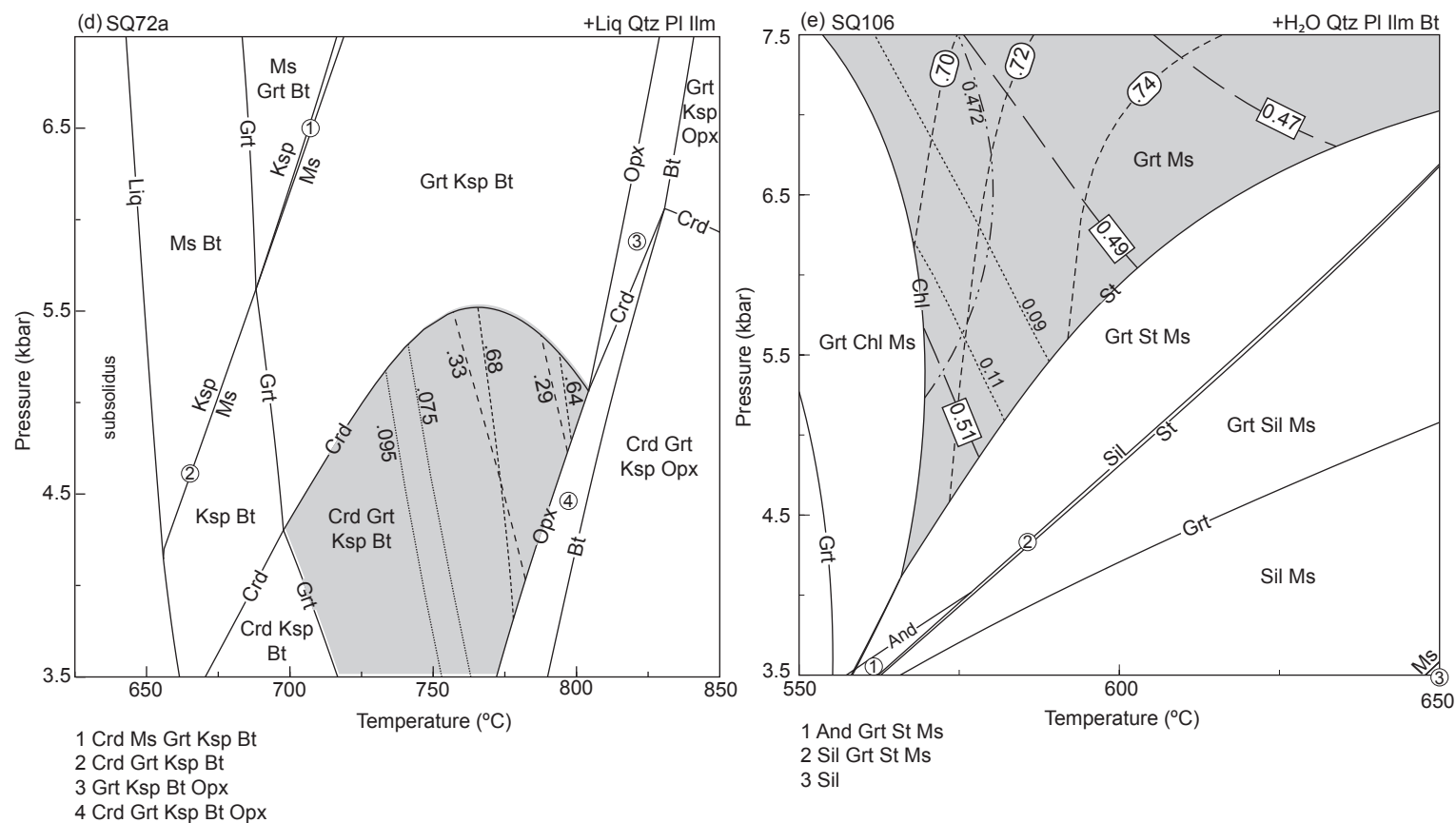
(d) SQ72a　　+Liq Qtz Pl Ilm

1 Crd Ms Grt Ksp Bt
2 Crd Grt Ksp Bt
3 Grt Ksp Bt Opx
4 Crd Grt Ksp Bt Opx

(e) SQ106　　+H₂O Qtz Pl Ilm Bt

1 And Grt St Ms
2 Sil Grt St Ms
3 Sil

Fig. B1. (continued)